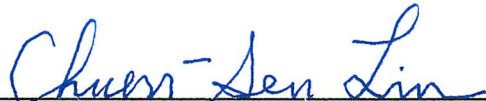
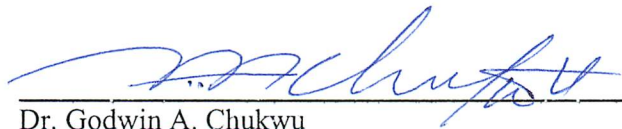


EXPERIMENTAL AND COMPUTATIONAL STUDIES OF NANOFLUIDS

By

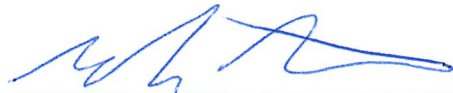
Ravikanth S. Vajjha


RECOMMENDED: 
Dr. Chuen-Sen Lin

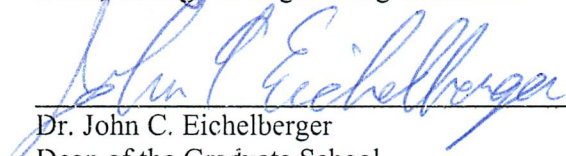

Dr. Godwin A. Chukwu



Dr. Yuri Shur


Dr. Debendra K. Das
Advisory Committee Chair


Dr. Rorik A. Peterson
Chair, Department of Mechanical Engineering

APPROVED: 
Dr. Douglas J. Goering
Dean, College of Engineering and Mines


Dr. John C. Eichelberger
Dean of the Graduate School


Date

EXPERIMENTAL AND COMPUTATIONAL STUDIES OF NANOFLUIDS

A
DISSERTATION

Presented to the Faculty
of the University of Alaska Fairbanks

in Partial Fulfillment of the Requirements
for the Degree of

DOCTOR OF PHILOSOPHY

By
Ravikanth S. Vajjha, M.S.

Fairbanks, Alaska

December 2014

Abstract

The goals of this dissertation were (i) to experimentally investigate the fluid dynamic and heat transfer performance of nanofluids in a circular tube, (ii) to study the influence of temperature and particle volumetric concentration of nanofluids on thermophysical properties, heat transfer and pumping power, (iii) to measure the rheological properties of various nanofluids and (iv) to investigate using a computational fluid dynamic (CFD) technique the performance of nanofluids in the flat tube of a radiator. Nanofluids are a new class of fluids prepared by dispersing nanoparticles with average sizes of less than 100 nm in traditional heat transfer fluids such as water, oil, ethylene glycol and propylene glycol. In cold regions of the world, the choice of base fluid for heat transfer applications is an ethylene glycol or propylene glycol mixed with water in different proportions. In the present research, a 60% ethylene glycol (EG) or propylene glycol (PG) and 40% water (W) by mass fluid mixture (60:40 EG/W or 60:40 PG/W) was used as a base fluid, which provides freeze protection to a very low level of temperature.

Experiments were conducted to measure the convective heat transfer coefficient and pressure loss of nanofluids flowing in a circular tube in the fully developed turbulent regime. The experimental measurements were carried out for aluminum oxide (Al_2O_3), copper oxide (CuO) and silicon dioxide (SiO_2) nanoparticles dispersed in 60:40 EG/W base fluid. Experiments revealed that the heat transfer coefficient of nanofluids showed an increase with the particle volumetric concentration. Pressure loss was also observed to increase with the nanoparticle volumetric concentration. New correlations for the Nusselt number and the friction factor were developed.

The effects of temperature and particle volumetric concentration on different thermophysical properties (e.g. viscosity, thermal conductivity, specific heat and density) and subsequently on the Prandtl number, Reynolds number and Nusselt number of three nanofluids were investigated. The three nanofluids studied were Al_2O_3 , CuO and SiO_2 nanoparticles dispersed in a base fluid of 60:40 EG/W. Results showed that the Prandtl number of nanofluids increased with increasing particle volumetric concentration and decreased with an increase in the temperature. The Reynolds number of nanofluids for a specified geometry and velocity increased

with an increase in temperature and decreased with an increase in particle volumetric concentration. The Mouromtseff numbers of nanofluids were higher than those of the conventional fluids under both laminar and turbulent flow conditions, proving the superiority of nanofluids in electronic cooling applications.

Experiments were performed to investigate the rheological properties of various nanoparticles dispersed in a 60:40 PG/W base fluid. The nanoparticles studied were; Al_2O_3 , CuO, SiO_2 , zinc oxide (ZnO), titanium oxide (TiO_2) with particle diameters ranging from 15 to 75 nm and particle volumetric concentrations of up to 6%. All the nanofluids exhibited a non-Newtonian Bingham plastic behavior at the lower temperature range of 243 K to 273 K and a Newtonian behavior in the temperature range of 273 K to 363 K. A new correlation was developed for the viscosity of nanofluids as a function of temperature, particle volumetric concentration, particle diameter, the properties of nanoparticles and those of the base fluid. Measurements were also conducted for single wall, bamboo-like structured and hollow structured multi-wall carbon nanotubes dispersed in a base fluid of 20:80 PG/W. A low-volume concentration (0.229%) of these carbon nanotubes (CNT) nanofluids revealed a non-Newtonian behavior over a measured temperature range of 273 K to 363 K. From the experimental data, a new correlation was developed which related viscosity to temperature and the Péclet number for CNT nanofluids.

A three-dimensional CFD study was performed to analyze the heat transfer and fluid dynamic performance of nanofluids flowing in the turbulent regime in a flat tube of an automotive radiator. Computations were carried out for the Al_2O_3 and CuO nanoparticles of 0 to 6% particle volumetric concentrations dispersed in a base fluid of 60:40 EG/W. The numerical study revealed that under equal pumping power basis, the Al_2O_3 and CuO nanofluids up to 3% and 2% particle volumetric concentrations respectively, provided higher heat transfer coefficients than those provided by the base fluid. From this study, several new correlations to determine the Nusselt number and friction factor for the nanofluids flowing in the flat tubes of a radiator were developed for the entrance as well as the fully developed regions.

Table of Contents

	Page
Signature Page	i
Title Page	iii
Abstract	v
Table of Contents	vii
List of Figures	xiii
List of Tables	xix
List of Appendices	xxi
Acknowledgements.....	xxiii
Chapter 1. Introduction	1
1.1 Introduction to Nanofluids	1
1.2 Nanoparticle Synthesis Methods.....	2
1.3 Dispersion of Nanoparticles in Liquids	3
1.3.1 Two-step process	3
1.3.2 Single-step process	4
1.4 Stabilization and Characterization of Nanofluids.....	5
1.5 Carbon Nanotubes.....	6
1.6 Nanofluids Thermophysical Properties.....	7
1.6.1 Density.....	7
1.6.2 Specific Heat	8
1.6.3 Thermal Conductivity.....	9
1.6.4 Viscosity	11
1.7 Applied Research in Nanofluids	12

	Page
1.7.1 Electronics Cooling Applications.....	13
1.7.2 Automotive Cooling Applications.....	13
1.7.3 Building Heating Systems	14
1.7.4 Other Applications	14
1.8 Agglomeration of Nanoparticles and Effects of pH	15
1.9 Erosion and Corrosion Effects of Nanofluids.....	16
1.10 Outline of the Present Research.....	16
1.11 Summary of Subsequent Chapters	16
1.12 Nomenclature	18
1.13 References.....	18
Chapter 2. Development of New Correlations for Convective Heat Transfer and Friction Factor in Turbulent Regime for Nanofluids	25
2.1 Abstract.....	25
2.2 Keywords	25
2.3 Nomenclature	25
2.4 Introduction.....	26
2.5 Determination of Thermophysical Properties.....	29
2.5.1 Viscosity.....	29
2.5.2 Thermal Conductivity.....	31
2.5.3 Specific Heat	32
2.5.4 Density.....	33
2.5.5 Base Fluid Properties.....	33
2.6 Pressure Loss and Heat Transfer Measurements	34
2.7 Heat Transfer Results.....	35

	Page
2.7.1 Benchmark Test Case	35
2.7.2 Effect of the Particle Volumetric Concentration	36
2.7.3 Effect of the Thermophysical Properties of Particles	37
2.7.4 Particle Size Effect on Heat Transfer	37
2.7.5 New Nusselt Number Correlation	38
2.7.6 Pressure Loss Measurement	39
2.7.7 Guidance from Experimental Observation	41
2.8 Conclusions	42
2.9 Acknowledgement	42
2.10 References	42
Chapter 3. A Review and Analysis on Influence of Temperature and Concentration of Nanofluids on Thermophysical Properties, Heat Transfer and Pumping Power	61
3.1 Abstract	61
3.2 Keywords	61
3.3 Nomenclature	61
3.4 Introduction	63
3.5 Convective Heat Transfer Theory of Nanofluids	71
3.6 Development of Correlations for Thermophysical Properties	73
3.6.1 Viscosity	73
3.6.2 Thermal Conductivity	74
3.6.3 Specific Heat	76
3.6.4 Density	77
3.6.5 Base Fluid Properties	78
3.7 Effect of Properties Variation	79

	Page
3.7.1 Effect on the Prandtl Number.....	79
3.7.2 Effect on the Reynolds Number	80
3.7.3 Effect on the Convective Heat Transfer Coefficient	81
3.7.4 Effect on Thermal Diffusivity	82
3.7.5 Effect on the Pumping Power.....	82
3.7.6 Effect on Mouromtseff number	83
3.7.7 Effect on Thermal and Fluid Dynamic Performance	84
3.8 Conclusions.....	85
3.9 References.....	86
Chapter 4. An Experimental Determination of the Viscosity of Propylene Glycol/Water Based Nanofluids and Development of New Correlations	101
4.1 Abstract.....	101
4.2 Introduction.....	101
4.3 Nanofluids preparation and characterization	104
4.4 Experimental setup for rheological properties measurements	105
4.5 Results and Discussion	107
4.5.1 Calibration and benchmark test case.....	107
4.5.2 Aluminum oxide nanofluid	107
4.5.3 Copper oxide nanofluid.....	109
4.5.4 Silicon dioxide nanofluid	109
4.5.5 Titanium oxide nanofluid	110
4.5.6 Zinc oxide nanofluid	110
4.5.7 Particle size effect	110
4.6 Development of new correlations	111

	Page
4.7 Carbon nanotubes.....	114
4.7.1 Effect of ultrasonication time on the viscosity of CNT nanofluids.....	116
4.8 Conclusions.....	118
4.9 Acknowledgments.....	118
4.10 References.....	118
Chapter 5. Development of New Correlations for the Nusselt Number and the Friction Factor under Turbulent Flow of Nanofluids in Flat Tubes	157
5.1 Abstract.....	157
5.2 Nomenclature.....	158
5.3 Introduction.....	159
5.4 Mathematical modeling	162
5.4.1 Problem geometry	162
5.4.2 Governing equations.....	163
5.4.3 Boundary conditions.....	165
5.5 Thermophysical properties.....	166
5.5.1 Conventional coolant (60:40 EG/W).....	166
5.5.2 Nanofluids	166
5.6 Numerical computation.....	169
5.6.1 Mesh independence study	169
5.6.2 Validation of the computational procedure.....	170
5.7 Results and discussion	171
5.7.1 Peripheral variation	171
5.7.2 Effect of nanoparticle concentration on local skin friction coefficient.....	172
5.7.3 Effect of nanoparticle concentration on local heat transfer coefficient.....	172

	Page
5.7.4 Effect of Reynolds number on average heat transfer coefficient	174
5.7.5 New correlations of Nusselt Number in fully developed and entrance regions of the flat tube.....	175
5.7.6 Effect of nanoparticle concentrations on pumping power.....	178
5.8 Conclusions.....	179
5.9 Acknowledgement	180
5.10 References.....	180
Chapter 6. Overall Conclusions	205
6.1 Conclusions for Development of New Correlations for Convective Heat Transfer and Friction Factor in Turbulent Regime for Nanofluids	205
6.2 Conclusions for a Review and Analysis on Influence of Temperature and Concentration of Nanofluids on Thermophysical Properties, Heat Transfer and Pumping Power.....	205
6.3 Conclusions for an Experimental Determination of the Viscosity of Propylene Glycol/Water based Nanofluids and Development of New Correlations.....	207
6.4 Conclusions for Development of New Correlations for the Nusselt Number and the Friction Factor under Turbulent Flow of Nanofluids in Flat Tubes	208
6.5 Suggestions for Future Research	209
Appendices.....	211

List of Figures

	Page
Figure 1.1. Comparison of thermal conductivities of metallic oxide nanoparticles and conventional heat transfer fluids at room temperature (300 K).	2
Figure 1.2. TEM image of a CuO nanofluid of average particle size 30 nm produced from inert gas condensation process. (Source: Eastman et al. [12])	3
Figure 1.3. Schematic diagram of nanofluids produced from the direct evaporation of materials into base fluids. (Source: Eastman et al. [12])	4
Figure 1.4. TEM image of a copper nanofluid of an average particle size of 10 nm produced from the direct evaporation process. (Source: Eastman et al. [12])	5
Figure 1.5. TEM images of (a) Al ₂ O ₃ nanoparticles of APS 20 nm and (b) SiO ₂ nanoparticles of APS 20 nm taken at the University of Alaska Fairbanks (UAF) laboratory.	6
Figure 1.6. TEM image of single-walled carbon nanotubes taken at the UAF laboratory.	7
Figure 1.7. Density variations with temperature of Al ₂ O ₃ nanofluid of several particle volumetric concentrations. (Source: Vajjha et al. [23])	8
Figure 1.8. Variation in the specific heat ratio of the Al ₂ O ₃ nanofluid with temperature for two particle volumetric concentrations. (Source: Vajjha and Das [25])	9
Figure 1.9. Thermal conductivity ratio variation with temperature at different particle volumetric concentrations of the CuO nanofluid. (Source: Vajjha and Das [27])	10
Figure 1.10. Measured viscosity values for different particle volumetric concentrations of the Al ₂ O ₃ nanofluid of APS 53 nm.	12
Figure 2.1. Experimental and curve-fit (Eq. 2.5) viscosity values for various particle concentrations of Al ₂ O ₃ nanofluid as a function temperatures.	48
Figure 2.2. Thermal conductivity ratio variation with temperature at different particle volumetric concentrations of CuO nanoparticles dispersed in 60:40 EG/W.	49
Figure 2.3. Comparison of experimental specific heat values with the correlation, Eq. (2.7) presented by Vajjha and Das [25].	50
Figure 2.4. A schematic diagram of the experimental set up to measure pressure loss and heat transfer of nanofluids.	51

	Page
Figure 2.5. Comparison between the experimental results and the theoretical values obtained from the equations of Dittus-Boelter, Eq. (2.16), and Gnielinski, Eq. (2.17).	52
Figure 2.6. The convective heat transfer coefficient of the Al ₂ O ₃ nanofluid in 60:40 EG/W.	53
Figure 2.7. Comparison of the heat transfer coefficient of three nanofluids at a particle volumetric concentration of 4% over the base fluid (0%).....	54
Figure 2.8. The effect of particle sizes on the heat transfer coefficient of 2% SiO ₂ nanoparticles suspended in 60:40 EG/W.....	55
Figure 2.9. Comparison of the experimental values with the values obtained from the proposed correlation, Eq. (2.18).....	56
Figure 2.10. Pressure loss of the Al ₂ O ₃ nanofluid measured at various particle volume concentrations as a function of the Reynolds number.....	57
Figure 2.11. Pressure loss variation with the Reynolds number for the base fluid (0%) and 2% particle concentration of SiO ₂ , Al ₂ O ₃ and CuO nanofluids.	58
Figure 2.12. Friction factor variation with the Reynolds number for the three nanofluids and the base fluid.	59
Figure 2.13. Comparison of the friction factor values calculated from the present correlation, Eq. (2.24) with the values obtained from the experiments.	60
Figure 3.1. Comparison of experimental values with correlations for different particle volumetric concentrations as a function of temperature (a) viscosity; (b) thermal conductivity.	92
Figure 3.2. Comparison of experimental values with correlations for different particle volumetric concentrations as a function of temperature (a) specific heat; (b) density.	93
Figure 3.3. Variation of (a) specific heat with temperature (b) volumetric heat capacity with particle volumetric concentration at 293 K.	94
Figure 3.4. Variation of Prandtl number with (a) particle volumetric concentration and (b) temperature.	95
Figure 3.5. Variation of Reynolds number with (a) temperature for three nanofluids and basefluid (b) particle volumetric concentrations for the SiO ₂ nanofluid at various nanofluids.	96
Figure 3.6. Effect of temperature variation (a) on the heat transfer coefficient and (b) on the thermal diffusivity.	97

	Page
Figure 3.7. Variation of pumping power per unit length (a) influence of temperature (b) influence of particle volumetric concentration.....	98
Figure 3.8. Variation of the ratio of Mouromtseff numbers (FOM) for three concentrations of the Al ₂ O ₃ nanofluid and the base fluid for laminar and turbulent internal flows.....	99
Figure 3.9. Variation of energy ratio with the Reynolds number for the Al ₂ O ₃ nanofluid at a temperature of 293 K.....	100
Figure 4.1. TEM images of (a) Al ₂ O ₃ nanoparticles of APS 20 nm and (b) BWCNT taken before conducting the rheological measurements.	134
Figure 4.2. Experimental setup for the viscosity measurement of nanofluids and carbon nanotubes.....	135
Figure 4.3. Benchmark test cases for the viscosity of 60:40 PG/W and DI water.....	136
Figure 4.4. Viscosity variation with shear strain rate of Al ₂ O ₃ nanofluid of 4% particle volume concentration for varying temperatures from 243 K (-30 °C) to 363 K (90 °C).....	137
Figure 4.5. Shear stress versus shear strain rate for a 4% particle volume concentration of Al ₂ O ₃ nanofluid at 243 K (-30°C) and 293 K (20°C).....	138
Figure 4.6. Viscosity variation with temperature at different particle volumetric concentrations of Al ₂ O ₃ nanoparticles of APS 53 nm suspended in 60:40 PG/W.....	139
Figure 4.7. Viscosity variation with temperature at different particle volumetric concentrations of Al ₂ O ₃ nanoparticles of APS 20 nm suspended in 60:40 PG/W.....	140
Figure 4.8. Viscosity variation with temperature at different particle volumetric concentrations of CuO nanoparticles of APS 29 nm suspended in 60:40 PG/W.	141
Figure 4.9. Viscosity variation with temperature at different particle volumetric concentrations of SiO ₂ nanoparticles of APS 30 nm suspended in 60:40 PG/W.	142
Figure 4.10. Viscosity variation with temperature at different particle volumetric concentrations of TiO ₂ nanoparticles of APS 10±5 nm suspended in 60:40 PG/W.	143
Figure 4.11. Viscosity variation with temperature at different particle volumetric concentrations of ZnO nanoparticles of APS 77 nm suspended in 60:40 PG/W.	144
Figure 4.12. Viscosity variation with temperature at different particle volumetric concentrations of ZnO nanoparticles of APS 50 nm suspended in 60:40 PG/W.	145

	Page
Figure 4.13. Effect of nanoparticle size on viscosity for varying temperatures at two different particle sizes and volumetric concentrations of Al ₂ O ₃ nanofluid in 60:40 PG/W.....	146
Figure 4.14. Effect of nanoparticle diameter on viscosity for varying temperatures at two different particle volumetric concentrations of ZnO nanofluid in 60:40 PG/W.	147
Figure 4.15. Comparison between several theoretical models and experimental data on viscosity for Al ₂ O ₃ -PG/Water nanofluids as a function of particle volumetric concentration at a room temperature of 293 K.	148
Figure 4.16. Comparison of the viscosity values calculated from the present correlation, Eq. (4.4) with the values obtained from the experiments.....	149
Figure 4.17. Viscosity variation with shear strain rate over a temperature range of 273 K to 363 K for a 0.229% volume concentration of (a) SWCNT, (b) BWCNT and (c) MWCNT. ...	150
Figure 4.18. Shear stress versus shear strain rate at 273 K and 313 K for a 0.229% particle volume concentration of (a) SWCNT, (b) BWCNT and (c) MWCNT after 90 minutes of ultrasonication.	152
Figure 4.19. Effect of ultrasonication time on the viscosity of BWCNT.	154
Figure 4.20. Effect of ultrasonication time on the viscosity of MWCNT.	155
Figure 4.21. Comparison of the viscosity values calculated from the present correlation, Eq. (4.7) with the values obtained from the experiments for the BWCNT at different shear rates.	156
Figure 5.1A. Typical configuration of an automobile radiator adopted from [21].....	188
Figure 5.1B. Dimensions and coordinate system of one quarter of a flat tube used in the present numerical study..	188
Figure 5.2. Mesh layout used in the present analysis.	189
Figure 5.3. Axial velocity and temperature profiles in the Y-Z plane at the outlet of the duct (Z=0.5m) and at the center (X=0) for four different mesh sizes.	190
Figure 5.4. Comparison of \overline{Nu} of the present numerical computations with the theoretical results for various Reynolds numbers in a flat tube.....	191
Figure 5.5. Comparison of \overline{C}_f of the present numerical computations with the correlations of other researchers for various Reynolds numbers.	192

	Page
Figure 5.6. Local heat transfer coefficient and local shear stress variation along the circumference (1-60 upper wall, 61-130 curved wall and 131-190 lower wall) of the tube at $Z=0.42$ m for the base fluid.	193
Figure 5.7. Contour plots of (a) Y velocity (m/s) and (b) Turbulent Kinetic Energy (m^2/s^2) at $Z = 0.25$ m and $Re = 5000$	194
Figure 5.8. Variation of h_{ZA} and τ_{ZA} on the upper, lower and semicircular walls along the length of the tube for the base fluid.	195
Figure 5.9. Variation of $C_{f\ avg}$ along the tube length for different particle volumetric concentrations of the CuO nanofluid.	196
Figure 5.10. Variation of h_{avg} along the tube length for various concentrations of the CuO nanofluid.	197
Figure 5.11. Variation of average heat transfer coefficient with velocity for base fluid and two nanofluids.	198
Figure 5.12. A comparison of the heat transfer coefficient at different friction powers per unit area for Al_2O_3 , CuO nanofluids of different concentrations and the base fluid.	199
Figure 5.13. Variation of the \bar{h} with Reynolds number for different particle volumetric concentrations of the Al_2O_3 nanofluid.	200
Figure 5.14. Variation of the \bar{h} with Reynolds number for different particle volumetric concentrations of the CuO nanofluid.	201
Figure 5.15. Comparison of the Nusselt number values calculated from the present correlation, Eq. (5.16) with the values obtained from the present numerical study in the fully developed region.	202
Figure 5.16. Comparison of the local Nusselt number values calculated from the correlation, Eq. (5.20a & b) with the values obtained from the present numerical study.	203

List of Tables

	Page
Table 2.1. Characteristics of nanoparticles.	46
Table 2.2. Constants of the viscosity correlation for different nanofluids.....	46
Table 2.3. Curve-fit relations proposed by Vajjha and Das [21] and Sahoo [22].....	47
Table 2.4. Curve-fit coefficients for different nanofluids.....	47
Table 3.1. Constants of the viscosity correlation for different nanofluids.....	91
Table 3.2. Curve-fit relations for β from experiments.....	91
Table 3.3. Curve-fit coefficients for specific heat of different nanofluids.	91
Table 4.1. Effective viscosity models proposed by researchers.	124
Table 4.2. Effective viscosity models for nanofluids proposed by researchers.....	125
Table 4.3. Characteristics of nanoparticles used in the present study as specified by the manufacturers.	130
Table 4.4. Characteristics of carbon nanotubes specified by the manufacturer.....	130
Table 4.5. Correlations for the viscosity of DI water and 60:40 PG/W.....	131
Table 4.6. Curve-fit coefficients of different nanofluids derived for Eq. (4.3).	132
Table 4.7. Curve-fit coefficients derived for Eq. (4.4) in two temperature regimes.	132
Table 4.8. Temperature dependence of flow consistency factor K and flow behavior index n for the CNT nanofluids.	133
Table 4.9. Curve-fit coefficients derived for Eq. (4.7) in two temperature regimes.	133
Table 5.1. Thermophysical property correlations for 60:40 EG/W.....	184
Table 5.2. Constants of the viscosity correlation for the Al_2O_3 and CuO nanofluids.....	184
Table 5.3. Curve-fit relations for β proposed from experiments of Vajjha and Das [9].	185
Table 5.4. Curve-fit coefficients for the specific heat of Al_2O_3 nanofluids [36].	185
Table 5.5. Mesh independence study.....	185
Table 5.6. Fully developed turbulent flow Nusselt number correlations used for comparison in the present numerical study.....	185
Table 5.7. Fully developed turbulent flow friction factor correlations used for comparison in the present study.....	186

Table 5.8. Comparison of various parameters for different concentrations of the Al_2O_3 nanofluid with the base fluid for a constant heat transfer.....187

List of Appendices

	Page
Appendix 1. Experimental and Numerical Investigations of Nanofluids Performance in a Compact Minichannel Plate Heat Exchanger	212
Appendix 2. Measurements of the pH of Three Nanofluids and Development of New Correlations	213
Appendix 3. Measurement of the Thermal Conductivity of Silicon Dioxide Nanofluid and Development of Correlations	214
Appendix 4. Electrical Conductivity Measurements of Nanofluids and Development of New Correlations	215
Appendix 5. Comparison of the Performance of Copper Oxide Nanofluid with Water in Electronic Cooling	216
Appendix 6. Application of Nanofluids in Heating Buildings and Reducing Pollution	217

Acknowledgements

First of all, I express my sincere thanks to my principal advisor, Dr. Debendra K. Das, for his constant support, encouragement, and invaluable guidance during my doctoral studies. I also greatly appreciate my advisory committee members Dr. Chuen-Sen Lin, Dr. Godwin A. Chukwu and Dr. Yuri Shur for their valuable suggestions and commitment to this dissertation.

The financial support from the Dean of the Graduate School at the University of Alaska Fairbanks and NASA EPSCoR are gratefully acknowledged. Special thanks to Petroleum Development Laboratory (PDL) for providing the experimental facilities to measure the viscosity.

I express my deepest gratitude to my parents, Mr. Ramakrishna and Mrs. Rupa Vajjha, for their unconditional love and support. Finally, I would like to thank my friends for their support and comments about my work.

Chapter 1. Introduction

1.1 Introduction to Nanofluids

Nanofluids are dilute suspensions of nanoparticles (typically 1-100 nm in size) in conventional heat transfer fluids such as water, ethylene glycol, propylene glycol and oils. The thermal properties of liquid coolants play a vital role in the ultrahigh-performance of industrial cooling systems. Particularly, the thermal conductivity of a liquid is an important physical property that determines its heat transfer performance. Compared to metals, most liquid coolants have low thermal conductivity. For example, a conventional liquid coolant, water has a thermal conductivity of 0.6 W/m. K [1], whereas aluminum oxide has a thermal conductivity 60 times greater at 36 W/m. K [2]. Figure 1.1 shows the thermal conductivities of metallic oxides of aluminum, copper (17.65 W/m. K [3]) and silicon (1.38 W/m. K [2]) compared with traditional coolants like water, 60:40 EG/W¹ (0.36 W/m. K [4]) and 60:40 PG/W² (0.3054 W/m. K [4]). Therefore, researchers have made great efforts to improve the inherently poor thermal conductivity of these conventional liquids by dispersing millimeter or micrometer sized metallic particles in liquids following the pioneering work of Maxwell's effective medium theory [5]. Since then, numerous experimental and theoretical studies have been performed to determine the heat transfer characteristics of these effective mixtures. However, the main drawback with the use of such large particles is that they are not uniformly dispersed and settle to the bottom due to gravity. This drawback can be overcome with the recent advancements in particle synthesis methods which enable us to produce metallic or nonmetallic nanoparticles. Masuda et al. [6] demonstrated experimentally that the thermal conductivity and viscosity of liquids are altered by dispersing the ultra-fine particles of γ -aluminum oxide, silicon dioxide and titanium dioxide. Subsequently, Choi [7] also conclusively established this finding from his experiments. He synthesized these nano-sized particles and dispersed them in conventional liquids to form a new type of engineered fluids known as nanofluids.

¹ 60 % ethylene glycol and 40 % water by mass

² 60 % propylene glycol and 40 % water by mass

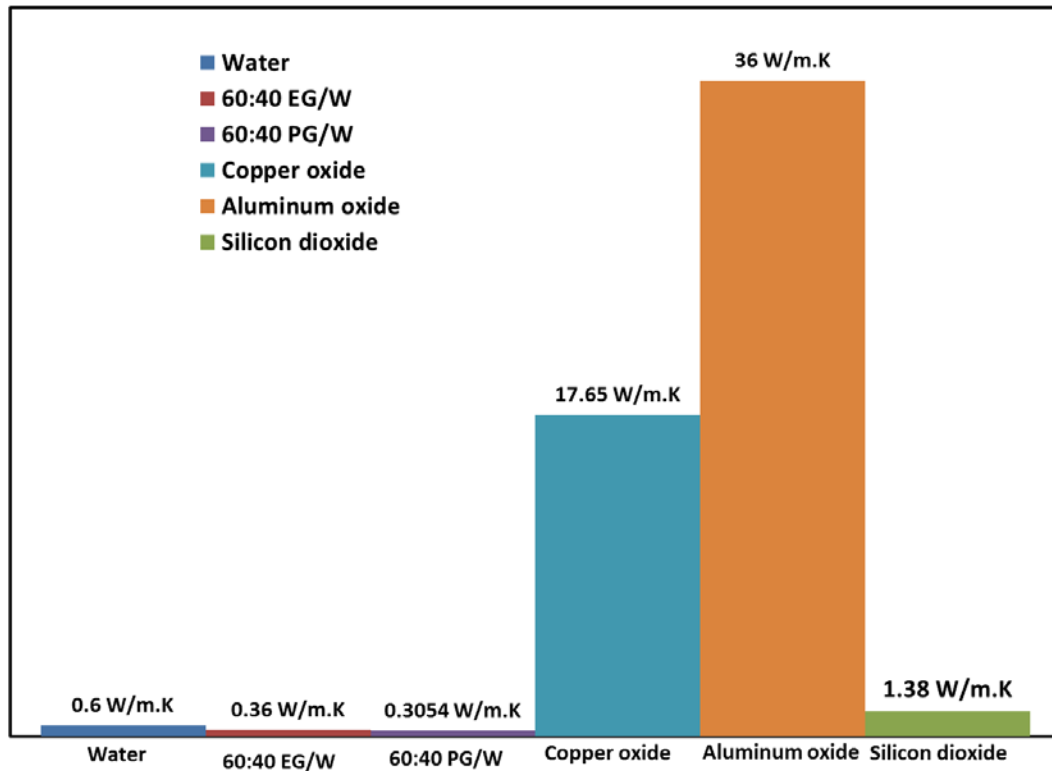


Figure 1.1. Comparison of thermal conductivities of metallic oxide nanoparticles and conventional heat transfer fluids at room temperature (300 K).

Nanoparticles used in nanofluids have been made of various materials such as; metals: aluminum (Al), copper (Cu), silver (Ag), gold (Au); metallic oxides: aluminum oxide (Al_2O_3), copper oxide (CuO), silicon dioxide (SiO_2), zinc oxide (ZnO), titanium oxide (TiO_2), iron oxide (Fe_3O_4), antimony-tin oxide ($\text{Sb}_2\text{O}_5:\text{SnO}_2$). In addition to the above nanoparticles, the nitrides of aluminum (AlN) and boron (BN) are also gaining much attention due to their high enhancements of thermal conductivity when dispersed in base fluids [8, 9].

1.2 Nanoparticle Synthesis Methods

The production of nanoparticles can be broadly classified into two categories as described in [10], (1) physical processes and (2) chemical processes. Typical physical synthesis methods include inert-gas condensation (IGC), and mechanical grinding. Chemical methods include chemical vapor deposition (CVD), chemical precipitation, micro emulsions, thermal spray and spray pyrolysis.

1.3 Dispersion of Nanoparticles in Liquids

Stable and uniform suspension of nanoparticles in conventional heat transfer fluids is critical in producing high quality nanofluids. Many two-step and one-step physical and chemical processes have been used in preparing nanofluids [11].

1.3.1 Two-step process

In a typical two-step process, nanoparticles are first produced using one of the above mentioned physical or chemical methods, such as inert gas condensation and chemical vapor deposition. Then these produced nanoparticles are dispersed into base fluids. This process is mostly used in producing nanofluids containing oxide nanoparticles and carbon nanotubes [10]. The major problem with the two-step processes is the agglomeration of nanoparticles due to strong attractive van der Waals forces between nanoparticles. The thermal conductivity of nanofluids produced from this process is low due to the poor dispersion quality. Therefore, in order to achieve higher thermal conductivity of nanofluids, a single step process is used to produce and suspend nearly monodispersed or nonagglomerated nanofluids. Figure 1.2 shows the transmission electron microscopy (TEM) image of a CuO nanofluid of an average particle size (APS) of 30 nm produced from the two-step process.

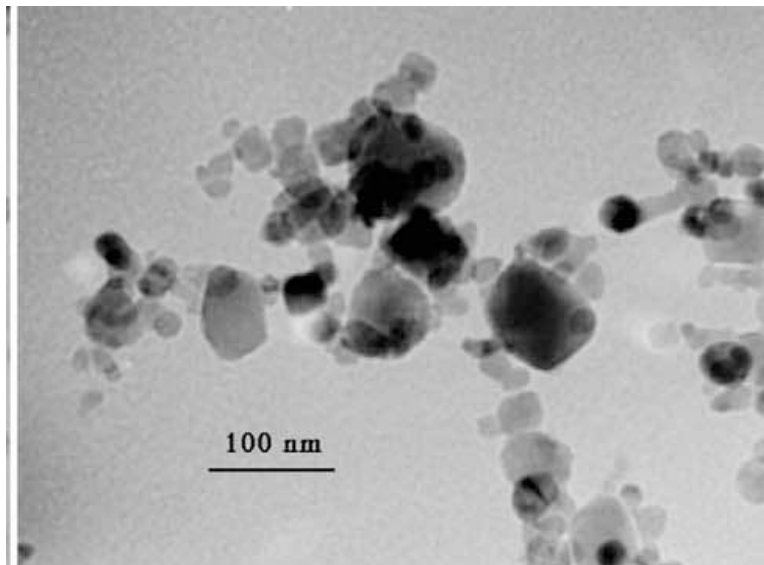


Figure 1.2. TEM image of a CuO nanofluid of average particle size 30 nm produced from inert gas condensation process. (Source: Eastman et al. [12])

1.3.2 Single-step process

The second successful and a promising technique for producing nanofluids is through direct evaporation. This process involves condensing nanophase powders from the vapor phase directly into a flowing low-vapor-pressure fluid [10]. The direct evaporation–condensation process yielded a uniform distribution of nanoparticles in a base fluid. The schematic of this direct evaporation technique is shown in Figure 1.3. Eastman et al. [12] used this single step process to produce nonagglomerating copper nanoparticles suspended in ethylene glycol base fluid. Figure 1.4 displays the TEM image of a copper nanofluid of an average particle size of 10 nm produced from the direct evaporation method.

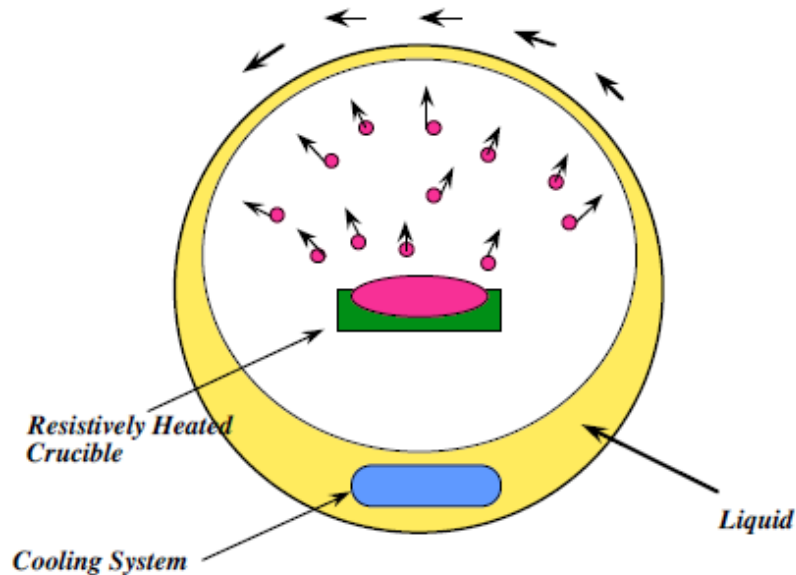


Figure 1.3. Schematic diagram of nanofluids produced from the direct evaporation of materials into base fluids. (Source: Eastman et al. [12])

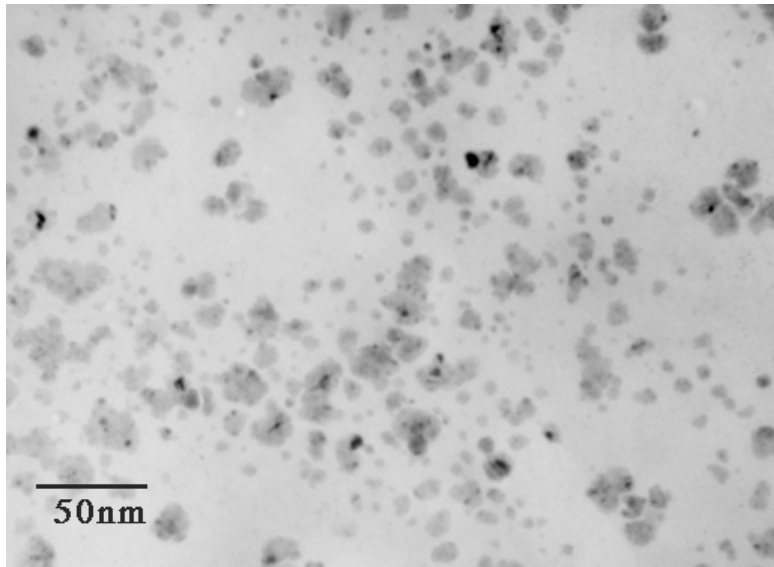


Figure 1.4. TEM image of a copper nanofluid of an average particle size of 10 nm produced from the direct evaporation process. (Source: Eastman et al. [12])

1.4 Stabilization and Characterization of Nanofluids

One of the concerns related to the use of nanofluids is to achieve a stable dispersion. The preparation of nanofluids containing mono-sized nanoparticles remains a technical challenge since the nanoparticles always form agglomerates in a host fluid due to strong van der Waals interactions between the particles. This undesirable agglomeration changes the size of the dispersed particles from nano to micro, which causes the particles to settle to the bottom due to their weight. Over the years, scientists have made many attempts to produce stable nanofluids. Physical or chemical treatments such as the addition of surfactants, electrostatic repulsion, and surface modification of suspended particles were used in dispersing the particles [10]. However, of the above mentioned treatments, the use of surfactants is widely used across the nanofluid community.

In the present study, nanofluids were procured from Alfa Aesar [13] and Nanostructured & Amorphous Materials, Inc. [14] as concentrated aqueous suspensions (up to 15-50% by mass) with various average particle sizes. These nanofluids were diluted to desired volumetric concentrations of 1 to 6% by adding the calculated amount of base fluid using a precise electronic mass balance. The nanofluids were subjected to ultrasonication to break down any agglomerated nanoparticles into their original particle sizes as specified by the manufacturer. In

order to ascertain the ultrasonication time, these nanofluids were best studied by transmission electron microscopy (TEM), which gives information on the shape and size of the particles. Figure 1.5 illustrates sample TEM images of the Al_2O_3 and SiO_2 nanoparticles. As observed, the average particle size of the nanoparticles is about 20 nm as specified by the manufacturer.

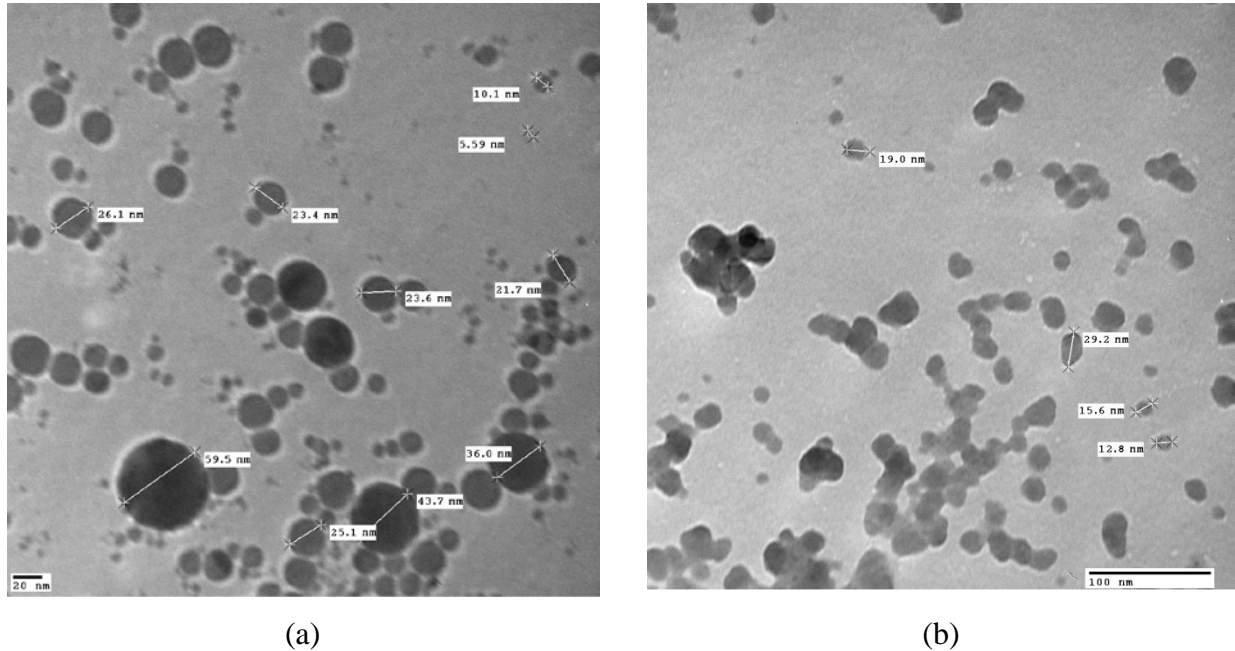


Figure 1.5. TEM images of (a) Al_2O_3 nanoparticles of APS 20 nm and (b) SiO_2 nanoparticles of APS 20 nm taken at the University of Alaska Fairbanks (UAF) laboratory.

1.5 Carbon Nanotubes

Since the discovery of carbon nanotubes by Iijima [15], they have gained much attention due to their exceptional thermal, electrical and mechanical properties. Measurements show that at room temperature, the thermal conductivity values are over 3000 W/m. K for individual multi-walled carbon nanotubes [16]. Carbon nanotubes can be categorized according to their structures. They are single-walled carbon nanotubes (SWCNT) and multi-walled carbon nanotubes (MWCNT). These two types of carbon nanotubes differ in the arrangement of their graphene cylinders. SWCNT have only a single layer of graphene cylinders while MWCNT have many layers. Carbon nanotubes typically have diameters ranging from of 1-50 nm and lengths several microns. Figure 1.6 shows the typical TEM image of single-wall carbon nanotubes.

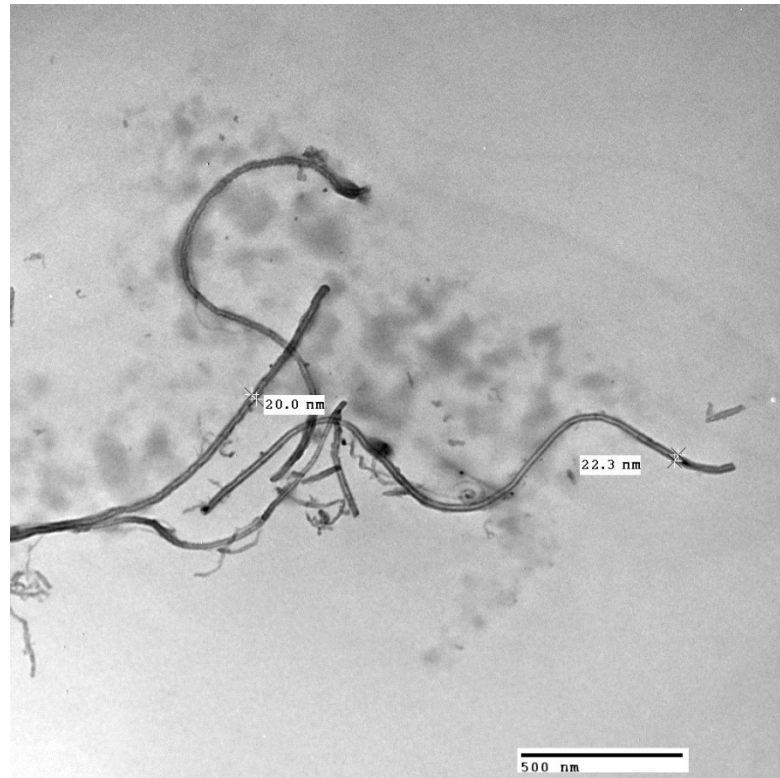


Figure 1.6. TEM image of single-walled carbon nanotubes taken at the UAF laboratory.

Similar to the dispersion of nanoparticles in conventional heat transfer fluids, carbon nanotubes are also suspended in base fluids like water, oil, or ethylene/propylene glycols. The experiments by various researchers [17-22] show substantial enhancements in the thermal conductivity and the convective heat transfer coefficient of CNT-based nanofluids. For example, the experiments of Assael et al. [17] show a thermal conductivity enhancement of 38% over the base fluid for 0.6% carbon nanotubes suspended in water.

1.6 Nanofluids Thermophysical Properties

1.6.1 Density

Vajjha et al. [23] measured the density of three nanoparticles: Al_2O_3 (APS 44 nm), $\text{Sb}_2\text{O}_5:\text{SnO}_2$ (APS 22-44 nm) and ZnO (APS 70 nm) dispersed in a base fluid of 60:40 EG/W and compared them with the theoretical equation for density, Eq. (1.1), presented by Pak and Cho [24]. They observed a good agreement between the theoretical equation and their experimental values. Figure 1.7 shows the density variations with the temperature of the Al_2O_3 nanofluid with an APS of 44 nm of several particle volumetric concentrations.

$$\rho_{nf} = \phi\rho_p + (1 - \phi)\rho_{bf} \quad (1.1)$$

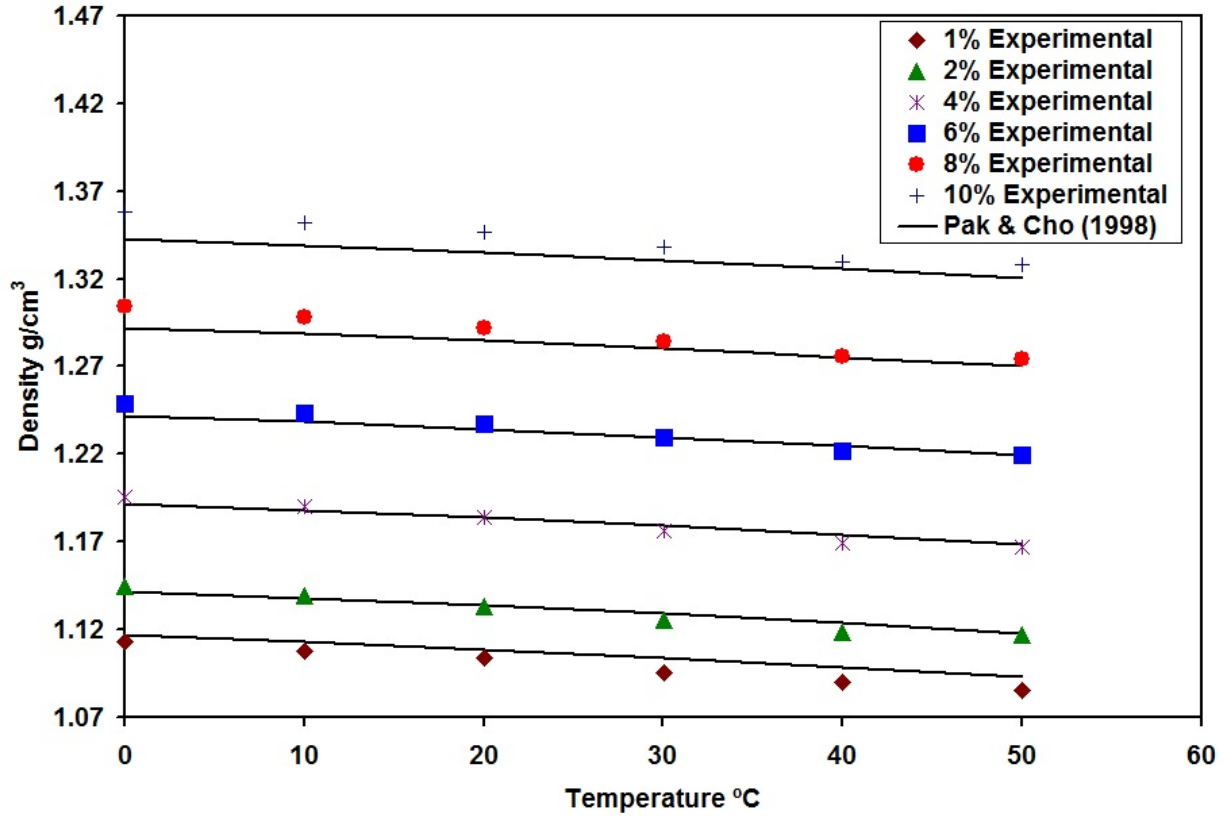


Figure 1.7. Density variations with temperature of Al_2O_3 nanofluid of several particle volumetric concentrations. (Source: Vajjha et al. [23])

1.6.2 Specific Heat

Vajjha and Das [25] measured the specific heat of three nanofluids containing Al_2O_3 (APS 44 nm), ZnO (70 nm) and SiO_2 (APS 20 nm) nanoparticles. The first two metallic oxide nanoparticles were dispersed in a base fluid of 60:40 EG/W and the non-metallic oxide nanoparticles in deionized (DI) water. The measured specific heat values were compared with the existing equation given by Xuan and Roetzel [26], Eq. (1.2), and a close agreement with the experimental data was not observed.

$$C_{pnf} = \frac{\phi\rho_p C_{pp} + (1 - \phi)\rho_{bf} C_{pbf}}{\rho_{nf}} \quad (1.2)$$

Therefore, from their study, they presented a new equation given by Eq. (1.3), where A, B and C are curved-fit constants given for each nanoparticle. Figure 1.8 displays the measured specific heat values for two particle volumetric concentrations of the Al₂O₃ nanofluid.

$$\frac{C_{p,nf}}{C_{p,bf}} = \frac{(A(T/T_0) + B(C_{p,p}/C_{p,bf}))}{(C + \phi)} \quad (1.3)$$

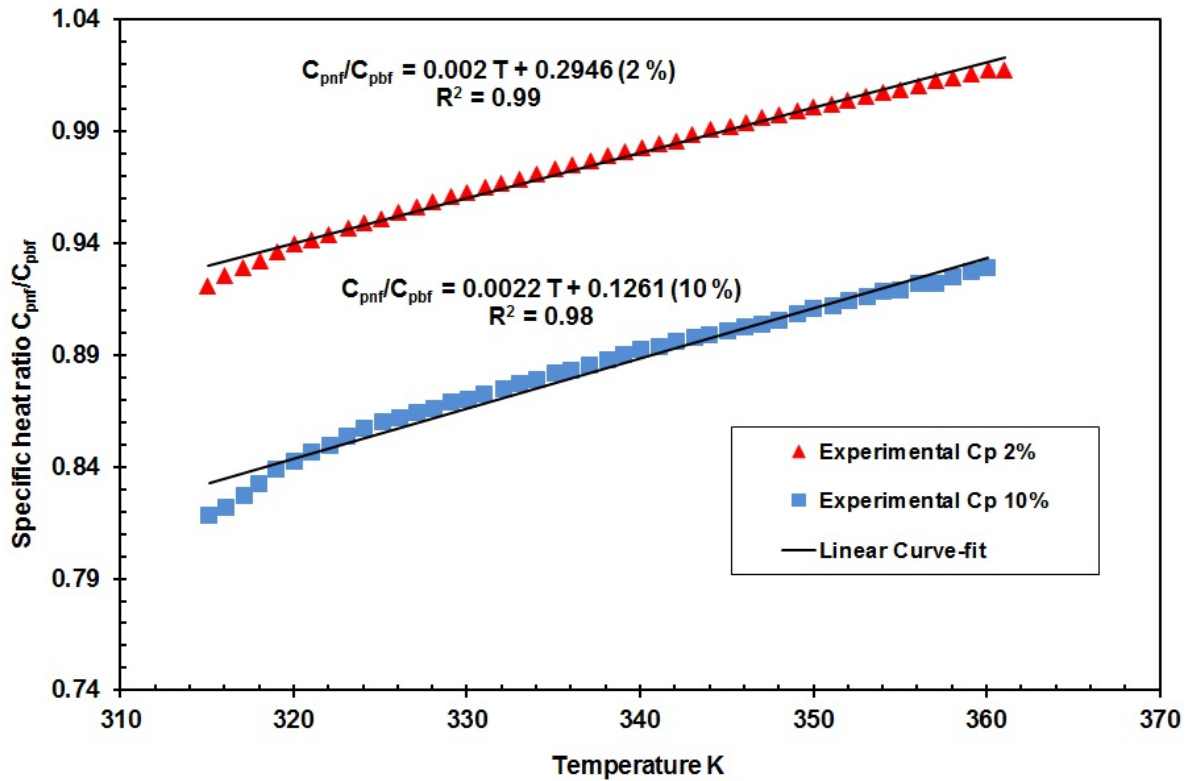


Figure 1.8. Variation in the specific heat ratio of the Al₂O₃ nanofluid with temperature for two particle volumetric concentrations. (Source: Vajjha and Das [25])

1.6.3 Thermal Conductivity

Vajjha and Das [27] and Sahoo et al. [28] conducted the thermal conductivity measurements of Al₂O₃ (APS 53 nm), CuO (APS 29 nm), ZnO (APS 29 & 77 nm) and SiO₂ (20 nm) nanoparticles dispersed in a base fluid of 60:40 EG/W. They developed a new correlation given by Eq. (1.4), following the work of Koo and Kleinstreuer [29]. The first part of the Eq.

(1.4a) is a static part proposed long ago by Maxwell; the second part of the equation is due to the Brownian motion of nanoparticles.

$$k_{nf} = \frac{k_p + 2k_{bf} - 2(k_{bf} - k_p)\phi}{k_p + 2k_{bf} + (k_{bf} - k_p)\phi} k_{bf} + 5 \times 10^4 \beta \phi \rho_{bf} C_{pbf} \sqrt{\frac{\kappa T}{\rho_p d_p}} f(T, \phi) \quad (1.4a)$$

$$f(T, \phi) = (2.8217 \times 10^{-2} \phi + 3.917 \times 10^{-3}) \left(\frac{T}{T_0}\right) + (-3.0669 \times 10^{-2} \phi - 3.91123 \times 10^{-3}) \quad (1.4b)$$

The parameter β is a curve-fit function of particle volumetric concentration ϕ for each nanoparticle. Figure 1.9 illustrates the thermal conductivity ratio variation with temperature at different particle volumetric concentrations of the CuO nanofluid of an average particle size of 29 nm.

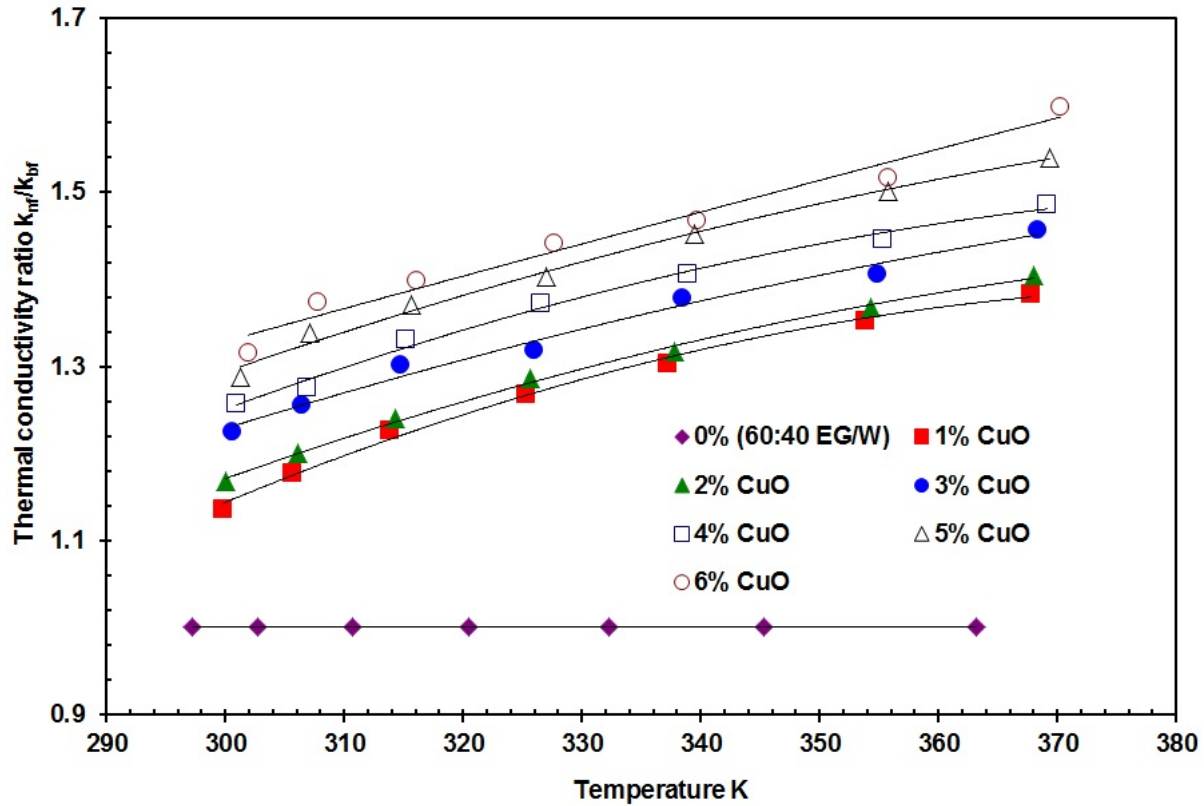


Figure 1.9. Thermal conductivity ratio variation with temperature at different particle volumetric concentrations of the CuO nanofluid. (Source: Vajjha and Das [27])

1.6.4 Viscosity

Kulkarni et al. [30] conducted experiments on the viscosity measurements of the CuO nanoparticles (APS 29 nm) dispersed in a base fluid of water. From their study they proposed a correlation for the viscosity of CuO nanofluid, given by Eq. (1.5), where the curve-fit parameters A_1 and B_1 are expressed as functions of the nanoparticle volume concentration.

$$\ln(\mu_{nf}) = A_1 \left(\frac{1}{T} \right) - B_1 \quad (1.5)$$

Kulkarni et al. [31] also measured the viscosity of the CuO nanoparticles (APS 29 nm) dispersed in a base fluid of 60:40 PG/W and developed a correlation, given by Eq. (1.6). In Eq. (1.6), the curve-fit parameters A_2 and B_2 are expressed as functions of temperature.

$$\mu_{nf} = A_2 (e^{B_2 \phi}) \quad (1.6)$$

Namburu et al. [32-34] conducted measurements of the viscosity of SiO₂ (APS 20, 50 & 100 nm), CuO (APS 29 nm) and Al₂O₃ (APS 53 nm) nanoparticles dispersed in 60:40 EG/W. They presented the following correlation for the viscosity of measured nanofluids. In Eq. (1.7), the curve-fit coefficients A_3 and B_3 are polynomial functions of particle volumetric concentration and are different for each nanofluid.

$$\log(\mu_{nf}) = A_3 e^{-B_3 T} \quad (1.7)$$

Sahoo et al. [35] extended the work of Namburu et al. [34] to higher temperatures and proposed a new correlation for the viscosity of Al₂O₃ nanofluid. In Eq. (1.8), A_4 , B_4 and C_4 were numerical constants and were not functions of particle volumetric concentration or temperature. However, these constants were different for each temperature regime. Figure 1.10 shows the measured viscosity values for the Al₂O₃ nanofluid of APS 53 nm.

$$\mu_{nf} = A_4 e^{\left(\frac{B_4}{T} + C_4 \phi \right)} \quad (1.8)$$

Having different types of equations for each nanofluid was cumbersome. Therefore, Vajjha and Das [36] developed a general correlation from the viscosity data of Namburu et al. [32-34] and Sahoo et al. [35], expressed in a non-dimensional form. In the generalized equation given by Eq. (1.9), A_5 and B_5 are constants.

$$\mu_{nf} = \mu_{bf}(A_5 e^{B_5 \phi}) \quad (1.9)$$

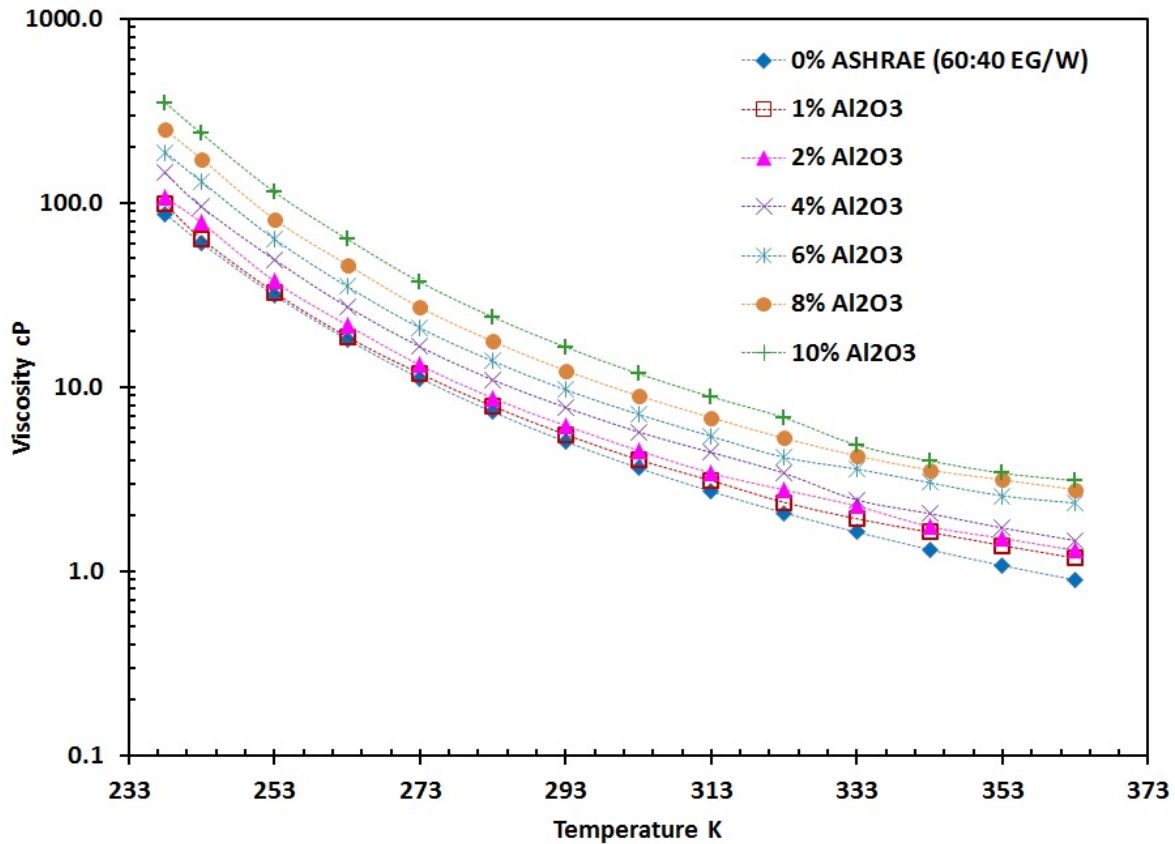


Figure 1.10. Measured viscosity values for different particle volumetric concentrations of the Al_2O_3 nanofluid of APS 53 nm.

1.7 Applied Research in Nanofluids

Nanofluids find most of their applications in the thermal management of heat transfer equipment used in industrial, commercial, residential and transportation sectors.

1.7.1 Electronics Cooling Applications

Due to the recent advancements in microprocessor chip technology, electronic chips generate an enormous amount of heat which must be dissipated in order to increase their performance and reliability. Chien et al. [37] experimentally showed the improvement in thermal performance of heat pipes by dispersing 17 nm of gold nanoparticles in water. Tsai et al. [38] conducted experiments for a heat pipe designed as a heat spreader for a CPU using gold nanoparticles of various particle sizes (5 to 75 nm) dispersed in DI water. Their results show a significant reduction in the thermal resistance of heat pipes with nanofluids over those with DI water. Chien and Huang [39] analytically studied the performance of copper nanoparticles dispersed in water as the coolant in silicon microchannel heat sink (MCHS). They observed an improved MCHS performance with nanofluids as a coolant when compared with water. Many similar experimental and numerical studies [40-42] show a significant improvement in the thermal performance of tested heat sink cooling systems with the use of nanofluids.

1.7.2 Automotive Cooling Applications

The use of nanofluids as coolants in automotive applications was first studied by researchers at Argonne national laboratory [43]. They observed a potential reduction in the frontal area of the radiator by up to 10% with the use of copper and aluminum nanoparticles. Vasu et al. [44] theoretically studied the application of the Al_2O_3 /water nanofluid as a coolant in a flat tube plain fin compact heat exchanger and observed a substantial increase in the cooling capacity compared to the base fluid. Vajjha et al. [45] numerically studied the fluid flow and heat transfer performance of Al_2O_3 and CuO nanoparticles dispersed in a base fluid of 60:40 EG/W circulating through the flat tubes of a radiator. They observed that for a 10% Al_2O_3 and 6% CuO nanofluids, the enhancement in the average heat transfer coefficient over the base fluid is about 94% and 89% respectively, at a Reynolds number of 2000. Chavan and Pise [46] experimentally studied the heat transfer performance of Al_2O_3 nanoparticles dispersed in a base fluid of water. For a 1% particle volumetric concentration of nanofluid, they observed a heat transfer enhancement of 40-45% over the base fluid. Similar studies conducted by other researchers [47-49] also showed an enhanced heat transfer performance with the use of nanofluids in automotive cooling systems.

1.7.3 Building Heating Systems

The use of nanofluids in conventional heat exchangers used in building heating systems could result in reduction in volumetric flow rate and savings in pumping power. Kulkarni et al. [50] analytically studied the performance of a liquid-air heat exchanger with the addition of Al_2O_3 , CuO and SiO_2 nanoparticles dispersed in a base fluid of 60:40 EG/W. The results showed that at a constant heat transfer coefficient, a 6% volume concentration of Al_2O_3 , CuO and SiO_2 nanofluids showed reductions in the volumetric flow rate of 37.22%, 28.95% and 22.18%, respectively, over the base fluid. For the same particle volumetric concentration and at a constant Reynolds number, they showed a reduction in the surface area of the heat exchanger by 17.3%, 20.37% and 8.5% for the Al_2O_3 , CuO and SiO_2 nanofluids, respectively. Strandberg and Das [51] theoretically analyzed the application of CuO nanofluids in hydronic building heating systems. At a mean fluid temperature of 323 K, the Nusselt number enhancement for the 4% CuO nanofluid is 87% relative to the base fluid for a Reynolds number of 14000. Their results showed that at a mean velocity of 1.52 m/s, the frictional pressure loss of a 4% CuO nanofluid is 44% higher than the base fluid at 323 K. Although the increase in the pumping power is significantly higher for the nanofluid, the enhancement in the heat transfer coefficient is proportionally greater under given flow conditions.

1.7.4 Other Applications

Other potential applications of nanofluids could be in biomedical, solar water heating, refrigeration systems, diesel electric generators, transformer cooling, nuclear cooling systems and so on. Although nanofluids were originally developed primarily for applications related to thermal management, they are currently being used in medical applications, including cancer therapy [10]. Iron nanoparticles can be used as delivery vehicles for drugs leaving the healthy tissues unharmed by guiding the nanoparticles up the bloodstream with magnets to a tumor cell [52]. Tyagi et al. [53] numerically compared the performance of aluminum/water nanofluids in a direct absorption solar receiver (DAR) with that of a typical flat-plate solar collector. They observed that the addition of nanoparticles to the base fluid, water, increased the absorption of incident radiation by more than 9 times, and the efficiency of a DAR using nanofluids as the absorbing medium was also found to be up to 10% higher than that of the flat-plate collector. Loaiza et al. [54] numerically illustrated the application of copper, Al_2O_3 , CuO and TiO_2

nanoparticles dispersed in water as secondary coolants in vapor compression refrigeration systems. Their simulation results show that for a given refrigeration capacity, the evaporator area and refrigerant side-pressure drop were reduced with the increase in the nanoparticle volume fraction and decrease in nanoparticle diameter. Kulkarni et al. [55] experimentally studied the application of aluminum oxide nanoparticles suspended in 50:50 EG/W base fluid as a coolant in a diesel electric generator (DEG). Their investigation revealed a reduction of cogeneration efficiency with the use of nanofluids. However, the efficiency of a waste-heat recovery heat exchanger increased for nanofluid. Xuan and Li and Yu et al. have illustrated that the heat transfer properties of transformer oils can be enhanced by the addition of nanoparticles. The improved cooling performance of these oils used in transformers could find an application in the power generation industry for reducing transformer size and weight.

A recent review of the research related to the nanofluids has been presented by Minkowycz et al. [56] addressing different aspects through a systematic exposition in ten chapters.

1.8 Agglomeration of Nanoparticles and Effects of pH

One of the challenges with nanofluids is to achieve a stable suspension. The long term stability of any particle in a colloidal solution can be predicted from the measurements of the zeta potential. The magnitude of zeta potential gives an indication of the stability of the dispersed particles. A low absolute value of zeta potential indicates a low amount of surface charge on the particle, which results in a very low repulsive force between the suspended particles to prevent their agglomeration. On the other hand, if the suspended particles have a large magnitude of zeta potential, then they will tend to repel each other preventing agglomeration and thus resulting in stable suspensions. The threshold of stability of a suspended particle in a colloidal solution in terms of the zeta potential is ± 30 mV [10]. Along with the use of surfactants, the value of zeta potential is affected primarily by pH. Konakanchi et al. [57] studied the effects of particle volumetric concentration, temperature and particle size on the pH of nanofluids and developed a new correlation. The studies of Xie et al. [58] and Lee et al. [59] indicate the influence of pH on thermal conductivity. Wamkam et al. [60] studied the influence of pH on thermal and fluid dynamic performance of nanofluids.

1.9 Erosion and Corrosion Effects of Nanofluids

In comparison with the suspension of larger sized microparticles, the very small size of nanoparticles and their low particle volumetric concentrations in the suspensions greatly reduce the erosion effects. On the corrosion effects, experimental studies are required to understand the corrosion behavior of nanoparticles on metal surfaces. At present, very limited research exists in the literature on corrosion effects of nanofluids. The work of Ismail et al. [61] showed that with the use of CNT based nanofluids the corrosion rates of copper, stainless steel and aluminum alloy did not change indicating better performance of fluids with CNT suspensions. More comprehensive and long term studies are required to understand the corrosion effects of various nanofluids flowing over metallic surfaces.

1.10 Outline of the Present Research

The goals of this dissertation were to:

1. Experimentally investigate the fluid dynamic and heat transfer performance of various nanofluids.
2. Determine the influence of temperature and the concentration of various nanofluids on thermophysical properties, heat transfer coefficient and pumping power.
3. Measure the viscosity of various nanofluids with varying temperatures, particle volumetric concentrations and particle diameters. Develop new viscosity correlations as a function of temperature, particle volume concentration, particle diameter, the properties of nanoparticles, and those of the base fluid.
4. Numerically model a three-dimensional turbulent flow and heat transfer of two different nanofluids in the flat tubes of an automotive radiator.

1.11 Summary of Subsequent Chapters

This dissertation has been written in manuscript format. Chapters 1 and 6 describe the general introduction and overall conclusions of the dissertation. Chapters 2 and 3 are already published in journals and Chapters 4 and 5 are submitted to journals for review towards publications.

Chapter 2 describes the experimental investigation of nanofluids comprised of Al_2O_3 , CuO and SiO_2 dispersed in 60:40 EG/W for their heat transfer and fluid dynamic performance. The experimental measurements were carried out in the fully-developed turbulent regime for the

above three nanofluids at various particle volumetric concentrations. The Reynolds number was varied between 3000 to 15000. To ensure the flow to be in turbulent regime, the lower range of Reynolds number was maintained above 3000 which is greater than the critical Reynolds number of 2300 [62], after which the flow is considered to be turbulent. It was found that the heat transfer coefficient of nanofluids showed an increase with the particle volumetric concentration. The pressure loss of nanofluids also increased with an increase in particle volume concentration. Typical values of percentage increase of the heat transfer coefficient and pressure loss are presented. New Nusselt number and friction factor correlations have been developed from this study.

Chapter 3 illustrates the influence of temperature and particle volumetric concentrations of three nanofluids (Al_2O_3 , CuO and SiO_2 dispersed in 60:40 EG/W base fluid) on thermophysical properties, heat transfer coefficient and pumping power. A comprehensive analysis has been performed to evaluate the effects on the performance of nanofluids due to variations of density, specific heat, thermal conductivity and viscosity, which are functions of nanoparticle volume concentration and temperature.

Chapter 4 describes the viscosity measurements of Al_2O_3 , CuO, SiO_2 , TiO_2 and ZnO nanoparticles dispersed in a base fluid of 60:40 PG/W. Measurements were conducted for particle volume concentrations of up to 6% and over a temperature range of 243 K to 363 K. The experiments reveal that all the tested nanofluids exhibited a Bingham plastic behavior at the lower temperatures of 243 K to 273 K and a Newtonian behavior in the temperature range of 273 K to 363 K. Measurements were also conducted for single-walled, bamboo-like structured and hollow-structured multi-walled carbon nanotubes dispersed in a base fluid of 20% propylene glycol and 80% water by mass. Measurements of these carbon nanotubes nanofluids were conducted for a particle volume concentration of 0.229% and over a temperature range of 273 K to 363 K, which exhibited a non-Newtonian behavior. The effect of ultrasonication time on the viscosity of carbon nanotubes nanofluids was investigated.

Chapter 5 presents the numerical study for the flow of Al_2O_3 and CuO nanofluids in the flat tubes of an automotive radiator under a turbulent regime. From the fluid dynamic and heat transfer computations, the magnitudes of increase in pressure loss and the convective heat transfer coefficient with the increasing particle volumetric concentrations of nanofluids are presented. From the present study, several new correlations to determine the Nusselt number and

friction factor for nanofluids flowing in the flat tubes of a radiator have been proposed for the entrance as well as the fully developed regions.

Chapter 6 summarizes the overall conclusions drawn from the present studies.

1.12 Nomenclature

C_p	specific heat, J/kg.K
d_p	nanoparticle diameter, m
k	thermal conductivity, W/m.K
T	temperature, K
T_0	reference temperature, 273 K

Greek symbols

κ	Boltzmann constant, 1.381×10^{-23} J/K
μ	viscosity, mPa.s
ρ	density, kg/m ³
ϕ	particle volumetric concentration, %

Subscripts

bf	base fluid
nf	nanofluid
p	nanoparticle

1.13 References

- [1] Bejan, A., 1993, Heat Transfer, John Wiley & Sons, Inc., New York, NY.
- [2] Bergman, T. L., Lavine, A. S., Incropera, F. P., and DeWitt, D. P., 2011, Introduction to Heat Transfer, Wiley, New York.
- [3] Bolz, R. E., and Tuve, G. L., 1973, CRC Handbook of Tables for Applied Engineering Science, Taylor & Francis, Boca Raton, FL.
- [4] American Society of Heating, Refrigerating Air-Conditioning Engineers, 2009, ASHRAE Handbook of Fundamentals, ASHRAE, Atlanta, GA.
- [5] Maxwell, J. C., 1873, A Treatise On Electricity and Magnetism, Clarendon Press, Oxford.

- [6] Masuda, H., Ebata, A., Teramae, K., and Hishinuma, N., 1993, "Alteration of thermal conductivity and viscosity of liquid by dispersing ultra-fine particles (dispersion of Al_2O_3 , SiO_2 and TiO_2 ultra-fine particles)," *Netsu Bussei*, 7(4), pp. 227-233.
- [7] Choi, S. U. S., 1995, "Enhancing Thermal Conductivity of Fluids with Nanoparticles," *Developments and Applications of Non-Newtonian Flows*, D. A. Singer, and H. P. Wang, eds., ASME FED-231/MD-66, New York, pp. 99-105.
- [8] Wozniak, M., Danelska, A., Rutkowski, P., and Kata, D., 2013, "Thermal Conductivity of Highly Loaded Aluminium Nitride–Poly(Propylene Glycol) Dispersions," *International Journal of Heat and Mass Transfer*, 65(1), pp. 592-598.
- [9] Li, Y., Zhou, J. e., Luo, Z., Tung, S., Schneider, E., Wu, J., and Li, X., 2011, "Investigation on Two Abnormal Phenomena about Thermal Conductivity Enhancement of BN/EG Nanofluids," *Nanoscale Research Letters*, 6(1), pp. 443-449.
- [10] Das, S. K., Choi, S. U., Yu, W., and Pradeep, T., 2007, *Nanofluids: Science and Technology*, John Wiley & Sons, Hoboken, NJ.
- [11] Choi, S. U. S., 2009, "Nanofluids: From Vision to Reality Through Research," *Journal of Heat Transfer*, 131(3), p. 9.
- [12] Eastman, J. A., Choi, S. U. S., Li, S., and Thomson, L. J., "Enhanced Thermal Conductivity Through the Development of Nanofluids," *Proc. Nanophase and Nanocomposite Materials II*, S. Komarneni, J. C. Parker, and H. J. Wollenberger, eds., Material Research Society, pp. 3-11.
- [13] AlfaAesar, 2013, www.alfa.com.
- [14] Nanostructured & Amorphous Materials, I., 2013, <http://www.nanoamor.com/>.
- [15] Iijima, S., 1991, "Helical Microtubules of Graphite Carbon," *Nature*, 354, pp. 56-58.
- [16] Gogotsi, Y., and Presser, V., 2006, *Carbon Nanomaterials*, Taylor & Francis, Boca Raton, FL.
- [17] Assael, M. J., Chen, C. F., Metaxa, I., and Wakeham, W. A., 2004, "Thermal Conductivity of Suspensions of Carbon Nanotubes in Water," *International Journal of Thermophysics*, 25(4), pp. 971-985.
- [18] Assael, M. J., Metaxa, I. N., Arvanitidis, J., Christofilos, D., and Lioutas, C., 2005, "Thermal Conductivity Enhancement in Aqueous Suspensions of Carbon Multi-Walled and Double-Walled Nanotubes in the Presence of Two Different Dispersants," *International Journal of Thermophysics*, 26(3), pp. 647-664.

- [19] Choi, S. U. S., Zhang, Z. G., Yu, W., Lockwood, F. E., and Grulke, E. A., 2001, "Anomalous Thermal Conductivity Enhancement in Nanotube Suspensions," *Applied Physics Letters*, 79(14), pp. 2252-2254.
- [20] Ding, Y., Alias, H., Wen, D., and Williams, R. A., 2006, "Heat Transfer of Aqueous Suspensions of Carbon Nanotubes (CNT Nanofluids)," *International Journal of Heat and Mass Transfer*, 49(1-2), pp. 240-250.
- [21] Garg, P., Alvarado, J. L., Marsh, C., Carlson, T. A., Kessler, D. A., and Annamalai, K., 2009, "An Experimental Study on the Effect of Ultrasonication on Viscosity and Heat Transfer Performance of Multi-Wall Carbon Nanotube-Based Aqueous Nanofluids," *International Journal of Heat and Mass Transfer*, 52(21-22), pp. 5090-5101.
- [22] Wen, D., and Ding, Y., 2004, "Effective Thermal Conductivity of Aqueous Suspensions of Carbon Nanotubes (Carbon Nanotube Nanofluids)," *Journal of Thermophysics and Heat Transfer*, 18(4), pp. 481-485.
- [23] Vajjha, R. S., Das, D. K., and Mahagaonkar, B. M., 2009, "Density Measurement of Different Nanofluids and Their Comparison With Theory," *Petroleum Science & Technology*, 27(6), pp. 612-624.
- [24] Pak, B. C., and Cho, Y. I., 1998, "Hydrodynamic and Heat Transfer Study of Dispersed Fluids With Submicron Metallic Oxide Particles," *Experimental Heat Transfer*, 11(2), pp. 151-170.
- [25] Vajjha, R. S., and Das, D. K., 2009, "Specific Heat Measurement of Three Nanofluids and Development of New Correlations," *Journal of Heat Transfer*, 131(7), pp. 1-10.
- [26] Xuan, Y., and Roetzel, W., 2000, "Conceptions for Heat Transfer Correlation of Nanofluids," *International Journal of Heat and Mass Transfer*, 43(19), pp. 3701-3707.
- [27] Vajjha, R. S., and Das, D. K., 2009, "Experimental Determination of Thermal Conductivity of Three Nanofluids and Development of New Correlations," *International Journal of Heat and Mass Transfer*, 52(21-22), pp. 4675-4682.
- [28] Sahoo, B. C., Das, D. K., Vajjha, R. S., and Satti, J. R., 2013, "Measurement of the Thermal Conductivity of Silicon Dioxide Nanofluid and Development of Correlations," *Journal of Nanotechnology in Engineering and Medicine*, 3(4), pp. 1-10.
- [29] Koo, J., and Kleinstreuer, C., 2005, "A New Thermal Conductivity Model for Nanofluids," *Journal of Nanoparticle Research*, 7(2-3), pp. 324-324.

- [30] Kulkarni, D. P., Das, D. K., and Chukwu, G. A., 2006, "Temperature Dependent Rheological Property of Copper Oxide Nanoparticles Suspension (Nanofluid)," *Journal of Nanoscience and Nanotechnology*, 6(4), pp. 1150-1154.
- [31] Kulkarni, D. P., Das, D. K., and Patil, S. L., 2007, "Effect of Temperature on Rheological Properties of Copper Oxide Nanoparticles Dispersed in Propylene Glycol and Water Mixture," *Journal of Nanoscience and Nanotechnology*, 7(7), pp. 2318-2322.
- [32] Namburu, P. K., Kulkarni, D. P., Dandekar, A., and Das, D. K., 2007, "Experimental Investigation of Viscosity and Specific Heat of Silicon Dioxide Nanofluids," *Micro Nano Letters*, 2(3), pp. 67-71.
- [33] Namburu, P. K., Kulkarni, D. P., Misra, D., and Das, D. K., 2007, "Viscosity of Copper Oxide Nanoparticles Dispersed in Ethylene Glycol and Water Mixture," *Experimental Thermal and Fluid Science*, 32(2), pp. 397-402.
- [34] Namburu, P. K., Das, D. K., Tanguturi, K. A., and Vajjha, R. S., 2009, "Numerical Study of Turbulent Flow and Heat Transfer Characteristics of Nanofluids Considering Variable Properties," *International Journal of Thermal Sciences*, 48(2), pp. 290-302.
- [35] Sahoo, B. C., Vajjha, R. S., Ganguli, R., Chukwu, G. A., and Das, D. K., 2009, "Determination of Rheological Behavior of Aluminum Oxide Nanofluid and Development of New Viscosity Correlations," *Petroleum Science & Technology*, 27(15), pp. 1757-1770.
- [36] Vajjha, R., and Das, D., 2010, *Measurements of Nanofluids Properties and Heat Transfer Computation : Correlations for Nanofluids Properties*, LAP Lambert Academic Publishing, Saarbrücken.
- [37] Hsin-Tang, C., Chien-In, T., Ping-Hei, C., and Po-Yeh, C., "Improvement on Thermal Performance of a Disk-Shaped Miniature Heat Pipe with Nanofluid," *Proc. Electronic Packaging Technology Proceedings, 2003. ICEPT 2003. Fifth International Conference on*, pp. 389-391.
- [38] Tsai, C. Y., Chien, H. T., Ding, P. P., Chan, B., Luh, T. Y., and Chen, P. H., 2004, "Effect of Structural Character of Gold Nanoparticles in Nanofluid on Heat Pipe Thermal Performance," *Materials Letters*, 58(9), pp. 1461-1465.
- [39] Chein, R., and Huang, G., 2005, "Analysis of Microchannel Heat Sink Performance using Nanofluids," *Applied Thermal Engineering*, 25(17-18), pp. 3104-3114.
- [40] Koo, J., and Kleinstreuer, C., 2005, "Laminar Nanofluid Flow in Microheat-Sinks," *International Journal of Heat and Mass Transfer*, 48(13), pp. 2652-2661.

- [41] Chein, R., and Chuang, J., 2007, "Experimental Microchannel Heat Sink Performance Studies using Nanofluids," *International Journal of Thermal Sciences*, 46(1), pp. 57-66.
- [42] Palm, S. J., Roy, G., and Nguyen, C. T., 2006, "Heat Transfer Enhancement with the use of Nanofluids in Radial Flow Cooling Systems Considering Temperature-Dependent Properties," *Applied Thermal Engineering*, 26(17–18), pp. 2209-2218.
- [43] Singh, D., Toutbort, J., Chen, G., Hull, J., Smith, R., Ajayi, O., and Yu, W., 2006, "Heavy Vehicle Systems Optimization Merit Review and Peer Evaluation," Argonne National Laboratory.
- [44] Vasu, V., Rama Krishna, K., and Kumar, A. C. S., 2008, "Thermal Design Analysis of Compact Heat Exchanger Using Nanofluids," *International Journal of Nanomanufacturing*, 2(3), pp. 271-288.
- [45] Vajjha, R. S., Das, D. K., and Namburu, P. K., 2010, "Numerical Study of Fluid Dynamic and Heat Transfer Performance of Al_2O_3 and CuO Nanofluids in the Flat Tubes of a Radiator," *International Journal of Heat and Fluid Flow*, 31(4), pp. 613-621.
- [46] Chavan, D., and Pise, A. T., 2013, "Performance Investigation of an Automotive Car Radiator Operated With Nanofluid as a Coolant," *Journal of Thermal Science and Engineering Applications*, 6(2), p. 5.
- [47] Peyghambarzadeh, S. M., Hashemabadi, S. H., Hoseini, S. M., and Seifi Jamnani, M., 2011, "Experimental Study of Heat Transfer Enhancement Using Water/Ethylene Glycol Based Nanofluids as a New Coolant for Car Radiators," *International Communications in Heat and Mass Transfer*, 38(9), pp. 1283-1290.
- [48] Hussein, A. M., Bakar, R. A., Kadrigama, K., and Sharma, K. V., 2014, "Heat Transfer Enhancement using Nanofluids in an Automotive Cooling System," *International Communications in Heat and Mass Transfer*, 53, pp. 195-202.
- [49] Ray, D. R., and Das, D. K., 2014, "Superior Performance of Nanofluids in an Automotive Radiator," *Journal of Thermal Science and Engineering Applications*, 6(4), p. 16.
- [50] Kulkarni, D. P., Das, D. K., and Vajjha, R. S., 2009, "Application of Nanofluids in Heating Buildings and Reducing Pollution," *Applied Energy*, 86(12), pp. 2566-2573.
- [51] Strandberg, R., and Das, D. K., 2010, "Influence of temperature and properties variation on nanofluids in building heating," *Energy Conversion and Management*, 51(7), pp. 1381-1390.

- [52] Nie, S., Xing, Y., Kim, G. J., and Simons, J. W., 2007, "Nanotechnology Applications in Cancer," *Annual Review of Biomedical Engineering*, 9(1), pp. 257-288.
- [53] Tyagi, H., Phelan, P., and Prasher, R., "Predicted Efficiency of a Nanofluid-Based Direct Absorption Solar Receiver," *Proc. ASME 2007 Energy Sustainability Conference*, ASME, Paper No. ES2007-36139, pp. 729-736.
- [54] Loaiza, J. C. V., Pruzaesky, F. C., and Parise, J. A. R., 2010, "A Numerical Study on the Application of Nanofluids in Refrigeration Systems," *Proc. International Refrigeration and Air Conditioning Conference*, Purdue e-Pubs, Paper 1145, pp. 1-8.
- [55] Kulkarni, D. P., Vajjha, R. S., Das, D. K., and Oliva, D., 2008, "Application of Aluminum Oxide Nanofluids in Diesel Electric Generator as Jacket Water Coolant," *Applied Thermal Engineering*, 28(14-15), pp. 1774-1781.
- [56] Minkowycz, W. J., Sparrow, E. M., and Abraham, J. P., 2013, *Nanoparticle Heat Transfer and Fluid Flow*, CRC Press/Taylor & Francis Group, Boca Raton, FL.
- [57] Konaknchi, H., Vajjha, R. S., Chukwu, G. A., Das, D. K., 2015, "Measurements of pH of Three Nanofluids and Development of New Correlations," *Heat Transfer Engineering*, 36 (1), pp. 81-90.
- [58] Xie, H. Q., Wang, J. C., Xi, T. G., Liu, Y., Ai, F., and Wu, Q. R., 2002, "Thermal Conductivity Enhancement of Suspensions Containing Nanosized Alumina Particles," *Journal of Applied Physics*, 91, pp. 4568-4572.
- [59] Lee, D., Kim, J. W., and Kim, B. G., 2006, "A New Parameter to Control Heat Transport in Nanofluids: Surface Charge State of the Particle in Suspension," *Journal of Physics and Chemistry B*, 110, pp. 4323-4328.
- [60] Wamkam, C. T., Opoku, M. K., Hong, H., and Smith, P., 2011, "Effects of pH on Heat Transfer Nanofluids Containing ZrO₂ and TiO₂ Nanoparticles," *Journal of Applied Physics*, 109(2), pp. 024305.
- [61] Ismail, A.F., Anuar, A., Rashmi, W., Yusaf, T., 2014, "Corrosion Effects of CNT-Nanofluids on Different Metals," *WIT Transactions on Engineering Sciences*, WIT Press Volume 87, pp. 139-146.
- [62] White, F.M., 2003, *Fluid Mechanics*, McGraw-Hill, New York, NY.

Chapter 2. Development of New Correlations for Convective Heat Transfer and Friction Factor in Turbulent Regime for Nanofluids *

2.1 Abstract

This paper presents new correlations for the convective heat transfer and the friction factor developed from experiments with nanoparticles comprised of aluminum oxide, copper oxide and silicon dioxide dispersed in 60% ethylene glycol and 40% water by mass. The experimental measurements were carried out in the fully-developed turbulent regime for the aforementioned three different nanofluids at various particle volumetric concentrations. First, the rheological and the thermophysical properties such as viscosity, density, specific heat and thermal conductivity were measured at different temperatures for varying particle volume concentrations. Next, these properties were used to develop the heat transfer coefficient correlation from experiments, as a function of these properties and the particle volumetric concentration. The pressure loss was also measured and a new correlation was developed to represent the friction factor for nanofluids.

2.2 Keywords

nanofluids, particle concentration, turbulent flow, convection correlation, pressure loss, friction factor

2.3 Nomenclature

C_p	specific heat, J/kg.K
d	inside diameter of tube, m
d_p	nanoparticle diameter, m
f	Darcy friction coefficient
h	heat transfer coefficient, $h = q'' / (T_w - T_b)$, W/m ² .K
k	thermal conductivity, W/m.K
L	length of the tube, m
\dot{m}	mass flow rate, kg/s

* Vajjha, R. S., Das, D. K., and Kulkarni, D. P., 2010, "Development of New Correlations for Convective Heat Transfer and Friction Factor in Turbulent Regime for Nanofluids," International Journal of Heat and Mass Transfer, 53(21-22), pp. 4607-4618.

Nu	Nusselt number, $Nu = (hd/K)$
Pe_d	particle Peclet number, $Pe = (Vd_p/\alpha_{nf})$
Pr	Prandtl number, $Pr = (\mu C_p/k)$
\dot{q}	rate of heat transfer, W
q''	heat flux, W/m^2
Re	Reynolds number, $Re = (\rho Vd/\mu)$
R^2	coefficient of determination
T	temperature, K
T_0	reference temperature, 273 K
V	velocity, m/sec
Greek symbols	
ΔP	differential pressure loss, Pa
ΔT	temperature difference, K
κ	Boltzmann constant, 1.381×10^{-23} J/K
μ	viscosity, mPa.s
ρ	density, kg/m^3
τ	shear stress, Pa
ϕ	particle volumetric concentration, %
Subscripts	
b	bulk
bf	base fluid
f	fluid
nf	nanofluid
p	nanoparticle
w	wall

2.4 Introduction

Nanostructured materials can have a major impact on the liquids used for the transport of heat in heat exchangers. When metallic or nonmetallic particles of higher thermal conductivity, whose dimensions are less than 100 nm, are dispersed in conventional heat transfer liquids, the

effective thermal conductivity of the resulting medium increases substantially. Masuda et al. [1] showed that the thermal conductivity and the viscosity of liquids are altered dramatically by dispersing ultra-fine particles of γ -aluminum oxide (Al_2O_3), silicon dioxide (SiO_2) and titanium dioxide (TiO_2). Subsequently, this finding was conclusively established from experiments of other researchers; notably, Choi [2], Wang et al. [3] and Eastman et al. [4]. For the same Nusselt number of fluid flow in a given flow passage, if the thermal conductivity increases then the convective heat transfer also increases in the same proportion. Nanofluids have valuable applications in the area of heating buildings through the hydronic coils, cooling automotive engines through the radiators and in heat exchangers in all types of industries. In all these applications the fluid flow is generally in the turbulent regime, because higher heat transfer is achieved through the turbulent flow.

Therefore, the fluid dynamic and heat transfer characteristics of nanofluids under the turbulent flow conditions must be known accurately to evaluate their performance. However, only a limited number of studies appear in the literature on the turbulent characteristics of nanofluids. Pak and Cho [5] performed the friction factor and convective heat transfer coefficient measurements on γ - Al_2O_3 and TiO_2 nanoparticles in water. They determined that the Darcy friction factor of the nanofluids of volume concentration ranging from 1 to 3% agreed well with the correlation for conventional single-phase fluid. They presented a new Nusselt number correlation for the turbulent heat transfer, which was similar to the well-known Dittus-Boelter correlation for the single-phase fluid with slight changes in the constant coefficient and the power of Prandtl number. Their friction factor and heat transfer measurements were limited to particle volumetric concentrations of 2.78% for the Al_2O_3 and 3.16% for the TiO_2 nanofluids. They also performed viscosity measurements up to a volume concentration of 10% and found that at that concentration level, the viscosity of γ - Al_2O_3 nanofluid was 200 times greater than that of the base fluid. For the TiO_2 nanofluid, at the same concentration the viscosity was 3 times greater than that of the base fluid. Xuan and Roetzel [6] presented a theoretical model for heat transfer as follows.

$$Nu = [1 + C^* Pef'(0)]\theta'(0) Re^m \quad (2.1)$$

Here f' and θ' are the derivatives of the dimensionless velocity and the dimensionless temperature respectively. They proposed that C^* was a constant to be determined from the experiment.

Following the suggestion of Xuan and Roetzel [6], Xuan and Li [7] carried out the experiments with copper nanoparticles dispersed in water to obtain a convective heat transfer equation for nanofluids under the turbulent flow condition.

$$Nu_{nf} = 0.0059(1 + 7.6286\phi^{0.6886} Pe_{d_p}^{0.001}) Re_{nf}^{0.9238} Pr_{nf}^{0.4} \quad (2.2)$$

Their experiment was limited to a 2% particle volumetric concentration. From their pressure loss experimental data, they found that the Cu-water nanofluid had nearly the same friction factor as water, which they attributed to the dilute concentration. Buongiorno [8] analyzed theoretically the boundary layer in nanofluid flow and proposed a Nusselt number correlation for turbulent flow, as a function of the Reynolds number, Prandtl number, friction factor and the laminar sublayer thickness. He presented an iterative procedure to calculate the Nusselt number until the nanoparticles volume fraction in the laminar sub-layer converges to a single value. Nguyen et al. [9] conducted experiments with Al_2O_3 -water nanofluid. They tested the nanofluid in the range of Reynolds number from 4000 to about 15000 and up to a particle volumetric concentration of 6.8%. They found that the heat transfer coefficient increased by 40 % over that of water for a 6.8% volumetric concentration of Al_2O_3 particle. They did not present a Nusselt number correlation and no pressure loss measurements were reported.

Williams et al. [10] conducted experiments with alumina and zirconia nanofluids in water. The alumina concentration tested was up to 3.6% and the zirconia up to 0.9%. They found that the viscous pressure losses were within $\pm 20\%$ of the theory of Blasius and McAdams which are for the single phase liquid. They did not present a Nusselt number correlation.

The objective of this study was to use more nanofluids and higher concentrations tested by prior researchers and develop the friction factor and Nusselt number correlations, so that they will be more general. The correlation of Xuan and Li [7] is based on the experiment on only one nanofluid. Pak and Cho [5] developed their correlation from two nanofluids. Furthermore, the particle volumetric concentrations tested thus far were low (less than 3.6%). Therefore, in the

present study three nanoparticles, Al_2O_3 , copper oxide (CuO) and SiO_2 (two metallic and one nonmetallic) were selected for the experiments because of their good thermal properties and easy availability. The base fluid was chosen to be 60% ethylene glycol and 40% water mixture by mass (60:40 EG/W), which is widely used as the heat transfer fluid in the cold regions of the world in building heating and in automobile radiators. First the thermophysical properties of these nanofluids were measured and correlations were developed. Then these properties correlations were used to develop the friction factor and heat transfer relations. The experiments revealed that the convective heat transfer and pressure loss of nanofluids are higher than the base fluid. The physical and mechanistic explanation for this enhancement may be due to multiple effects; higher thermal conductivity, Brownian motion, thermophoresis, transport mechanisms of nanoparticles and fluid properties variation in the near-wall region. All these effects should be examined in the future research.

2.5 Determination of Thermophysical Properties

Three types of nanofluids, Al_2O_3 , CuO and SiO_2 were tested in this study. The nanofluids were procured from Alfa Aesar [11] at a particle mass concentration of 50% in water. Then properly calculated mass of 60:40 EG/W mixture was added to the concentrated nanofluid and careful mass measurement of the resulting fluid in a precise electronic mass balance was conducted to arrive at the desired particle volumetric concentration of nanofluids of 1, 2, 4, 6, 8, and 10%. Before using any nanofluid sample for measurements, it was subjected to ultrasonication for several hours in a bath type sonicator to ensure proper dispersion of the nanoparticles. The characteristics of nanoparticles used in this study are summarized in Table 2.1 below.

2.5.1 Viscosity

Measurements of viscosity of copper oxide nanoparticles dispersed in 60:40 EG/W were conducted using the LV DV-II+ Brookfield viscometer [15] with a Julabo computer controlled temperature bath to set the nanofluid's temperature at different values. Namburu et al. [16] carried out the measurements and presented the following correlation for the viscosity of CuO nanofluid as a function of concentration and temperature.

$$\log \mu_{nf} = Ae^{(-BT)} \quad (2.3)$$

where A and B are second order polynomial functions of particle volumetric concentration ϕ . This correlation was based on volumetric concentration of $0 \leq \phi \leq 0.06$ and between a temperature range of $-35^\circ C < T < 50^\circ C$ for their application in cold regions.

Namburu et al. [17] further conducted similar measurements on SiO₂ nanofluids and developed a correlation similar to Eq. (2.3), but the curve-fit coefficients A and B were different. The coefficient A was a third order polynomial and B was a second order polynomial function of particle volumetric concentration ϕ . Sahoo et al. [18] measured the rheological properties of Al₂O₃ nanofluids with the same experimental setup that was used by Namburu et al. They developed two correlations for the viscosity; one in the low temperature regime and one in the high temperature regime.

$$\mu_{nf} = Ae^{\left(\frac{B}{T} + C\phi\right)} \quad (2.4)$$

where A, B and C were numerical constants and not functions of ϕ . However, these constants were different for each temperature regimes. Having different types of equations or different coefficients for each nanofluid were cumbersome. Therefore, Vajjha [19] carefully analyzed all the data of Namburu et al. [16, 17] and Sahoo et al. [18] and supplemented them with additional measurements up to a temperature of 90°C to develop a general correlation for viscosity of nanofluids. He derived a correlation which expresses the viscosity in a non-dimensional form, valid for all three nanofluids.

$$\frac{\mu_{nf}}{\mu_{bf}} = A_1 e^{(A_2\phi)} \quad (2.5)$$

In the above generalized correlation, A_1 and A_2 are constants and not functions of ϕ , unlike previous correlations. The values of constants A_1 and A_2 are shown in Table 2.2. This table also

lists the range of concentrations (e.g. $\phi=0.06$ meaning a 6% particle volumetric concentration) and particle sizes from which this correlation is derived. It is observed that μ_{bf} (i.e., the viscosity of the base fluid) takes care of the temperature effect on viscosity in Eq. (2.5) so that no additional term involving T is necessary. The above correlation is applicable in the temperature range of $273K(0^{\circ}C) < T < 363K(90^{\circ}C)$, which encompasses the operating range of heat transfer fluids in building heating and cooling, automobile radiators and outdoor heat exchangers in industrial plants in cold regions of the world.

2.5.1.1 Particle Size Effect on Viscosity

Namburu et al. [17] and Vajjha [19] analyzed the viscosity measurements on SiO₂ nanofluids for three particle sizes: 20, 50 and 100 nm. They observed, for the same volumetric concentration, as the particle size increased the viscosity decreased. This observation is consistent with that presented by Cheremisinoff [20] for microparticles. This is possibly due to the fact that there are more number of smaller particles present in the same volumetric concentration and the total particle surface area interacting with the liquid phase is more than that for the larger particles. Since only SiO₂ nanofluid of different particle diameter was measured, there was a lack of sufficient data to include the particle size as a parameter in the viscosity equation. In the future, measurements of several nanofluids, each with different average particle diameters will be a valuable contribution in including the particle size into the viscosity relation. Figure 2.1 shows the experimental and curve-fit values predicted by Eq. (2.5) of viscosity against temperature for the Al₂O₃ nanofluid for different volumetric concentration of particles in 60:40 EG/W. In Fig. 2.1, the maximum deviation between the data and correlation is of the order of $\pm 12\%$, except at a temperature of 363 K. At this temperature, the deviation is a bit higher because the viscometer is operating near its lowest measuring limit.

2.5.2 Thermal Conductivity

Measurements of the thermal conductivity of CuO, Al₂O₃, ZnO and SiO₂ nanofluids of several volumetric concentrations in the 60:40 EG/W base fluid were conducted by Vajjha and Das [21] and Sahoo [22] with a P.A. Hilton [23] thermal conductivity apparatus suitable for liquids and gases. Vajjha and Das measured the thermal conductivity of CuO and Al₂O₃ nanofluids and Sahoo extended the work to the SiO₂ nanofluid. Following the work of Koo and

Kleinstreuer [24], they developed a thermal conductivity model, which is a two-term function. The first term is called the static part and the second term is due to the Brownian motion. The second term takes into account the effect of particle size, particle volumetric concentration, temperature and properties of base fluid, as well as nanoparticles subjected to Brownian motion. The effective thermal conductivity of a nanofluid is given by Eq. (2.6a). The term $f(T, \phi)$ in Eq. (2.6a) is a function of temperature and particle volume concentration given by Eq. (2.6b) and the correlations for β (fraction of the liquid volume which travels with a particle) is given in Table 2.3 for the three nanofluids.

$$k_{nf} = \frac{k_p + 2k_{bf} - 2(k_{bf} - k_p)\phi}{k_p + 2k_{bf} + (k_{bf} - k_p)\phi} k_{bf} + 5 \times 10^4 \beta \phi \rho_{bf} C_{pbf} \sqrt{\frac{\kappa T}{\rho_p d_p}} f(T, \phi) \quad (2.6a)$$

$$f(T, \phi) = (2.8217 \times 10^{-2} \phi + 3.917 \times 10^{-3}) \left(\frac{T}{T_0} \right) + (-3.0669 \times 10^{-2} \phi - 3.91123 \times 10^{-3}) \quad (2.6b)$$

Figure 2.2 shows the variation of the thermal conductivity ratio (k_{nf} / k_{bf}) with temperature for various volumetric concentrations of CuO nanofluid. It is observed that the thermal conductivity increases with the particle volumetric concentration and the temperature. For example at 350 K the thermal conductivity is increased by 50% for the CuO nanofluid of 6% concentration. The best-fit curves are provided for the visualization purpose and to aid the reader to interpolate values between the experimental points.

2.5.3 Specific Heat

Vajjha and Das [25] conducted the specific heat measurements of three different nanofluids (Al_2O_3 , SiO_2 and ZnO) and developed a general correlation given by Eq. (2.7), where the values of A, B and C are given in Table 2.4. In Figure 2.3, a comparison between the experimental data and the proposed correlation, Eq. (2.7) is shown. Vajjha and Das determined the uncertainty in the specific heat measurement to be 3.1%.

$$\frac{C_{pnf}}{C_{pbf}} = \frac{\left(\left(A * \left(\frac{T}{T_0} \right) \right) + B * \left(\frac{C_{pp}}{C_{pbf}} \right) \right)}{(C + \phi)} \quad (2.7)$$

Since we did not have the measured data of the specific heat of CuO nanofluids we used the equation presented by Xuan & Roetzel [6]. This correlation assumes thermal equilibrium between the nanoscale solid particles and the liquid phase.

$$C_{pnf} = \frac{\phi \rho_p C_{pp} + (1 - \phi) \rho_{bf} C_{pbf}}{\rho_{nf}} \quad (2.8)$$

2.5.4 Density

Vajjha et al. [26] measured the density of Al₂O₃ and other nanofluids using the Anton Paar digital density meter [27]. They observed a good agreement between their experimental values and the equation given by Pak and Cho [5].

$$\rho_{nf} = \rho_p \phi + \rho_{bf} (1 - \phi) \quad (2.9)$$

2.5.5 Base Fluid Properties

The thermophysical properties equations summarized in the above sections require the values of the properties of the base fluid, which in the present case was 60:40 EG/W. The properties of this fluid were obtained from the ASHRAE Handbook [28] and were curve fitted as a function of the temperature with the following equations.

Density: $\rho_{bf} = -0.0024T^2 + 0.963T + 1009.8 \quad (2.10)$

Viscosity: $\mu_{bf} = A_4 e^{\left(\frac{B_4}{T}\right)} \quad (2.11)$

where $A_4 = 0.555 \times 10^{-3}$; $B_4 = 2664$

$$\text{Thermal Conductivity: } K_{bf} = -3 \times 10^{-6} T^2 + 0.0025 T - 0.1057 \quad (2.12)$$

$$\text{Specific Heat: } C_{pbf} = 4.2483 T + 1882.4 \quad (2.13)$$

The above equations are valid within the temperature range of $293 \text{ K} \leq T \leq 363 \text{ K}$.

2.6 Pressure Loss and Heat Transfer Measurements

Figure 2.4 shows the schematic diagram of the apparatus used to measure the fluid dynamic and heat transfer characteristics of nanofluids. The test section consists of a 4.76 mm (3/16 inch) nominal diameter (3.14 mm inside diameter) copper tube of length 1.168 m (46 inch). It is surrounded by copper blocks over which four electrical strip heaters each of 1,000 W capacity are installed. Each of these heaters are individually controlled by a variac and the heat input is measured by the power meter. The test section is covered with a 15-cm thick fiber glass insulation which minimizes the heat loss to the environment. The fluid inlet, outlet and wall temperature measurements along the test section are determined by eight copper-constantan thermocouples. Two plastic fittings with thermowells at the inlet and outlet sections of the copper tube provide a thermal barrier to axial heat conduction. For turbulent flow, the hydrodynamic and thermal entry length in a tube is $X/d = 10$. In the experimental setup, this length is 3.14 cm, beyond which all measurements are taken to ensure that the readings are taken in the fully developed regions. The nanofluids are heated uniformly by the electric resistance strip heaters under a constant heat flux boundary condition. After exiting the test section the heated nanofluid is cooled by water in an annular counter flow four-pass heat exchanger, so that the nanofluid re-enters the test section at a consistent inlet temperature. The nanofluid is circulated by a single stage regenerative turbine pump. In order to vary the flow through the test section to attain different Reynolds numbers, a flow control loop is provided with a bypass valve. Volumetric flow rates of nanofluids are measured by a turbine flow meter and a totalizer. Pressure loss measurements across the test section are recorded by a differential pressure

transducer. The data logger is programmed to record the temperatures, flow rates and pressures at each Reynolds number by monitoring the parameters until they reach a steady state.

Using the measured data from the experiment, the convective heat transfer coefficient can be calculated as:

$$h_{nf} = \frac{q''}{(T_w - T_b)} \quad (2.14)$$

where q'' is the heat flux supplied to the test section by the heaters, T_w is the average outside wall temperature and T_b is the average of fluid inlet and outlet temperatures. The heat flux is derived from \dot{q} , the rate of heat gained by the fluid flowing through the test section, which is given as:

$$\dot{q} = \dot{m}C_p \Delta T_f \quad (2.15)$$

where \dot{m} is the mass flow rate, C_p is the specific heat of nanofluid and ΔT_f is the difference between outlet and inlet temperatures of the nanofluid. Dividing the heat transfer rate by the inside surface area of the tube, the heat flux is obtained. As checkups, energy balance between the heat provided by the heaters from the power meter readings and the heat absorbed by the fluid from Eq. (2.15) were done for each runs and an agreement within about 2% accounting for a heat loss through the insulation was determined.

2.7 Heat Transfer Results

2.7.1 Benchmark Test Case

Figure 2.5 presents the benchmark test case to verify the experimental set up and the procedure adopted for the convective heat transfer coefficient evaluation. In the test loop shown in Fig. 2.4, first the single phase liquid, 60:40 EG/W mixture, was circulated at varying Reynolds numbers while it was being heated by a constant heat flux with electrical strip heaters on the boundary. Then using the measured data in Eq. (2.14), the heat transfer coefficient was

calculated. Applying the curve-fit equation for the thermal conductivity of the 60:40 EG/W mixture, derived from the ASHRAE data, Eq. (2.12), corresponding Nusselt numbers for each test Reynolds number were calculated. In a similar manner, the viscosity and specific heat of the 60:40 EG/W mixture were evaluated from the ASHRAE data, which provided the value of Prandtl number for each measurement. Using the Nusselt number and the Prandtl number values, the data were plotted against the Reynolds numbers. In Figure 2.5 comparisons between the experimental data and the theoretical predictions by Dittus-Boelter [29] and Gnielinski [30] equations have been shown. The Dittus-Boelter equation for the fluid being heated is given as:

$$Nu = 0.023 Re^{0.8} Pr^{0.4} \quad (2.16)$$

where $0.6 \leq Pr \leq 100$, $3000 \leq Re \leq 10^6$

The equation given by Gnielinski [30] for liquids is:

$$Nu = 0.012(Re^{0.87} - 280) Pr^{0.4} \quad (2.17)$$

where $1.5 \leq Pr \leq 500$, $3000 \leq Re \leq 10^6$

The present experimental data points of the benchmark test case showed a closer agreement with the equation of Gnielinski. It is explained by Bejan [31] that the maximum deviation between experimental data and the values predicted by the Dittus-Boelter equation, Eq. (2.16) can be of the order of 40%. However, the equation by Gnielinski is accurate within $\pm 10\%$ and it can be used for both constant heat flux and constant wall temperature boundary conditions. After this benchmark test case, the measurements of three nanofluids of various concentrations were performed.

2.7.2 Effect of the Particle Volumetric Concentration

Figure 2.6 presents the results of convective heat transfer measurements of the Al_2O_3 nanofluid of particle volumetric concentrations ranging up to 10%. Kulkarni et al. [32] have shown that the uncertainty in the heat transfer coefficient measurements in this experiment is less than 3%. It is observed from Fig. 2.6 that the heat transfer coefficient increases with the particle

concentration. At higher concentrations, more particles are taking part in heat transport and there is higher surface area of particles interacting with the base fluid, thereby enhancing the heat transfer process. As an example, at a Reynolds number of 8000, an Al_2O_3 nanofluid of 6% concentration has a convective heat transfer coefficient that is approximately 50% higher than that produced by the base fluid. Notice that at the 10% concentration level, the high viscosity of the nanofluid limited the pump to circulate at a maximum Reynolds number of about 7000.

2.7.3 Effect of the Thermophysical Properties of Particles

In Figure 2.7 we compare the heat transfer coefficients of three nanofluids of the same particle concentration with the base fluid. This diagram shows that the type of nanoparticle influences the heat transfer characteristics of nanofluids. This behavior is due to their differing thermophysical properties. The two metallic particles CuO and Al_2O_3 have higher density, higher thermal conductivity and produce more viscous nanofluid compared to the non-metallic SiO_2 particle. The specific heats of the three particles are comparable as observed from Table 2.1. Because of the higher values of the properties of the metallic particles, the nanofluids containing them generate higher heat transfer coefficients than the non-metallic particle. At a Reynolds number of 10,000 the heat transfer coefficient is 29% greater for the SiO_2 , 40% for the Al_2O_3 and 43 % for the CuO nanofluids, over the base fluid. The combined effects of these particle properties play the role in enhancing the heat transfer coefficient of nanofluids.

2.7.4 Particle Size Effect on Heat Transfer

Figure 2.8 presents the heat transfer coefficient variation with Reynolds number for three different SiO_2 nanoparticles of average particle sizes; 20, 50 and 100 nm. For a 2% concentration nanofluid, it is observed that at a constant Reynolds number, the heat transfer coefficient data are coincident upon one another for all three particle sizes, and the variations are within the uncertainties of the measurements. The results obtained from the 4% concentration SiO_2 nanofluid were also similar to the observations of the 2%. Therefore, we may infer that at lower concentrations, particle size does not have any noticeable effect on the convective heat transfer coefficient.

We had measured the particle size effect of only one nanofluid, SiO_2 , which possess a lower thermal conductivity. The other nanofluids tested were of single average particle sizes. Therefore, the particle size effect remains to be explored and should be an important topic in the

future to conduct comprehensive experiments with several particle sizes of the higher thermal conductivity nanofluids of various concentrations to conclusively evaluate the particle size effect at higher concentrations.

2.7.5 New Nusselt Number Correlation

Pak and Cho [5] had shown that for nanofluids the Nusselt number is a function of Reynolds number and Prandtl number and a correlation of the Dittus-Boelter [29] type was adequate to represent the forced convection heat transfer in nanofluids. However, their correlation did not include any dependence on the particle volumetric concentration. Xuan and Li [7] presented their correlation in which Nusselt number was a function of concentration, particle size (through a particle Peclet number), Reynolds number and Prandtl number. From our experimental observation in Fig. 2.6, we noticed that increasing the particle volume concentration increased the heat transfer coefficient and from Fig. 2.8, we noticed that particle size had no measurable effect on the heat transfer coefficient. The Nusselt number Nu , by definition, is a function of the heat transfer coefficient h and the thermal conductivity k of the nanofluid. Both h and k vary with the particle concentration of the nanofluid. Therefore, Nu must be a function of the particle concentration of the nanofluid. With this argument we developed a Nusselt number correlation as a function of ϕ , Re and Pr . Experimental value of Nusselt number was obtained by converting the experimental h to the Nusselt number via the thermal conductivity correlations of three nanofluids presented in Section 2.5.2. The Reynolds number and the Prandtl number were determined from each measured velocity and the thermophysical properties evaluated at the bulk mean temperature (average of inlet and outlet temperatures). The equations for μ and C_p were taken from sections 2.5.1 and 2.5.3 respectively.

After carefully analyzing the data of all three nanofluids, a correlation similar to the well-known Gnielinski [30] equation was derived. This new correlation, which contains an additional term for particle concentration to account for nanofluids, is given as:

$$Nu_{nf} = 0.065(Re^{0.65} - 60.22)(1 + 0.0169\phi^{0.15})Pr^{0.542} \quad ; \quad R^2=0.97 \quad (2.18)$$

This equation has maximum deviations of $\pm 10\%$ and an average deviation of 2% when compared with the experimental data points. The correlation is valid for $3000 < \text{Re} < 16000$, $0 < \phi < 0.06$ for CuO and SiO₂ nanofluids and $0 < \phi < 0.1$ for the Al₂O₃ nanofluid.

2.7.6 Pressure Loss Measurement

Figure 2.10 displays the pressure loss measured in the test section at varying Reynolds number for particle volumetric concentrations of 0 to 10% for the Al₂O₃ nanofluid. Kulkarni et al. [32] measured the pressure drop with an Omega differential pressure transducer. The accuracy of this transducer was $\pm 0.25\%$. At a constant Reynolds number, as the nanofluid concentration increases the pressure loss increases. As an example; at a Reynolds number of 6000 the pressure drop for the 6 % concentration is nearly three times that of the base fluid.

White [33] presents the following equation for the pressure drop in a horizontal pipe at low turbulent Reynolds number using the Blasius friction factor relation.

$$\Delta P = \frac{fL\rho V^2}{2d} = 0.158L\rho^{3/4}\mu^{1/4}d^{-5/4}V^{7/4} \quad (2.19)$$

One notices that the pressure loss is dependent on density and viscosity of the fluid. With an increase in the particle volumetric concentration in the nanofluids the density and viscosity increases and hence they cause an increased pressure drop as shown in Fig. 2.11. An important point to notice from the exponents of the density and viscosity in Eq. (2.19) is that ΔP and f vary weakly with viscosity but strongly with density.

Figure 2.11 shows a comparison of measured pressure losses for varying Reynolds number for three different nanofluids of the same particle volumetric concentration of 2%. The density and viscosity of copper oxide are higher than those of the other two nanofluids. Therefore, the CuO nanofluid encounters the highest pressure loss among the three fluids shown here. The aluminum oxide nanofluid has its density and viscosity in the middle range when compared with the other two fluids and therefore, its pressure loss is also in the middle range. For the SiO₂ nanofluid, the pressure loss is lower than the CuO and Al₂O₃ nanofluids, because its density and viscosity are lower than those of the other two nanofluids. The base fluid without any nanoparticles, 60:40 EG/W, produces the lowest pressure loss at a constant Reynolds

number, because of the lowest values of density and viscosity. For example, at a Reynolds number of 8000 the base fluid encounters half the pressure loss as that experienced by the CuO nanofluid.

The friction factor obtained from measured pressure loss data using Eq. (2.19) is plotted in Fig. 2.12. This figure compares the variation of the friction factor with Reynolds number for the three nanofluids and the base fluid. The bottom most curve in this figure is a bench mark test case. It compares the experimental Darcy friction factor for the 60:40 EG/W base fluid with the Blasius correlation from White [33] for low Reynolds number turbulent flow in a pipe. The Blasius equation from White for a single phase fluid is:

$$f = 0.3164 \text{Re}^{-0.25} \quad 4000 < \text{Re} < 10^5 \quad (2.20)$$

For the 60:40 EG/W a good agreement between the data and the classical Blasius equation is observed. The maximum deviation between the equation and the data is 7% and the average deviation is 0.5%. Therefore, the benchmark test validates our experimental setup and the procedure.

When the nanofluids friction factor data were plotted, it was observed that they group together nicely for each individual nanofluids. The copper oxide nanofluid is at the top of the figure followed by the Al₂O₃ and the SiO₂ nanofluids. These data fall according to the higher densities and viscosities of various nanofluids. Next, following the Blasius type equation, we developed correlations from the data of the three nanofluids.

For the CuO nanofluid: $f = 0.9027 \text{Re}^{-0.336} ; R^2=0.98$ (2.21)

where $4000 < \text{Re} < 16000 ; 0 \leq \phi \leq 0.06$. The maximum deviation is 5.8% and an average deviation is 0.03%.

For the Al₂O₃ nanofluid: $f = 0.5814 \text{Re}^{-0.2986} ; R^2=0.99$
(2.22)

where $4000 < Re < 16000$; $0 \leq \phi \leq 0.1$. The maximum deviation is 3.8% and an average deviation is 0.02%.

For the SiO₂ nanofluid: $f = 0.3607 Re^{-0.2518}$; $R^2=0.964$ (2.23)

where $4000 < Re < 16000$; $0 \leq \phi \leq 0.06$. The maximum deviation is 4.9% and an average deviation is 0.02%.

From this analysis, it is promising to find that the friction factor of nanofluids obey a similar trend as the well-established single-phase fluid. However, separate correlations for each nanofluid are cumbersome and undesirable. Therefore, we proceeded to seek a more general correlation for the friction factors of all three nanofluids.

2.7.7 Guidance from Experimental Observation

Examining the Fig. 2.12, we observe that at a constant Reynolds number the friction factors of nanofluids increase in proportion to their increase in density and viscosity over that of the base fluid. Therefore, a general correlation for the friction factor must be functions of the base fluid friction factor supplemented by multipliers which are functions of the density and the viscosity. The general correlation is maintained dimensionless, by adopting the multipliers to be ratios of density and viscosity of nanofluids to those of the base fluid. With careful statistical analysis we have minimized deviations between the empirical correlation and the friction factor data for three nanofluids and the base fluid, and have derived the generalized equation, Eq. (2.24).

$$f_{nf} = 0.3164 Re^{-0.25} \left(\frac{\rho_{nf}}{\rho_{bf}} \right)^{0.797} \left(\frac{\mu_{nf}}{\mu_{bf}} \right)^{0.108} \quad (2.24)$$

This equation is valid in the range $4000 < Re < 16000$, $0 \leq \phi \leq 0.06$ for CuO and SiO₂ nanofluids and $0 \leq \phi \leq 0.1$ for the Al₂O₃ nanofluid. Figure 2.13 shows the experimental friction factor values versus predicted values obtained from the Eq. (2.24). The two dashed lines shown in this figure are the 95% prediction bounds. Given any specific nanofluid, we are 95% confident

that the friction factor for that particular nanofluid lies between the upper and lower prediction limits.

2.8 Conclusions

The convective heat transfer and pressure loss characteristics of three nanofluids flowing in a circular tube in the turbulent regime were investigated experimentally. The heat transfer and pressure loss data were analyzed using new rheological and thermophysical properties correlations developed from experiments. Heat transfer coefficient of nanofluids showed an increase with the particle volumetric concentration. For example, at a Reynolds number of 7240, the percentage increase in the heat transfer coefficient over the base fluid for a 10% Al_2O_3 nanofluid is 81.74%. The pressure loss of nanofluids also increases with an increase in particle volume concentration. The increase of pressure loss for a 10% Al_2O_3 nanofluid at a Reynolds number of 6700 is about 4.7 times than that of the base fluid. This is due to the increase in the viscosity of the nanofluid with concentration. A new Nusselt number correlation similar to the Gnielinski equation for single phase liquid has been developed. This new equation is a function of the nanoparticle volume concentration in addition to the Reynolds number and the Prandtl number. Furthermore, a new correlation for the friction factor has been developed following the Blasius friction factor equation supplemented by the density and viscosity of nanofluids.

2.9 Acknowledgement

Financial assistance from the Dean of the Graduate School at the University of Alaska Fairbanks is gratefully acknowledged.

2.10 References

1. H. Masuda, A. Ebata, K. Teramae, N. Hishinuma, Alteration of thermal conductivity and viscosity of liquid by dispersed ultra-fine particles (dispersion of $\gamma\text{-Al}_2\text{O}_3$, SiO_2 , and TiO_2 ultra-fine particles), *Netsu Bussei (Japan)* 4 (1993) 227–233.
2. S.U.S. Choi, Enhancing thermal conductivity of fluids with nanoparticles. in: D.A. Siginer and H.P. Wang, Editors, *Developments and Applications of Non-Newtonian Flows*, FED-vol. 231/MD-vol. 66, ASME, New York (1995), pp. 99–105.

3. X. Wang, X. Xu , S.U.S. Choi, Thermal conductivity of nanoparticle-fluid mixture, *J. Thermophys. Heat Transfer* 13 (1999) 474–480.
4. J.A. Eastman, S.U. S Choi, S. Li, W. Yu, L.J. Thompson, Anomalously increased effective thermal conductivities of ethylene glycol-based nanofluids containing copper nanoparticles, *Appl. Phys. Lett.* 78 (6) (2001) 718–720.
5. B.C. Pak, Y.I. Cho, Hydrodynamic and heat transfer study of dispersed fluids with submicron metallic oxide particles, *Exp. Heat Transfer* 11(2) (1998) 151-170.
6. Y. Xuan, W. Roetzel, Conceptions of heat transfer correlation of nanofluids, *Int. J. Heat Mass Transfer* 43 (2000) 3701-3707.
7. Y. Xuan, Q. Li, Investigation on convective heat transfer and flow features of nanofluids, *J. Heat Transfer* 125 (2003) 151-155.
8. J. Buongiorno, Convective transport in nanofluids, *J. Heat Transfer* 128 (2006) 240-250.
9. C.T. Nguyen, G. Roy, C. Gauthier, N. Galanis, Heat transfer enhancement using Al_2O_3 -water nanofluid for an electronic liquid cooling system, *Appl. Therm. Eng.* 27 (8-9) (2007) 1501–1506.
10. W. C. Williams, J. Buongiorno, L. W. Hu, Experimental investigation of turbulent convective heat transfer and pressure loss of alumina/water and zirconia/water nanoparticle colloids (nanofluids) in horizontal tubes, *J. Heat Transfer* 130 (2008) 042412-1 to 7.
11. Alfa Aesar. Available from: <<http://www.alfaesar.com/>>, 2007.
12. F.P. Incropera, D.P. DeWitt, *Introduction to Heat Transfer*, third ed., John Wiley & Sons, Inc., New York, 1996.
13. D.R. Lide, *Handbook of Chemistry and Physics*, 84th ed.; CRC Press: Boca Raton, FL., 2003.
14. R. Bolz, G. Tuve, *Handbook of Tables for Applied Engineering Science*, second ed., CRC Press, 2007.
15. Brookfield DV-IIC Programmable Viscometer Manual, Brookfield Engineering Laboratories Inc., No. M/97-164-D1000. Middleboro, MA, 1999.
16. P.K. Namburu, D.P. Kulkarni, D. Misra, D.K. Das, Viscosity of copper oxide nanoparticles dispersed in ethylene glycol and water mixture, *Exp. Therm. Fluid Sci.* 32 (2007) 67-71.

17. P.K. Namburu, D.P. Kulkarni, A. Dandekar, D.K. Das, 2007, Experimental investigation of viscosity and specific heat of silicon dioxide nanofluids, *Micro & Nano Letters* 2 (3) (2007) 67–71.
18. B.C. Sahoo, R.S. Vajjha, R. Ganguli, G.A. Chukwu, D.K. Das, Determination of rheological behavior of aluminum oxide nanofluid and development of new viscosity correlations, *Petro. Sci. Tech.* 27 (15) (2009) 1757-1770.
19. R.S. Vajjha, Measurements of Thermophysical Properties of Nanofluids and Computation of Heat Transfer Characteristics. M.S. thesis, Mech. Engineering Dept., University of Alaska Fairbanks, Fairbanks, AK, 2008.
20. N.P. Cheremisinoff, *Encyclopedia of Fluid Mechanics, Rheology and Non-Newtonian Flows*, vol. 7, Gulf Publishing Company, Houston, Tex., 1988.
21. R.S. Vajjha, D.K. Das, Measurement of thermal conductivity of three nanofluids and development of new correlations, *Int. J. Heat Mass Transfer* 52 (2009) 4675-4682.
22. B.C. Sahoo, Measurement of Rheological and Thermal Properties and the Freeze-Thaw Characteristics of Nanofluids, Department of Mining and Geological Engineering, University of Alaska Fairbanks, Fairbanks, AK, 2008.
23. *Experimental Operating and Maintenance Procedures for Thermal Conductivity of Liquids and Gases Unit*, P.A. Hilton Ltd., Hampshire, England, 2005.
24. J. Koo, C. Kleinstreuer, A new thermal conductivity model for nanofluids, *J. Nanoparticle Res.* 6 (2004) 577–588.
25. R.S. Vajjha, D.K. Das, Specific heat measurement of three nanofluids and development of new correlations, *J. Heat Transfer* 131 (2009) 071601-1 to 7.
26. R.S. Vajjha, D.K. Das, B.M. Mahagaonkar, Density measurements of different nanofluids and their comparison with theory, *Petro. Sci. Tech.* 27 (6) (2009) 612-624.
27. Anton Paar Digital Density Meter for Liquids and Gases. DMA 45, A-8054, Graz, Austria, 1986.
28. ASHRAE Handbook, Fundamentals, American Society of Heating, Refrigerating and Air-Conditioning Engineers Inc., Atlanta, GA, 2005.
29. F.W. Dittus, L.M.K. Boelter, Heat transfer in automobile radiators of the tubular type, *Univ. of Calif. Publ. in Eng.* 11 (1930) 443-461.

30. V. Gnielinski, Equations for heat and mass transfer in turbulent pipe and channel flow, Int. Chem. Eng. 16 (1976) 359–368.
31. A. Bejan, Heat Transfer, John Wiley & Sons, Inc., New York, 1993.
32. D.P. Kulkarni, P.K. Namburu, H.E. Bargar, D.K. Das, Convective heat transfer and fluid dynamic characteristics of SiO₂- ethylene glycol/water nanofluid, Heat Transfer Engineering 29 (12) (2008) 1027-1035.
33. F.M. White, Fluid Mechanics, second ed., McGraw-Hill, Inc., New York, 1986.

Table 2.1. Characteristics of nanoparticles.

Type of material	Density , kg/m ³	Specific heat, J/kgK	Thermal conductivity, W/m K
Al ₂ O ₃ (45 nm)	3600[11]	765[12]	36[12]
CuO (29 nm)	6500[11]	533[13]	17.65[14]
SiO ₂ (20, 50, 100 nm)	2220[11]	745[12]	1.4[12]

Table 2.2. Constants of the viscosity correlation for different nanofluids.

Nanoparticle	A ₁	A ₂	Average Particle Size (nm)	Concentration (%)
Al ₂ O ₃	0.983	12.959	45	0 < ϕ < 0.1
CuO	0.9197	22.8539	29	0 < ϕ < 0.06
SiO ₂	1.092	5.954	20	0 < ϕ < 0.1
SiO ₂	0.9693	7.074	50	0 < ϕ < 0.06
SiO ₂	1.005	4.669	100	0 < ϕ < 0.06

Table 2.3. Curve-fit relations proposed by Vajjha and Das [21] and Sahoo [22].

Type of particles	β	Concentration	Temperature
Al ₂ O ₃	$8.4407(100\phi)^{-1.07304}$	$1\% \leq \phi \leq 10\%$	298 K ≤ T ≤ 363 K
CuO	$9.881(100\phi)^{-0.9446}$	$1\% \leq \phi \leq 6\%$	298 K ≤ T ≤ 363 K
SiO ₂	$1.9526 (100\phi)^{-1.4594}$	$1\% \leq \phi \leq 10\%$	298 K ≤ T ≤ 363 K

Table 2.4. Curve-fit coefficients for different nanofluids.

Nanofluid	A	B	C
Al ₂ O ₃	0.0008911	0.5179	0.4250
SiO ₂	0.001769	1.1937	0.8021

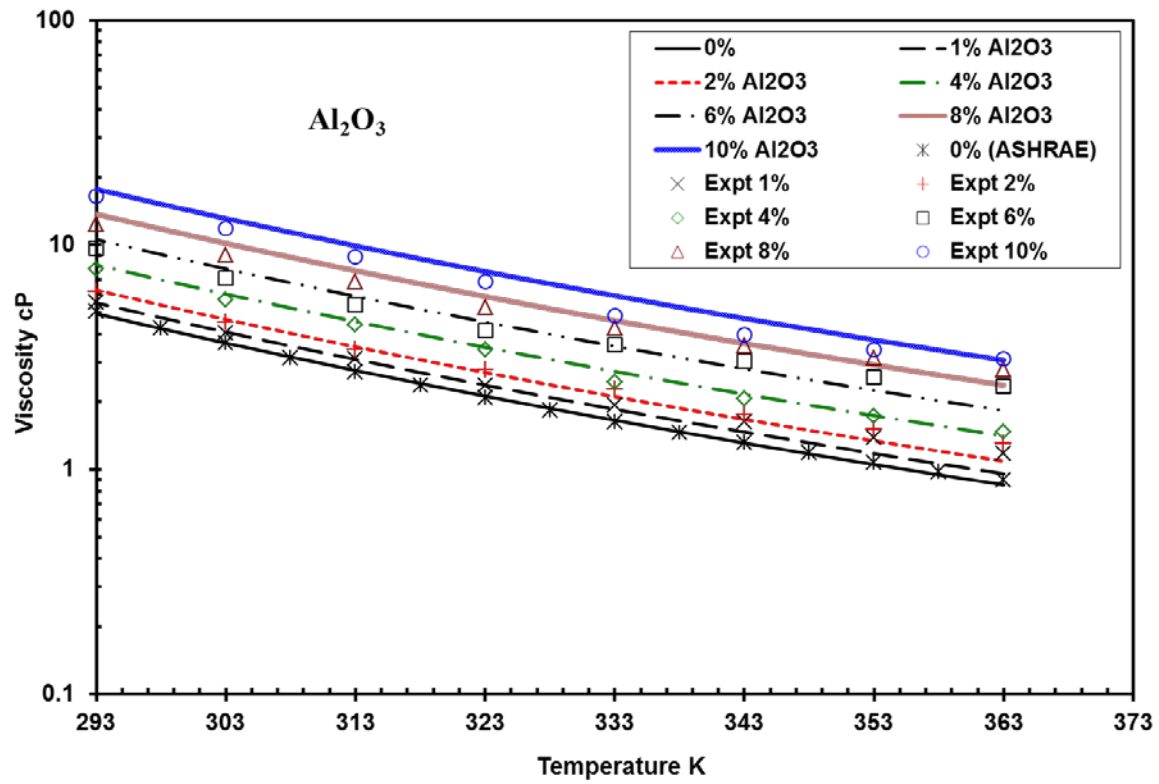


Figure 2.1. Experimental and curve-fit (Eq. 2.5) viscosity values for various particle concentrations of Al_2O_3 nanofluid as a function temperatures.

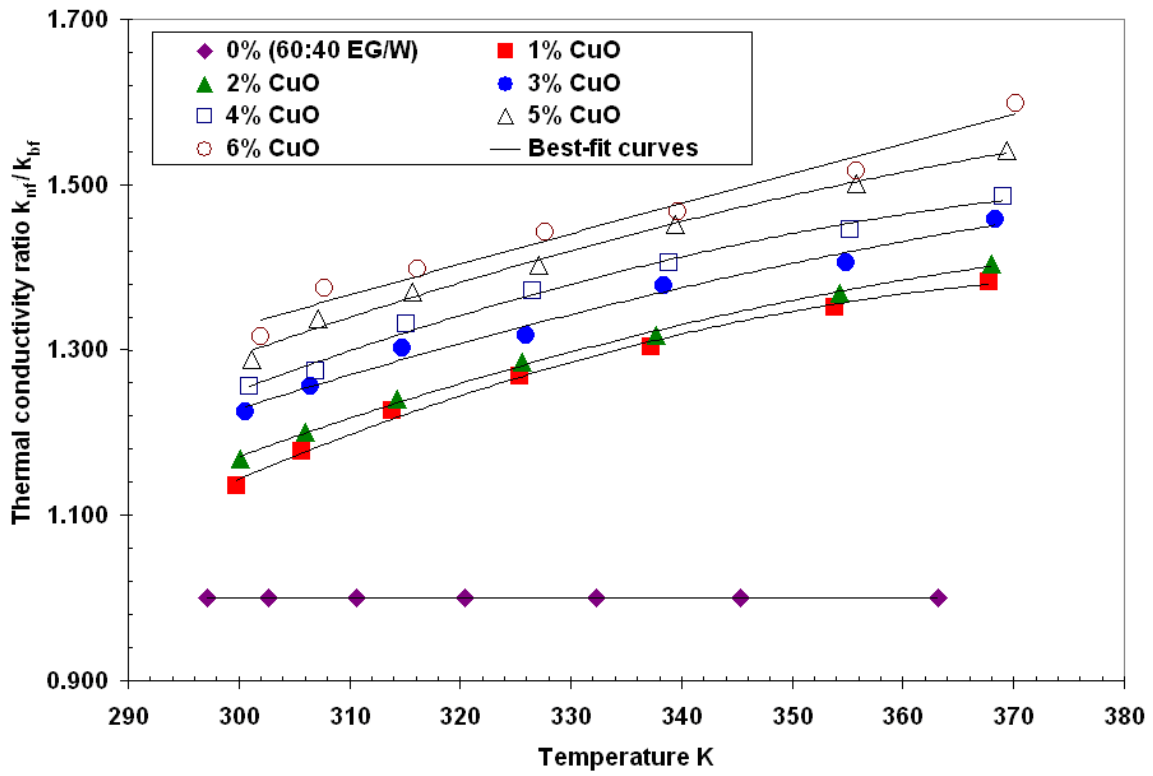


Figure 2.2. Thermal conductivity ratio variation with temperature at different particle volumetric concentrations of CuO nanoparticles dispersed in 60:40 EG/W.

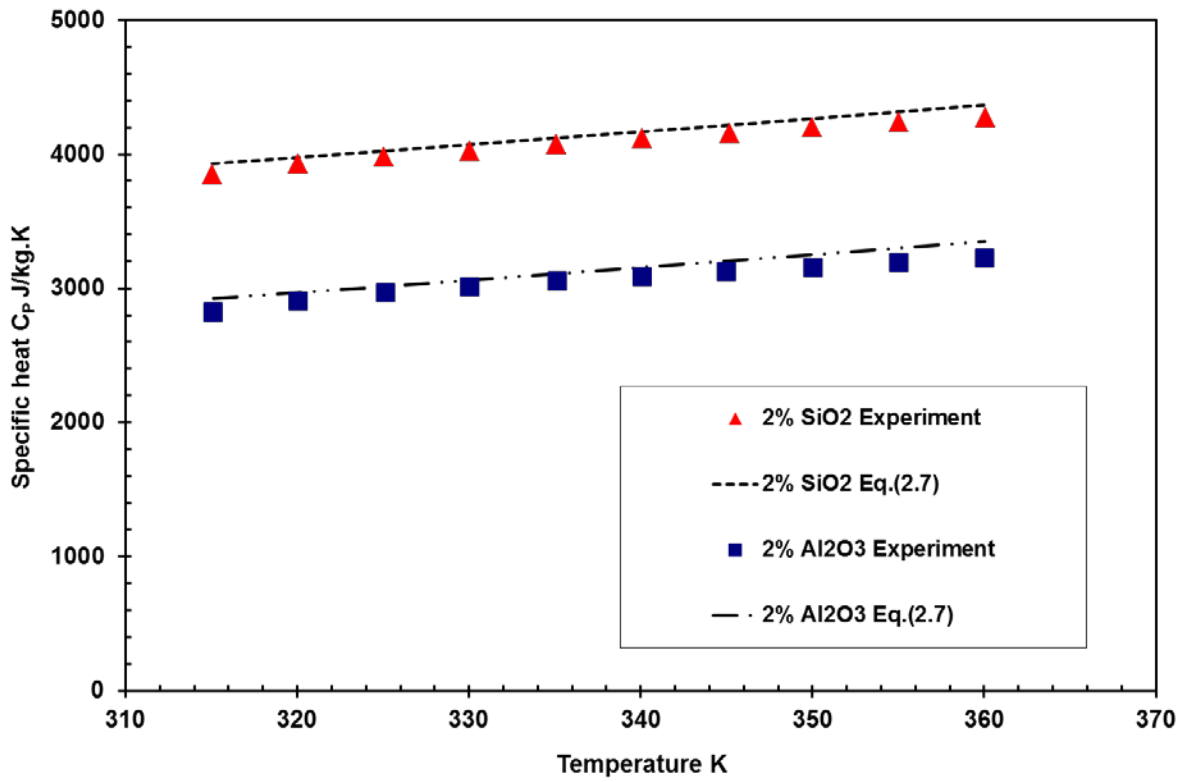


Figure 2.3. Comparison of experimental specific heat values with the correlation, Eq. (2.7) presented by Vajjha and Das [25].

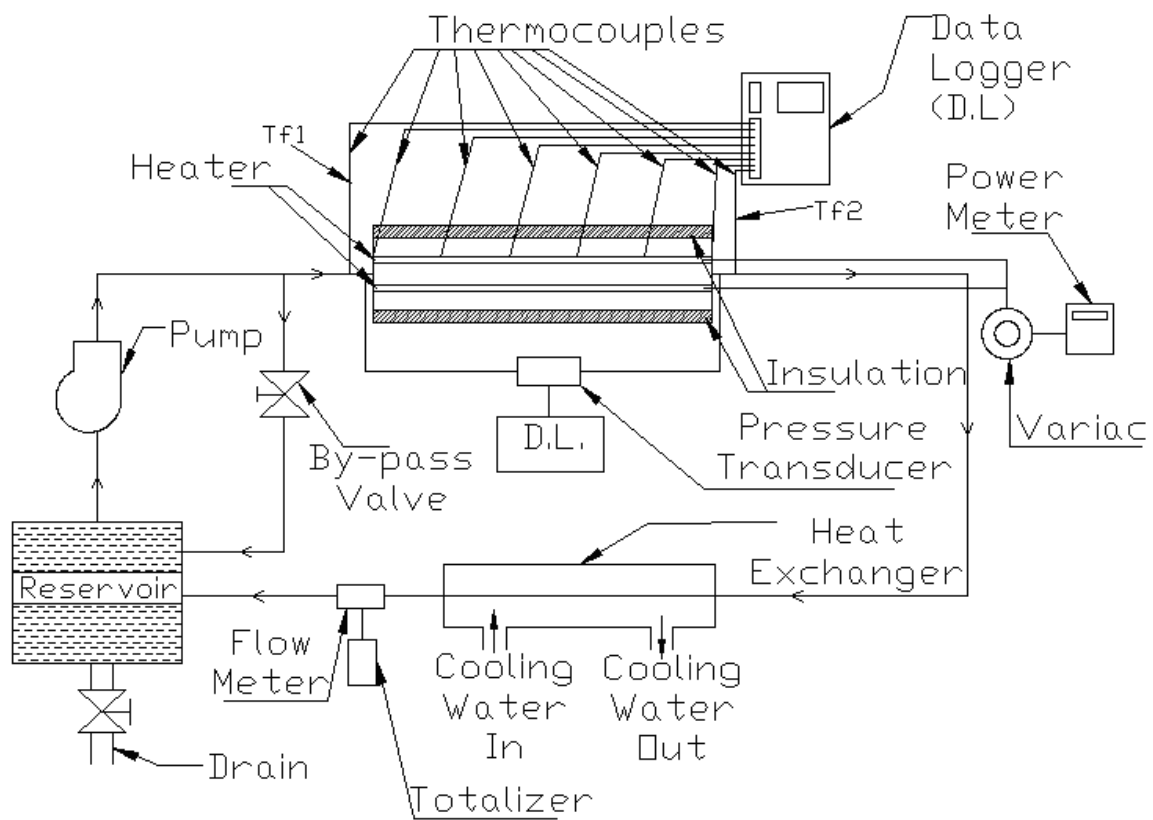


Figure 2.4. A schematic diagram of the experimental set up to measure pressure loss and heat transfer of nanofluids.

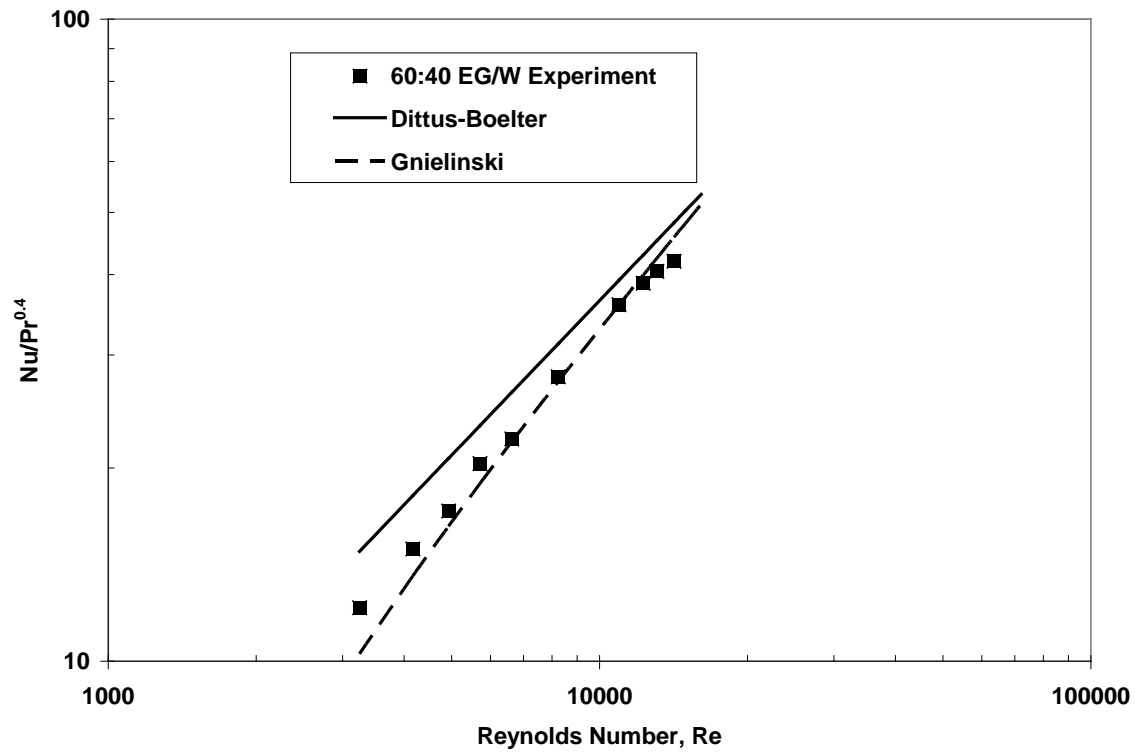


Figure 2.5. Comparison between the experimental results and the theoretical values obtained from the equations of Dittus-Boelter, Eq. (2.16), and Gnielinski, Eq. (2.17).

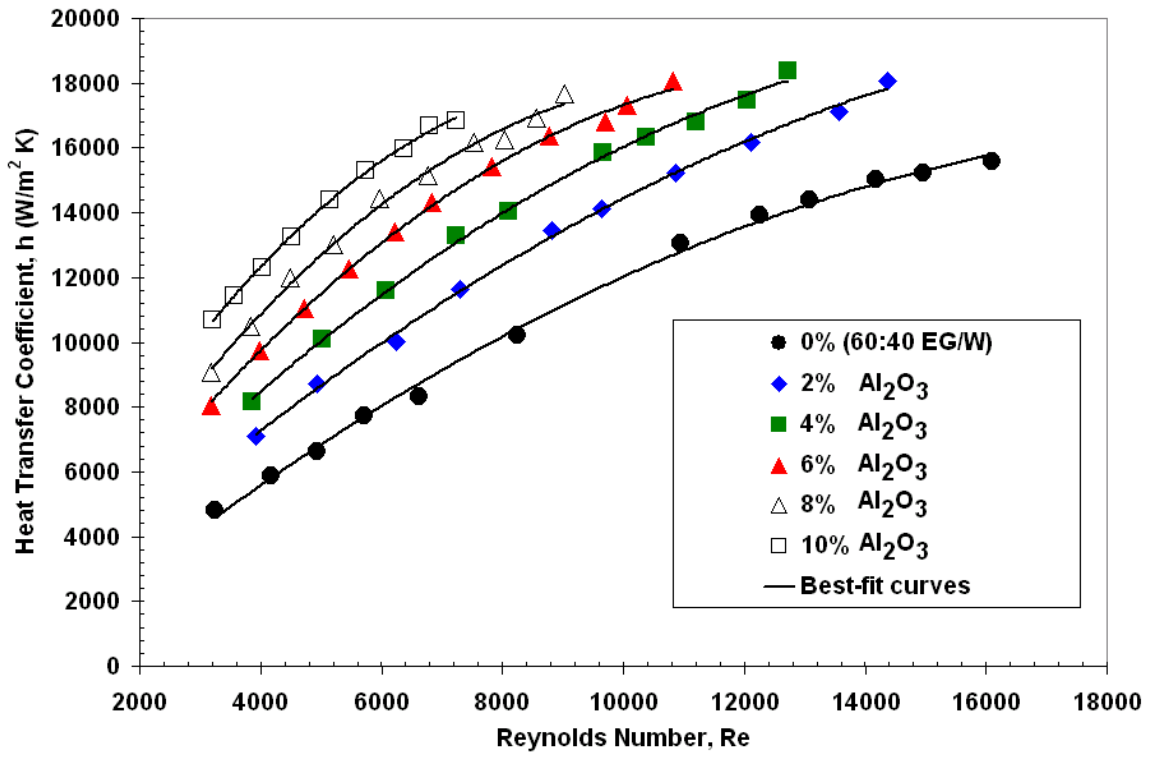


Figure 2.6. The convective heat transfer coefficient of the Al₂O₃ nanofluid in 60:40 EG/W.

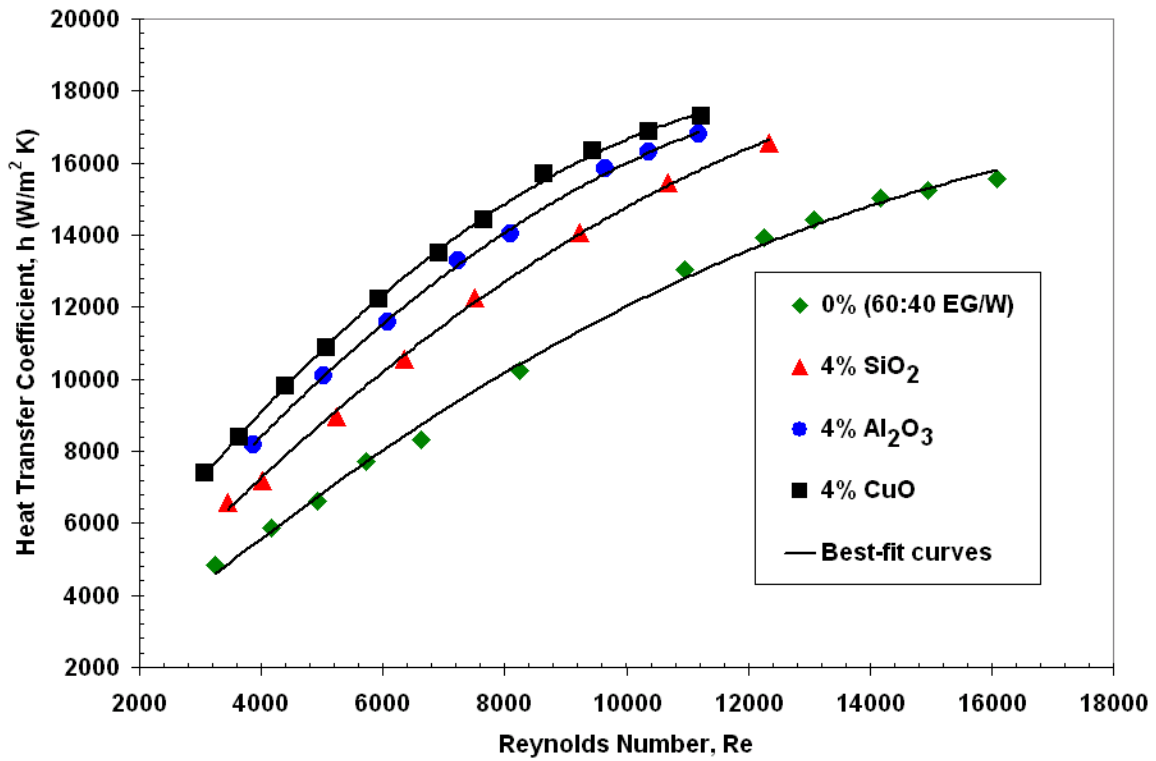


Figure 2.7. Comparison of the heat transfer coefficient of three nanofluids at a particle volumetric concentration of 4% over the base fluid (0%).

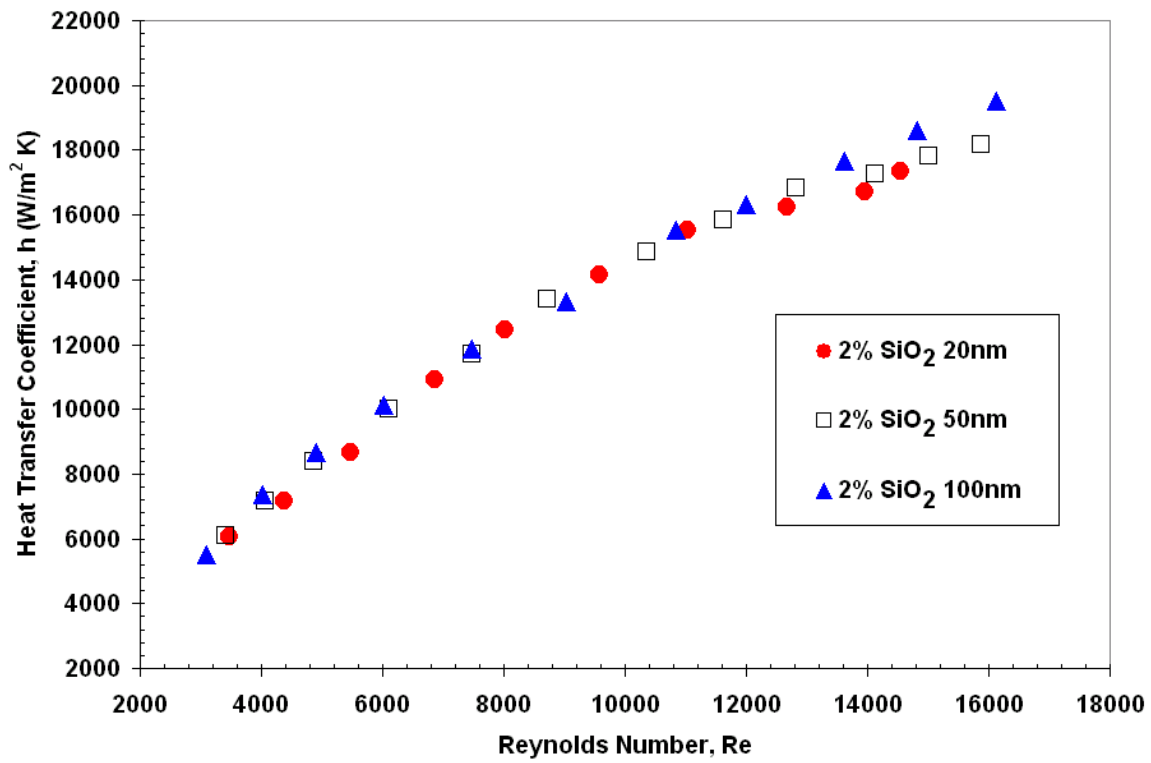


Figure 2.8. The effect of particle sizes on the heat transfer coefficient of 2% SiO₂ nanoparticles suspended in 60:40 EG/W.

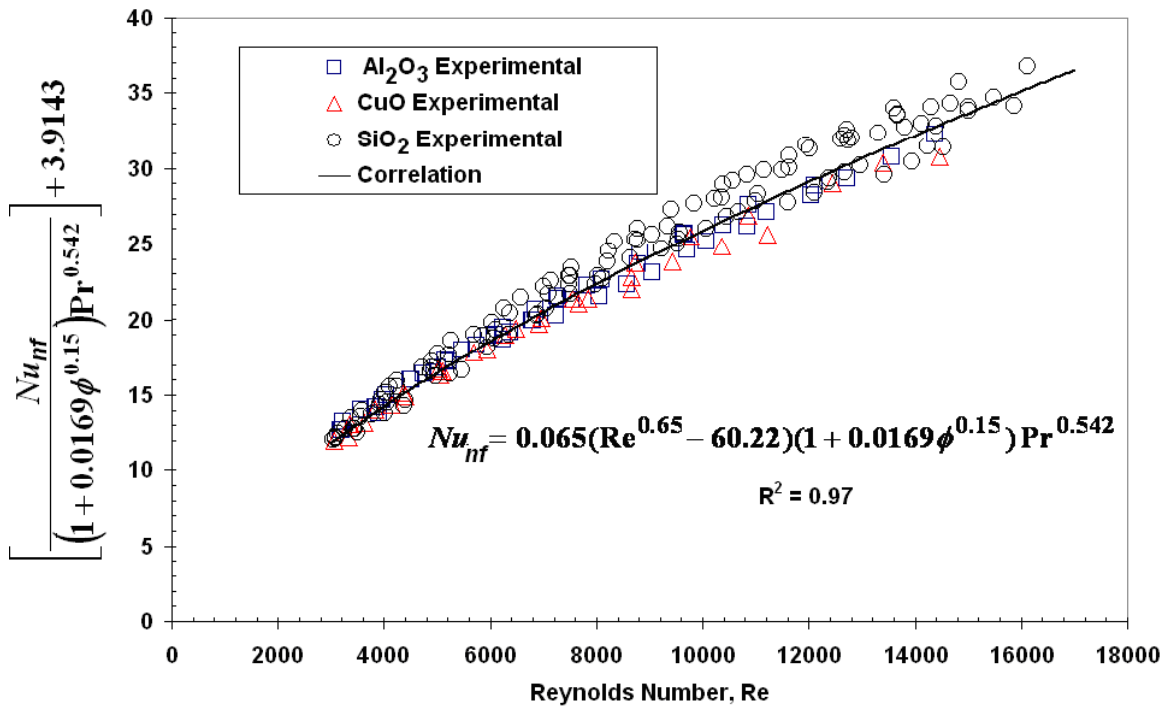


Figure 2.9. Comparison of the experimental values with the values obtained from the proposed correlation, Eq. (2.18).

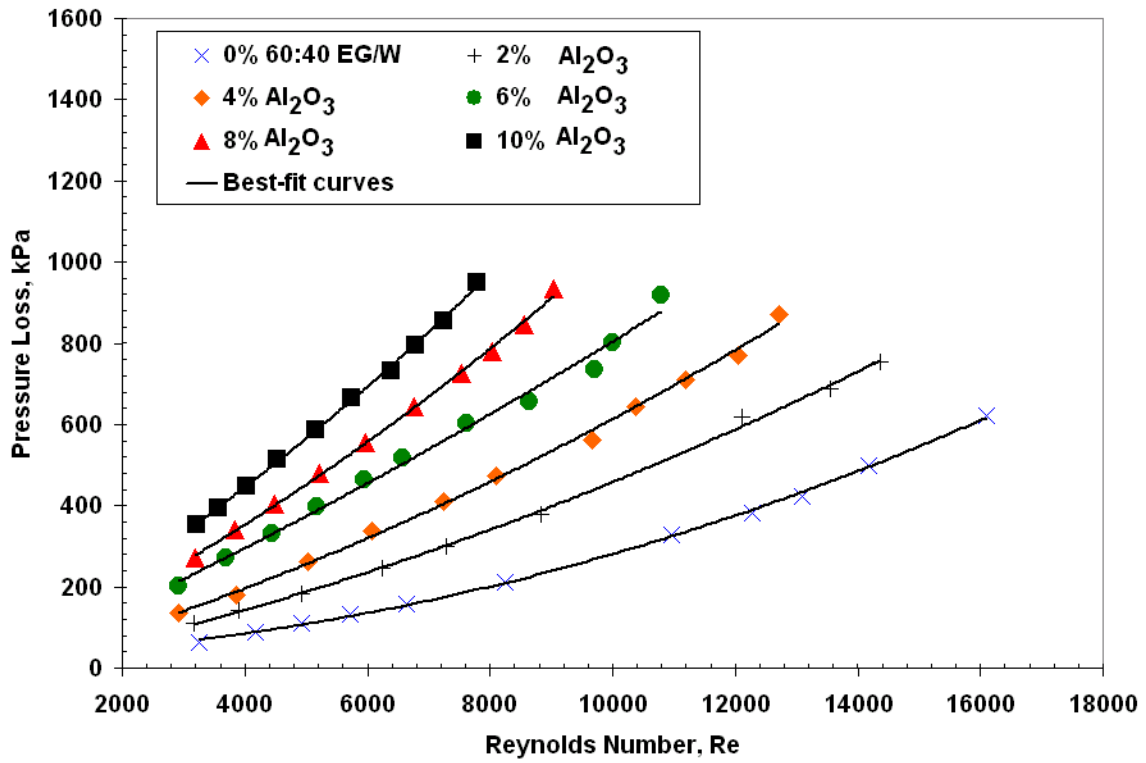


Figure 2.10. Pressure loss of the Al₂O₃ nanofluid measured at various particle volume concentrations as a function of the Reynolds number.

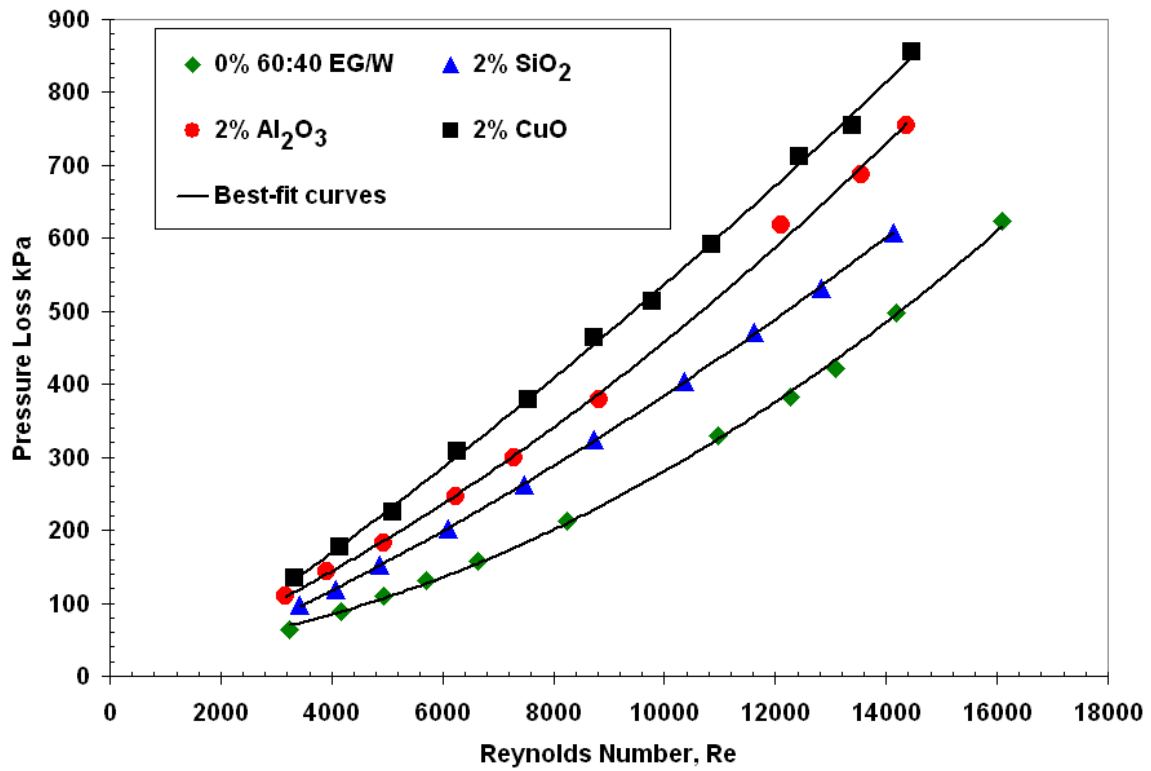


Figure 2.11. Pressure loss variation with the Reynolds number for the base fluid (0%) and 2% particle concentration of SiO₂, Al₂O₃ and CuO nanofluids.

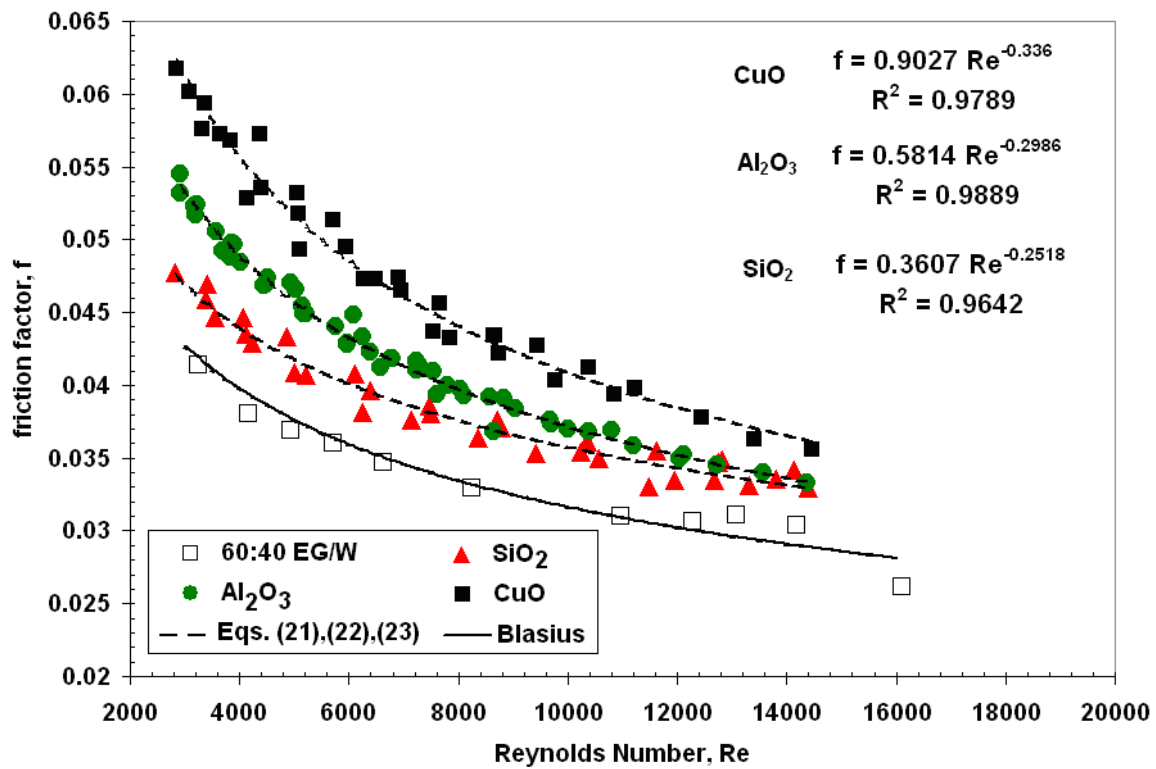


Figure 2.12. Friction factor variation with the Reynolds number for the three nanofluids and the base fluid.

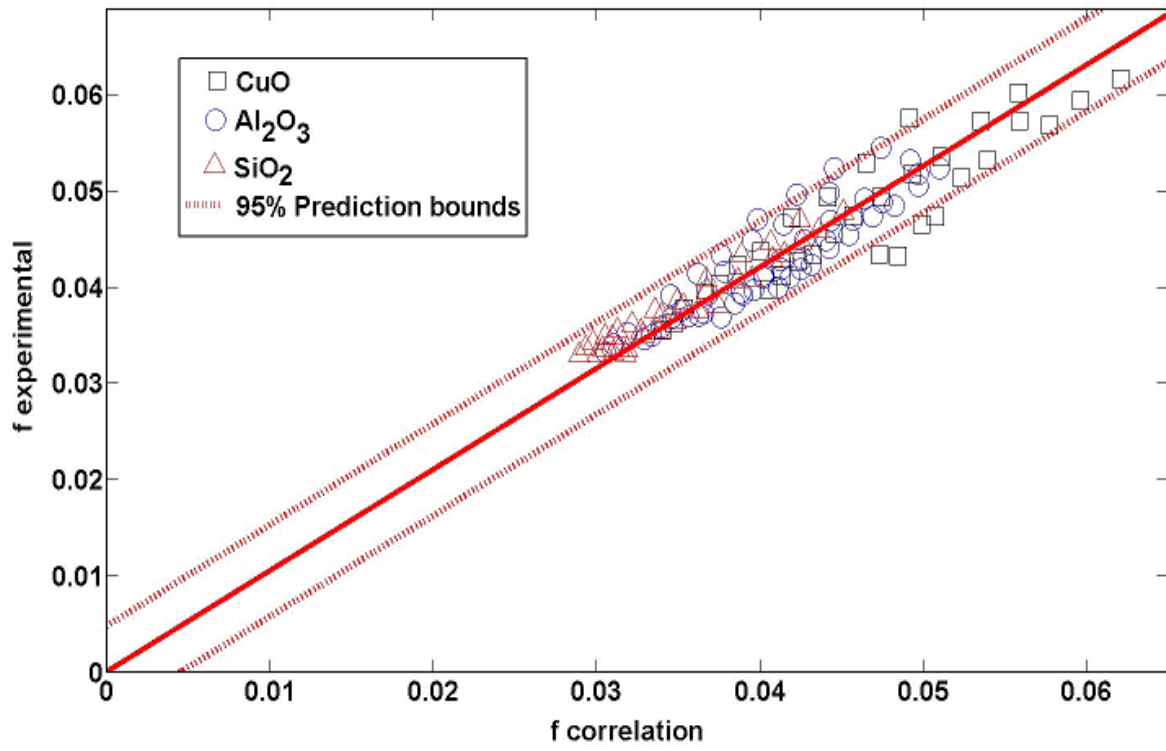


Figure 2.13. Comparison of the friction factor values calculated from the present correlation, Eq. (2.24) with the values obtained from the experiments.

Chapter 3. A Review and Analysis on Influence of Temperature and Concentration of Nanofluids on Thermophysical Properties, Heat Transfer and Pumping Power *

3.1 Abstract

The Prandtl number, Reynolds number and Nusselt number are functions of the thermophysical properties of nanofluids and these numbers strongly influence the convective heat transfer coefficient. The pressure loss and the required pumping power for a given amount of heat transfer depend on the Reynolds number of flow. The thermophysical properties vary with temperature and the volumetric concentration of nanofluids. Therefore, a comprehensive analysis has been performed to evaluate the effects on the performance of nanofluids due to variations of density, specific heat, thermal conductivity and viscosity, which are functions of nanoparticle volume concentration and temperature. Two metallic oxides, aluminum oxide (Al_2O_3), copper oxide (CuO) and one nonmetallic oxide, silicon dioxide (SiO_2), dispersed in an ethylene glycol and water mixture (60:40 by weight) as the base fluid have been studied.

3.2 Keywords

Convective heat transfer, Euler number, Friction factor, Mouromtseff number, Nanofluids, Nusselt number, Prandtl number, Reynolds number, Thermal diffusivity, Thermophysical properties.

3.3 Nomenclature

C_p	specific heat, J/kg K
d	inner diameter of a tube, m
d_p	particle diameter, m
Eu	Euler number, $Eu = \Delta P / \left(\frac{1}{2} \rho V^2 \right)$
f	Darcy friction coefficient

* Vajjha, R. S., and Das, D. K., 2012, "A Review and Analysis on Influence of Temperature and Concentration of Nanofluids on Thermophysical Properties, Heat Transfer and Pumping Power," International Journal of Heat and Mass Transfer, 55(15–16), pp. 4063-4078.

h	convective heat transfer coefficient, $\text{W/m}^2 \text{K}$
k	thermal conductivity, W/m K
L	length of the tube, m
Mo	Mouromtseff number, $Mo = (k^a \rho^b C_p^d) / \mu^e$
Nu	Nusselt number, $Nu = hd/k$
Pe_d	Peclet number for particle, $Pe_d = (Vd_p) / \alpha_{nf}$
Pr	Prandtl number, $Pr = (\mu C_p) / k$
Re	Reynolds number, $Re = (\rho Vd) / \mu$
T	temperature, K
T_0	reference temperature, 273 K
V	mean velocity, m/s
\dot{W}	pumping power, W

Greek Letters

ΔP	differential pressure loss, Pa
α	thermal diffusivity, $\alpha = k / (\rho C_p)$, m^2/s
μ	coefficient of dynamic viscosity of the fluid, kg/m s
ϕ	particle volumetric concentration
ρ	density, kg/m^3
κ	Boltzmann constant, $1.381 \times 10^{-23} \text{ J/K}$

Subscripts

b	bulk
bf	base fluid
f	fluid
nf	nanofluid
p	particle
w	wall

3.4 Introduction

Nanofluids are prepared by dispersing nanometer-sized particles, generally less than 100 nm, in a base fluid such as water, ethylene glycol, propylene glycol, oil and other conventional heat transfer fluids. Addition of high thermal conductivity metallic nanoparticles (e.g., copper, aluminum, silver) etc. to the base fluid increases the thermal conductivity of such mixtures, thus enhancing their overall heat transfer capability. In the past decade and half, there have been abundant experimental as well as numerical studies to explore the advantages of nanofluids under wide variety of conditions. Several bibliographical references on various aspects of nanofluids research are discussed below.

Choi [1] in 1995 showed from a series of calculations that the thermal conductivity of a fluid can be enhanced by adding nanoparticles. Using the assumption that the Dittus and Boelter [2] correlation, Eq. (3.1), also holds for nanofluids, which appears valid for low particle concentrations, he derived that $h_{nf}/h_{bf} = (k_{nf}/k_{bf})^{2/3}$.

$$Nu=0.023 Re^{0.8}Pr^{0.4} \quad (3.1)$$

Pak and Cho [3] conducted experiments on water based nanofluids containing γ -Al₂O₃ and TiO₂ nanoparticles of mean diameters 13 and 27 nm respectively, and for volumetric concentration ϕ up to 3% to determine their heat transfer and frictional characteristics under turbulent flow conditions. Conducting viscosity measurements up to a high level of 10% volumetric concentration, they found that the viscosity of nanofluids increased substantially with an increase in particle concentration. They presented a Nusselt number correlation for dilute dispersions, which was similar in format to the Dittus-Boelter correlation (Eq. 3.1), except the constant multiplier and the power of Prandtl number were 0.021 and 0.5 respectively. Also for these dilute nanofluids concentrations, the friction factor results agreed with the standard correlation available for single-phase fluids. These results in early stages of nanofluids development gave the hope that dilute concentrations of nanofluids can be modeled as a single-phase fluid. Lee et al. [4] measured thermal conductivity of Al₂O₃ (mean diameter 38 nm) and CuO (mean diameter 23.6 nm) nanofluids in deionized (DI) water and ethylene glycol up to about 4% volumetric concentration, using the transient hot-wire method. Their experimental results showed that for a

copper oxide-ethylene glycol nanofluid the thermal conductivity can be enhanced by more than 20% with a particle volumetric concentration of 4%. Comparison between their measured thermal conductivity of CuO nanofluids with that obtained from the model of Hamilton and Crosser [5] did not agree. Therefore, the Hamilton-Crosser model, which was originally developed for microparticles was found to be inadequate to predict the thermal conductivity of nanofluids correctly and new correlations were necessary. From theoretical analysis, Xuan and Roetzel [6] presented a conceptual form of a correlation for the Nusselt number of nanofluids as a function of Reynolds number, Prandtl number, ratio of thermal conductivities of the solid nanoparticles and that of the base fluid, ratio of the volumetric heat capacities ($C_V = \rho C_p$) of nanoparticles and the base fluid, particle volume fraction, and the particle Peclet number, which is related to the particle size and thermal diffusivity of nanofluids. Eastman et al. [7] used transient hot wire method to measure the thermal conductivity of Cu nanoparticle of mean diameter < 10 nm in ethylene glycol. They found that the effective thermal conductivity increased by up to 40% with approximately 0.3% volumetric concentration of Cu nanoparticles over the base fluid. Koblinski et al. [8] studied the mechanism of heat transfer in nanofluids by considering Brownian motion, liquid/particle interface and the effect of nanoparticles clustering. They drew conclusions that Brownian motion was too slow to transport significant amount of heat, so thermal conductivity enhancements was due to a highly conductive layered structure around the particles and also due to cluster of particles separated by liquid layers thin enough to allow rapid heat flow among particles. Xuan and Li [9] conducted an experiment with copper nanoparticles of below 100 nm diameter seeded in DI water, in the Reynolds number range of 10,000 to 25,000 for developing heat transfer coefficient and friction factor correlations for turbulent flow guided by the conceptual correlation of Xuan and Roetzel [6]. They used dilute nanofluid up to 2% volumetric concentration. They presented a Nusselt number correlation under turbulent flow condition as a function of Reynolds number, Prandtl number, particle Peclet number and the particle volumetric concentration. Their friction factor measurements of dilute nanofluid matched with the correlation for the base fluid, water, implying that the single-phase fluid friction correlation can apply to dilute nanofluids. Das et al. [10] presented the temperature dependency of thermal conductivity of nanofluids with water-based CuO and Al₂O₃ nanoparticles of average particle diameter 28.6 nm and 30.4 nm respectively. Their measured thermal conductivity values of CuO-water nanofluid of 4 % volumetric concentration exhibited

an increment from 14 to 36% over the base fluid with temperature increasing from 21°C to 51°C. They also showed that at temperatures above the room temperature, the Hamilton and Crosser [5] model failed to predict the correct values of thermal conductivities for both Al₂O₃ and CuO nanofluids, consistently under-predicting the correct values. Putra et al. [11] conducted experimental investigation on natural convection in two types of water-based nanofluids. The average diameters were 87 nm and 131 nm for the CuO and Al₂O₃ nanoparticles respectively. Under natural convection, they found that the Nusselt number of nanofluid was lower than that of the base fluid for the same Rayleigh number. We notice that this characteristic is different than the general trend under forced convection, where the Nusselt number may generally be higher than that of the base fluid for the same Reynolds number. However, even if the Nusselt number is lower for the nanofluid, the h_{nf} can still be higher, if k_{nf} is sufficiently enhanced. Wang et al. [12] presented a model based on the fractal theory for the determination of the effective thermal conductivity of nanofluids. They compared the fractal model prediction to experimental data with 50 nm CuO particles in DI water of less than 0.5% volumetric concentration. They mentioned that beyond this dilute limit, the model needs to be refined by taking into account possible deposition effect. Koo and Kleinstreuer [13] derived a model for the effective thermal conductivity of nanofluids that combines the conventional static part represented by Hamilton-Crosser equation plus a dynamic part due to the Brownian motion. This model includes the effects of particle size, volume concentration, temperature, properties of the base fluid and the nanoparticles and the motion of the surrounding fluid moving with the particles. Using their model of effective thermal conductivity and viscosity, Koo and Kleinstreuer [14] showed through a numerical laminar flow analysis that there was an increase in the heat transfer performance of micro-heat sinks with the addition of CuO nanoparticles of particle diameter 20 nm and particle concentration of up to 4% in the base fluids of both water and ethylene glycol.

Wen and Ding [15] conducted experiment with the γ - Al₂O₃ nanoparticle with a size range of 27-56 nm in DI water and presented Nusselt number versus Reynolds number data at the entrance region of a tube under laminar flow condition. They found that the heat transfer enhancement was significantly higher in the entrance region in comparison to the base fluid and decreased along the axial distance. Ding et al. [16] performed experiment on aqueous suspension of multi-walled carbon nanotubes and reported an impressive maximum enhancement of heat

transfer coefficient of 3.5 times compared to the basefluid at Reynolds number of 800, with 0.5% by weight of carbon nanotubes. Khaled and Vafai [17] showed by numerical analysis that heat transfer enhancement can occur with nanofluids flowing through a channel by controlling the thermal dispersion effect across the channel. Maiga et al. [18], through a numerical analysis under laminar flow condition, proved that the γ - Al_2O_3 nanoparticles in water and ethylene glycol had enhanced heat transfer coefficients and Nusselt numbers compared to the base fluid for flow inside a tube and also for radial flow between parallel coaxial heated disks. Their computations revealed a new finding that, as the volumetric concentration of nanofluid increased the length of the thermal entry region decreased. Yang et al. [19] measured laminar flow characteristics of graphite non-spherical nanoparticles of aspect ratio $L/d \approx 0.02$ in automatic transmission oil and synthetic oils. They presented a convective heat transfer correlation of the form $\Omega = a \text{Re}^b$ where Ω is a function of Nu, Pr, L/d and μ_b/μ_w and the constants a and b were curve-fit values obtained from their experimental data. Heris et al. [20] investigated experimentally the behavior of CuO and Al_2O_3 nanofluids of particle size 50-60 nm and 20 nm respectively in water under laminar flow with a constant wall temperature condition and exhibited enhancement of heat transfer coefficient and Nusselt number as volume concentration increased at a fixed Peclet number ($\text{Pe} = \text{Re} \cdot \text{Pr}$). Prasher et al. [21] showed through an order-of-magnitude analysis that the enhancement of thermal conductivity of nanofluids was due to the localized convection caused by the Brownian motion of nanoparticles. They presented a thermal conductivity correlation containing the Maxwell-Garnet model multiplied by functions of Reynolds number, Prandtl number and particle volumetric concentration. Buongiorno [22] evaluated the relative magnitudes of inertia, Brownian diffusion, thermophoresis, diffusiophoresis, Magnus effect, fluid drainage and gravity on convective thermal transport in nanofluids and concluded that Brownian diffusion and thermophoresis were important slip mechanisms in nanofluids. He derived a Nusselt number correlation as a function of Reynolds number, friction factor, Prandtl number and the laminar sub-layer thickness. Liu et al. [23] reported the synthesis of copper nanoparticles in water by a chemical reduction method in which no surfactant was employed to disperse the nanoparticles. They reported a thermal conductivity enhancement of 23.8% with only 0.1 volume percent copper particles. They noticed that the thermal conductivity of their nanofluid exhibited a time dependent behavior, decreasing

considerably with time. We believe this decrease may be due to the agglomeration of nanoparticles in the absence of any surfactant. Wang and Mujumdar [24] presented a review of nanofluids research summarizing in a tabular form 16 different correlations proposed by researchers for the effective thermal conductivity of liquid-particle suspensions. They further summarized a list of 11 experiments on the convective heat transfer measurements on different nanofluids. Mansour et al. [25] studied the effect of uncertainties in physical properties of water- $\gamma\text{Al}_2\text{O}_3$ nanofluid and observed that the heat transfer and pumping power comparisons of different concentrations of nanofluids and the base fluid are quite sensitive to these physical properties. Kim et al. [26] applied Cu, CuO and Al_2O_3 nanoparticles to ammonia-water solution in an absorption refrigeration system. They found that the addition of surfactants and nanoparticles enhanced the absorption performance by 5.32 times over the base fluid. Li et al. [27] compared thermal conductivity measurements of the Al_2O_3 -water nanofluid by transient and steady state methods. They found that at room temperature the results from the steady state and transient methods presented nearly identical values. However, at higher temperatures, natural convection resulted in higher thermal conductivity values with transient method over the steady state method. Jung et al. [28] conducted experiments to study the laminar forced convective heat transfer of nanofluids containing the Al_2O_3 nanoparticles ($d_p=170$ nm; ϕ up to 1.8%) in microchannels. They presented a heat transfer correlation $\text{Nu}=0.014\phi^{0.095}\text{Re}^{0.4}\text{Pr}^{0.6}$ for water-based nanofluid under laminar flow in microchannels. The Al_2O_3 nanoparticle of 1.8% volume concentration dispersed in both the base fluids, water and a mixture of water and ethylene glycol, showed an increase in the convective heat transfer coefficient without any major increase in frictional losses. Nguyen et al. [29] experimentally investigated the heat transfer enhancement of Al_2O_3 nanofluids ($d_p=36$ nm & 47 nm; ϕ up to 6.8%) with water, in a system used for cooling microprocessors. Their experimental data showed that for the Al_2O_3 nanofluid of particle diameter 36 nm and for a particle concentration of 6.8%, the heat transfer coefficient increased by 40% when compared to that of the base fluid. They also found that the convective heat transfer coefficient was higher for 36 nm particle than that of 47 nm particles under equal mass flow rate and volume concentration. Fotukian and Esfahany [30, 31] experimentally investigated the turbulent convective heat transfer and pressure loss of the γ - Al_2O_3 -water ($d_p=20$ nm; ϕ up to 0.14%) and CuO-water ($d_p=30$ -50 nm; ϕ up to 0.236%) nanofluids inside a circular tube. The

results showed that for the Al_2O_3 nanofluid with particle volume concentration of 0.054%, the heat transfer coefficient increased by 48% compared to pure water at a Reynolds number of 10,000. For the CuO nanofluid with particle volume concentration 0.3%, the heat transfer coefficient increased by 25% compared to pure water. The maximum increase in pressure drop was about 20% for the CuO nanofluid of 0.03% volume concentration compared to pure water. For the $\gamma\text{-Al}_2\text{O}_3$ nanofluid with volume concentration of 0.135 % the pressure drop increased by 30% at a Reynolds number of 20,000 compared to pure water.

Sharma et al. [32] conducted experiments on the Al_2O_3 -water nanofluid ($d_p=47$ nm; ϕ up to 0.1%) to evaluate the heat transfer coefficient and friction factor in a circular tube with twisted tape inserts in the transition flow regime. Their results showed that at Reynolds numbers of 3000 and 9000, the heat transfer enhancement in circular tube with 0.1% particle volume concentration are 13.77 % and 23.69% respectively when compared to water. Furthermore, for the same particle volume concentration of 0.1%, the heat transfer enhancement with twisted tape insert inside a circular tube were 36.96% and 44.71% at Reynolds numbers of 3000 and 9000 respectively, when compared to flow of nanofluid in a plain tube. They presented new correlations for Nusselt number and friction factor for nanofluid flow with twisted tape inserts as a function of the twist ratio. Noie et al. [33] experimentally analyzed the heat transfer enhancement in a two-phase closed thermosyphon using the Al_2O_3 -water nanofluid ($d_p=20$ nm; ϕ up to 3%). Their study showed that with the use of nanofluids the efficiency of the thermosyphon increased by up to 14.7%. Farajollahi et al. [34] carried out experiments to evaluate the heat transfer characteristics of $\gamma\text{-Al}_2\text{O}_3$ -water ($d_p=25$ nm; ϕ up to 2%) and TiO_2 -water ($d_p=10$ nm; ϕ up to 0.75%) nanofluids in a shell and tube heat exchanger under turbulent flow condition. From their experimental data they proposed that, there existed two different optimum nanoparticle volumetric concentrations for the two different nanofluids used, beyond which the convective heat transfer coefficient decreased with an increase in the particle volumetric concentration, at a constant Peclet number. They presented that the convective heat transfer coefficients for 0.3, 0.5, 0.75, 1 and 2% of the $\gamma\text{-Al}_2\text{O}_3$ -water nanofluids were about 46, 56, 46, 38 and 19% higher than those of water respectively. Similarly, the convective heat transfer coefficients for 0.15, 0.3, 0.5 and 0.75% of the TiO_2 -water nanofluids were about 20, 56, 33 and 18% higher than those of water respectively. This finding is new and additional research

is warranted to confirm this characteristic. Ferrouillat et al. [35] conducted experimental study on the convective heat transfer and frictional losses using the SiO₂-water nanofluids ($d_p=22$ nm; 5-34 weight %, equivalent to $\phi=2.31-18.79$ vol %) in a horizontal tube with constant wall temperature boundary condition. They performed the measurements at three different conditions (isothermal, heating and cooling) as well as at different inlet temperatures of 20 °C, 50 °C, 70°C with various Reynolds numbers ranging from 200 to 10,000. They concluded that for all the measurements for Reynolds number higher than 1000, a significant heat transfer enhancement of about 50% was observed with the nanofluid volume concentration of 18.79%. To our knowledge, a nanofluid of this volume concentration is the highest measured thus far. They used Performance Evaluation Criterion (PEC) defined as the ratio of heat transferred to the required pumping power in the test section showing that PEC decreases with an increase in the nanoparticle concentration. We believe due to the lower density and viscosity of the SiO₂ nanofluid compared to other nanofluids the pumping power may not be prohibitively high. Lee et al. [36] experimentally measured the effective convection coefficient, viscosity and the thermal conductivity in microtubes for the oxide nanoparticles (Al₂O₃, CuO and ZnO) and carbon nanotubes suspended in DI water. They measured particle sizes in the nanofluids using dynamic light scattering technique and reported that their measured particle sizes were at least four times larger than the nominal particle size claimed by the vendor. This was due to the agglomeration of nanoparticles. They reported an effective convective coefficient increase of 5% for the Al₂O₃ nanofluid of volume concentration 3%, 13.3% for the CuO nanofluid of volume concentration 4% and 11.6% for the carbon nanotube of volume concentration 0.2%. From their measurements they proposed an useful conclusion, that nanofluid is effective as long as the increase in the thermal conductivity of the nanofluid is higher than the one third power of the viscosity increase. Xie et al. [37] experimentally showed an increase in the convective heat transfer coefficient of nanofluids in laminar flow inside a circular copper tube with constant wall temperature. They conducted experiments using four different nanoparticles, MgO, Al₂O₃, TiO₂ and ZnO suspended in 55% distilled water and 45% ethylene glycol by volume as the base fluid. They reported an increase in the heat transfer coefficient of about 252, 40, 18 and 10% for the MgO, Al₂O₃, ZnO and TiO₂ nanofluids of 0.01 % volume concentration respectively, when compared with the base fluid at a Reynolds number of 1000. This highest convective heat transfer

enhancement of 252% for the MgO nanofluid is quite intriguing. Further research should be performed on the MgO nanofluid to confirm this finding. If the pressure loss penalty of this nanofluid is not too severe, this may be an excellent candidate. Sarah et al. [38] conducted experiments on mass transfer to a rotating disk electrode with the CuO nanoparticles (30-50 nm) in distilled water. They presented a new correlation for the Sherwood number as a function of volume concentration, Reynolds number and Schmidt number. From their measurements they concluded that an increase in mass transfer up to 50 % can be attained by adding a small amount of nanoparticles of the order of $\phi=1.94$ %. Kalteh et al. [39] presented a two-phase numerical simulation of Cu-water nanofluid under laminar flow in a microchannel. The conservation equations of the liquid and the solid phases were solved simultaneously. They used microparticle correlations for nanoparticles as new correlations are not available yet. Their analyses showed that the Nusselt number predicted by the two-phase model was much higher than that predicted by a homogeneous single-phase model. Peng et al. [40] measured pressure loss of R113 refrigerant containing the CuO nanoparticles under flow boiling inside a tube for mass fractions of nanoparticle up to 0.5 weight %. Using their experimental data, they presented a nanoparticle impact factor correlation, which can be used for frictional pressure loss calculation for refrigerant based nanofluid.

All these literatures discussed in the preceding paragraphs, support the notion that nanofluids are good candidates for future generation of heat transfer fluids. Reviewing the literatures carefully, we observe that the fluid dynamic and thermal performances of nanofluids are strongly dependent upon their thermophysical properties. And the thermophysical properties of nanofluids are strongly dependent upon temperature, the volumetric concentration and the properties of the dispersed particles. However, no concentrated investigation has appeared in the literature thus far, studying how changes in thermophysical properties due to temperature and concentration variation would affect the heat transfer coefficient and pumping power requirement of nanofluids. In the present paper, our objective is to present such a comprehensive analyses. First we developed correlations of thermophysical properties from measurements of three nanofluids (CuO, Al₂O₃, SiO₂ in 60:40 EG/W). Using those correlations, we studied in detail how variation of nanofluids' properties with concentration and temperature, affect the Prandtl number, Reynolds number, Nusselt number, Muromtseff number, thermal diffusivity etc.

Subsequently we analyze their influence on the heat transfer coefficient, the friction factor and the pumping power. Our study is focused on a base fluid of ethylene glycol and water mixture, because in cold regions of the world, this is the fluid of choice for heat transfer. We have selected a 60:40 EG/W mass ratio because this ratio provides protection against freezing down to the lowest level of -48.3°C as specified in the ASHRAE handbook. Long period of building heating consumes about 40-60% of total energy use in cold regions like Alaska. This study will be useful for applications in cold regions where nanofluids may be successful, in building heating systems, automobile radiators and outdoor heat exchangers in industrial plants.

3.5 Convective Heat Transfer Theory of Nanofluids

Heat transfer coefficient of any fluid is directly proportional to the Nusselt number via the relation $h = (Nu.k)/d$. Pak and Cho [3] were possibly the first to propose an experimentally derived correlation for the Nusselt number for nanofluids, very similar to the well-known correlation due to Dittus-Boelter [2] for single-phase fluids. Pak and Cho proposed

$$Nu_{nf} = 0.021 Re_{nf}^{0.8} Pr_{nf}^{0.5} \quad (3.2)$$

Xuan and Li [9, 41] presented two equations for the Nusselt number of copper-water nanofluids which included the particle Peclet number influence.

$$Nu_{nf} = 0.4328(1.0 + 11.285\phi^{0.754} Pe_d^{0.218}) Re_{nf}^{0.333} Pr_{nf}^{0.4} \quad (\text{For laminar flow}) \quad (3.3)$$

$$Nu_{nf} = 0.0059(1.0 + 7.6286\phi^{0.6886} Pe_d^{0.001}) Re_{nf}^{0.9238} Pr_{nf}^{0.4} \quad (\text{For turbulent flow}) \quad (3.4)$$

The correlations given above (Eqs. 3.2, 3.3 and 3.4) were limited to dilute concentrations (ϕ up to 3 % by Pak and Cho and 2% for Xuan and Li). Both Pak and Choi and Xuan and Li found that the friction factor of nanofluids could be represented by the correlation available for single-phase base fluids. However, for higher nanoparticles concentrations this is not true. Maiga et al. [18] proposed the following correlations from numerical analysis on laminar flow in a tube.

$$Nu_{nf} = 0.086 Re_{nf}^{0.55} Pr_{nf}^{0.5} \text{ (for constant wall heat flux)} \quad (3.5)$$

$$Nu_{nf} = 0.28 Re_{nf}^{0.35} Pr_{nf}^{0.36} \text{ (for constant wall temperature)} \quad (3.6)$$

For turbulent flow, Maiga et al. [42] presented the following correlation from numerical results obtained with flow in a tube using the Al₂O₃ nanoparticles suspension in water.

$$Nu_{nf} = 0.085 Re_{nf}^{0.71} Pr_{nf}^{0.35} \quad (3.7)$$

Buongiorno [22] proposed the following correlation for nanofluid heat transfer in turbulent flow.

$$Nu_{nf} = \frac{\frac{f}{8} (Re_{nf} - 1000) Pr_{nf}}{1 + \delta_v^+ \sqrt{\frac{f}{8} (Pr_v^{2/3} - 1)}} \quad (3.8)$$

where δ_v^+ is dimensionless thickness of laminar sub-layer and Pr_v is the Prandtl number in the laminar sub-layer. Vajjha et al. [43] performed experiments on three nanofluids under constant heat flux boundary conditions and proposed the following heat transfer correlation for flow in the turbulent regime similar in form to the well-known Gnielinski's equation for a single-phase fluid.

$$Nu_{nf} = 0.065 (Re_{nf}^{0.65} - 60.22) (1 + 0.0169 \phi^{0.15}) Pr_{nf}^{0.542} \quad (3.9)$$

To represent the friction factor of nanofluids they developed an equation that reproduced the well-known Blasius equation in the degenerate case of a base fluid.

$$f_{nf} = 0.3164 Re_{nf}^{-0.25} \left(\frac{\rho_{nf}}{\rho_{bf}} \right)^{0.797} \left(\frac{\mu_{nf}}{\mu_{bf}} \right)^{0.108} \quad (3.10)$$

It is noted that the heat transfer coefficient of nanofluids are strongly dependent upon the Reynolds number, Prandtl number and the fluid friction is dependent up on the Reynolds number. These dimensionless numbers are functions of the thermophysical properties of nanofluids, which are investigated in the following sections.

3.6 Development of Correlations for Thermophysical Properties

3.6.1 Viscosity

Namburu et al. [44] conducted measurements of viscosity of copper oxide nanoparticles dispersed in 60:40 EG/W using the LV DV-II+ Brookfield viscometer [45] with a Julabo computer controlled temperature bath to set the nanofluid's temperature at different values. They presented the following correlation for the viscosity of CuO nanofluid as a function of concentration and temperature.

$$\log \mu_{nf} = C_1 e^{(-C_2 T)} \quad (3.11)$$

where $C_1 = 1.8375(\phi)^2 - 29.643(\phi) + 165.56$ with $R^2 = 0.9873$ and $C_2 = 4 \times 10^{-6}(\phi)^2 - 0.001(\phi) + 0.0186$ with $R^2 = 0.9881$. This correlation, Eq. (3.11), was based on volumetric concentration of $0 \leq \phi \leq 0.06$ and within a temperature range of $-35^\circ C < T < 50^\circ C$ for their application in cold regions.

Namburu et al. [46] further conducted similar measurements on SiO₂ nanofluids and developed a correlation similar to Eq. (3.11). Sahoo et al. [47] measured the rheological properties of Al₂O₃ nanofluids from -35°C to 90°C and developed two correlations for the viscosity; one in the low temperature regime (-35°C to 0°C) and the other in the high temperature regime (0°C to 90°C) given by

$$\mu_{nf} = D e^{\left(\frac{E}{T} + F\phi\right)} \quad (3.12)$$

where D, E and F were numerical constants. This was an improvement over the correlation previously given by Namburu et al. as these coefficients were not functions of ϕ . However, these

constants were different for each temperature regimes. Having different types of equations for each nanofluid were cumbersome. Therefore, Vajjha and Das [48] carefully analyzed all the data of Namburu et al. [44, 46] and Sahoo et al. [47] to develop a general correlation for viscosity of these nanofluids. They derived a correlation which expressed the viscosity in a non-dimensional form, valid for all three nanofluids.

$$\frac{\mu_{nf}}{\mu_{bf}} = A_1 e^{(A_2 \phi)} \quad (3.13)$$

In the above generalized correlation, A_1 and A_2 are constants and not functions of ϕ , unlike previous correlations. The values of constants A_1 and A_2 are given in Table 3.1.

It is observed that μ_{bf} , the viscosity of the base fluid takes care of the temperature dependency on viscosity in Eq. (3.13), so that no additional term involving T is necessary as in Eqs. (3.11,3.12). The above correlation is applicable in the temperature range of $273K(0^\circ C) < T < 363K(90^\circ C)$, which encompasses the operating range of heat transfer fluids in building heating and cooling and in automobile radiators in cold regions of the world.

Figure 3.1(a) shows the experimental and curve-fit values predicted by Eq. (3.13) of viscosity against temperature for the Al_2O_3 nanofluid for different volumetric concentration of particles in 60:40 EG/W. The viscosity decreases with an increase in temperature and increases with an increase in the particle volumetric concentration. The average deviation between the data and correlation is of the order of 1%. Notice that the viscosity of Al_2O_3 nanofluid of 6% volumetric concentration at 323 K is 2.18 times that of the base fluid. Therefore, the viscosity of a fluid is highly impacted by the addition of nanoparticles. This shows that viscosity plays a strong role in influencing the performance of nanofluids.

3.6.2 Thermal Conductivity

From recent literatures it is noticed that the thermal conductivity is the most widely studied property of nanofluids. It has been measured by many researchers and several models have been proposed. Most of the research has concentrated on water-based nanofluids and only a limited amount of data exists for ethylene or propylene glycol-based nanofluids, which are required in the cold regions. Prasher et al. [21] developed a convective-conductive model, which

is a combination of Maxwell-Garnett conduction model plus the convection caused by the Brownian motion of suspended nanoparticles. Their equation is expressed as

$$\frac{k_{nf}}{k_{bf}} = (1 + A \text{Re}^m \text{Pr}^{0.333} \phi) \left(\frac{[k_p(1 + 2\alpha) + 2k_m] + 2\phi[k_p(1 - \alpha) - k_m]}{[k_p(1 + 2\alpha) + 2k_m] - \phi[k_p(1 - \alpha) - k_m]} \right) \quad (3.14)$$

where A and m are constants for a particular fluid, $k_m = k_{bf} [1 + (1/4) \text{Re} \cdot \text{Pr}]$ is called the matrix conductivity; $\text{Re} = \frac{1}{\nu} \sqrt{\frac{18\kappa T}{\pi \rho_p d_p}}$ is the Brownian-Reynolds number; $\alpha = 2R_b k_m / d_p$ is the nanoparticle Biot number and R_b is the interfacial thermal resistance between nanoparticles and the fluid.

Koo and Kleinstreuer [13] presented a different type of model for spherical nanoparticles combining the well-known Hamilton-Crosser conduction term with a Brownian motion driven convective term presented below.

$$k_{nf} = \frac{k_p + 2k_{bf} - 2(k_{bf} - k_p)\phi}{k_p + 2k_{bf} + (k_{bf} - k_p)\phi} k_{bf} + 5 \times 10^4 \beta \phi \rho_{bf} C_{\rho bf} \sqrt{\frac{\kappa T}{\rho_p d_p}} f(T, \phi) \quad (3.15)$$

The factor β is a function of ϕ and is dependent on the type of nanoparticles. The term $f(T, \phi)$ is functions of T and ϕ . Both β and $f(T, \phi)$ are derived as curve-fit constants from the experimental data.

Vajjha and Das [49] measured the thermal conductivity of CuO, Al₂O₃ and ZnO nanofluids of several volumetric concentrations in the 60:40 EG/W base fluid. Subsequently Sahoo [50] extended that work to the thermal conductivity of SiO₂ nanofluid. Vajjha and Das and Sahoo found their experimental data on these four nanofluids to agree well with the model of Koo and Kleinstreuer [13]. Vajjha and Das developed the functional relationships for β and $f(T, \phi)$ from their experimental data. The effective thermal conductivity of these four nanofluids can be represented by Eq. (3.15). The first term represents the static conductivity part and the second term is the dynamic part arising due to the enhancement in conductivity caused by the Brownian

motion. The second term includes the effect of particle size, particle volumetric concentration, temperature and properties of base fluid, as well as the influence of Brownian motion. Vajjha and Das derived the function $f(T, \phi)$ denoted by Eq. (3.16) for the four nanofluids CuO, Al₂O₃, ZnO and SiO₂.

$$f(T, \phi) = (2.8217 \times 10^{-2} \phi + 3.917 \times 10^{-3}) \left(\frac{T}{T_0} \right) + (-3.0669 \times 10^{-2} \phi - 3.91123 \times 10^{-3}) \quad (3.16)$$

They developed the correlation for β (fraction of the liquid volume that travels with a particle) from their experimental data presented in Table 3.2 for all four nanofluids.

Figure 3.1(b) shows the variation of the thermal conductivity with temperature for various volumetric concentrations of the CuO nanofluid from the experimental results of Vajjha and Das [49]. It is observed that the thermal conductivity increases with an increase in the particle volumetric concentration and also with an increase in the temperature. There is a significant enhancement of thermal conductivity of nanofluids over the base fluid. For example, at 323 K the thermal conductivity is increased by about 40% for the CuO nanofluid of 6% particle concentration over the base fluid.

3.6.3 Specific Heat

An early equation for the specific heat of nanofluids was given by Pak and Cho [3], which had also appeared in the literature for microparticles and liquid mixtures. Subsequently, Xuan & Roetzel [6] presented an improved correlation given by Eq. (3.17), which assumed thermal equilibrium between the nanoscale solid particles and the liquid phase.

$$C_{pnf} = \frac{\phi \rho_p C_{pp} + (1 - \phi) \rho_{bf} C_{pbf}}{\rho_{nf}} \quad (3.17)$$

The equation proposed by Pak and Cho and Eq. (3.17) were all theoretical relations and experimental studies on this property of nanofluids are very limited. Vajjha and Das [51] carried out measurements of specific heat of three different nanofluids (Al₂O₃, SiO₂ and ZnO) to

develop appropriate correlations. From their experimental data, they developed a general correlation given by Eq. (3.18), where the values of A, B and C are given in Table 3.3. The maximum and average deviation between measured data and curve-fit Eq. (3.18) are given in this table. In Figure 3.3, a comparison between the experimental data, the proposed correlation, Eq. (3.18) and the theoretical equation given by Eq. (3.17) is shown.

$$\frac{C_{pmf}}{C_{pbf}} = \frac{(A(T/T_0) + B(C_{pp}/C_{pbf}))}{(C + \phi)} \quad (3.18)$$

For the base fluid, the maximum deviation between the ASHRAE data and our measurements is 8% occurring at 358 K. The deviation between the theoretical relation, Eq.(3.17), and the experimental data in Fig. 3.2(a) may be due to the fact that the particles may not be in thermal equilibrium with the surrounding liquid due to the random motion and differing thermal properties of particles from the fluid. The specific heats of these nanofluids decrease with an increase in the particle volumetric concentration. This is attributed to the fact that solid particles have lower specific heat compared to the base fluid.

Using correlations, Eqs. (3.17) and (3.18), the specific heats of SiO₂, Al₂O₃ and CuO nanofluids of 2% volumetric concentration were calculated and plotted in Fig. 3.3(a). It was observed from the plot that the CuO nanofluid had the lowest specific heat because this material had lower specific heat compared to the other two nanoparticles. The changes in specific heats are modest compared to the changes in the viscosity and thermal conductivity of nanofluids due to the addition of the same volume concentration of nanoparticles. As the temperature of the nanofluid increases, the effective specific heat also increases very modestly indicating that nanofluids possess slightly better thermal capacity at higher temperature.

3.6.4 Density

Vajjha et al. [52] measured the density of three different nanofluids containing aluminum oxide, antimony-tin oxide and zinc oxide nanoparticles in a base fluid of 60:40 EG/W, using the Anton Paar digital density meter. These measurements were compared with the theoretical equation given by Pak and Cho [3].

$$\rho_{nf} = \rho_p \phi + \rho_{bf} (1 - \phi) \quad (3.19)$$

In Figure 3.2(b), the comparisons between experimental values and prediction via Eq. (3.19) for the Al₂O₃ nanofluid have been shown. A good agreement between the measured and predicted values is observed. Vajjha et al. further showed that the CuO and SiO₂ nanofluids also exhibited similar close agreement. Hence Eq. (3.19) can be accepted as a general correlation for all types of nanofluids. The density of nanofluids increases with an increase in the volumetric concentration of the particles as their densities are higher than that of the base fluid. The density of nanofluid decreases very modestly with temperature mostly due to the effect on the fluid.

To compare the increase in densities, we calculate using Eq. (3.19) the values for CuO, Al₂O₃ and SiO₂ nanofluids. By the addition of 2% volume of nanoparticles at 323 K, the densities of CuO, Al₂O₃ and SiO₂ nanofluids increase by 10.14, 4.73, 2.15%, respectively in comparison to the base fluid. This is due to the higher densities of nanoparticles (CuO= 6500 kg/m³, Al₂O₃= 3600 kg/m³, SiO₂=2220 kg/m³) compared to the base fluid.

Figure 3(b) shows the volumetric heat capacity ($C_v = \rho C_p$) variation of the three nanofluids with particle volumetric concentration at room temperature (293 K). The specific heat of a nanofluid diminishes and its density increases with an increase in particle concentration. We observe that for the CuO nanofluid, the volumetric heat capacity remains practically the same as the concentration is increased. For the other two nanofluids, the C_v diminishes moderately (1.12% for the Al₂O₃ nanofluid and 3.1% for the SiO₂ nanofluid at 6% volumetric concentration compared to the base fluid) with an increase in particle concentration. This shows that the volumetric requirement for nanofluids is not too different from the base fluid to transfer the same amount of heat.

3.6.5 Base Fluid Properties

The thermophysical properties equations summarized in the preceding sections are functions of the properties of the base fluid, which in our case is the 60:40 EG/W. The properties of this fluid were obtained from the data provided in the ASHRAE Handbook [53] and were curve-fitted as a function of the temperature with the following equations.

Density:
$$\rho_{bf} = -0.0024T^2 + 0.963T + 1009.8; R^2=1 \quad (3.20)$$

Viscosity:
$$\mu_{bf} = A_4 e^{\left(\frac{B_4}{T}\right)} ; R^2=0.97; A_4 = 0.555 \times 10^{-3}; B_4 = 2664 \quad (3.21)$$

Thermal Conductivity:
$$K_{bf} = -3 \times 10^{-6} T^2 + 0.0025T - 0.1057 ; R^2=1 \quad (3.22)$$

Specific Heat:
$$C_{pbf} = 4.2483T + 1882.4 ; R^2=1 \quad (3.23)$$

The above equations are valid within the temperature range of $293 \text{ K} \leq T \leq 363 \text{ K}$, which is suitable for building heating and automobile radiators.

For the base fluid the Nusselt number is given by Gnielinski's equation cited in Bejan [54] as

$$Nu = 0.012(Re^{0.87} - 280)Pr^{0.4} \quad \text{valid for } 1.5 \leq Pr \leq 500, 3000 \leq Re \leq 10^6 \quad (3.24)$$

The friction factor equation is the Blasius correlation presented by White [55] given as

$$f = 0.3164 Re^{-0.25} \quad (3.25)$$

3.7 Effect of Properties Variation

3.7.1 Effect on the Prandtl Number

The Prandtl number is dependent on fluid properties, μ , C_p and k , which in turn are dependent on T and ϕ . Figure 3.4(a) shows how adding different volumes of nanoparticles affect the Prandtl number of nanofluids at the room temperature. As the volume concentration of particles increases, the Prandtl number increases more rapidly for the CuO nanofluid. As typical numbers, by adding nanoparticles of 6% volume, the Prandtl number can be enhanced by 124%, 50%, 29% for CuO, Al_2O_3 and SiO_2 nanofluids respectively in comparison with the base fluid at the room temperature of 293 K. As the Nusselt number is proportional to $(Pr)^n$ from Eqs. (3.1) - (3.9), an increase in the Prandtl number will result in an increase in the Nusselt number and subsequently in the convective heat transfer coefficient h .

Figure 3.4(b) shows a comparison of the Prandtl number of CuO, Al₂O₃ and SiO₂ nanofluids of 6% particle concentration as a function of temperature. All three nanofluids offer higher Prandtl number than the base fluid. It is observed that the Prandtl number of all fluids decrease with an increase in temperature. In this case, the viscosity variation takes a dominant role. The specific heat increases very modestly, and the thermal conductivity increases moderately with an increase in temperature. However, the viscosity diminishes substantially with an increase in temperature. Therefore, viscosity's effect is dominant and overcomes the increase of specific heat and thermal conductivity, resulting in a lowering of the Prandtl number. The CuO nanofluid possesses highest Prandtl number among the three nanofluids at a given temperature due to its higher viscosity.

From Figs. 3.4(a) and 3.4(b), we conclude that the concentration and temperature are intertwined to influence the Prandtl number of a nanofluid. Therefore, the Prandtl number of nanofluids can be enhanced either by increasing the concentration or by operating at a lower temperature. The dominant thermophysical property here is viscosity, which is higher at lower temperature and higher at higher particle concentration. For obtaining maximum benefit from nanofluids, optimal temperature and concentration should be found from parametric analysis.

3.7.2 Effect on the Reynolds Number

Figure 3.5(a) shows the variation of the Reynolds number of three nanofluids with temperature for a particle volume concentration of 4%. In this case the velocity and the diameter of the flow passage are held constant for different nanofluids at the values taken from the experiment of Vajjha et al. [43] ($d=0.00337\text{m}$, $V=7\text{m/sec}$) to ensure flow in the turbulent regime. The Reynolds number is a function of density and viscosity. As the temperature increases the density of a nanofluid decreases slightly but the viscosity decreases in a higher proportion, in comparison with the base fluid. The end result is that the Reynolds number increases with an increase in temperature which will increase the Nusselt number. Since the CuO nanofluid possesses higher viscosity than the other two nanofluids at a given temperature, it has the lowest Reynolds number.

In Figure 3.5(b), we present the variation of Reynolds number with particle volumetric concentration for a SiO₂ nanofluid at various temperatures. There is a gradual decrease in the Reynolds number with an increase in particle volumetric concentration at all temperatures.

Increase in particle concentration increases the density and the viscosity of the nanofluids. However, the proportion of increase in viscosity value is much higher than the increase in the density value. Therefore, the end result is that there is a decrease in the Reynolds number due to an increase in the concentration. This leads us to conclude that a low particle concentration of nanofluid would be preferable to keep the Reynolds number higher and achieve a higher heat transfer coefficient. The other two nanofluids also exhibit the same trend.

The analyses under sections 3.7.1 and 3.7.2 show that the thermophysical properties of nanofluids affect the Prandtl number and the Reynolds number in a conflicting manner. Higher concentration and lower temperature are better for nanofluids operation in enhancing the Prandtl number and heat transfer. On the other hand, lower concentration and higher temperature are the desirable ingredients to attain higher Reynolds number for nanofluids and enhance the heat transfer. Therefore, the important lesson learned from the present analyses is that before finalizing a design, a careful parametric study should be performed for various combinations of temperatures and concentrations of different nanofluids to eventually arrive at the optimal condition to maximize the heat transfer. This should further be linked to the pumping power requirement on the basis of equal heat transfer, which we have analyzed under Section 3.7.5.

3.7.3 Effect on the Convective Heat Transfer Coefficient

Using Eq. (3.9) and the experimental data of Vajjha et al. [43] ($d=0.00337\text{m}$, $V=7\text{m/sec}$), the convective heat transfer coefficient were calculated for 1 % concentration of nanofluids. The base fluid heat transfer coefficient was obtained from Gnielinski equation, Eq. (3.24). Figure 3.6(a) shows the heat transfer coefficient comparison as a function of temperature. As recommended in the Section 3.7.2, using a low concentration of 1%, the heat transfer coefficient is found to be higher than that of the base fluid up to a temperature of 323 K. However, if the concentration is increased, the decrease in the Reynolds number becomes more dominant than the increase in the Prandtl number and the advantage of nanofluids over the base fluid is diminished. It is noticed that the CuO and Al₂O₃ nanofluids of 1% concentration perform nearly equally in enhancing the heat transfer coefficient h .

3.7.4 Effect on Thermal Diffusivity

Figure 3.6(b) displays the variation of the thermal diffusivity of nanofluids $\alpha_{nf} = k_{nf} / (\rho_{nf} C_{p,nf})$ with respect to the temperature. The thermal diffusivity increases with an increase in temperature and also with an increase in particle concentration, which are positive attributes of nanofluid. Nanofluids will diffuse heat much faster than the base fluid. Therefore, it would be preferred, where a faster rate of heating or cooling is critical. For example, nanofluids will be a better fluid in cooling automobile engines, where the stagnant fluid can be heated up faster, when the engine is starting. Similar benefit applies to nanofluids being heated in a household furnace where the liquid in the loop gets warmed up quickly when the furnace fires. Reviewing the heat transfer correlation of Xuan and Li [9], the Nusselt number is a function of the particle Peclet number, which is inversely proportional to the α_{nf} . An increase in the α_{nf} will result in a decrease in the Nusselt number. However, for nanofluids the particle Peclet number is very small and for turbulent flow Eq. (3.4), the power of Pe is 0.001, which will have a negligible effect on the magnitude of Nusselt number. The CuO nanofluid shows the highest thermal diffusivity at a given temperature among the three nanofluids due to its high value of thermal conductivity.

3.7.5 Effect on the Pumping Power

The pumping power in turbulent flow, with velocity V through a tube of diameter d is given by $\dot{W} = (\pi / 4)(d^2 V)(\Delta P)$, where

$$\Delta P = \frac{fL\rho V^2}{2d} \quad (3.26).$$

Using Eq. (3.26), the pumping power per unit length becomes

$$\frac{\dot{W}}{L} = \frac{\pi}{8} dV^3 [f\rho] \quad (3.27).$$

Let us consider the pumping power required on the basis of equal heat transfer. The heat transfer rate $\dot{q} = hA_s(T_w - T_{bm})$. If surface area A_s and the wall to fluid temperature difference are maintained constant, as in the case of constant heat flux boundary condition, then the heat transfer coefficient h for all fluids will be the same. Adopting a constant value for h and a diameter $d=0.00337$ m from the experimental data of Vajjha et al. [43], we computed the Reynolds number from Eq. (3.9) and Eq. (3.24) for nanofluids and the base fluid respectively. Then we calculated the friction factor for nanofluids and the base fluid from the Eq. (3.10) and Eq. (3.25) respectively, and the velocities were calculated from the Reynolds numbers for different fluids. Finally, the pumping power per unit length was calculated from Eq. (3.27) for a 2% volumetric concentration and plotted in Fig. 3.7(a) as a function of temperature. Figure 3.7(a) shows that at a given temperature, all three nanofluids require less pumping power than the base fluid for the same amount of heat transfer and their performance is superior at lower temperatures. The Al_2O_3 nanofluid shows the best performance requiring the least amount of pumping power among the three nanofluids on the basis of equal heat transfer.

The variation of pumping power with particle volumetric concentration of nanofluids at the room temperature of 293K is displayed in Fig. 3.7(b). The calculations follow the same procedure of equal heat transfer basis used in generating the plots in Fig. 3.7(a). We notice from Fig. 3.7(b) that Al_2O_3 and SiO_2 nanofluids require less pumping power than the base fluid, whereas the CuO nanofluid would require more pumping power than the base fluid beyond a volumetric concentration of about 3%. This is due to the high viscosity value of the CuO nanofluid compared to the other two nanofluids.

3.7.6 Effect on Mouromtseff number

Simons [56] presented the effectiveness of various liquid coolants for electronic cooling using the concept of Mouromtseff number, Mo . The Mouromtseff number is a Figure of Merit (FOM) for comparing the relative heat transfer capability of different fluids. This number is proportional to the convective heat transfer coefficient h and only considers the contributions of thermophysical properties of the fluid for a fixed geometry and velocity. Higher Mo indicates better heat transfer capability of fluids. The Mouromtseff number for fully developed internal flow is given by [56]:

$$Mo = \frac{k^a \rho^b c_p^d}{\mu^e} \quad (3.28)$$

where the exponents a, b, d, and e take on values appropriate to the heat transfer mode of interest and the corresponding heat transfer correlation. For fully developed internal laminar flow, $Mo_{nf}/Mo_{bf} \approx h_{nf}/h_{bf} \approx K_{nf}/K_{bf}$, since Nusselt number is constant for both fixed wall temperature and fixed heat flux conditions. For internal turbulent flow:

$$Mo_{nf}/Mo_{bf} \approx \{h_{nf} \text{ from Eq. (3.2)} / h_{bf} \text{ from Eq. (3.1)}\}. Mo_{nf} \propto h_{nf} = \frac{\rho_{nf}^{0.8} C_{pnf}^{0.5} k_{nf}^{0.5}}{\mu_{nf}^{0.3}} \text{ and}$$

$$Mo_{bf} \propto h_{bf} = \frac{\rho^{0.8} C_p^{0.4} k^{0.6}}{\mu^{0.4}}.$$

Figure 3.8 shows the relative heat transfer rate (Mo_{nf} / Mo_{bf}) versus temperature for different nanofluids and the base fluid under laminar as well as turbulent flow regimes. In both cases the FOM is greater than 1 indicating that nanofluids are superior to the base fluid under both laminar and turbulent conditions. It turns out that dilute concentration of nanofluid works better under turbulent flow, whereas higher concentration works better for laminar flow.

3.7.7 Effect on Thermal and Fluid Dynamic Performance

An early equation for the efficiency of heat and momentum transfer was given by Engasser and Horvath [57]; expressed as $(Nu/Eu) = (d/4L)Re$. The same concept may be extended to evaluate nanofluids, for comparing their thermal and fluid dynamic performances. The Nusselt number represents a measure of heat transfer and the Euler number (Eu) represents a measure of pressure loss due to pumping effort to achieve that heat transfer. Thus, this ratio can be considered as a ratio of thermal energy transferred to the mechanical energy needed. The Energy Ratio $ER = Nu/Eu$, where Eu is given by Shah and Sekulic [58].

From our experimental data [43] we have used a tube diameter $d = 0.003337$ m, $V = 7$ m/sec for flow in the turbulent regime. The Nusselt number is calculated by Eq. (3.9) for nanofluids and Eq. (3.24) for the base fluid. The Euler number is calculated from the pressure loss per unit length of the tube based on Eq. (3.26). The friction factors were calculated using Eq. (3.10) for nanofluids and Eq. (3.25) for the base fluid. Figure 3.9 shows the thermal and fluid dynamic

performance ratio for the Al_2O_3 nanofluid up to 6% concentration and the base fluid at the room temperature of 293 K as a function of the Reynolds number. The ER improves as the concentration of the nanofluid is increased at equal Reynolds number. Other nanofluids exhibit a similar characteristic.

3.8 Conclusions

Addition of nanoparticles to a liquid increases the viscosity significantly and the thermal conductivity moderately, however the specific heat and density change modestly. For example, the viscosity of the Al_2O_3 nanofluid of 6% volumetric concentration increases by 91% in comparison to the base fluid of 60:40 EG/W at the room temperature of 293 K. Under the same conditions the thermal conductivity of the same nanofluid increases by 22.4%, the density by 13.9% and the specific heat decreases by 13.2%. Prandtl number of nanofluids increases as particle volume concentration increases (e.g. for the CuO nanofluid of 6% concentration the increase is 124%), but decreases with an increase in the temperature. Reynolds number of nanofluid for a specified geometry and velocity increases with temperature and decreases with an increase in particle volumetric concentration. As an example, for the SiO_2 nanofluid of 4% concentration examined in this paper, the Reynolds number increases from 3900 at 293 K to 11395 at 333 K, an increase of 192%, predominantly due to the decrease in viscosity. The convective heat transfer coefficient of nanofluids increases with an increase in temperature and concentration and is significantly higher than that of the base fluid. As an example, for a 1% Al_2O_3 nanofluid the convective heat transfer coefficient can increase by 31.9% compared to the base fluid at room temperature. There exists an optimal range of temperature and concentration at the dilute level, where the benefits of nanofluids can be maximized. The thermal diffusivity of nanofluid increases with an increase in particle concentration and temperature. This increase is primarily due to the increase in thermal conductivity while the product of (ρC_p) remains nearly constant. The increase in thermal diffusivity for a 2% CuO nanofluid at 333 K is 28%, which is a desirable property for some applications. For a constant rate of heat transfer, the pumping power for the nanofluid can be lower than that of the base fluid. For example, the 60:40 EG/W base fluid would require 83.3% higher pumping power in comparison to a 2% Al_2O_3 nanofluid at the room temperature of 293 K for the same amount of heat transfer. The Mouriomtseff numbers of nanofluids are higher than that of the base fluid proving that nanofluids can be more efficient

than the conventional fluids under both laminar and turbulent flow conditions. The energy ratio (ER) for the nanofluid is higher than that of the base fluid at equal Reynolds number. From the pumping power requirement study, we observe that a dilute concentration of the Al_2O_3 nanofluid has the best combination of properties over the other fluids to yield a superior level of heat transfer at lower pumping power and may become an effective new generation heat transfer fluid.

3.9 References

1. S.U.S. Choi, Enhancing thermal conductivity of fluids with nanoparticles. in: D.A. Siginer and H.P. Wang, Editors, *Developments and Applications of Non-Newtonian Flows*, FED-vol. 231/MD-vol. 66, ASME, New York (1995), pp. 99–105.
2. F.W. Dittus, L.M.K. Boelter, Heat transfer in automobile radiators of the tubular type, *Univ. of Calif. Publ. in Eng.* 11 (1930) 443-461.
3. B.C. Pak, Y.I. Cho, Hydrodynamic and heat transfer study of dispersed fluids with submicron metallic oxide particles, *Exp. Heat Transfer* 11(2) (1998) 151-170.
4. S. Lee, S.U.S. Choi, S. Li, J.A. Eastman, Measuring thermal conductivity of fluids containing oxide nanoparticles, *J. Heat Transfer* 121 (1999) 280-289.
5. R.L. Hamilton, O.K. Crosser, Thermal conductivity of heterogeneous two-component system, I and EC Fundamentals 1 (1962) 187-191.
6. Y. Xuan, W. Roetzel, Conceptions of heat transfer correlation of nanofluids, *Int. J. Heat Mass Transfer* 43 (2000) 3701-3707.
7. J.A. Eastman, S.U. S Choi, S. Li, W. Yu, L.J. Thompson, Anomalous increased effective thermal conductivities of ethylene glycol-based nanofluids containing copper nanoparticles, *Appl. Phys. Lett.* 78 (6) (2001) 718–720.
8. P. Keblinski, S.R. Phillot, S.U.S. Choi, J.A. Eastman, Mechanisms of heat flow in suspensions of nano-sized particles (nanofluids), *Int. J. Heat and Mass Transfer* 45 (2002) 855-863.
9. Y. Xuan, Q. Li, Investigation on convective heat transfer and flow features of nanofluids, *J. Heat Transfer* 125 (2003) 151-155.
10. S.K. Das, N. Putra, P. Thiesen, W. Roetzel, Temperature dependence of thermal conductivity enhancement for nanofluids, *J. Heat Transfer* 125 (2003) 567-574.

11. N. Putra, W. Roetzel, S.K. Das, Natural convection of nano-fluids, *Heat and Mass Transfer* 39 (2003) 775-784.
12. B-X. Wang, L.-P. Zhou, X.-F. Peng, A fractal model for predicting the effective thermal conductivity of liquid with suspension of nanoparticles, *Int. J. Heat Mass Transfer* 46 (2003) 2665-2672.
13. J. Koo, C. Kleinstreuer, A new thermal conductivity model for nanofluids, *J. Nanoparticle Res.* 6 (2004) 577–588.
14. J. Koo, C. Kleinstreuer, Laminar nanofluid flow in microheat-sinks, *Int. J. Heat Mass Transfer* 48 (2005) 2652-2661.
15. D. Wen, Y. Ding, Experimental investigation into convective heat transfer of nanofluids at the entrance region under laminar flow conditions, *Int. J. Heat and Mass Transfer* 47 (2004) 5181-5188.
16. Y. Ding, H. Alias, D. Wen, R.A. Williams, Heat transfer of aqueous suspensions of carbon nanotubes (CNT nanofluids), *Int. J. Heat and Mass Transfer* 49 (2006) 240-250.
17. A.R.A. Khaled, K. Vafai, Heat transfer enhancement through control of thermal dispersion effects, *Int. J. Heat and Mass Transfer* 48 (2005) 2172-2185.
18. S.E.B. Maiga, S.J. Palm, C.T. Nguyen, G. Roy, N. Galanis, Heat transfer enhancement by using nanofluids in forced convection flows, *Int. J. Heat and Fluid Flow* 26 (2005) 530-546.
19. Y. Yang, Z.G. Zhang, E.A. Grulke, W.B. Anderson, G. Wu, Heat transfer properties of nanoparticles-in-fluid dispersions (nanofluids) in laminar flow, *Int. J. Heat and Mass Transfer* 48 (2005) 1107-1116.
20. S.Z. Heris, S.G. Etemad, M.N. Esfahany, Experimental investigation of oxide nanofluids laminar flow convective heat transfer, *Int. J. Heat and Mass Transfer* 33 (2006) 529-535.
21. R. Prasher, P. Bhattacharya, P.E. Phelan, Brownian-motion-based convective-conductive model for the effective thermal conductivity of nanofluids, *J. Heat Transfer* 128 (2006) 588-595.
22. J. Buongiorno, Convective transport in nanofluids, *J. Heat Transfer* 128 (2006) 240-250.
23. M.S. Liu, M.C.-C. Lin, C.Y. Tsai, C.-C. Wang, Enhancement of thermal conductivity with Cu for nanofluids using chemical reduction method, *Int. J. Heat Mass Transfer* 49 (2006) 3028-3033.

24. X.-Q. Wang, A.S. Mujumdar, Heat transfer characteristics of nanofluids: a review, *Int. J. of Thermal Sciences* 46 (2007) 1-19.
25. R.B. Mansour, N. Galanis, C.T. Nguyen, Effect of uncertainties in physical properties on forced convection heat transfer with nanofluids, *Applied Thermal Engineering* 27 (2007) 240-249.
26. J.K. Kim, J.Y. Jung, Y.T. Kang, Absorption performance enhancement by nano-particles and chemical surfactants in binary nanofluids, *Int. J. Refrigeration* 30 (2007) 50-57.
27. C. H. Li, W. Williams, J. Buongiorno, L.-W. Hu, G.P. Peterson, Transient and steady-state experimental comparison study of effective thermal conductivity of Al_2O_3 /water nanofluids, *J. Heat Transfer* 130 (2008) 042407.
28. J.Y. Jung, H.S. Oh, H.Y. Kwak, Forced convective heat transfer of nanofluids in microchannels, *Int. J. Heat and Mass Transfer* 52 (2009) 466-472.
29. C.T. Nguyen, G. Roy, C. Gauthier, N. Galanis, Heat transfer enhancement using Al_2O_3 -water nanofluid for an electronic liquid cooling system, *Appl. Therm. Eng.* 27 (8-9) (2007) 1501–1506.
30. S.M. Fotukian, M.N. Esfahany, Experimental investigation of turbulent convective heat transfer of dilute γ - Al_2O_3 /water nanofluid inside a circular tube, *Int. J. Heat and Fluid Flow* 31 (2010) 606-612.
31. S.M. Fotukian, M.N. Esfahany, Experimental study of turbulent convective heat transfer and pressure drop of dilute CuO /water nanofluid inside a circular tube, *Int. Comm. Heat and Mass Transfer* 37 (2010) 214-219.
32. K.V. Sharma, L.S. Sundar, P.K. Sarma, Estimation of heat transfer coefficient and friction factor in the transition flow with low volume concentration of Al_2O_3 nanofluid flowing in a circular tube with twisted tape insert, *Int. Comm. Heat and Mass Transfer* 36 (2009)503-507.
33. S.H. Noie, S.Z. Heris, M. Kahani, S.M. Nowee, Heat transfer enhancement using Al_2O_3 /water nanofluid in a two-phase closed thermosyphon. *Int. J. Heat and Fluid Flow* 30 (2009) 700-705.
34. B. Farajollahi, S.G. Etemad, M. Hojjat, Heat transfer of nanofluids in a shell and tube heat exchanger, *Int. J. Heat and Mass Transfer* 53 (2010) 12-17.

35. S. Ferrouillat, A. Bontemps, J.P. Ribeiro, J.A. Gruss, O. Soriano, Hydraulic and heat transfer study of SiO₂/water nanofluids in horizontal tubes with imposed wall temperature boundary conditions, *Int. J. Heat and Fluid Flow* 32 (2011) 424-439.
36. J. Lee, P.E. Gharagozloo, B. Kolade, J.K. Eaton, K.E. Goodson, Nanofluid convection in microtubes, *J. Heat Transfer* 132 (2010) 092401-1 to 5.
37. H. Xie, Y. Li, W. Yu, Intriguingly high convective heat transfer enhancement of nanofluid coolants in laminar flows, *Physics Letters A* 374 (2010) 2566-2568.
38. O.N. Sara, F. Icer, S. Yapici, B. Sahin, Effect of suspended CuO nanoparticles on mass transfer to a rotating disc electrode, *Expt. Thermal and Fluid Science* 35 (2011) 558-564.
39. M. Kalteh, A. Abbassi, M.S. Avval, J. Harting, Eulerian-Eulerian two-phase numerical simulation of nanofluid laminar forced convection in a microchannel, *Int. J. Heat and Fluid Flow* 32 (2011) 107-116.
40. H. Peng, G. Ding, W. Jiang, H. Hu, Y. Gao, Measurement and correlation of frictional pressure drop of refrigerant-based nanofluid flow boiling inside a horizontal smooth tube, *Int. J. Refrigeration* 32 (2009) 1756-1764.
41. Q. Li, Y. Xuan, Convective heat transfer and flow characteristics of Cu-water nanofluid, *Science in China* (45) (4) (Series E) (2002) 408-416.
42. S.B. Maiga, C.T. Nguyen, N. Galanis, G. Roy, T. Mare, M. Coqueux, Heat transfer enhancement in turbulent tube flow using Al₂O₃ nanoparticle suspension, *Int. J. Numerical Methods for Heat and Fluid Flow* (16) (3) (2006) 275-292.
43. R.S. Vajjha, D.K. Das, D.P. Kulkarni, Development of new correlations for convective heat transfer and friction factor in turbulent regime for nanofluids, *Int. J. Heat and Mass Transfer* 53 (2010) 4607-4618.
44. P.K. Namburu, D.P. Kulkarni, D. Misra, D.K. Das, Viscosity of copper oxide nanoparticles dispersed in ethylene glycol and water mixture, *Exp. Therm. Fluid Sci.* 32 (2007) 67-71.
45. Brookfield DV-IIC Programmable Viscometer Manual, Brookfield Engineering Laboratories Inc., No. M/97-164-D1000. Middleboro, MA, 1999.
46. P.K. Namburu, D.P. Kulkarni, A. Dandekar, D.K. Das, 2007, Experimental investigation of viscosity and specific heat of silicon dioxide nanofluids, *Micro & Nano Letters* 2 (3) (2007) 67-71.

47. B.C. Sahoo, R.S. Vajjha, R. Ganguli, G.A. Chukwu, D.K. Das, Determination of rheological behavior of aluminum oxide nanofluid and development of new viscosity correlations, *Petro. Sci. Tech.* 27 (15) (2009) 1757-1770.
48. R.S. Vajjha, D.K. Das, *Measurements of Thermophysical Properties of Nanofluids and Computation of Heat Transfer Characteristics*, LAP Lambert Academic Publishing, ISBN: 978-3-8383-7214-3, 2010.
49. R.S. Vajjha, D.K. Das, Measurement of thermal conductivity of three nanofluids and development of new correlations, *Int. J. Heat Mass Transfer* 52 (2009) 4675-4682.
50. B.C. Sahoo, *Measurement of Rheological and Thermal Properties and the Freeze-Thaw Characteristics of Nanofluids*, M.S. thesis, University of Alaska Fairbanks, Fairbanks, AK, 2008.
51. R.S. Vajjha, D.K. Das, Specific heat measurement of three nanofluids and development of new correlations, *J. Heat Transfer* 131 (2009) 071601-1 to 7.
52. R.S. Vajjha, D.K. Das, B.M. Mahagaonkar, Density measurements of different nanofluids and their comparison with theory, *Petro. Sci. Tech.* 27 (6) (2009) 612-624.
53. *ASHRAE Handbook, Fundamentals*, American Society of Heating, Refrigerating and Air-Conditioning Engineers Inc., Atlanta, GA, 2005.
54. A. Bejan, *Heat Transfer*, John Wiley & Sons, Inc., New York, 1993.
55. F.M. White, *Fluid Mechanics*, second ed., McGraw-Hill, Inc., New York, 1986.
56. R.E. Simons, Comparing heat transfer rates of liquid coolants using the Mouromtseff number, *Electronics Cooling* 12 (2) (2006).
57. J.M. Engasser, C. Horvath, Efficiency of mass and momentum transport in homogeneous and two-phase flow, *Industrial & Engineering Chemistry Fundamentals* 14 (2) (1975) 107-110.
58. R.K. Shah, D.P. Sekulic, *Fundamentals of Heat Exchanger Design*, John Wiley & Sons, Inc., New Jersey, 2003.

Table 3.1. Constants of the viscosity correlation for different nanofluids.

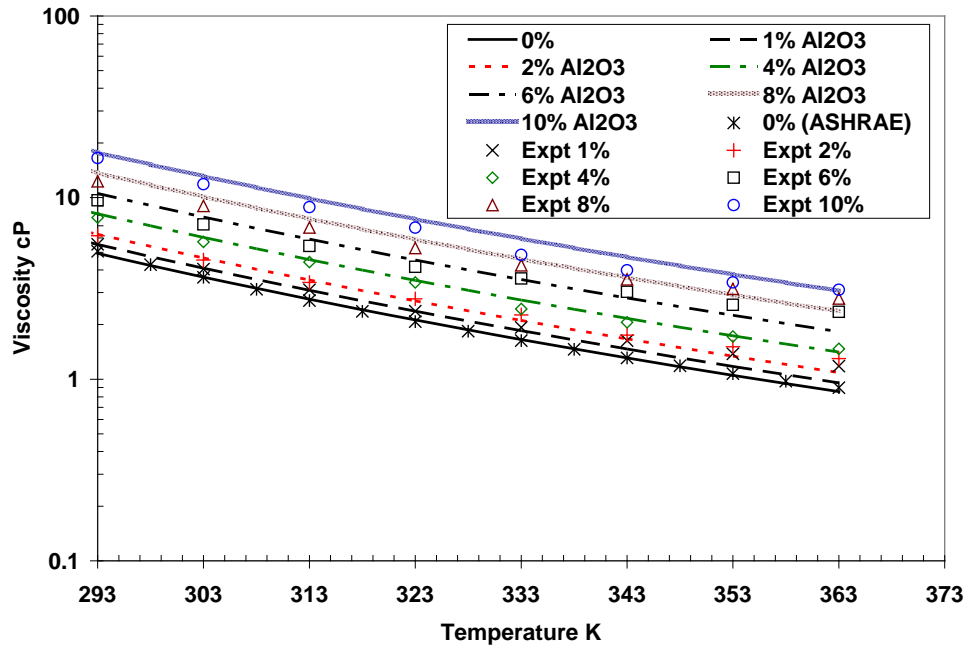
Nanoparticles	A ₁	A ₂	Average Particle Size (nm)	Concentration (%)
Al ₂ O ₃	0.983	12.959	45	0 < ϕ < 0.1
CuO	0.9197	22.8539	29	0 < ϕ < 0.06
SiO ₂	1.092	5.954	20	0 < ϕ < 0.1
SiO ₂	0.9693	7.074	50	0 < ϕ < 0.06
SiO ₂	1.005	4.669	100	0 < ϕ < 0.06

Table 3.2. Curve-fit relations for β from experiments.

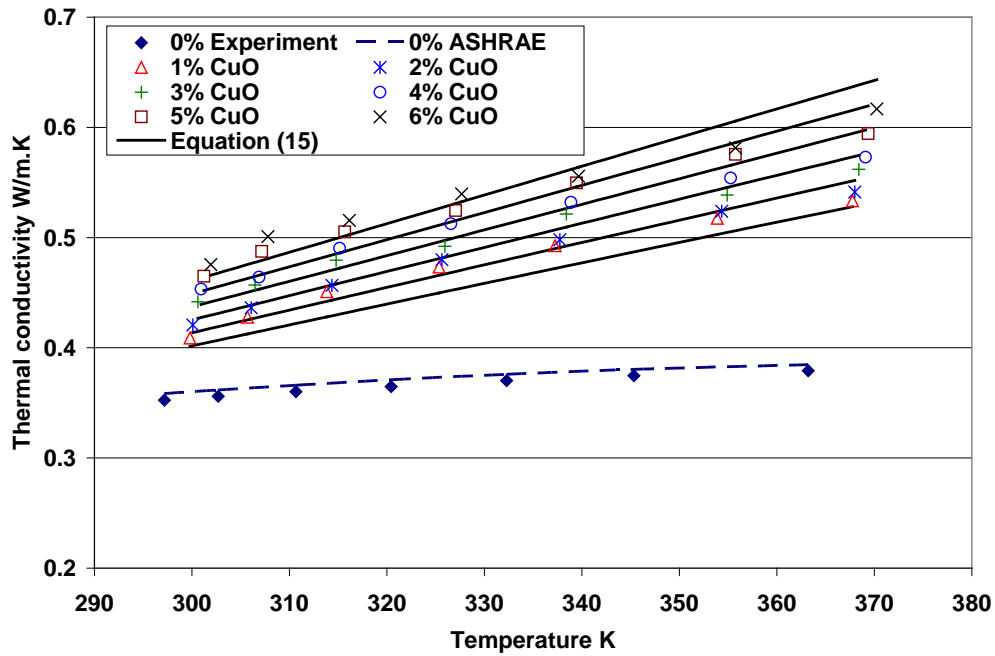
Type of particles	β	Concentration	Avg. Particle size (nm)	Temperature (K)
Al ₂ O ₃	$8.4407(100\phi)^{-1.07304}$	1% ≤ ϕ ≤ 10%	53	298 ≤ T ≤ 363
ZnO	$8.4407(100\phi)^{-1.07304}$	1% ≤ ϕ ≤ 7%	29 & 77	298 ≤ T ≤ 363
CuO	$9.881(100\phi)^{-0.9446}$	1% ≤ ϕ ≤ 6%	29	298 ≤ T ≤ 363
SiO ₂	$1.9526(100\phi)^{-1.4594}$	1% ≤ ϕ ≤ 10%	30	298 ≤ T ≤ 363

Table 3.3. Curve-fit coefficients for specific heat of different nanofluids.

Nanofluid	A	B	C	Max. deviation %	Avg. absolute deviation %
Al ₂ O ₃	0.0008911	0.5179	0.4250	5	2.28
SiO ₂	0.001769	1.1937	0.8021	3.1	1.5
ZnO	0.0004604	0.9855	0.299	4.4	2.7

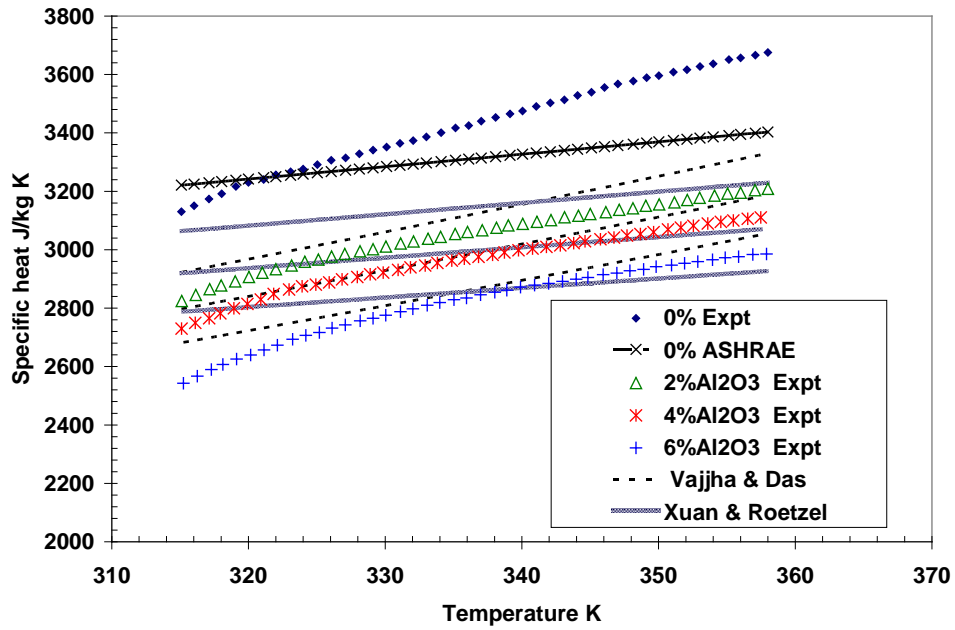


(a)

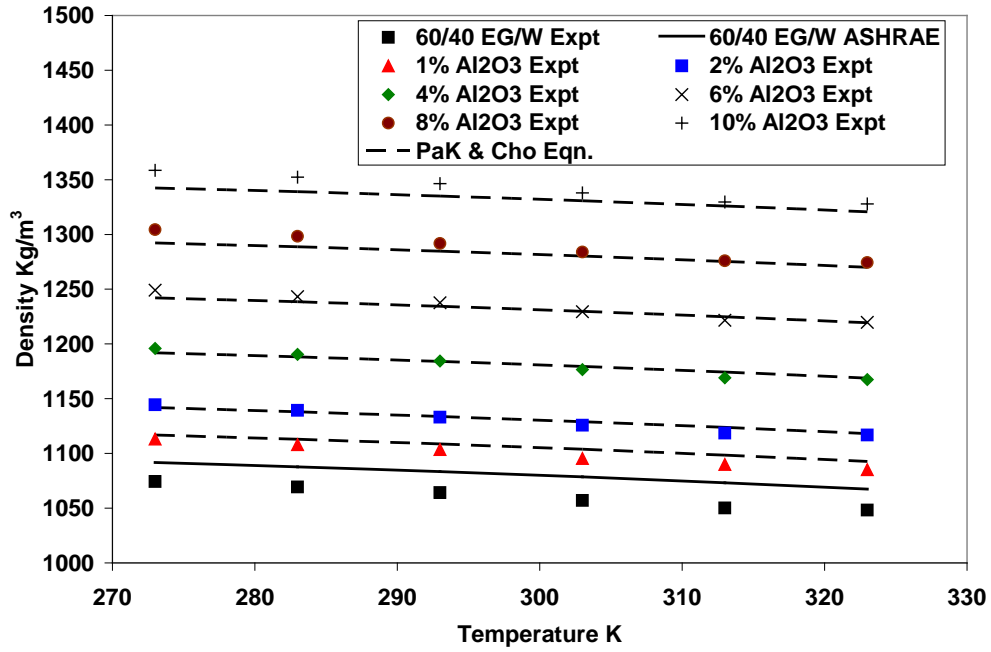


(b)

Figure 3.1. Comparison of experimental values with correlations for different particle volumetric concentrations as a function of temperature (a) viscosity; (b) thermal conductivity.

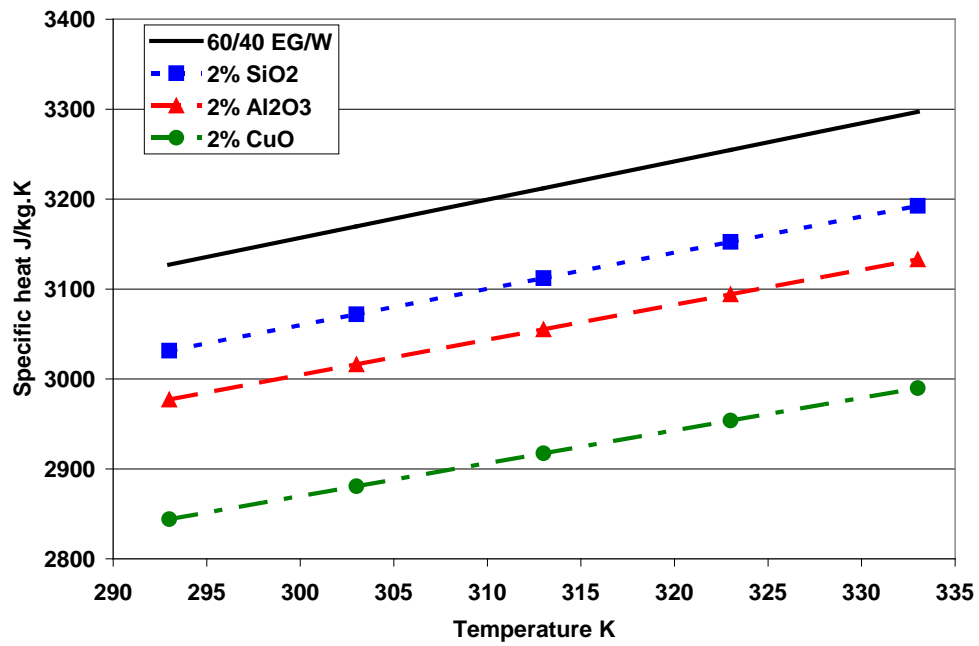


(a)

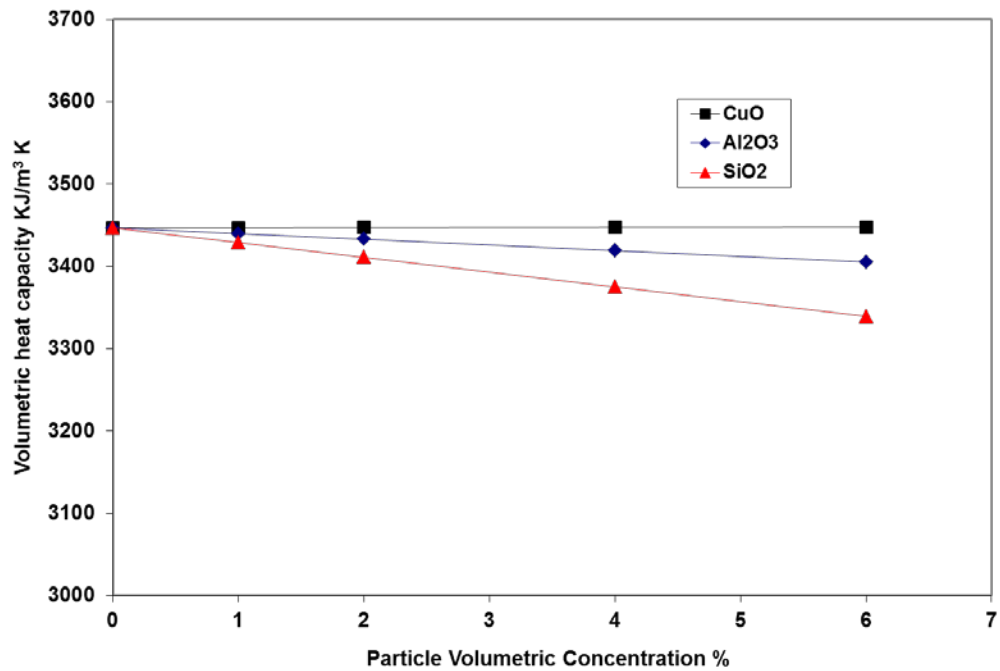


(b)

Figure 3.2. Comparison of experimental values with correlations for different particle volumetric concentrations as a function of temperature (a) specific heat; (b) density.

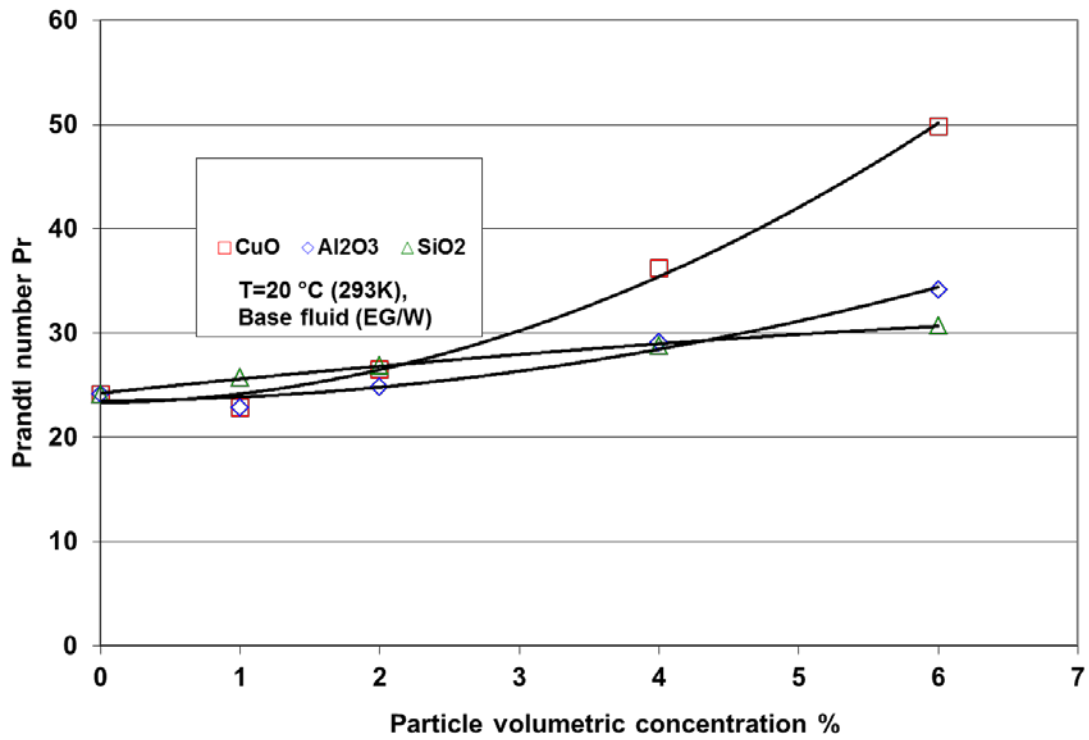


(a)

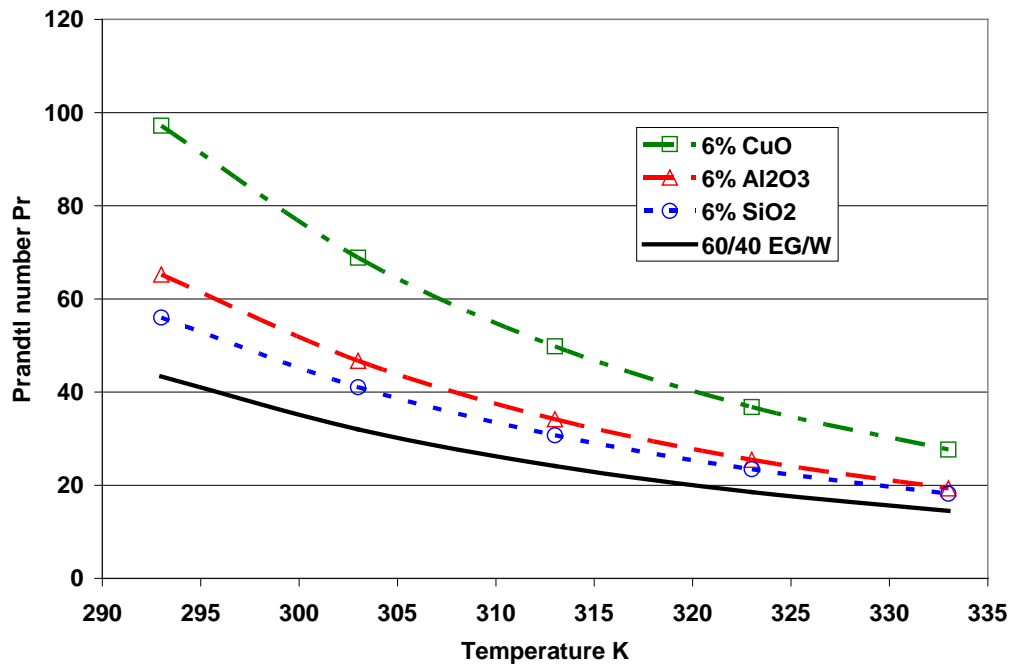


(b)

Figure 3.3. Variation of (a) specific heat with temperature (b) volumetric heat capacity with particle volumetric concentration at 293 K.

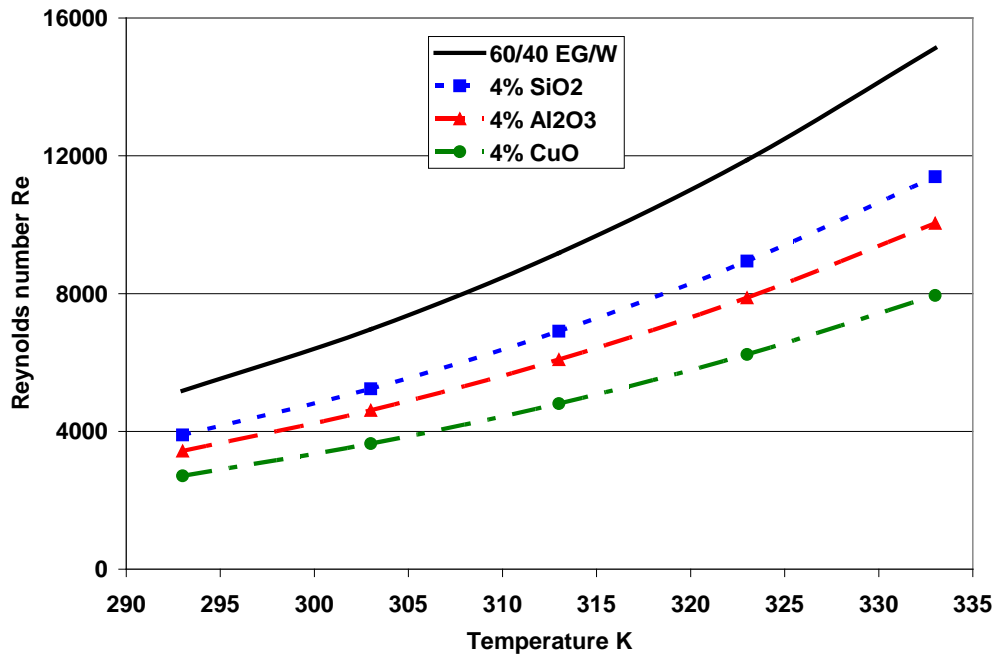


(a)

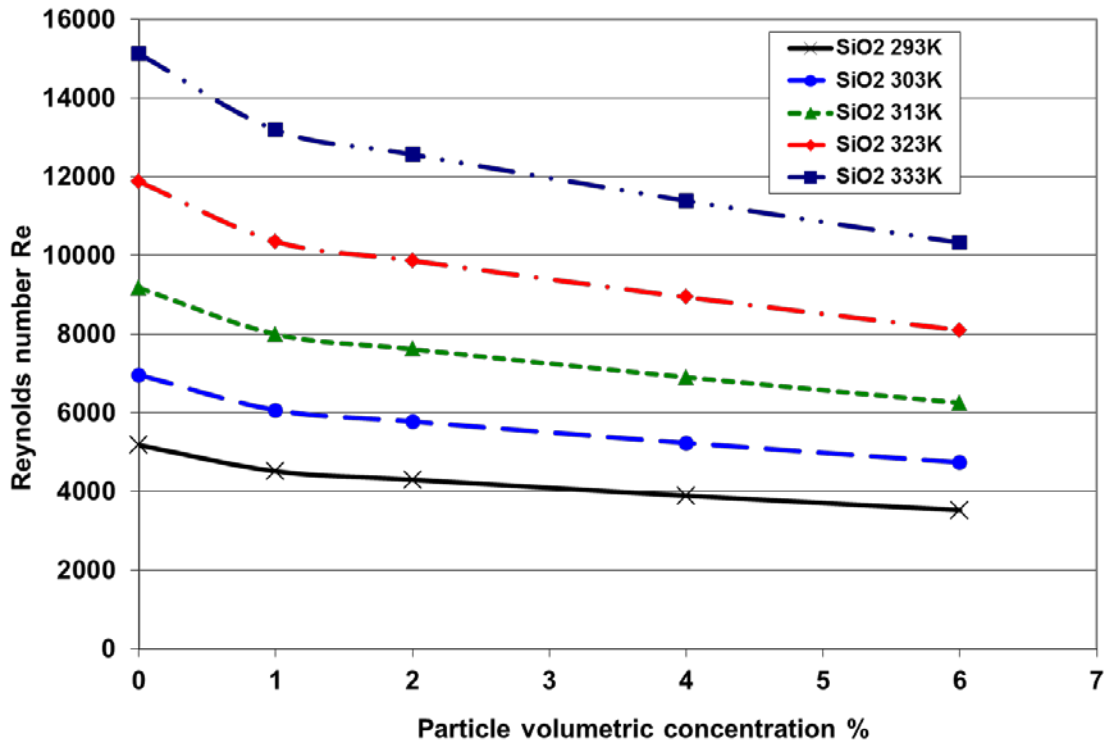


(b)

Figure 3.4. Variation of Prandtl number with (a) particle volumetric concentration and (b) temperature.

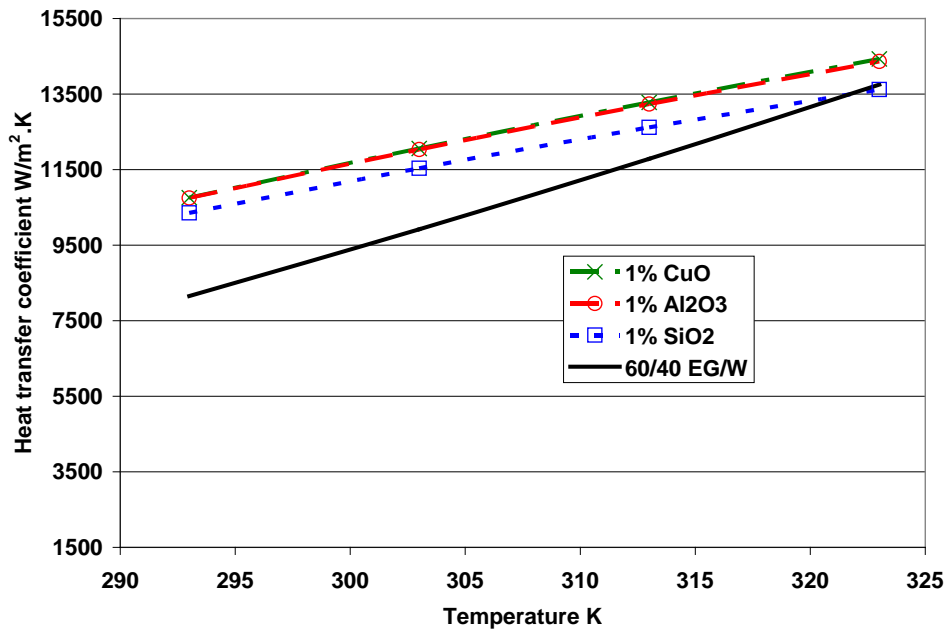


(a)

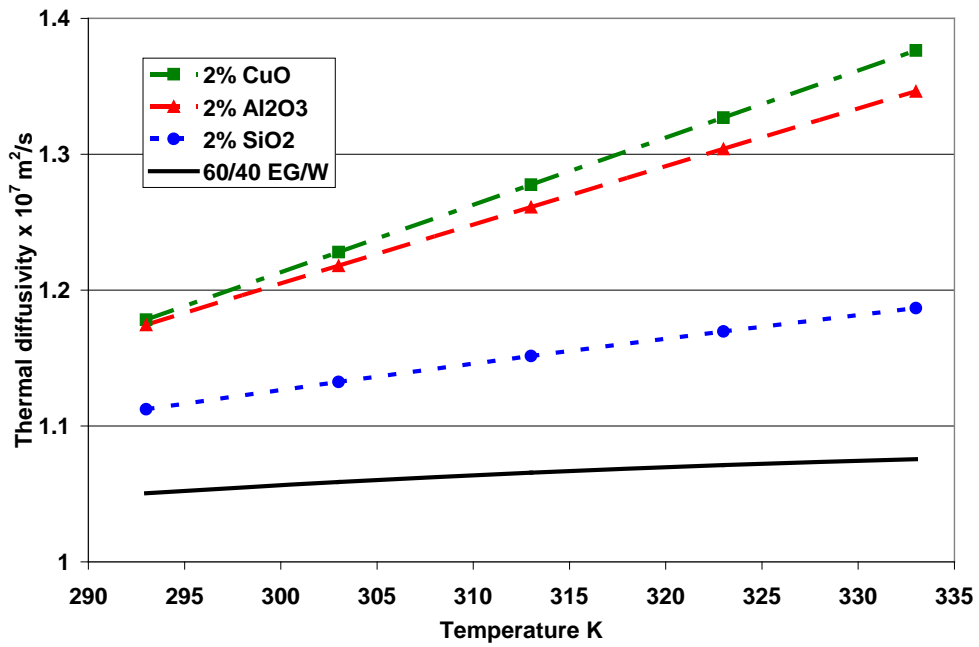


(b)

Figure 3.5. Variation of Reynolds number with (a) temperature for three nanofluids and basefluid (b) particle volumetric concentrations for the SiO₂ nanofluid at various nanofluids.

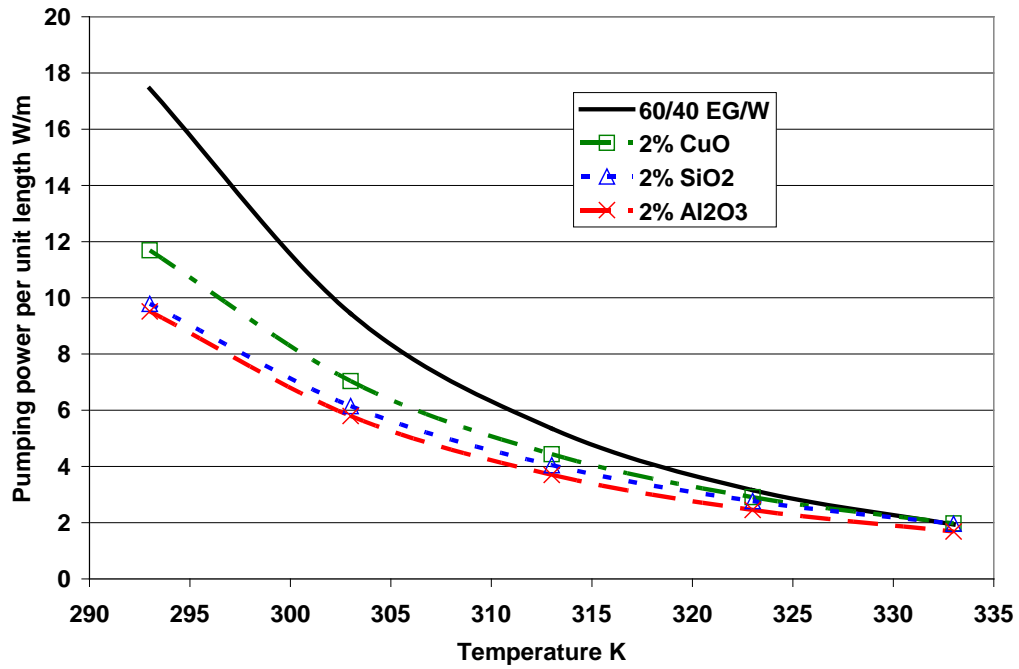


(a)

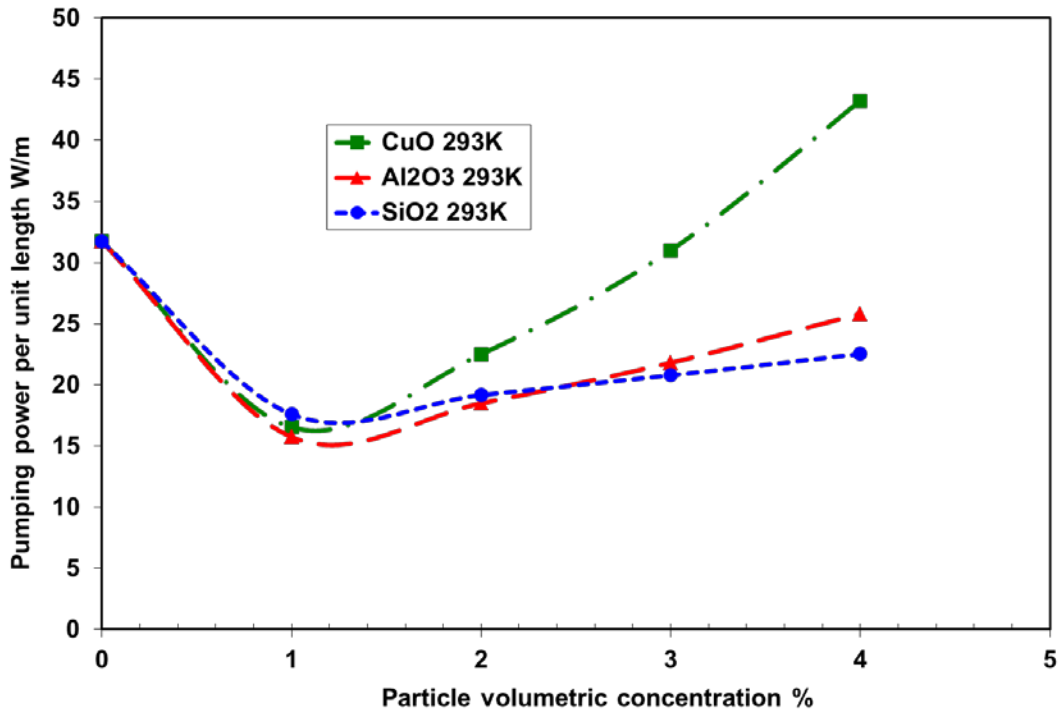


(b)

Figure 3.6. Effect of temperature variation (a) on the heat transfer coefficient and (b) on the thermal diffusivity.



(a)



(b)

Figure 3.7. Variation of pumping power per unit length (a) influence of temperature (b) influence of particle volumetric concentration.

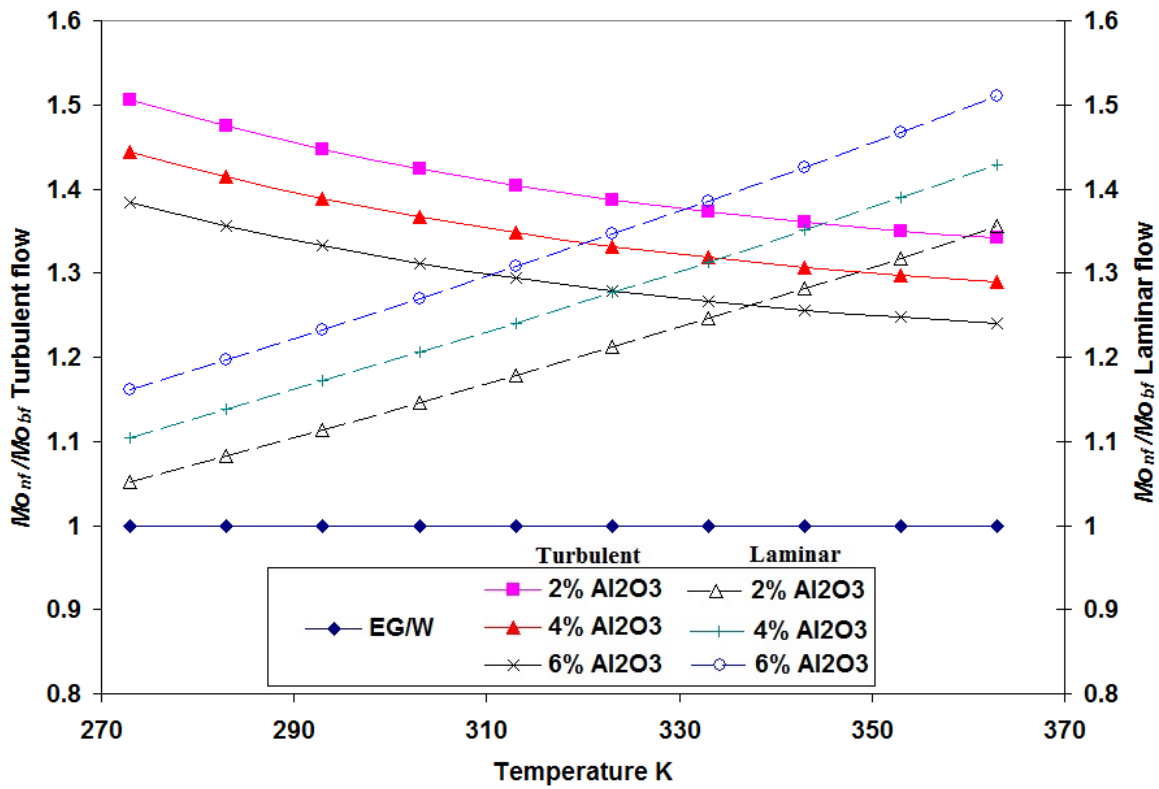


Figure 3.8. Variation of the ratio of Mouromtseff numbers (FOM) for three concentrations of the Al_2O_3 nanofluid and the base fluid for laminar and turbulent internal flows.

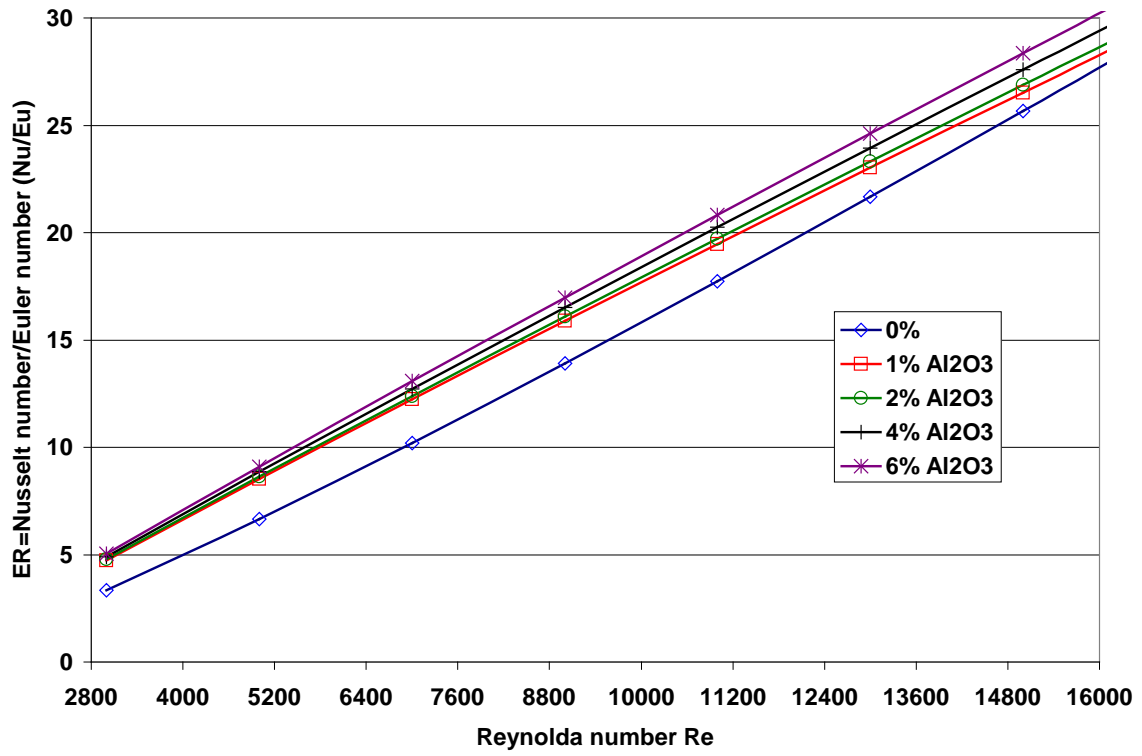


Figure 3.9. Variation of energy ratio with the Reynolds number for the Al₂O₃ nanofluid at a temperature of 293 K.

Chapter 4. An Experimental Determination of the Viscosity of Propylene Glycol/Water Based Nanofluids and Development of New Correlations*

4.1 Abstract

Measurements have been carried out for determining the viscosity of several nanofluids, in which different nanoparticles were dispersed in a base fluid of 60% propylene glycol and 40% water by mass. The nanoparticles were aluminum oxide, copper oxide, silicon dioxide, titanium oxide and zinc oxide with different average particle diameters. Measurements were conducted for particle volume concentrations of up to 6% and over a temperature range of 243 K to 363 K. All the nanofluids exhibited a Bingham plastic behavior at the lower temperatures of 243 K to 273 K and a Newtonian behavior in the temperature range of 273 K to 363 K. Comparisons of the experimental data with several existing models show that they do not exhibit good agreement. Therefore, a new model has been developed for the viscosity of nanofluids as a function of temperature, particle volume concentration, particle diameter, the properties of nanoparticles, and those of the base fluid. Measurements were also conducted for single-walled, bamboo-like structured and hollow-structured multi-walled carbon nanotubes dispersed in a base fluid of 20% propylene glycol and 80% water by mass. Measurements of these carbon nanotubes nanofluids were conducted for a particle volume concentration of 0.229% and over a temperature range of 273 K to 363 K, which exhibited a non-Newtonian behavior. The effect of ultrasonication time on the viscosity of carbon nanotubes nanofluids was investigated. From the experimental data of carbon nanotubes nanofluids, a new correlation was developed which relates the viscosity to temperature and the Péclet number.

4.2 Introduction

The suspension of solid particles in traditional heat transfer fluids to improve the poor thermal conductivity of these fluids dates back to Maxwell's [1] theoretical work. Since then, numerous experimental and theoretical studies have been performed on thermophysical,

* Vajjha, R. S., Chukwu, G.A., and Das, D. K., 2014, "An experimental Determination of the Viscosity of Propylene Glycol/Water based Nanofluids and Development of New Correlations," Currently Under Review in ASME Journal of Fluids Engineering.

rheological and heat transfer characteristics of these fluids. However, these studies were limited to dispersions of micro or millimeter sized particles. The main drawback of these micro or millimeter sized particles is that they are not uniformly dispersed and settle to the bottom due to gravity. Choi [2] recognized that this drawback can be overcome by nano-sized particles. He gave the name of this new type of engineered fluids as nanofluids, which are the dispersions of nanometer-sized particles with average particle sizes of less than 100 nm, in base fluids such as water, oil, ethylene glycol, propylene glycol etc. Similar to those of micro or millimeter sized particle-fluid mixtures, these nano-engineered heat transfer fluids exhibited superior thermal conductivity mainly attributed to dispersion of metallic or non-metallic particles that have higher thermal conductivities compared to those of the base fluids. Since its discovery, many researchers [3-6] have studied the thermal conductivity of several nanofluids, generally prepared from copper and aluminum oxides. Comparatively, much less research has appeared in the literature on the viscosity of nanofluids. It should be noted that although the increase in thermal conductivity is what makes the nanofluids more attractive compared to base fluids, the increase in viscosity of nanofluids can hinder its performance. Therefore, the accurate determination of viscosity of nanofluids is important as it plays a crucial role in determining the Reynolds number, Prandtl number and the pumping power in a fluid flow. Table 4.1 chronologically summarizes some of the important theoretical correlations proposed by different researchers for calculating the effective viscosity μ_{eff} of a mixture, as a function of the viscosity of base fluids μ_{bf} , when particles are suspended.

This research first started with the pioneering work of Einstein [7] to predict the effective viscosity of a fluid in which solid spheres are suspended. He derived an analytical solution for the effective viscosity as a function of particle volume fraction ϕ (less than 2%), considering the hydrodynamics around an isolated sphere. Ever since this work was published, several equations have been developed by other researchers to extend Einstein's theory to higher particle volume fractions. For example, Vand [9] and Brinkmann [11] considered the higher order coefficients neglected by Einstein in an effort to validate his equation to higher particle volume fraction. Batchelor [14] improved the correlation of Einstein and Vand by incorporating the effect of Brownian motion on the effective viscosity of suspended spherical particles in a liquid. The research of Krieger and Dougherty [12], Frankel and Acrivos [13], Leighton and Acrivos [16]

included the maximum attainable concentration ϕ_m as a parameter influencing the effective viscosity. Graham [15] expressed the effective viscosity of suspensions in terms of particle radius r_p and the inter particle spacing h of the spherical particles. Thomas and Muthukumar [17] derived the effective viscosity of a dilute suspension of hard spheres from the fully hydrodynamic interactions involving three spheres.

The correlations summarized in Table 4.1 were developed to predict the viscosity of micro or millimeter sized dispersions in base fluids. However, when they were applied to the viscosity measurements on nanofluids at the initial stage by Masuda [18] and Pak and Cho [19], it was found that these correlations failed to correctly predict the effective viscosity of nano-sized suspensions in base fluids. Therefore, this new discovery started a phase of research in recent years to develop new accurate correlations from experimental data and theoretical analysis using different nanoparticles and base fluids. A representative list for the rheological properties of nanofluids correlations developed for different nanoparticles suspended in a variety of base fluids are summarized in Table 4.2. Tseng and Lin [20], Nguyen et al. [28] and Williams et al. [31] present nanofluid viscosity μ_{nf} as exponential functions of particle volume concentration. Maiga et al. [21], Buongiorno [22] and Chen et al. [30] follow a Batchelor type correlation. Kulkarni et al. [24, 25], Namburu et al. [26, 27], Sahoo et al. [33] and Rohini et al. [39] derived Andrade [40] type correlation, where constants A and B were changed to functions of ϕ and T. Only the correlations of Avsec and Oblak [29], Masoumi et al. [34], Corcione [36] and Khanafer and Vafai [38] include a dependence of the particle diameter.

In the arctic and sub-arctic regions of the world, due to severe winter conditions ethylene or propylene glycol mixed with water in different mass proportions are used as heat transfer fluids in building heating systems, automobile radiators and in industrial heat exchangers. For example, a mixture of 60 % propylene glycol and 40 % water by mass (60:40 PG/W) has a freezing point of -51.5 °C [41]. Compared with propylene glycol solutions, ethylene glycol solutions have better thermophysical properties, especially at lower temperatures. However, due to its nontoxic nature, the propylene glycol is preferred over the ethylene glycol in residential building heating systems where possible contact of the potable water and the building heating fluid is possible due to the sharing of the same furnace. Due to the long heating season in cold regions of the world, nanofluids promises to be an attractive heat transfer fluid. Therefore, the

objective of the present research is to study the rheological properties of 60:40 PG/W based nanofluids. These nanofluids will find wide application as the heat transfer fluids in building heating air coils and in baseboard heaters. Except the work of Kulkarni et al. [24], no rheological data is currently available in the literature for nanoparticles dispersed in 60:40 PG/W base fluid. In the present study a wide spectrum of nanoparticles have been considered to develop generalized viscosity correlations and to compare their magnitudes. The nanoparticles studied are: aluminum oxide (Al_2O_3) of average particle sizes (APS) d_p , 53 nm and 20 nm, copper oxide (CuO) of APS 29 nm, silicon dioxide (SiO_2) of APS 30 nm, zinc oxide (ZnO) of APS 77 nm and 50 nm, titanium oxide (TiO_2) of APS (10 ± 5) nm, single-walled carbon nanotubes (SWCNT), hollow-structured multi-walled carbon nanotubes (MWCNT) and bamboo-like structured multi-walled carbon nanotubes (BWCNT).

4.3 Nanofluids preparation and characterization

The nanofluids were procured from Alfa Aesar [42] and Nanostructured & Amorphous Materials, Inc. [43] as concentrated aqueous suspensions (up to 15-50% by mass) with various average particle sizes. Table 4.3 summarizes the average particle sizes of various nanoparticles used in the present study and their density values at room temperature (300 K). The preparation of nanofluid samples for the viscosity measurements involved two steps. In the first step, the parent nanofluids were subjected to ultrasonication for about 6 hours in a Branson sonicator under a frequency of 40 kHz and a power of 185 W. This process makes the agglomerated nanoparticles to break down into their original particle sizes specified by the manufacturer. Then these ultrasonicated parent samples were diluted to desired volumetric concentrations of 1 to 6% by adding calculated amount of propylene glycol and water using a precise electronic mass balance. The second step involved ultrasonication of these diluted nanofluids for about 3 hours. The adequacy of the ultrasonication time was ascertained by taking a small amount of diluted nanofluid sample and examining it under the transmission electron microscope (TEM). Figure 4.1(a) illustrates a sample TEM image of the Al_2O_3 nanoparticles. As observed from the Fig. 4.1(a) the particles are not agglomerated, the shape of the Al_2O_3 nanoparticles are perfectly spherical and the average particle size is about 20 nm as specified by the manufacturer. It should be noted that in preparing nanofluids, manufacturers use surfactants to enhance the dispersion stability of the nanoparticles in fluids. Unfortunately the manufacturers did not provide any data

on the surfactants used in nanofluids, treating those as proprietary information. However, they express that the amount of surfactant added is minute to not influence the viscosity measurably.

The carbon nanotubes were obtained from Nanolab [44] as dispersions in 20% propylene glycol and 80% water (20:80 PG/W) with a concentration of 0.3% by weight. The nanotubes provided by Nanolab are Carboxyl (COOH) functionalized carbon nanotubes produced by chemical-vapor deposition method. The purity of this COOH functionalized CNT is specified to be greater than 95% by the manufacturer. The dimensions of CNT provided by the manufacturer are given in Table 4.4. A sample TEM image of a BWCNT shown in Fig. 4.1(b) confirms an average tube diameter of 15 nm as specified by the manufacturer and the lengths were found to be between 1 to 5 μm . There were some entanglements observed in the image, since the TEM measured a dry sample. The long slender tubes are prone to breakage depending upon the time of sonication which would affect the rheological properties. In order to study the effect of ultrasonication time on the rheological properties of carbon nanotubes, the samples were ultrasonicated for 45, 90 and 180 minutes. Rheological properties were measured in identical manner after each ultrasonication period.

4.4 Experimental setup for rheological properties measurements

The experimental setup for measuring the rheological properties of nanofluids is shown in Fig. 4.2. It consists of two Brookfield programmable viscometers, namely; (1) LVDV II+ Small Sample Adapter and Thermosel (SSA & T), and (2) LVDV II+ Cone/Plate. There is a Julabo temperature controlled bath connected to a computer to control the temperature of the sample, whose properties are being measured.

LVDV II+ SSA & T Viscometer: The principle of operation of the DV II + viscometer is to drive the spindle which is immersed in the test fluid through a calibrated spring attached to the spindle. The deflection in the spring measures the viscous drag of the fluid against the spindle. The measurement range of a DV II+ viscometer depends on the rotational speed of the spindle, the size and shape of the spindle, the container in which the spindle is rotating in, and the full scale torque of the calibrated spring. This viscometer has a viscosity measurement range of 1.5 to 4,790,000 cP (1cP = 0.001 kg/m.s) and has the temperature sensing range of 173 K (-100 °C) to 573 K (300 °C). The sample chamber is fitted with a RTD probe to record the temperature of the sample during viscosity measurements.

The computer controlled Julabo temperature bath was very effective in maintaining the test fluid at a desired temperature. A SC4-18 spindle was used which has a viscosity measuring range of 1.5 to 30,000 cP. For this spindle, a wide variety of speeds are selected such that the applied torque remained between 10 to 100 % of the maximum possible torque. This range is recommended by the viscometer manufacturer. The measurements were performed from a temperature range of 243 K (-30 °C) to 333 K (60 °C). Computer connected to the viscometer collects the data through the Wingather[®] software. The recorded data includes speed in rpm, torque in %, viscosity in cP, shear stress in dyne/cm², shear rate in 1/sec, temperature in °C and time duration in seconds for which each reading was taken. All the viscosity readings were taken only after thermal equilibrium has been attained by the test fluid.

LVDV II+ Cone/Plate Viscometer: At higher temperatures, the 60:40 PG/W based nanofluids have very low viscosity values approaching lower operational limit which is 1.5 cP for the LVDV II+ SSA & T viscometer. For this reason a cone/plate viscometer was used for measuring the viscosity of nanofluids in the temperature range of 60 °C to 90 °C. The cone/plate viscometer with CPE-40 spindle has a viscosity measurement range of 0.15 to 3,065 cP. To ensure accurate readings, the most critical aspect in using the cone/plate viscometer is adjusting/verifying the “gap” between the cone and the plate, as emphasized by the equipment vendor. The gap should be set such that the pin in the center of the cone is separated from the plate by 0.013mm (0.0005 inch), otherwise the measurements will be erroneous. This is accomplished by turning the toggle switch towards on position; a pilot light (red light) is illuminated enabling the electronic gap setting feature. If the yellow contact light is illuminated, slowly turn the micrometer adjustment ring clockwise until the yellow contact light is just breaking contact or begins to flicker. Similarly, if the yellow contact light is not illuminated, slowly turn the micrometer adjustment ring counter-clockwise until the yellow light first turns on or begins to flicker. This is the hit point where the pin in the center of the cone touches the surface of the plate. Adjust the sliding reference marker, right or left, to the closest full scale division mark and turn the micrometer adjustment ring one scale division to the left to meet the line on the sliding reference marker. The yellow contact light should go off, indicating that, at this stage the correct gap is established and the measurement can begin. For each temperature setting of the sample fluid, this procedure must be repeated.

The RTD probes used for recording the temperature has an accuracy of ± 1 °C between -100 °C to +149 °C. The viscometer has an accuracy of $\pm 1\%$ of full scale range, while the repeatability of the apparatus is $\pm 0.2\%$.

4.5 Results and Discussion

4.5.1 Calibration and benchmark test case

The calibration of the apparatus was done using Brookfield's silicone viscosity standard fluid having a viscosity value of 9.7 cP at 298 K (25 °C). The measured value obtained from the experiment showed a deviation of 3% from the true value. After calibration was done, benchmark tests were conducted with de-ionized (DI) water and 60:40 PG/W fluids to verify the accuracy of the apparatus and the experimental procedure. The experimental results were compared with the values published by White [45] and Kestin et al. [46] for DI water and in ASHRAE handbook [41] for 60:40 PG/W. Figure 4.3 shows the comparison between the measured viscosity values and the data from White, Kestin et al. and ASHRAE handbook. A good agreement is observed between the current measurements and the published data. An average deviation of 3.6% for DI water and 7.4% for 60:40 PG/W were observed between the measurements and the data from White, Kestin et al. and ASHRAE. Table 4.5 presents the viscosity correlations for DI water given by White and Kestin et al. and viscosity correlation developed from the present study for 60:40 PG/W fluid using ASHRAE data. The correlation for 60:40 PG/W follows the log-quadratic empirical fit recommended by White for liquids. To improve the accuracy of the 60:40 PG/W viscosity correlation presented at the bottom row of the Table 4.5, the temperature range was split into two segments; $238 \leq T \leq 273$ K and $273 \leq T \leq 393$ K, achieving a maximum deviation of $\pm 0.5\%$. These two equations are used for the base fluid viscosity value subsequently in developing the viscosity correlation of nanofluids.

4.5.2 Aluminum oxide nanofluid

After confirming the accuracy of measured values of base fluid viscosities and the procedure followed with the apparatus via the benchmark tests, the same experimental setup was used for measuring the viscosities of nanofluids. The viscosity measurements were conducted over a temperature range of 243 K (-30 °C) to 363 K (90 °C) for the Al₂O₃ nanofluids with an average particle size of 53 nm and for particle volumetric concentrations of 1 to 6%. One of the

primary objectives of this study was to understand whether nanofluid displayed Newtonian or non-Newtonian behavior with variations of particle volumetric concentration and temperature. Figure 4.4 displays the viscosity versus shear rate for a 4% Al₂O₃ nanofluid over a temperature range. It was observed that nanofluids showed a non-Newtonian behavior in the lower temperature range of 243 K (-30 °C) to 273 K (0 °C) and a Newtonian behavior in the temperature range of 273 K (0 °C) to 363 K (90 °C). This trend was observed for all the measured particle volumetric concentrations of the Al₂O₃ nanofluid. At negative Celsius temperatures, the measured viscosity value decreased with an increase in the shear rate showing that fluid behaved like a non-Newtonian fluid. This observed non-Newtonian behavior is possibly due to the system getting dynamically arrested specially at low temperatures as suggested by Wagner and Brady [47]. But once the shear stress exceeds a certain yield value, the fluid starts to flow and its viscosity decreases with the increasing shear rate. They also proposed that this decrease in viscosity with increasing shear rate was a direct consequence of rearrangement of suspended particles due to the applied shear.

The plot of shear stress versus shear rate shown in Fig. 4.5 clearly distinguishes the rheological behavior of this nanofluid. At 243 K (-30 °C), the nanofluid exhibits a non-Newtonian fluid characteristic of Bingham plastic model given by Eq. (4.1). For this kind of fluid, the shear stress beyond the yield stress is linearly proportional to the shear rate.

$$\tau = \tau_y + \mu_{pl}\dot{\gamma} \quad (4.1)$$

where τ is the shear stress, τ_y is the yield stress, μ_{pl} is the plastic viscosity and $\dot{\gamma}$ is the shear rate. While, at 293 K (20 °C) the nanofluid follows a Newtonian behavior. These observations are in agreement with the prior studies on viscosity measurements done by Namburu et al. [26] and Sahoo et al. [33].

A summary of the variations of viscosities with temperature for various particle volumetric concentrations of the Al₂O₃ nanofluid is displayed in Fig. 4.6. The viscosities diminish exponentially [40] as the temperature of the fluid increases. As an example, for a 6% particle volumetric concentration, the viscosity decreases by 277 times from 686.92 cP to 2.48 cP between 243 K to 363 K. Furthermore, with an increase in particle volumetric concentration,

the nanofluid viscosity increases. For the same 6% nanofluid at temperatures of 243 K and 303 K, the viscosity increases over the base fluid by 94% and 71% respectively. It was noticed that as the temperature increased from 243 K to 363 K, the percentage enhancement in the viscosity of nanofluid over the base fluid decreased. Similar trend was observed for the Al_2O_3 nanofluid with an average particle size of 20 nm. Figure 4.7 shows the viscosity versus temperature for various particle volumetric concentrations of the Al_2O_3 nanofluid of APS 20 nm. The effect of particle size has a noticeable effect on the viscosity of nanofluids. This topic is covered in Section 4.5.7.

4.5.3 Copper oxide nanofluid

Figure 4.8 presents the viscosity variation with temperature for different particle volumetric concentrations of a CuO nanofluid of an average particle size of 29 nm. As observed earlier for Al_2O_3 nanofluids, the viscosity of a CuO nanofluid increases with an increase in particle volumetric concentration and decreases with an increase in temperature. To examine the magnitude of some typical values, a 4% CuO nanofluid viscosity decreases with temperature by a factor of 354 from 926.33 cP to 2.62 cP between 243 K to 363 K. Considering the influence of concentration, a 5% CuO nanofluid viscosity is increased by about 3.34 times and 2.6 times over that of the base fluid at temperatures of 243 K and 303 K respectively. It was observed in the experiments that the viscosity of CuO nanofluid increased at a higher proportion with the addition of nanoparticles when compared with other nanoparticles studied in the present research. Since the CuO has the highest density among particles used in this study, this indicates that the higher is the density of nanoparticles, the higher would be the viscosity.

4.5.4 Silicon dioxide nanofluid

Figure 4.9 shows the viscosity variation of the SiO_2 nanofluid as a function of temperature and particle volumetric concentration. Similar to the observations made for the Al_2O_3 and CuO nanofluids, the viscosity decreases with an increase in temperature and increases with an increase in particle volume concentration. For this nanofluid of 5% particle volumetric concentration, the viscosity value is decreased from 495.68 cP to 1.89 cP i.e., by a factor of about 262 between 243 K to 363 K. Also for the same 5% concentration nanofluid, the viscosity increases by 40% and 33% over the base fluid at temperatures of 243 K and 303 K respectively.

4.5.5 Titanium oxide nanofluid

The variation of TiO₂ nanofluid with temperature and particle volumetric concentration is presented in Fig. 4.10. Manufacturer could only provide this nanofluid at a low aqueous mass concentration of 15%, which yielded a maximum volumetric concentration of 1.5% for our sample, when dispersed in a 60:40 PG/W base fluid. The trend in viscosity variation is very similar to the observations made for the previous nanofluids. For example, when the temperature of a 1% TiO₂ nanofluid is increased from 243 K to 363 K, the viscosity value decreased by 302 times. For the same 1% concentration nanofluid the viscosity increased by 23.4% and 16.5% over the base fluid at temperatures of 243 K and 303 K respectively.

4.5.6 Zinc oxide nanofluid

Figures 4.11 and 4.12 present the viscosity variation with temperature and particle volume concentration for the ZnO nanofluids of average particle sizes 77 nm and 50 nm respectively. Similar observations were made on viscosities of these nanofluids with respect to changes in temperature and particle volumetric concentration. For example, when the temperature increased from 243 K to 363 K, the viscosity decreased by a factor of 292 and 297 for a 4 % concentration of APS 77 nm and 50 nm respectively. Similarly, for the same 4% volume concentration and at a temperature of 243 K, the viscosity of nanofluid increases over the base fluid by 55% and 68% for the ZnO nanofluid of APS 77 nm and 50 nm respectively. At a temperature of 303 K, for the same 4% volume concentration, the viscosity of nanofluid increases over the base fluid by 44% and 51% for the ZnO nanofluid of APS 77 nm and 50 nm respectively. The effect of particle size on the viscosity of nanofluids is discussed in Section 4.5.7.

4.5.7 Particle size effect

The experimental data obtained for the Al₂O₃ nanofluid of APS 53 nm and 20 nm and for the ZnO nanofluid of APS 77 nm and 50 nm were analyzed to determine the effect of particle size on the viscosity. Figure 4.13 shows this effect on the viscosity with variation of temperature for two different particle volumetric concentrations of 1% and 4% for the Al₂O₃ nanofluid. It is observed that the viscosity is lower with a larger size particle at the same temperature and for the same concentration. This is because, for the same particle volumetric concentration of suspended nanoparticles, fluid with lower average particle size will have more number of particles. Higher

number of particles results in increased surface area of interaction between the solid particles and liquid and increased drag, which results in increasing the viscosity. Similar observations were made by Chermisinoff [48] for the micro particles and by Namburu et al. [26] for the nanoparticles suspended in fluids. Same trend was also recorded for the ZnO nanofluids of two different concentrations of 3% and 5% as depicted in Fig. 4.14. From Figs. 4.13 & 4.14, it is also noticed that at a constant temperature, with an increase in particle volumetric concentration, the percentage increase in viscosity is higher between the two particle sizes of the same nanofluid. For example, at the room temperature of 303 K and at a volumetric concentration of 1%, the Al₂O₃ nanofluid's viscosity is 9.2% higher for the 20 nm particle over that of the 53 nm particle. At the same temperature of 303 K, when the volumetric concentration is 4%, the viscosity is 45.65% higher for the 20 nm particle over that of the 53 nm particle. Similarly, for the ZnO nanofluid at 303 K, the viscosity is 5.23% higher for the 50nm particle over that of the 77 nm particle at volumetric concentrations of 3%. At the same temperature, when the volumetric concentration is 5%, the viscosity is 9% higher for the 50 nm particle over that of the 77 nm particle.

The measured viscosities between two different average particle sizes of the same nanoparticle showed that the Al₂O₃ nanoparticle has a higher percentage increase in viscosity when compared with the ZnO nanoparticle. This is because the ratio of particle diameters between the two Al₂O₃ nanoparticles is higher compared to the ratio between the two ZnO nanoparticles.

4.6 Development of new correlations

From the present study of viscosity measurements of various nanoparticles dispersed in 60:40 PG/W base fluid, a total of 458 experimental data points were collected. The comparison of the experimental data with several well-known theoretical equations presented in Table 4.1 showed that they all underpredict the viscosity values for nanofluids, when compared with the experimental data. This is clearly demonstrated in Fig. 4.15. Similarly, the viscosity correlations presented in Table 4.2 which are developed from the experimental work of nanofluids also failed to agree with experimental data of the present study.

Therefore, new correlations need to be developed for the nanofluids. In the present study, initially an exponential form given by Eq. (4.2), originally proposed by Andrade [40] was used to derive the viscosity values of nanofluids as a function of temperature.

$$\mu = \exp\left(B + \frac{C}{T}\right) \quad (4.2)$$

Equation (4.2) needed modification by including a ϕ term to account for the dependence of viscosity of nanofluids on particle volumetric concentration. A non-dimensional form of expressing the viscosity of nanofluid divided by that of the base fluid following the historical equations summarized in Table 4.1 was adopted. In order to make the right hand side of Eq. (4.3) non-dimensional, a reference temperature T_0 was introduced.

$$\frac{\mu_{nf}}{\mu_{bf}} = A \exp\left(B\phi + C \frac{T_0}{T}\right) \quad (4.3)$$

In Eq. (4.3), A , B , C are the curve-fit constants which are different for different nanofluids and T_0 is a reference temperature which could be set to any value and was selected to be 273 K (0 °C) for convenience. The values of constants A , B and C are given in Table 4.6. A maximum deviation of about $\pm 6\%$ was observed between the experimental and curve-fit values for all the nanofluids examined.

It had been observed earlier from Fig. 4.4, describing the variation of viscosity versus shear rate that two different behaviors of nanofluids in two temperature regimes occurred. In the lower temperature regime (243 K to 273 K), nanofluids behaved like a non-Newtonian fluid whereas in the upper temperature regime (273 K to 363 K), nanofluids behaved like a Newtonian fluid. Therefore, two sets of constants A , B , C were developed for each nanofluid of a particular particle size to accurately describe the viscous behavior of nanofluids. These different constants are summarized in Table 4.6, reflecting one set of curve-fit constants in the lower temperature regime and another set of curve-fit constants in the higher temperature regime, for each nanofluid.

However, having different curve-fit constants for each nanofluid were cumbersome and lacked generality. Therefore, a single general correlation applicable for the calculation of the viscosity of all nanofluids as functions of concentration, temperature, particle size and densities of particles ρ_p and that of the base fluid ρ_{bf} were conceived in the form of Eq. (4.4).

$$\mu_{nf} = \mu_{bf}(1 + 2.5\phi + 6.2\phi^2) + A_1 \left[\exp \left(A_2\phi + A_3 \frac{T_0}{T} + A_4 \frac{d_{bf}}{d_p} + A_5 \frac{\rho_p}{\rho_{bf}} \right) \right] \left[\frac{\rho_p V_B d_p^2}{72\delta} \right] \quad (4.4)$$

The first part of the Eq. (4.4) is a theoretical equation developed by Batchelor [14] that includes the effect of concentration. But this term alone failed to predict the effective viscosity of nanofluid as it underpredicted the experimental values observed in Fig. 4.15. To augment the underprediction, a second term was needed to bring in the influence of other relevant parameters. The second term of Eq. (4.4) was derived as a result of observations made from the present study. The first part of the second term in Eq. (4.4) is adopted following Eq. (4.3) which showed that the nanofluid viscosity variation with temperature and particle volume concentration was best described by the exponential form. The two terms containing the diameter and density effects are based on the following logic. From Figs. 4.13 and 4.14, we observe that the viscosity of nanofluid is inversely proportional to the particle diameter which has been nondimensionalized by the base fluid molecule diameter d_{bf} . The equivalent diameter of a base fluid (60:40 PG/W) molecule was found to be 0.543 nm, calculated following the equation $d_{bf} = 0.1[6M/(N\pi\rho_{bf0})]^{1/3}$ [49], where M is the molecular weight of the base fluid, N is the Avogadro number, ρ_{bf0} is the density of the base fluid calculated at a temperature of 293 K. The density effect of a nanoparticle is directly proportional to the viscosity. This is observed by comparing the viscosity values of similar size nanoparticles at same temperature and particle volume concentration. The Al_2O_3 nanoparticle of APS 53 nm having a particle density of 3600 kg/m^3 and ZnO nanoparticle of APS 50nm having a particle density of 5600 kg/m^3 have viscosities of 13.12 cP and 14.28 cP respectively at a room temperature of 293 K and for a particle volume concentration of 4% from Figs. 4.6 and 4.12. Similar observations were also made by comparing the viscosity values of CuO and SiO_2 nanofluids of APS 30 nm from Figs. 4.8 and 4.9 respectively, at the same temperature and particle volume concentration. Therefore,

when the density of the particle is higher, it makes the viscosity of the nanofluid higher. The last term $(\rho_p V_B d_p^2 / 72 \delta)$ represents the influence due to fluid flow over spherical nanoparticles proposed by Masoumi et al. [34]. This term takes into account the Brownian velocity (V_B) of the particles suspended in the fluid and the inter-particle spacing (δ). The inter-particle spacing is given by $\delta = d_p (\pi / 6 \phi)^{1/3}$.

With these observations, curve-fit coefficients A_1 to A_5 of Eq. (4.4) were derived using the statistical software Minitab [50]. Table 4.7 gives the curve-fit coefficients derived for all the nanofluids studied, in two temperature regimes. This new correlation Eq. (4.4) has a maximum deviation of $\pm 20\%$ in both temperature regimes and an average absolute deviation of 11.6% and 9.14% in the range of $243 \text{ K} \leq T \leq 273 \text{ K}$ and $273 \text{ K} < T \leq 363 \text{ K}$ respectively. Figure 4.16 shows the experimental viscosity values versus predicted values obtained from Eq. (4.4).

4.7 Carbon nanotubes

Carbon nanotubes have gained much attention due to their superior thermal, electrical and mechanical properties. Currently, very limited experimental data is available on the viscosity of CNT-based nanofluids. Kinloch et al. [51] studied the rheological behavior of oxidized carbon nanotubes dispersed in water at volume concentrations of 0.5% to 10%. They observed shear thinning behavior under steady shear for the dispersions up to a Péclet number of 1 to 10 and at higher Péclet numbers the shear thinning followed the Ostwald-de Waele power law. Ding et al. [52] conducted the viscosity measurements of aqueous suspensions of multi walled carbon nanotubes at 25 °C, 40 °C and for weight concentrations of 0.1% and 0.5%. The shear thinning behavior was also observed by them. For a fixed concentration, they observed the viscosity of CNT nanofluids decreased with an increase in temperature and at a given shear rate, the viscosity increased with an increase in dispersion concentration. Garg et al. [53] experimentally studied the effect of ultrasonication time on viscosity of a 1% by weight aqueous MWCNT at 15 °C and 30 °C. From their experiments, they noticed a non-Newtonian (shear thinning or pseudoplastic) behavior especially at 15 °C. They also observed that the viscosity of MWCNT first increased, when the ultrasonication time was increased from 20 minutes to 40 minutes, and thereafter decreased with an increase in the ultrasonication time. This finding stresses that ultrasonication time is an important factor for the CNT nanofluids. Aladag et al. [54] investigated experimentally the effects due to temperature and shearing time on the rheological properties of

water based CNT nanofluids of weight concentration 1%. They observed a thixotropic shear time dependent phenomenon when the stress was gradually increased and decreased. Halelfadl et al. [55] studied the influence of concentration and temperature on the viscosity of water-based CNT nanofluids. The particle volume concentration tested varied from 0.0055% to 0.55% and the temperature ranged from 0 °C to 40 °C. Their results showed that for low particle volume concentrations ($< 0.055\%$), the nanofluid showed Newtonian behavior and for higher particle volume concentrations, a shear thinning non-Newtonian behavior was observed. They also reported that although temperature affected the viscosity of nanofluids, at higher shear rates the relative viscosity (μ_{nf}/μ_{bf}) was independent of temperature.

The present study covers the experiments on rheological properties of three different types of carbon nanotubes; SWCNT, BWCNT and MWCNT as a function of temperature. The three kinds of carbon nanotubes were dispersed in the base fluid of 20:80 PG/W with a particle weight concentration of 0.3% which corresponds to a particle volume concentration of 0.229%. The ϕ value for the CNT dispersions is generally low compared to nanoparticles to avoid entanglement of tubes that hinders uniform dispersion. The measurements were conducted over a temperature range of 273 K to 363 K (0 °C to 90 °C). Figures 4.17 (a), (b) and (c) show the plot of viscosity versus shear rate for SWCNT, BWCNT and MWCNT respectively. These plots show the non-Newtonian behavior of nanofluids especially at lower temperatures. This non-Newtonian (pseudoplastic) behavior is due to development of entangled network of suspended carbon tubes. Under shear these tubes become oriented and points of entanglement are reduced which results in decrease in fluid viscosity. It was observed that at same shear rate, the viscosity of MWCNT $>$ BWCNT $>$ SWCNT, for a fixed volume concentration and temperature of the fluid. For example, at a shear rate of 92.4 (1/sec) and at a temperature of 283 K, the viscosities of MWCNT, BWCNT and SWCNT are 38.9 cP, 26.4 cP and 24.9 cP respectively. At a given concentration, the viscosity of the MWCNT is higher compared to that of the BWCNT and the SWCNT at the same temperature and shear rate. The data presented in these figures are measured after an ultrasonication time of 90 minutes. Aladag et al. [54] had pointed out the influence of the ultrasonication time on the rheological behavior of CNT nanofluids. The effects of ultrasonication time on the viscosity of carbon nanotubes are discussed in the next section.

The measurements revealed that the SWCNT and MWCNT suspensions behaved like a pseudoplastic fluid up to a temperature of 313 K (30 °C) and thereafter they behaved as Bingham

plastic fluid. On the other hand, the BWCNT behaved like a Bingham plastic fluid with over the entire temperature range of 273 K to 363 K. Figures 4.18(a), 18(b), 18(c) compare plots of shear stress versus shear rate for SWCNT, BWCNT and MWCNT nanofluids respectively at 273 K (0 °C) and 313 K (40 °C). Examining the experimental data in Figs. 4.18(a) & (c), SWCNT and MWCNT were well represented to a great deal of fidelity ($R^2=0.999$) by the Herschel-Bulkley model given by Eq. (4.5) confirming the pseudoplastic behavior.

$$\tau = \tau_y + K\dot{\gamma}^n \quad (4.5)$$

where τ_y is the yield stress, K is the flow consistency factor and n is the flow behavior index. For pseudoplastic fluids $n < 1$ and a low value of n indicate a strong non-Newtonian behavior of a fluid. Table 4.8 provides the equations fitted in Figs. 4.18 (a), (b) & (c) at 273 K and 313 K for SWCNT, BWCNT and MWCNT. Comparing the fitted correlations, between 273 K and 313 K, with an increase in temperature the flow behavior index n increased while the flow consistency factor K and yield stress τ_y decreased. And from a temperature beyond 303 K (30 °C), the SWCNT and the MWCNT followed the Bingham plastic fluid model given by Eq. (4.1).

4.7.1 Effect of ultrasonication time on the viscosity of CNT nanofluids

The effects of ultrasonication times on SWCNT, BWCNT and MWCNT nanofluids were studied at three time intervals; 45, 90 and 180 minutes. The ultrasonication was done under a frequency of 40 kHz and a power of 185 W. Approximately 80 ml of each 0.3% by weight CNT sample was taken for ultrasonication. Figures 4.19 and 4.20 show the plots of viscosity versus shear rate for a BWCNT and MWCNT respectively. It was observed that the rheological properties of BWCNT showed very little change when the ultrasonication times were varied from 45 to 180 minutes. On the other hand, the MWCNT showed a decrease in the viscosity with an increase in ultrasonication time. Yang et al. [56] has also observed similar behavior for the MWCNT dispersed in oil. In our experiments, for example, with an increase in ultrasonication time from 45 to 90 minutes, the viscosity of MWCNT decreased by about 22%, 21% and 13% at 273 K (0 °C), 283 K (10 °C) and 293 K (20 °C) respectively. This may be due to the effect that breakage of MWCNT increased with an increase in ultrasonication time. This breakage reduced

their aspect ratio, which in turn reduced the viscosity. The BWCNT is reinforced by the intermediate graphene layers and does not yield to breakage at the same rate as the MWCNT.

Stickel and Powell [57] and Mueller, Llewellyn and Mader [58] had proposed viscosity as a function of dimensionless Péclet number, which correlates the shear rate of a flow to the particle's diffusion rate. The Péclet number includes the influence of Brownian motion and is given by Eq. (4.6)

$$Pe = \frac{6\pi\mu_{bf}a^3\dot{\gamma}}{\kappa T} \quad (4.6)$$

where $\kappa = 1.38 \times 10^{-23}$ J/K is the Boltzmann constant, T is the absolute temperature (K), μ_{bf} is the base fluid viscosity (kg/m.s), $\dot{\gamma}$ is the shear rate (1/sec) and a is the particle radius (m). For a non-spherical particle, the radius is obtained by calculating the equivalent radius of non-spherical particle on an equal volume basis. An equation for the relative viscosity ($\mu_{r_{CNT}} = \mu_{CNT}/\mu_{bf}$) of CNT, $\mu_{r_{CNT}} = f(T, Pe_{\dot{\gamma}})$ has been developed from the present measurements of viscosity of SWCNT and BWCNT which is given by Eq. (4.7)

$$\frac{\mu_{CNT}}{\mu_{bf}} = a_1 (Pe)^{a_2} \left(\frac{T}{T_0}\right)^{a_3} \quad (4.7)$$

where a_1 , a_2 , a_3 are the curve-fit coefficients given in Table 4.9, $T_0 = 273$ K is the reference temperature. Viscosity would be a function of particle volume concentration (ϕ), but our measurements were limited to only one concentration obtained from the nanofluid manufacturer. Therefore, this correlation may be treated as a preliminary one.

Two sets of curve-fit coefficients were derived for two temperature regimes. The maximum percentage deviation of Eq. (4.7) from the experimental values is $\pm 10\%$. Figure 4.21 shows the experimental viscosity values versus predicted values at different shear rates obtained from Eq. (4.7) for the BWCNT nanofluids. No correlation was derived for the MWCNT as rheological properties of these carbon nanotubes varied steadily with the ultrasonication time.

Further studies are recommended to establish a suitable time of ultrasonication for the MWCNT to reach an equilibrium state, beyond which the rheological properties change may be minimal.

4.8 Conclusions

The viscosities of five nanoparticles (Al_2O_3 , CuO , SiO_2 , TiO_2 and ZnO) dispersed in a base fluid of 60:40 PG/W exhibit a non-Newtonian behavior within a lower temperature range of 243 K to 273 K and a Newtonian behavior within the higher temperature range of 273 K to 363 K. The non-Newtonian behavior followed a Bingham plastic viscosity model with small yield stress values. The yield stress decreases with an increase in temperature and with a decrease in particle volumetric concentration. The viscosity of nanofluids increases with an increase in particle volumetric concentration and decreases with an increase in temperature. At the same particle volumetric concentration and temperature, if the nanoparticle diameter is larger, the viscosity of nanofluid becomes lower. Existing correlations in the literature do not predict the viscosity of nanofluids accurately. Therefore, a new model was developed from 458 experimental data points of five nanofluids. The SWCNT and BWCNT showed that the viscosity practically did not change after an ultrasonication time of 45 minutes under a prescribed power and sample volume. A correlation for the viscosity of CNT nanofluids as a function of temperature and shear rate, involving the Péclet number has been proposed from the measured values for SWCNT and BWCNT at a fixed volumetric concentration.

4.9 Acknowledgments

Financial support from the Alaska NASA EPSCoR grant # AK- NNX11AM16A is gratefully acknowledged. Authors are thankful to Petroleum Development Laboratory for providing the experimental facilities to measure the viscosity.

4.10 References

- [1] Maxwell, J. C., 1904, A Treatise On Electricity and Magnetism, Dover Publications, Inc., New York.
- [2] Choi, S. U. S., and Eastman, J. A., 1995, "Enhancing thermal conductivity of fluids with nanoparticles," International mechanical engineering congress and exhibition, D. A. Siginer, and H. P. Wang, eds. San Francisco, United States, p. 8.

- [3] Das, S. K., Putra, N., Thiesen, P., and Roetzel, W., 2003, "Temperature dependence of thermal conductivity enhancement for nanofluids," *ASME J. of Heat Transfer*, 125(4), pp. 567-574.
- [4] Koo, J., and Kleinstreuer, C., 2005, "A new thermal conductivity model for nanofluids," *Journal of Nanoparticle Research*, 6(6), pp. 577-588.
- [5] Vajjha, R. S., Das, D. K., and Kulkarni, D. P., 2010, "Development of new correlations for convective heat transfer and friction factor in turbulent regime for nanofluids," *International Journal of Heat and Mass Transfer*, 53(21-22), pp. 4607-4618.
- [6] Prasher, R., Bhattacharya, P., and Phelan, P. E., 2006, "Brownian-motion-based convective-conductive model for the effective thermal conductivity of nanofluids," *Journal of Heat Transfer*, 128(6), p. 588.
- [7] Einstein, A., 1906, "A new determination of the molecular dimensions," *Annalen der Physik*, 19(2), pp. 289-306.
- [8] Bruijn, H. d., 1942, "The viscosity of suspensions of spherical particles. (The fundamental η - c and ϕ - c relations)," *Recueil des travaux chimiques des pays Bas*, 61(12), pp. 863-874.
- [9] Vand, V., 1948, "Viscosity of solutions and suspensions. I. Theory," *Journal of Chemical Physics*, 52 (2), pp. 277-299.
- [10] Mooney, M., 1951, "The viscosity of a concentrated suspension of spherical particles," *Journal of Colloid Science*, 6(2), pp. 162-170.
- [11] Brinkman, H. C., 1952, "The viscosity of concentrated suspensions and solutions," *Journal of Chemical Physics*, 20, pp. 571-581.
- [12] Krieger, I. M., and Dougherty, T. J., 1959, "A mechanism for non-newtonian flow in suspensions of rigid spheres," *Journal of Rheology*, 3(1), pp. 137-152.
- [13] Frankel, N. A., and Acrivos, A., 1967, "On the viscosity of a concentrated suspension of solid spheres," *Chemical Engineering Science*, 22, pp. 847-853.
- [14] Batchelor, G. K., 1977, "The effect of Brownian motion on the bulk stress in a suspension of spherical particles," *Journal of Fluid Mechanics*, 83, pp. 97-117.
- [15] Graham, A., 1981, "On the viscosity of suspensions of solid spheres," *Applied Scientific Research*, 37, pp. 275-286.
- [16] Leighton, D., and Acrivos, A., 1987, "The shear-induced migration of particles in concentrated suspensions," *Journal of Fluid Mechanics*, 181, pp. 415-439.

- [17] Thomas, C. U., and Muthukumar, M., 1991, "Three-body hydrodynamic effects on viscosity of suspensions of spheres," *Journal of Chemical Physics*, 94(7), pp. 5180-5189.
- [18] Masuda, H., Ebata, A., Teramae, K., and Hishinuma, N., 1993, "Alteration of thermal conductivity and viscosity of liquid by dispersing ultra-fine particles (dispersion of Al_2O_3 , SiO_2 and TiO_2 ultra-fine particles)," *Netsu Bussei*, 7(4), pp. 227-233.
- [19] Pak, B. C., and Cho, Y. I., 1998, "Hydrodynamic and heat transfer study of dispersed fluids with submicron metallic oxide particles," *Experimental Heat Transfer*, 11(2), pp. 151-170.
- [20] Tseng, W. J., and Lin, K. C., 2003, "Rheology and colloidal structure of aqueous TiO_2 nanoparticle suspensions," *Materials Science and Engineering: A*, 355(1-2), pp. 186-192.
- [21] Maïga, S. E. B., Palm, S. J., Nguyen, C. T., Roy, G., and Galanis, N., 2005, "Heat transfer enhancement by using nanofluids in forced convection flows," *International Journal of Heat and Fluid Flow*, 26(4), pp. 530-546.
- [22] Buongiorno, J., 2006, "Convective transport in nanofluids," *J Heat Trans-T Asme*, 128(3), pp. 240-250.
- [23] Prasher, R., Song, D., Wang, J., and Phelan, P. E., 2006, "Measurements of nanofluid viscosity and its implications for thermal applications," *Applied Physics Letters*, 89(13), p. 3.
- [24] Kulkarni, D. P., Das, D. K., and Chukwu, G. A., 2006, "Temperature dependent rheological property of copper oxide nanoparticles suspension (nanofluid)," *Journal of Nanoscience and Nanotechnology*, 6(4), pp. 1150-1154.
- [25] Kulkarni, D. P., Das, D. K., and Patil, S. L., 2007, "Effect of temperature on rheological properties of copper oxide nanoparticles dispersed in propylene glycol and water mixture," *Journal of Nanoscience and Nanotechnology*, 7(7), pp. 2318-2322.
- [26] Namburu, P. K., Kulkarni, D. P., Dandekar, A., and Das, D. K., 2007a, "Experimental investigation of viscosity and specific heat of silicon dioxide nanofluids," *Micro Nano Lett*, 2(3), pp. 67-71.
- [27] Namburu, P. K., Kulkarni, D. P., Misra, D., and Das, D. K., 2007b, "Viscosity of copper oxide nanoparticles dispersed in ethylene glycol and water mixture," *Experimental Thermal and Fluid Science*, 32(2), pp. 397-402.
- [28] Nguyen, C. T., Desgranges, F., Roy, G., Galanis, N., Maré, T., Boucher, S., and Angue Mintsu, H., 2007, "Temperature and particle-size dependent viscosity data for water-based

nanofluids – Hysteresis phenomenon," *International Journal of Heat and Fluid Flow*, 28(6), pp. 1492-1506.

[29] Avsec, J., and Oblak, M., 2007, "The calculation of thermal conductivity, viscosity and thermodynamic propoerties for nanofluids on the basis of statistical nanomechanics," *International Journal of Heat and Mass Transfer*, 50(21-22), pp. 4331-4341.

[30] Chen, H., Ding, Y., He, Y., and Tan, C., 2007, "Rheological behaviour of ethylene glycol based titania nanofluids," *Chemical Physics Letters*, 444(4-6), pp. 333-337.

[31] Williams, W., Buongiorno, J., and Hu, L. W., 2008, "Experimental investigation of turbulent convective heat transfer and pressure loss of alumina/water and zirconia/water nanoparticle colloids (nanofluids) in horizontal tubes," *Journal of Heat Transfer*, 130(4), p. 042412.

[32] Namburu, P. K., Das, D. K., Tanguturi, K. A., and Vajjha, R. S., 2009, "Numerical study of turbulent flow and heat transfer characteristics of nanofluids considering variable properties," *International Journal of Thermal Sciences*, 48(2), pp. 290-302.

[33] Sahoo, B. C., Vajjha, R. S., Ganguli, R., Chukwu, G. A., and Das, D. K., 2009, "Determination of rheological behavior of aluminum oxide nanofluid and development of new viscosity correlations," *Petrol Sci Technol*, 27(15), pp. 1757-1770.

[34] Masoumi, N., Sohrabi, N., and Behzadmehr, A., 2009, "A new model for calculating the effective viscosity of nanofluids," *Journal of Physics D: Applied Physics*, 42(5), p. 055501.

[35] Kole, M., and Dey, T. K., 2010, "Viscosity of alumina nanoparticles dispersed in car engine coolant," *Experimental Thermal and Fluid Science*, 34(6), pp. 677-683.

[36] Corcione, M., 2011, "Rayleigh-Bénard convection heat transfer in nanoparticle suspensions," *International Journal of Heat and Fluid Flow*, 32(1), pp. 65-77.

[37] Kole, M., and Dey, T. K., 2011, "Effect of aggregation on the viscosity of copper oxide–gear oil nanofluids," *International Journal of Thermal Sciences*, 50(9), pp. 1741-1747.

[38] Khanafer, K., and Vafai, K., 2011, "A critical synthesis of thermophysical characteristics of nanofluids," *International Journal of Heat and Mass Transfer*, 54(19-20), pp. 4410-4428.

[39] Rohini Priya, K., Suganthi, K. S., and Rajan, K. S., 2012, "Transport properties of ultra-low concentration CuO–water nanofluids containing non-spherical nanoparticles," *International Journal of Heat and Mass Transfer*, 55(17-18), pp. 4734-4743.

[40] Andrade, E. N. d. C., 1930, "The Viscosity of Liquids," *Nature*, 125, pp. 309-310.

- [41] American Society of Heating, R., and Engineers, A.-C., 2009, ASHRAE Handbook of Fundamentals, ASHRAE, Atlanta, United States.
- [42] AlfaAesar, 2013, www.alfa.com.
- [43] Nanostructured & Amorphous Materials, I., 2013, <http://www.nanoamor.com/>.
- [44] NanoLab, 2013, <http://www.nano-lab.com/>.
- [45] White, F. M., 2005, Viscous fluid flow, McGraw-Hill New York.
- [46] Kestin, J., Sokolov, M., and Wakeham, A. W., 1978, "Viscosity of liquid water in the range -8°C to 150°C ," Journal of Physical and Chemical Reference Data, 7(3), pp. 941-948.
- [47] Wagner, N. J., and Brady, J. F., 2009, "Shear thickening in colloidal dispersions," Physics Today, 62(10), pp. 27-32.
- [48] Chermisinoff, N. P., 1988, Encyclopedia of Fluid Mechanics: Rheology and non-Newtonian flows, Gulf Publishing Company, Houston, United States.
- [49] Corcione, M., 2012, "Natural Convection in Nanofluids," Nanoparticle Heat Transfer and Fluid Flow, W. J. Minkowycz, E. M. Sparrow, and J. P. Abraham, eds., CRC Press, New York, pp. 277-318.
- [50] "Minitab 16 Statistical Software (2013). [Computer software].", Minitab, Inc. (www.minitab.com), State College, PA.
- [51] Kinloch, I. A., Roberts, S. A., and Windle, A. H., 2002, "A rheological study of concentrated aqueous nanotube dispersions," Polymer, 43, pp. 7483-7491.
- [52] Ding, Y., Alias, H., Wen, D., and Williams, R. A., 2006, "Heat transfer of aqueous suspensions of carbon nanotubes (CNT nanofluids)," International Journal of Heat and Mass Transfer, 49(1-2), pp. 240-250.
- [53] Garg, P., Alvarado, J. L., Marsh, C., Carlson, T. A., Kessler, D. A., and Annamalai, K., 2009, "An experimental study on the effect of ultrasonication on viscosity and heat transfer performance of multi-wall carbon nanotube-based aqueous nanofluids," International Journal of Heat and Mass Transfer, 52(21-22), pp. 5090-5101.
- [54] Aladag, B., Halelfadl, S., Doner, N., Maré, T., Duret, S., and Estellé, P., 2012, "Experimental investigations of the viscosity of nanofluids at low temperatures," Applied Energy, 97, pp. 876-880.

- [55] Halelfadl, S., Estellé, P., Aladag, B., Doner, N., and Maré, T., 2013, "Viscosity of carbon nanotubes water-based nanofluids: Influence of concentration and temperature," *International Journal of Thermal Sciences*, 71, pp. 111-117.
- [56] Yang, Y., Grulke, E. A., Zhang, Z. G., and Wu, G., 2006, "Thermal and rheological properties of carbon nanotube-in-oil dispersions," *Journal of Applied Physics*, 99(11), p. 8.
- [57] Stickel, J. J., and Powell, R. L., 2005, "Fluid mechanics and rheology of dense suspensions," *Annual Review of Fluid Mechanics*, 37(1), pp. 129-149.
- [58] Mueller, S., Llewellyn, E. W., and Mader, H. M., 2010, "The rheology of suspensions of solid particles," *Proceeding of the Royal Society of London. Series A, Mathematical and Physical Sciences*, 466, pp. 1201-1228.

Table 4.1. Effective viscosity models proposed by researchers.

Researchers	Effective viscosity Models
Einstein [7]	$\mu_{eff} = \mu_{bf} \left(1 + \frac{5}{2} \phi \right)$
de Bruijn [8]	$\mu_{eff} = \mu_{bf} \left(\frac{1}{1 - 2.5\phi + 1.552\phi^2} \right)$
Vand [9]	$\mu_{eff} = \mu_{bf} (1 + 2.5\phi + 7.349\phi^2 + \dots)$
Mooney [10]	$\mu_{eff} = \mu_{bf} \exp \left(\frac{2.5\phi}{1 - k\phi} \right)$
Brinkman [11]	$\mu_{eff} = \mu_{bf} \frac{1}{(1 - \phi)^{2.5}}$
Krieger and Dougherty [12]	$\mu_{eff} = \mu_{bf} \left[1 - \frac{\phi}{\phi_m} \right]^{-[\eta]\phi_m}$
Frankel and Acrivos [13]	$\mu_{eff} = \mu_{bf} \left(\frac{9}{8} \right) \left[\frac{(\phi/\phi_m)^{1/3}}{1 - (\phi/\phi_m)^{1/3}} \right]$
Batchelor [14]	$\mu_{eff} = \mu_{bf} (1 + 2.5\phi + 6.2\phi^2)$
Graham [15]	$\mu_{eff} = \mu_{bf} \left[1 + 2.5\phi + 4.5 \left(\frac{1}{\frac{h}{r_p} \left[2 + \frac{h}{r_p} \right] \left[1 + \frac{h}{r_p} \right]^2} \right) \right]$
Leighton and Acrivos [16]	$\mu_{eff} = \mu_{bf} \left[1 + \frac{0.5\mu_{in}\phi}{1 - (\phi/\phi_m)} \right]$
Thomas and Muthukumar [17]	$\mu_{eff} = \mu_{bf} (1 + 2.5\phi + 4.8292\phi^2 + 6.4028\phi^3 + \dots)$

Table 4.2. Effective viscosity models for nanofluids proposed by researchers.

<p align="center">Researchers & nanofluids viscosity models</p>	<p align="center">Specifications regarding nanoparticle material, base fluid, d_p, ϕ, T</p>
<p align="center">Tseng and Lin [20]</p> $\mu_{nf} = \mu_{bf}(13.47e^{35.98\phi})$	<p align="center">TiO₂, water, 7-20 nm, 0-2.5%, 293-333 K</p>
<p align="center">Maiga et al. [21]</p> $\mu_{nf} = \mu_{bf}(1 + 7.3\phi + 123\phi^2)$ $\mu_{nf} = \mu_{bf}(1 - 0.19\phi + 306\phi^2)$	<p align="center">Al₂O₃, water, 13&28 nm, 0-5%, 298 K Al₂O₃, ethylene glycol, 28 nm, 0-5%, 298 K</p>
<p align="center">Buongiorno [22]</p> $\mu_{nf} = \mu_{bf}(1 + 39.11\phi + 533.9\phi^2)$ $\mu_{nf} = \mu_{bf}(1 + 5.45\phi + 108.2\phi^2)$	<p align="center">Al₂O₃, water, 13 nm, 0-10%, 298 K TiO₂, water, 27 nm, 0-10%, 298 K</p>
<p align="center">Prasher et al. [23]</p> $\mu_{nf} = \mu_{bf}(1 + 10\phi)$	<p align="center">Al₂O₃, propylene glycol, 27 nm, 40 nm & 50 nm, 0-3%, 303-333 K Al₂O₃, ethylene glycol, 28 nm, 0-4%, 298 K Al₂O₃, water, 28 nm, 0-4%, 298 K Al₂O₃, water, 38 nm, 0-4%, 293-333 K Al₂O₃, water, 27 nm, 40 nm & 50 nm, 0-3%, 303-333 K</p>

Table 4.2 continued...

<p>Kulkarni et al. [24]</p> $\ln(\mu_{nf}) = A \left(\frac{1}{T} \right) - B$ <p>where $A = 1078.3 + 15857\phi + 20587\phi^2$; $B = 2.8715 + 53.548\phi - 107.12\phi^2$</p>	<p>CuO, water, 29 nm, 5-15%, 278-323 K</p>
<p>Kulkarni et al. [25]</p> $\mu_{nf} = A(e^{B\phi})$ <p>where $\ln(A) = 736.9e^{-0.0199T}$; $B = 44.794 - 0.0765T$</p>	<p>CuO, 60:40 PG/W, 29 nm, 0-5%, 238 -323 K</p>
<p>Namburu et al. [26]</p> $\log(\mu_{nf}) = A e^{-BT}$ <p>where $A = 167.17 - 2.245\phi - 1.9289\phi^2 + 0.1193\phi^3$; $B = 0.0192 - 0.0004\phi - 7 \times 10^{-6}\phi^2$</p>	<p>SiO₂,60:40 EG/W, 20 nm, 50 nm & 100 nm, 0-10%, 238-323 K</p>
<p>Namburu et al. [27]</p> $\log(\mu_{nf}) = Ae^{-BT}$ <p>where $A = 165.56 - 29.643\phi + 1.8375\phi^2$; $B = 0.0186 - 0.001\phi - 4 \times 10^{-6}\phi^2$</p>	<p>CuO, 60:40 EG/W, 29 nm, 0-6%, 238-323 K</p>
<p>Nguyen et al. [28]</p> $\mu_{nf} = \mu_{bf}(0.904e^{0.148\phi})$ $\mu_{bf} = \mu_{nf}(1 + 0.025\phi + 0.015\phi^2)$ $\mu_{bf} = \mu_{nf}(1.475 - 0.319\phi + 0.051\phi^2 + 0.009\phi^3)$	<p>Al₂O₃,water, 47 nm, 0-12%, 293-348 K Al₂O₃,water, 36 nm, 0-12%, 293-348 K CuO,water,29 nm, 0-12%, 293-348 K</p>

Table 4.2 continued...

<p>Avsec & Oblak [29]</p> $\mu_{nf} = \mu_{bf} [1 + (2.5\alpha_e) + (2.5\alpha_e)^2 + (2.5\alpha_e)^3 + (2.5\alpha_e)^4 + \dots];$ <p>where $\alpha_e = \phi \left(1 + \frac{2h}{d_p}\right)^3$ and h is the liquid layer thickness</p>	<p>A theoretical model tested with Al_2O_3, water, 13 nm, 0-10%, 298 K TiO_2, water, 27 nm, 0-10%, 298 K</p>
<p>Chen et al. [30]</p> $\mu_{nf} = \mu_{bf} [1 + (10.6\phi) + (10.6\phi)^2]$	<p>TiO_2, ethylene glycol, 25 nm, 0-3%, 293-333 K</p>
<p>Williams et al. [31]</p> $\mu_{nf} = \mu_{bf} e^{\left[\frac{4.91\phi}{0.2092-\phi}\right]}$ $\mu_{nf} = \mu_{bf} e^{\left[\frac{11.19\phi}{0.1960-\phi}\right]}$	<p>Al_2O_3, water, 46 nm, 0-3.6%, 293-353 K ZrO_2, water, 60 nm, 0-0.9%, 293-353 K</p>
<p>Namburu et al. [32]</p> $\log(\mu_{nf}) = Ae^{-BT}$ <p>Where $A = 236.11 - 55.444\phi + 6.7388\phi^2 - 0.29956\phi^3$; $B = (20341 - 1478.5\phi + 140.03\phi^2 - 6.4745\phi^3) \times 10^{-6}$</p>	<p>Al_2O_3, 60:40 EG/W, 53 nm, 0-10%, 238-323 K</p>
<p>Sahoo et al. [33]</p> $\mu_{nf} = (1.2200 \times 10^{-6}) e^{\left(\frac{4285}{T} + 0.1448\phi\right)}$ $\mu_{nf} = (2.3920 \times 10^{-4}) e^{\left(\frac{2903}{T} + 0.1265\phi\right)}$	<p>Al_2O_3, 60:40 EG/W, 53 nm, 0-10%, 238-273 K Al_2O_3, 60:40 EG/W, 53 nm, 0-10%, 273-</p>

Table 4.2 continued...

<p>Masoumi et al. [34]</p> $\mu_{nf} = \mu_{bf} \left(1 + \frac{\rho_p V_B d_p^2}{72 \delta C \mu_{bf}} \right); \text{ where the correction factor}$ $C = \mu_{bf}^{-1} (1.133e^{-06} d_p - 2.771e^{-06}) \phi + (9e^{-08} d_p - 3.93e^{-07})$	<p>An empirical model tested with</p> <p>Al₂O₃, water, 36 nm, 0-5%, 298-338 K</p> <p>Al₂O₃, water, 28 nm, 0-5%, 295-333 K</p> <p>TiO₂, ethylene glycol, 25 nm, 0-2.3% 295-333 K</p> <p>CuO, water, 29 nm, 0-4.5%, 295-333 K</p> <p>CuO, 60:40 EG/W, 29 nm, 0-6%, 243-323 K</p>
<p>Kole and Dey [35]</p> <p>$\log(\mu_{nf}) = Ae^{BT}$; where A & B are curve-fit parameters derived for different concentrations</p>	<p>Al₂O₃, 50:50 PG/W, 50 nm, 0-1.5%, 283- 323 K</p>
<p>Corcione [36]</p> $\frac{\mu_{nf}}{\mu_{bf}} = \frac{1}{1 - 34.87(d_p/d_{bf})^{-0.3} \phi^{1.03}}$ <p>where d_{bf} is the equivalent diameter of base fluid molecule;</p> $d_{bf} = 0.1 \left[\frac{6M}{N\pi\rho_{bf}o} \right]^{1/3}$	<p>Empirical correlation from the viscosity data of various researchers</p>
<p>Kole and Dey [37]</p> <p>$\ln(\mu_{nf}) = A + 1000 B/(T + C)$; where A, B & C are curve-fit parameters derived for different concentrations</p>	<p>CuO, gear oil, 40 nm, 0-2.5%, 283-353 K</p>

Table 4.2 continued...

<p style="text-align: center;">Khanafer and Vafai [38]</p> $\mu_{nf} = -0.4491 + \frac{28.837}{T} + 0.574\phi - 0.1634\phi^2 + 23.053 \left(\frac{\phi}{T}\right)^2$ $+ 0.0132\phi^3 - 2354.735 \frac{\phi}{T^3} + 23.498 \left(\frac{\phi}{d_p}\right)^2$ $- 3.0185 \frac{\phi^3}{d_p^2}$	<p style="text-align: center;">Empirical correlation from the viscosity data of various researchers</p> <p style="text-align: center;">Al₂O₃, water, 13 ≤ d_p ≤ 131 nm, 1-9%, 293-343 K</p>
<p style="text-align: center;">Rohini et al. [39]</p> $\frac{\mu_{nf}}{\mu_{bf}} = (1 + 120.62\phi + 7576.86\phi^2)e^{(0.28\phi+332.86\phi^2)T}$	<p style="text-align: center;">CuO, water, cylindrical particle aspect ratio (d/l)=10, 0-1.6%, 301-328 K</p>

Table 4.3. Characteristics of nanoparticles used in the present study as specified by the manufacturers.

Type of nanoparticle	Density (kg/m ³)	Average particle size (nm)
Al ₂ O ₃	3600	53 and 20
CuO	6500	29
SiO ₂	2220	30
TiO ₂	4230	10±5
ZnO	5600	77 and 50

Table 4.4. Characteristics of carbon nanotubes specified by the manufacturer.

Properties	Carboxyl-SWCNT	Carboxyl-BWCNT	Carboxyl-MWCNT
Diameter (nm)	1.5	15±5	15±5
Length (µm)	1-5	1-5	1-5
No. of walls	1	10	10

Table 4.5. Correlations for the viscosity of DI water and 60:40 PG/W.

Fluid	Correlation	Max. dev.*
Water [45]	$\ln\left(\frac{\mu}{\mu_0}\right) = 7.003\left(\frac{T_0}{T}\right)^2 - 5.306\left(\frac{T_0}{T}\right) - 1.704$ $273 \text{ K} \leq T \leq 363 \text{ K}; \mu_0 = 0.001788 \text{ kg/(m.s)},$ $T_0=273 \text{ K}$	±0.5%
Water [46]	$\log_{10}\left(\frac{\mu}{1.002}\right) = \frac{20 - T}{T + 96} [1.2378 - 1.303E$ $- 03(20 - T) + 3.06E - 06(20 - T)^2$ $+ 2.55E - 08(20 - T)^3]$ $-8 \text{ }^\circ\text{C} \leq T \leq 150 \text{ }^\circ\text{C}; \text{ Here } T \text{ is in } ^\circ\text{C}$	±0.26%
60:40 PG/W (present study)	$\ln\left(\frac{\mu}{\mu_0}\right) = 6.1855\left(\frac{T_0}{T}\right)^2 + 5.9484\left(\frac{T_0}{T}\right) - 12.139$ $238 \text{ K} \leq T < 273 \text{ K}; R^2 = 1; \mu_0 = 0.03132 \text{ kg/(m.s)},$ $T_0=273 \text{ K}$	±0.5%
	$\ln\left(\frac{\mu}{\mu_0}\right) = 17.659\left(\frac{T_0}{T}\right)^2 - 17.435\left(\frac{T_0}{T}\right) - 0.2229$ $273 \text{ K} \leq T \leq 393 \text{ K}; R^2 = 1; \mu_0 = 0.03132 \text{ kg/(m.s)},$ $T_0=273 \text{ K}$	±0.5%

*Maximum deviation is between the literature data and the curve-fit correlation

Table 4.6. Curve-fit coefficients of different nanofluids derived for Eq. (4.3).

Type of nanofluid	<i>A</i>	<i>B</i>	<i>C</i>	<i>d_p</i> (nm)	<i>T</i> (K)	ϕ (%)	% Max. Deviation
Al₂O₃	0.087113	10.0778	2.2663	53	243 to 273	1 to 6	± 6.27
	3.22478	9.40463	-1.33429		273 to 363		
	0.083941	21.5655	2.25491	20	243 to 273	1 to 4	± 6.65
	2.22043	17.1297	-0.89042		273 to 363		
CuO	0.056853	23.7352	2.61494	29	243 to 273	1 to 5	± 6.71
	1.7225	18.7338	-0.60339		273 to 363		
SiO₂	0.11855	6.79704	1.96651	30	243 to 273	1 to 5	± 6.46
	3.11747	6.11298	-1.2898		273 to 363		
TiO₂	0.101304	30.6188	2.00325	15	243 to 273	1 & 1.5	± 3.48
	1.90537	27.4305	-0.87336		273 to 363		
ZnO	0.105222	10.2897	2.06659	77	243 to 273	1 to 6	± 6.26
	2.76754	9.29369	-1.1526		273 to 363		
	0.092579	13.336	2.16365	50	243 to 273	1 to 5	± 5.27
	2.78555	11.2954	-1.17814		273 to 363		

Table 4.7. Curve-fit coefficients derived for Eq. (4.4) in two temperature regimes.

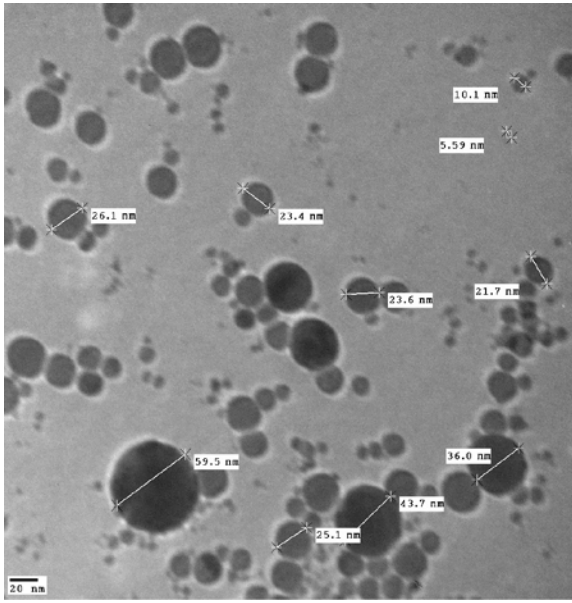
Temp. regime	<i>A₁</i>	<i>A₂</i>	<i>A₃</i>	<i>A₄</i>	<i>A₅</i>
243 K < T ≤ 273 K	3.420224E-5	36.3093	24.6829	42.394	0.180571
273 K < T ≤ 363 K	1490.8033	23.3085	8.23538	-14.282	0.10304

Table 4.8. Temperature dependence of flow consistency factor K and flow behavior index n for the CNT nanofluids.

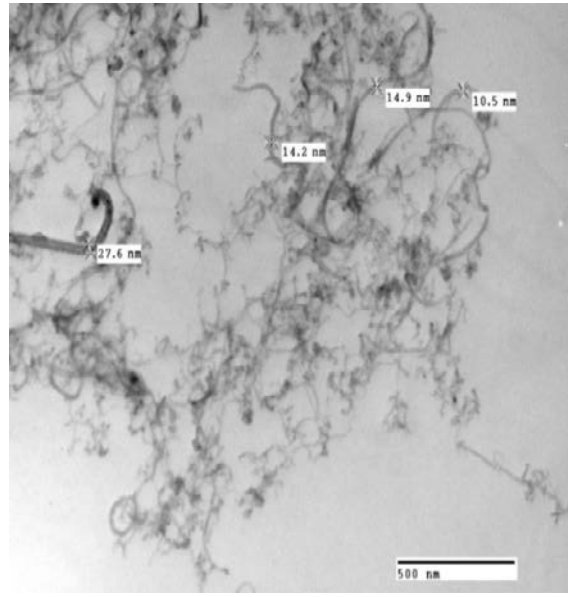
Type of CNT	T (K)	Type of model	Equation
SWCNT	273	Herschel-Bulkley	$\tau = 1.2464 + 0.7691\dot{\gamma}^{0.8689}$
	313	Bingham plastic	$\tau = 0.0455 + 0.04224\dot{\gamma}$
BWCNT	273	Bingham plastic	$\tau = 1.1916 + 0.5091\dot{\gamma}$
	313	Bingham plastic	$\tau = 0.5483 + 0.0665\dot{\gamma}$
MWCNT	273	Herschel-Bulkley	$\tau = 2.5304 + 1.9629\dot{\gamma}^{0.7727}$
	313	Bingham plastic	$\tau = 1.6537 + 0.0723\dot{\gamma}$

Table 4.9. Curve-fit coefficients derived for Eq. (4.7) in two temperature regimes.

Temp.(K)	SWCNT			BWCNT			Max. Deviation%
	a_1	a_2	a_3	a_1	a_2	a_3	
$273 \leq T \leq 303$	2.70922	-0.20887	-6.1012	9.96377	-0.0985	-6.6796	± 10
$303 < T \leq 363$	2.0457	-0.16819	-1.5097	4.62117	-0.1377	-1.5652	± 10



(a)



(b)

Figure 4.1. TEM images of (a) Al_2O_3 nanoparticles of APS 20 nm and (b) BWCNT taken before conducting the rheological measurements.

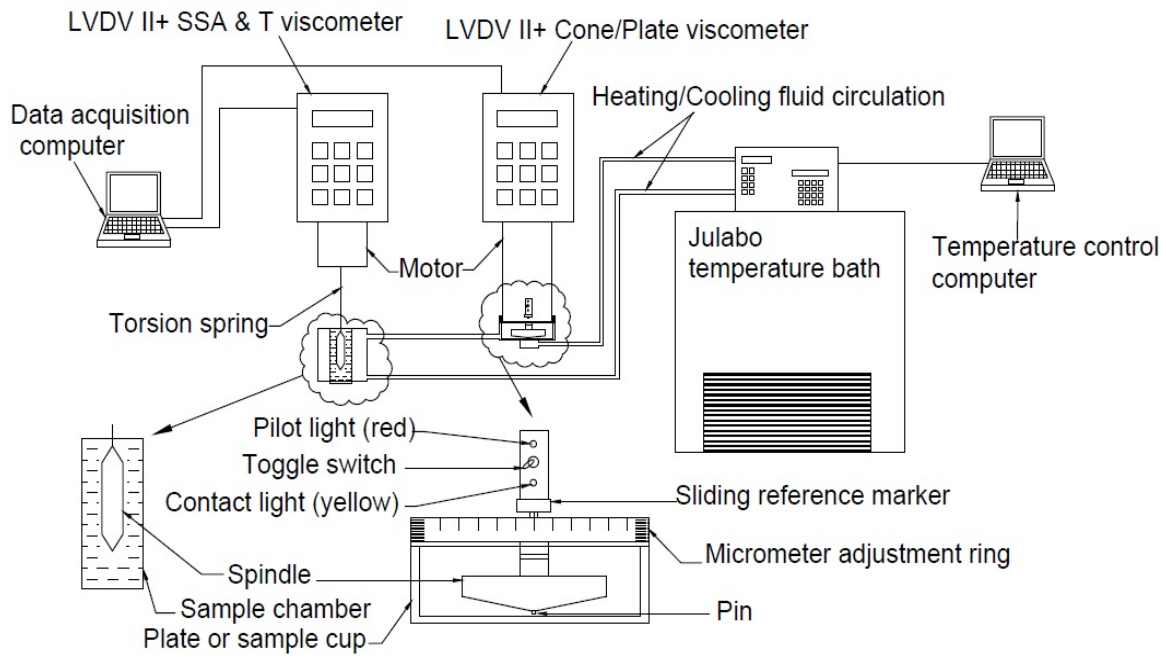


Figure 4.2. Experimental setup for viscosity measurement of nanofluids and carbon nanotubes.

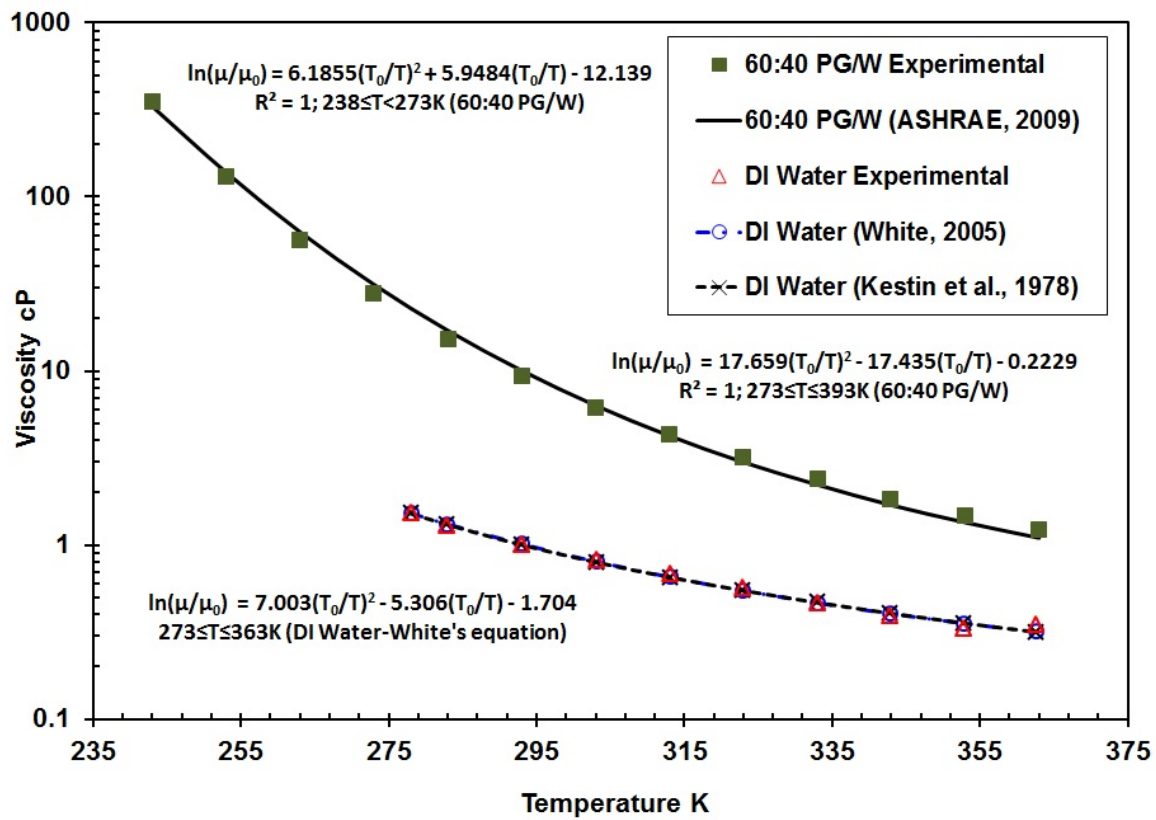


Figure 4.3. Benchmark test cases for the viscosity of 60:40 PG/W and DI water.

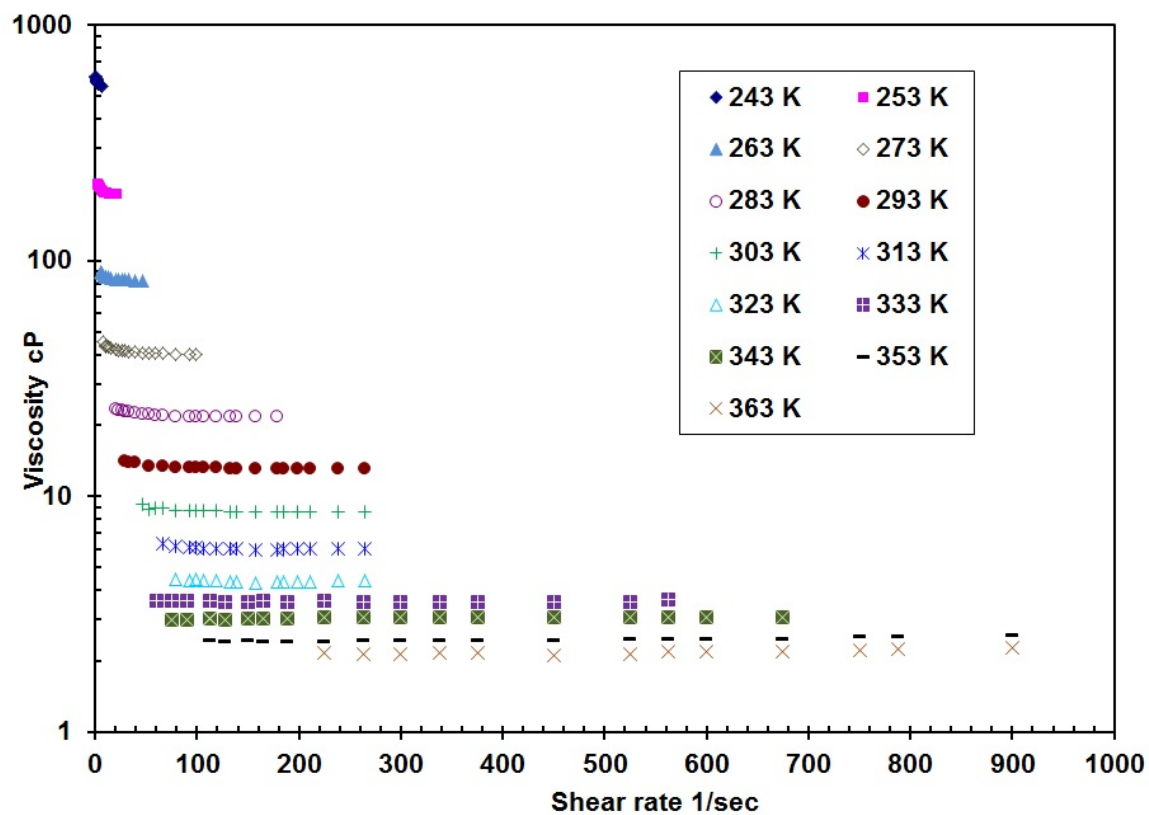


Figure 4.4. Viscosity variation with shear strain rate of Al_2O_3 nanofluid of 4% particle volume concentration for varying temperatures from 243 K (-30 °C) to 363 K (90 °C).

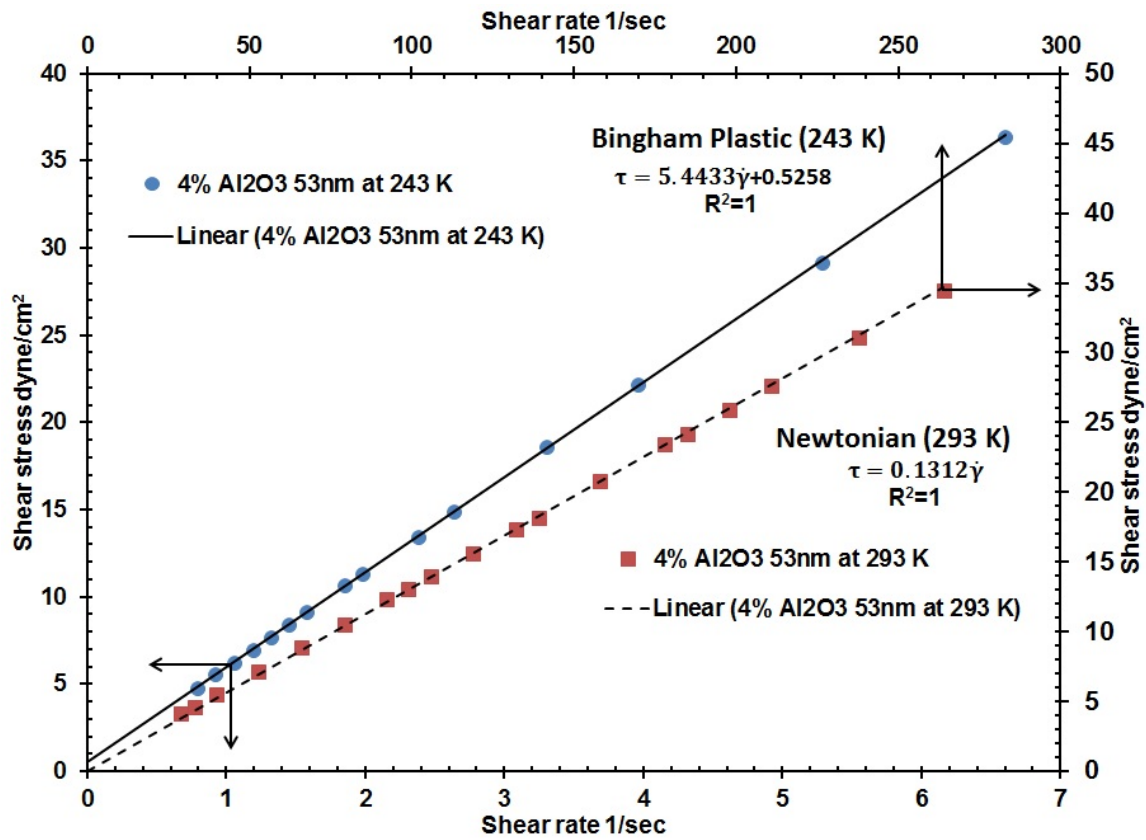


Figure 4.5. Shear stress versus shear strain rate for a 4% particle volume concentration of Al₂O₃ nanofluent at 243 K (-30°C) and 293 K (20°C).

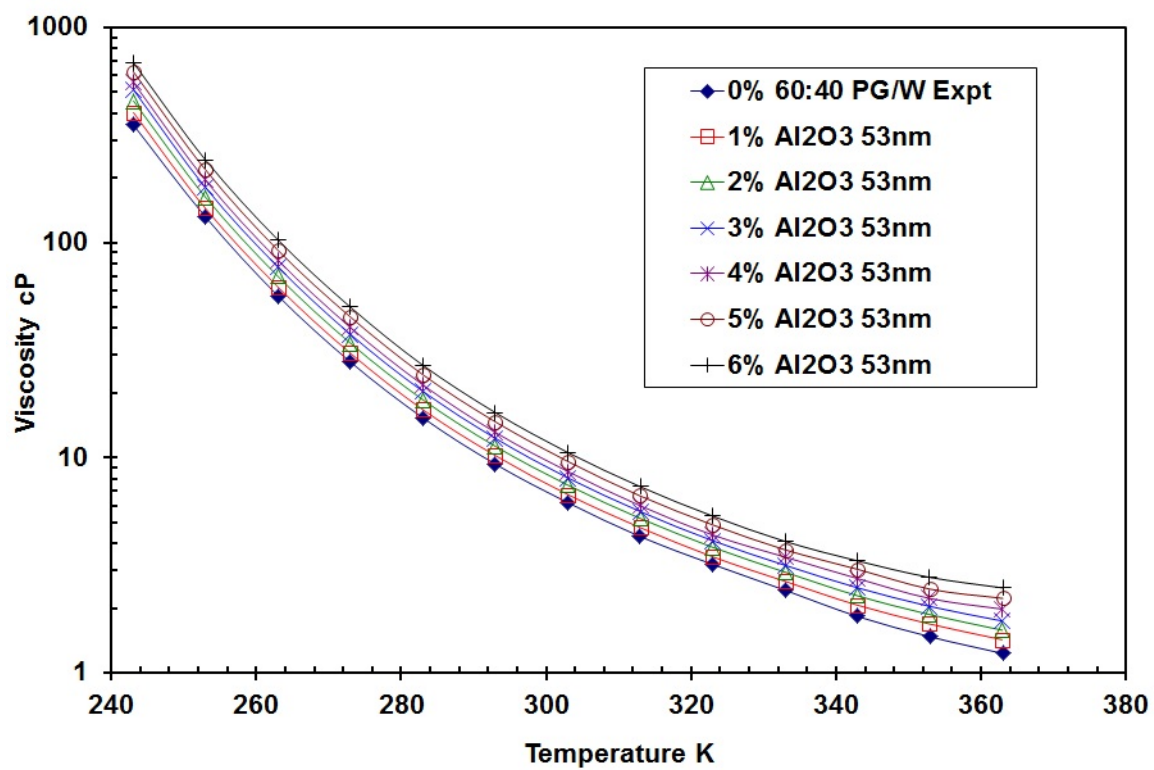


Figure 4.6. Viscosity variation with temperature at different particle volumetric concentrations of Al₂O₃ nanoparticles of APS 53 nm suspended in 60:40 PG/W.

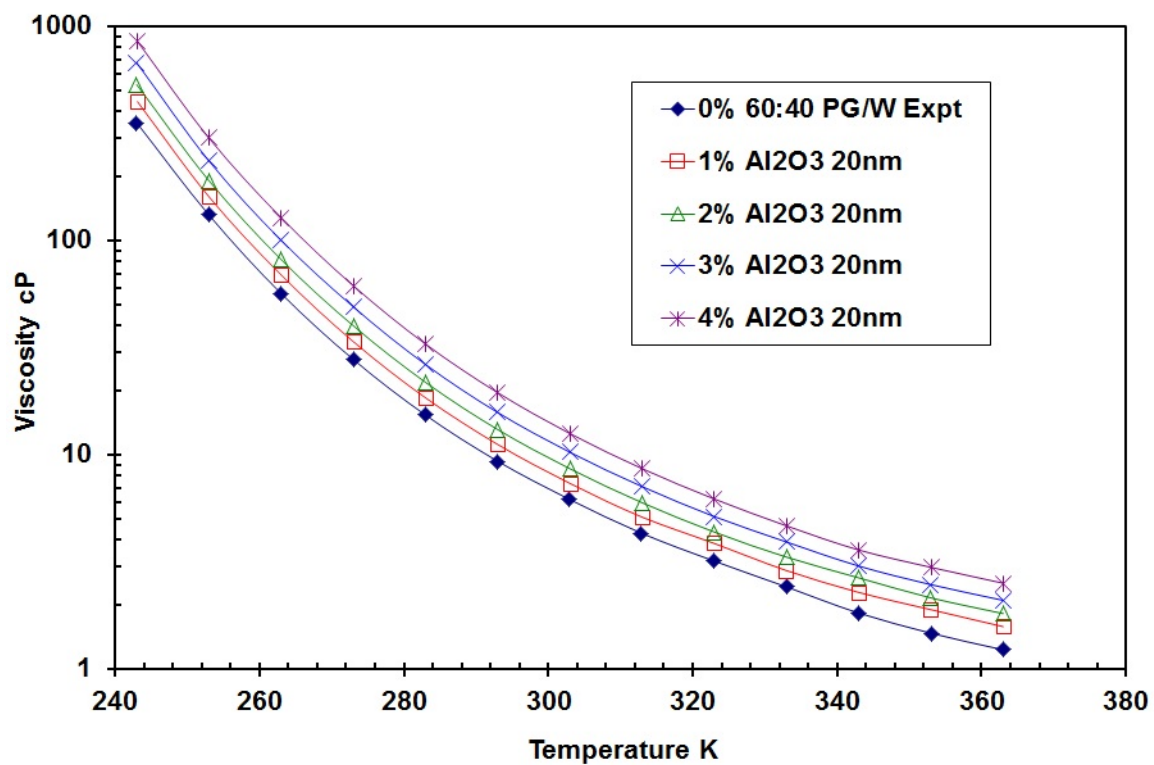


Figure 4.7. Viscosity variation with temperature at different particle volumetric concentrations of Al₂O₃ nanoparticles of APS 20 nm suspended in 60:40 PG/W.

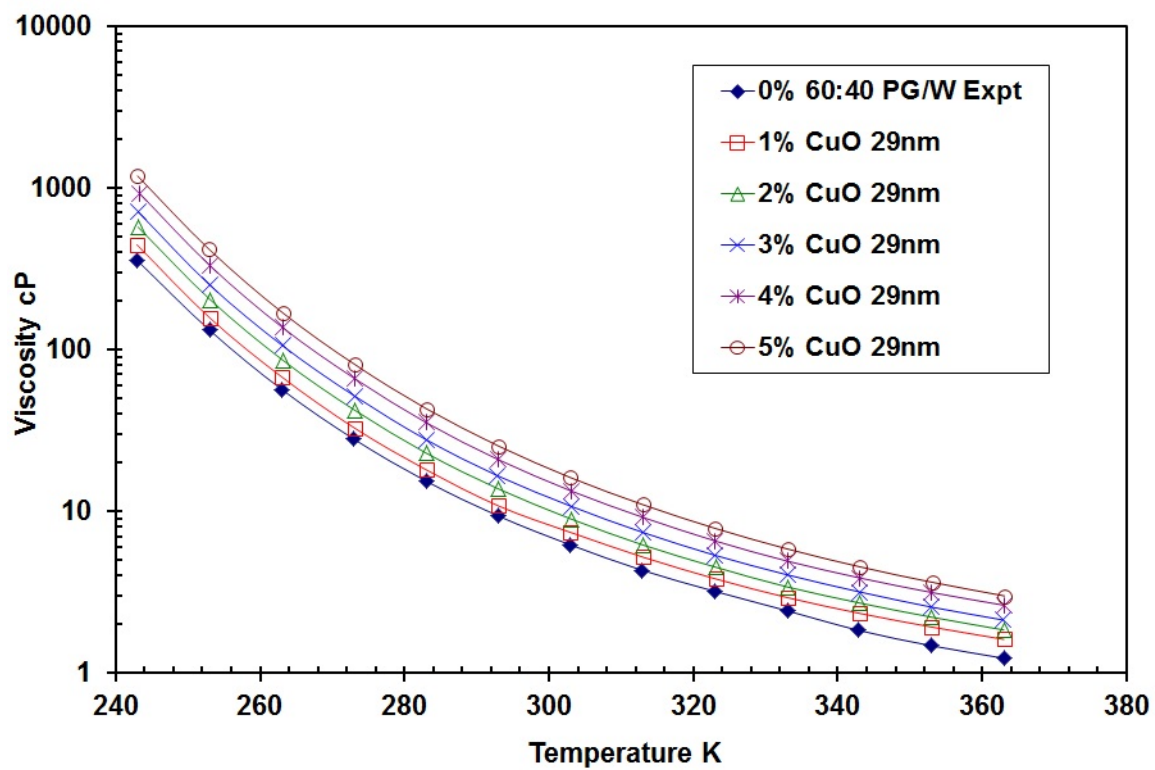


Figure 4.8. Viscosity variation with temperature at different particle volumetric concentrations of CuO nanoparticles of APS 29 nm suspended in 60:40 PG/W.

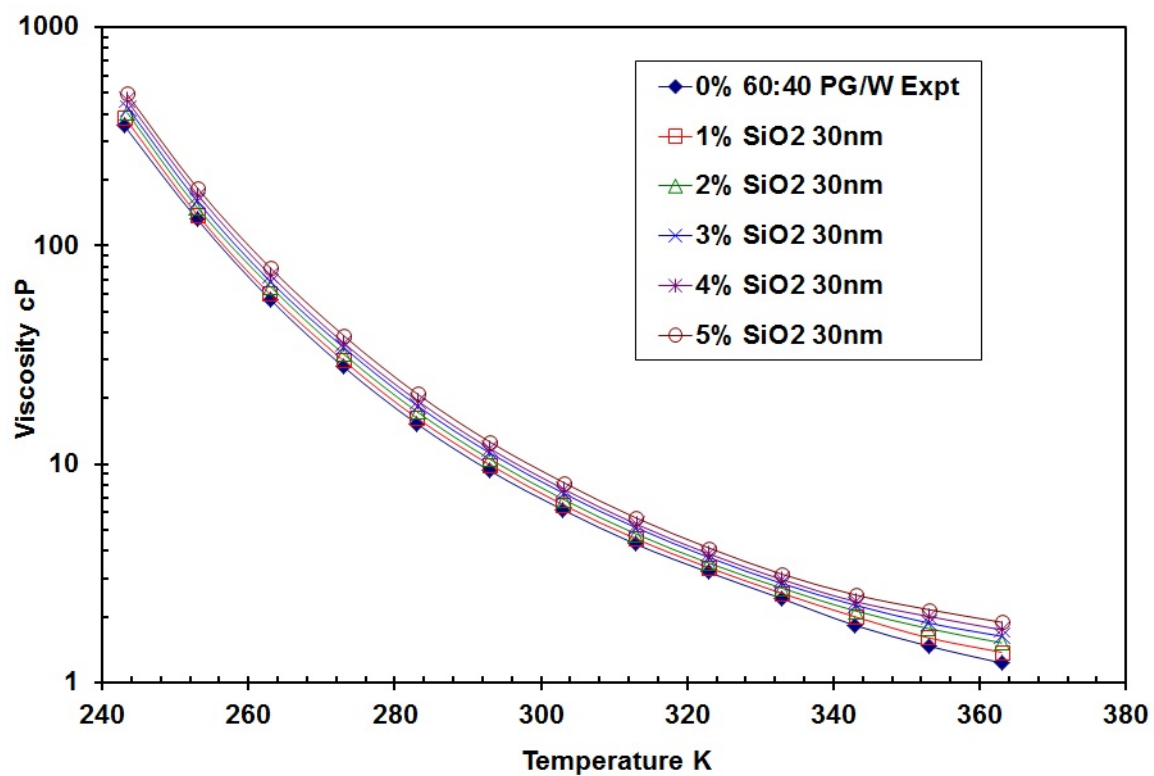


Figure 4.9. Viscosity variation with temperature at different particle volumetric concentrations of SiO₂ nanoparticles of APS 30 nm suspended in 60:40 PG/W.

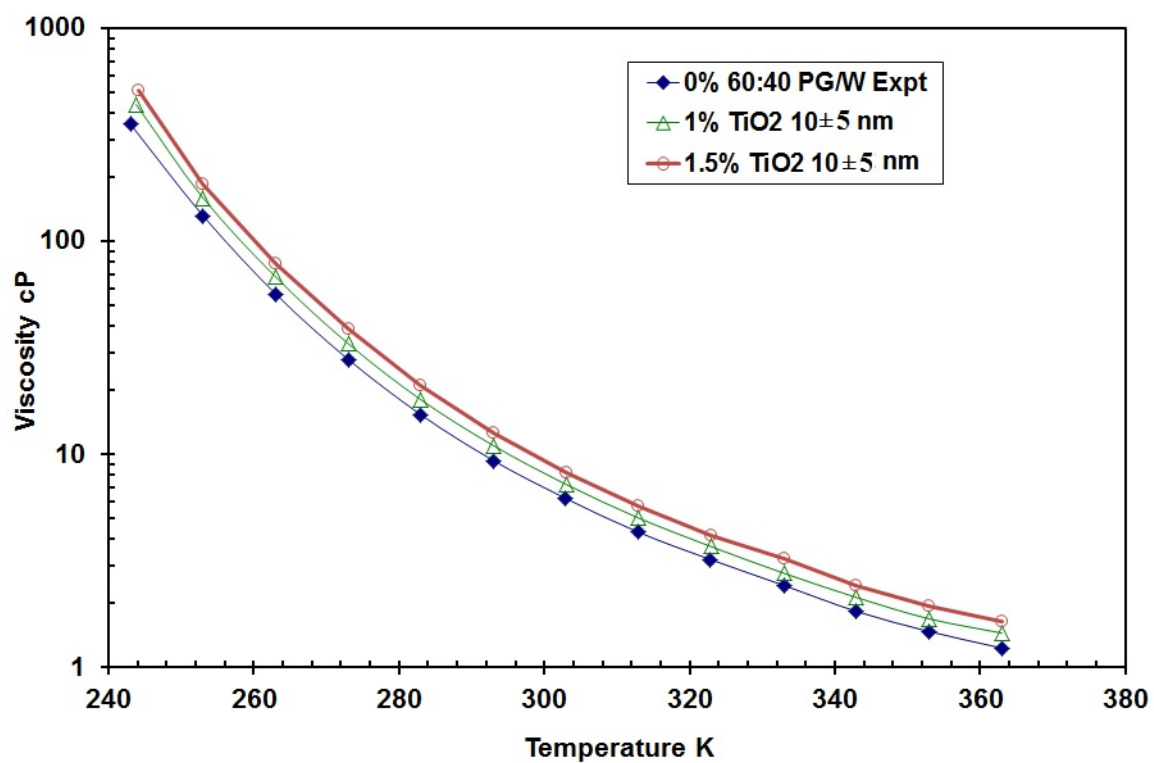


Figure 4.10. Viscosity variation with temperature at different particle volumetric concentrations of TiO₂ nanoparticles of APS 10±5 nm suspended in 60:40 PG/W.

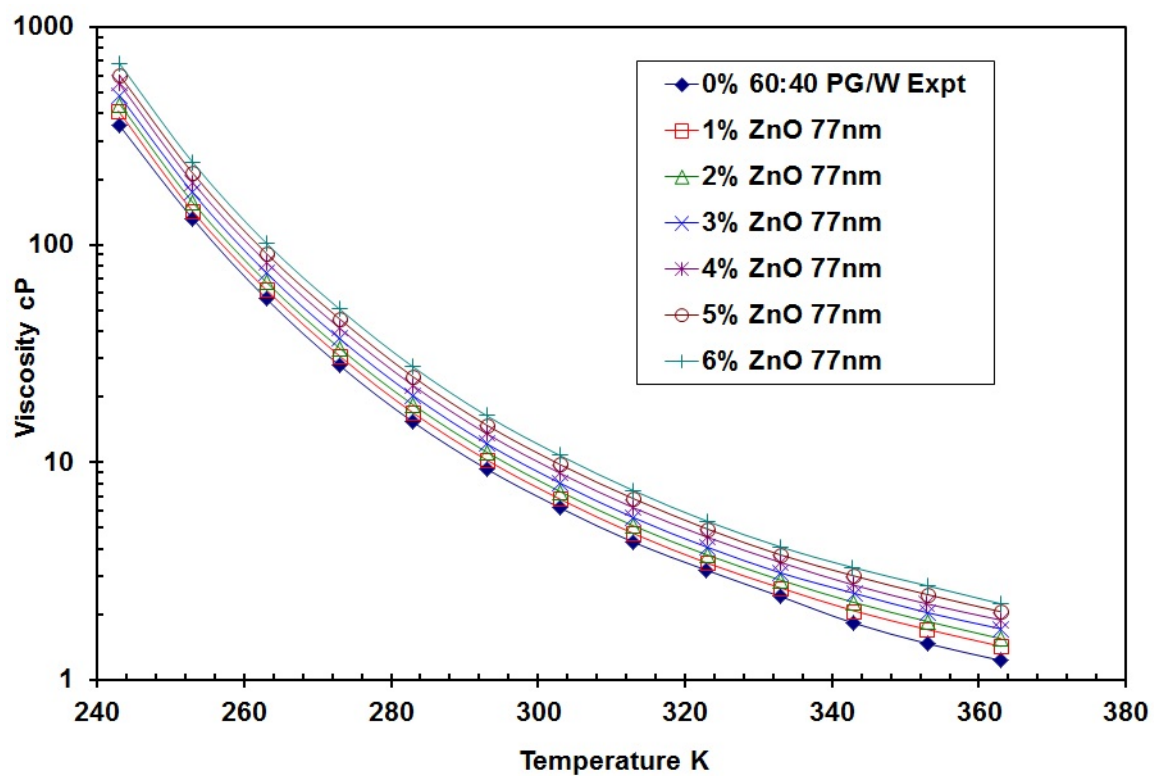


Figure 4.11. Viscosity variation with temperature at different particle volumetric concentrations of ZnO nanoparticles of APS 77 nm suspended in 60:40 PG/W.

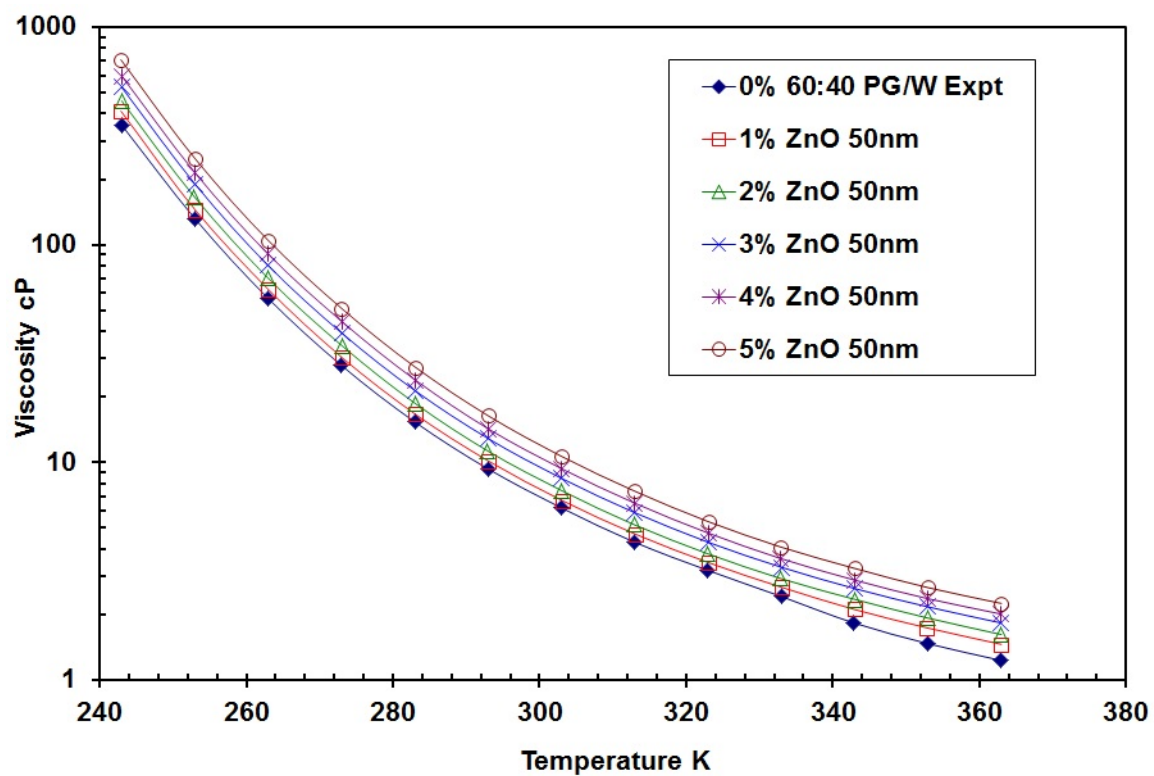


Figure 4.12. Viscosity variation with temperature at different particle volumetric concentrations of ZnO nanoparticles of APS 50 nm suspended in 60:40 PG/W.

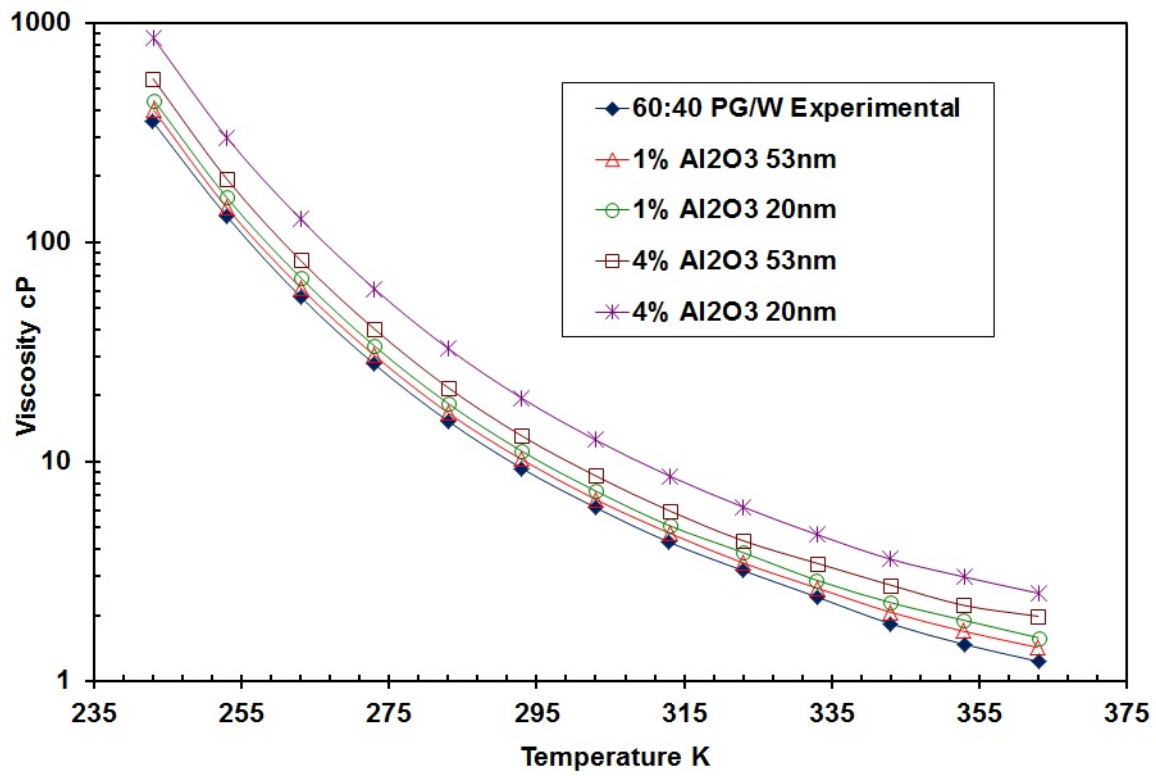


Figure 4.13. Effect of nanoparticle size on viscosity for varying temperatures at two different particle sizes and volumetric concentrations of Al₂O₃ nanofluid in 60:40 PG/W.

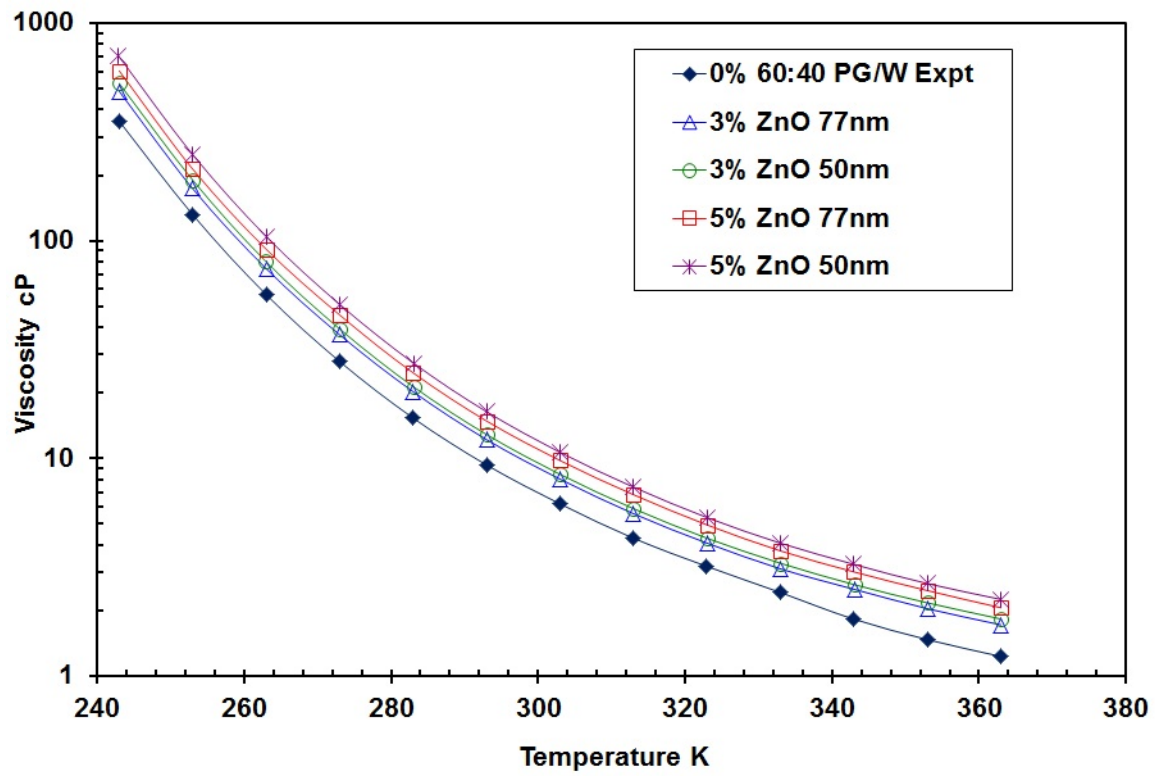


Figure 4.14. Effect of nanoparticle diameter on viscosity for varying temperatures at two different particle volumetric concentrations of ZnO nanofluid in 60:40 PG/W.

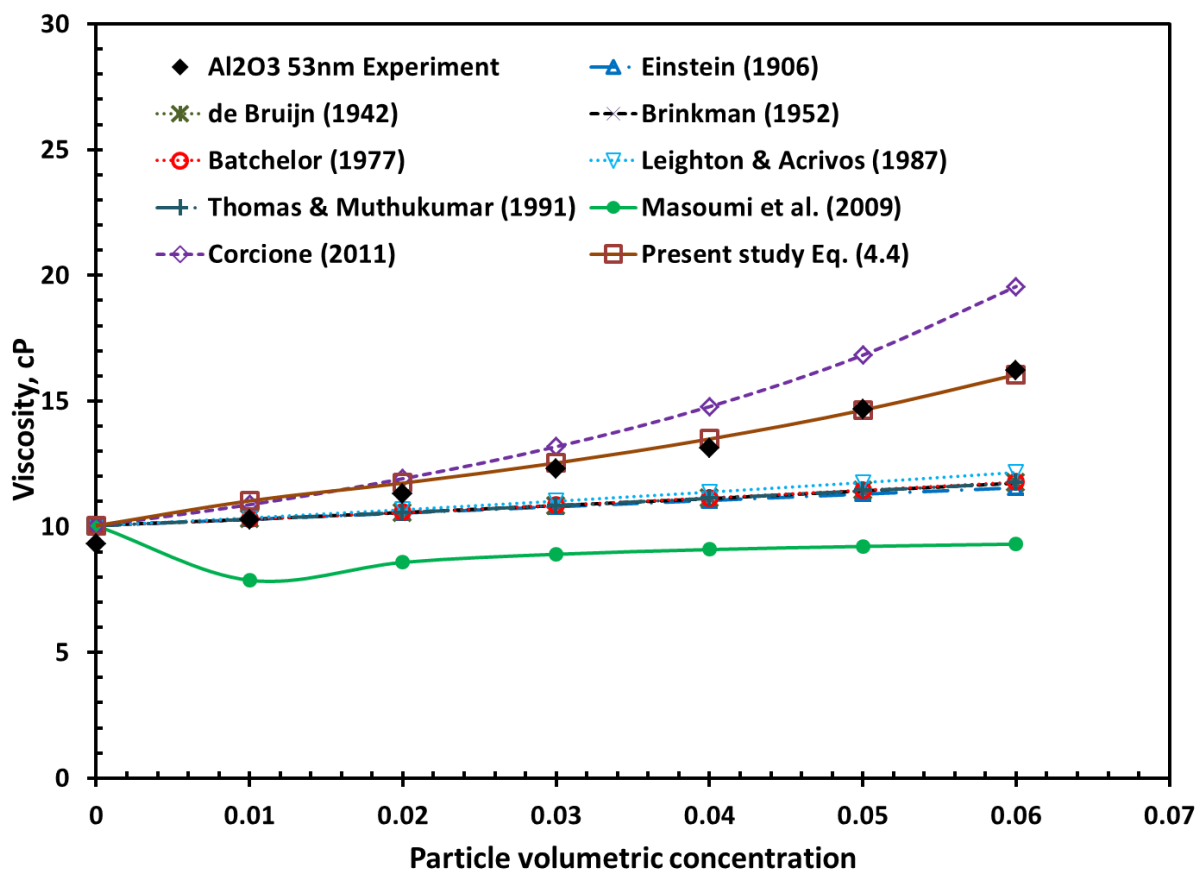


Figure 4.15. Comparison between several theoretical models and experimental data on viscosity for Al₂O₃-PG/Water nanofluids as a function of particle volumetric concentration at a room temperature of 293 K.

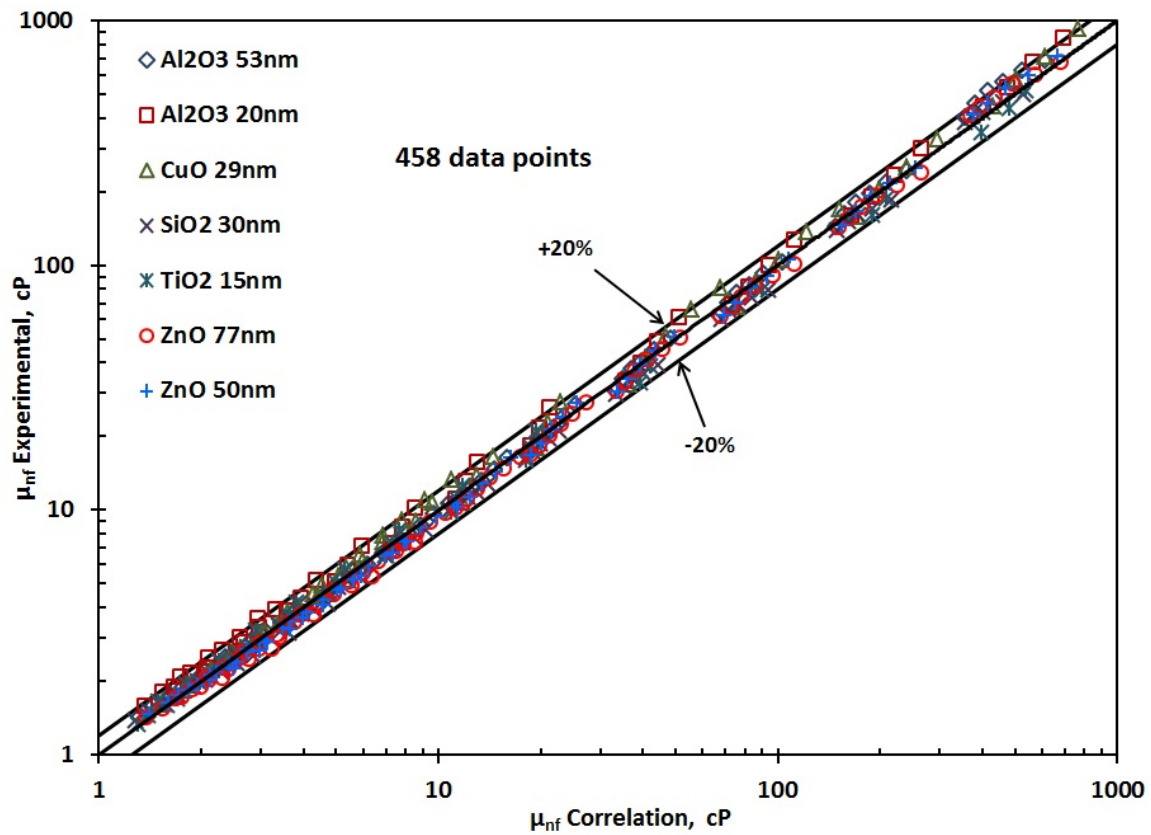
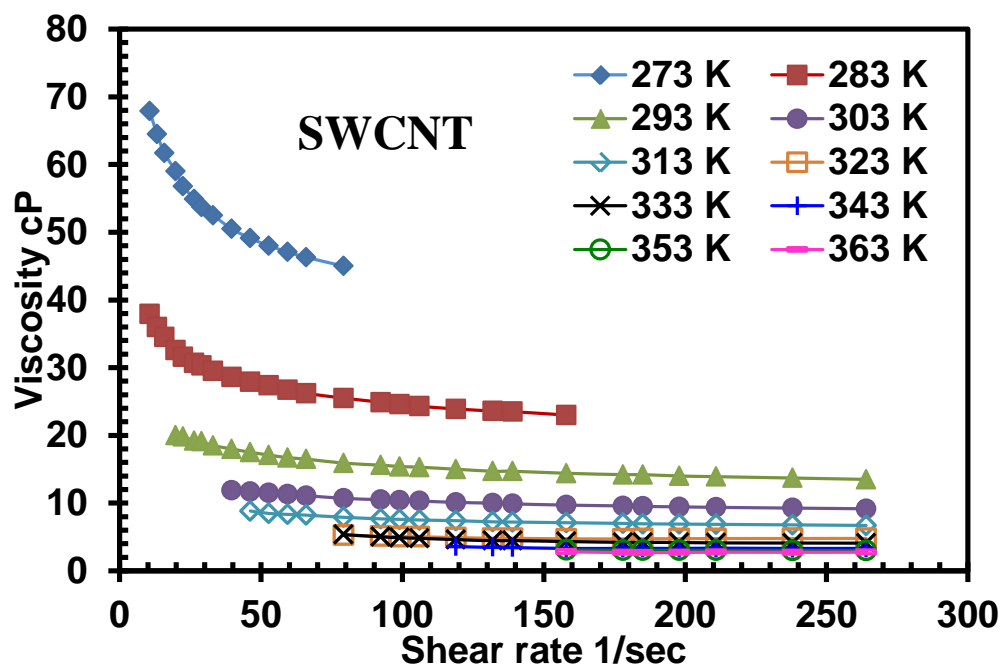
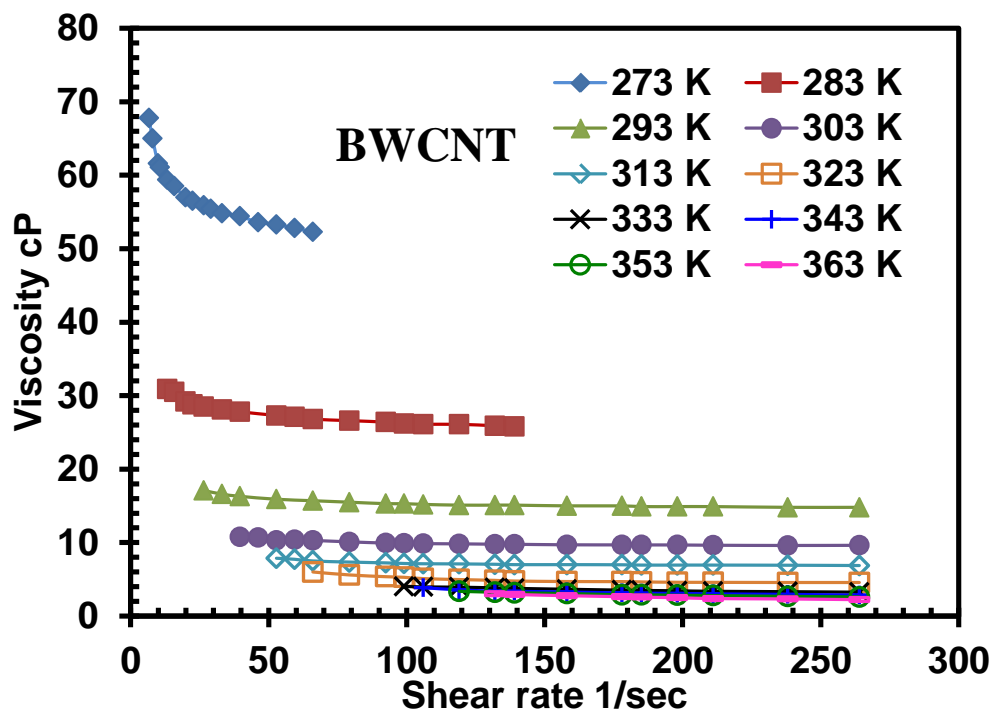


Figure 4.16. Comparison of the viscosity values calculated from the present correlation, Eq. (4.4) with the values obtained from the experiments.

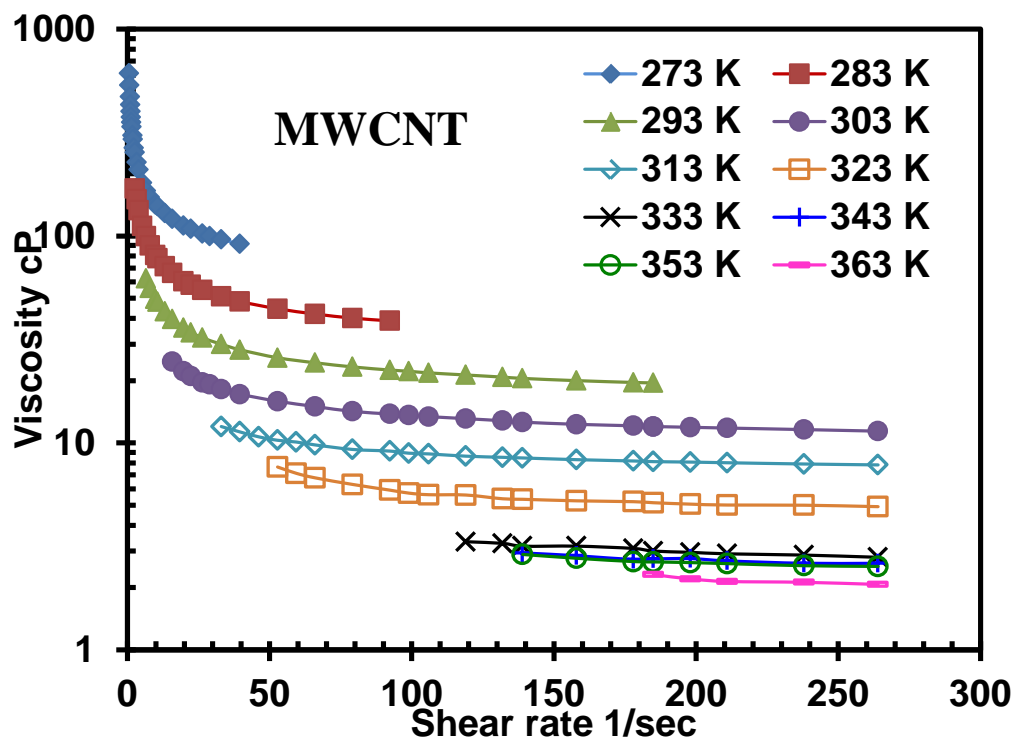


(a)



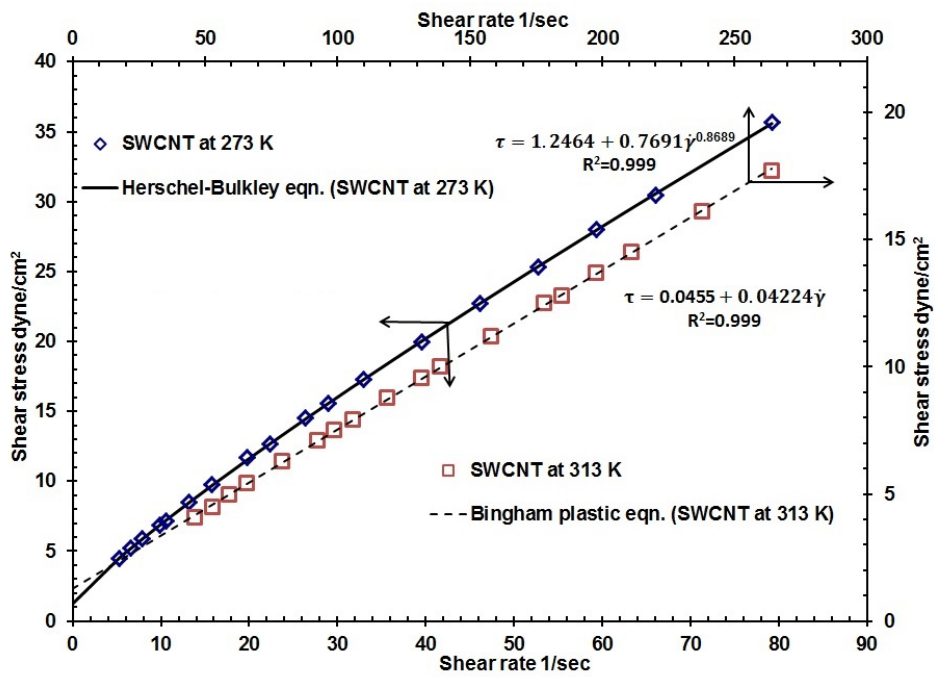
(b)

Figure 4.17. Viscosity variation with shear strain rate over a temperature range of 273 K to 363 K for a 0.229% volume concentration of (a) SWCNT, (b) BWCNT and (c) MWCNT.

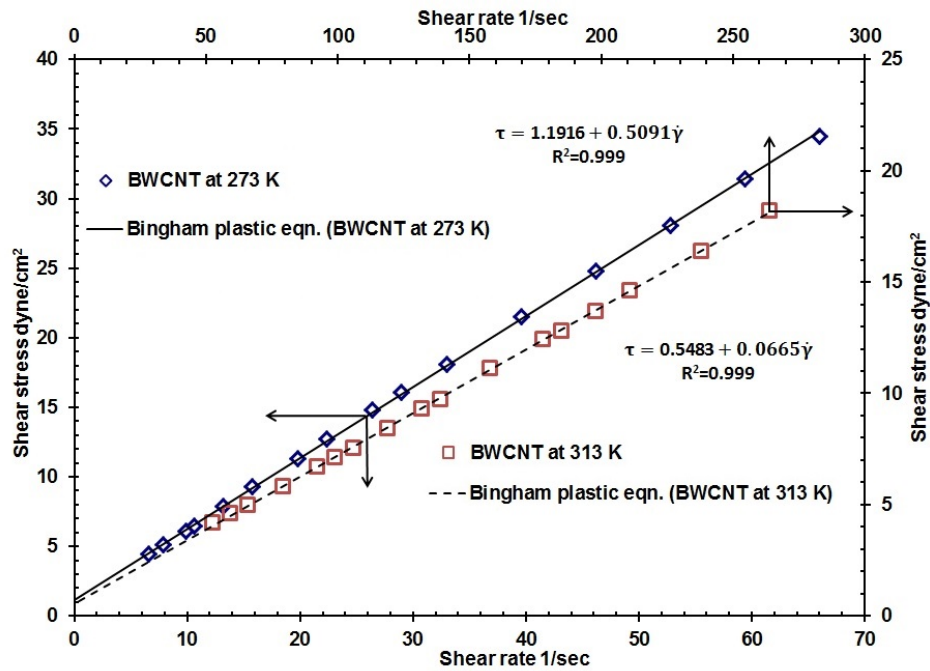


(c)

Figure 4.17 continued...

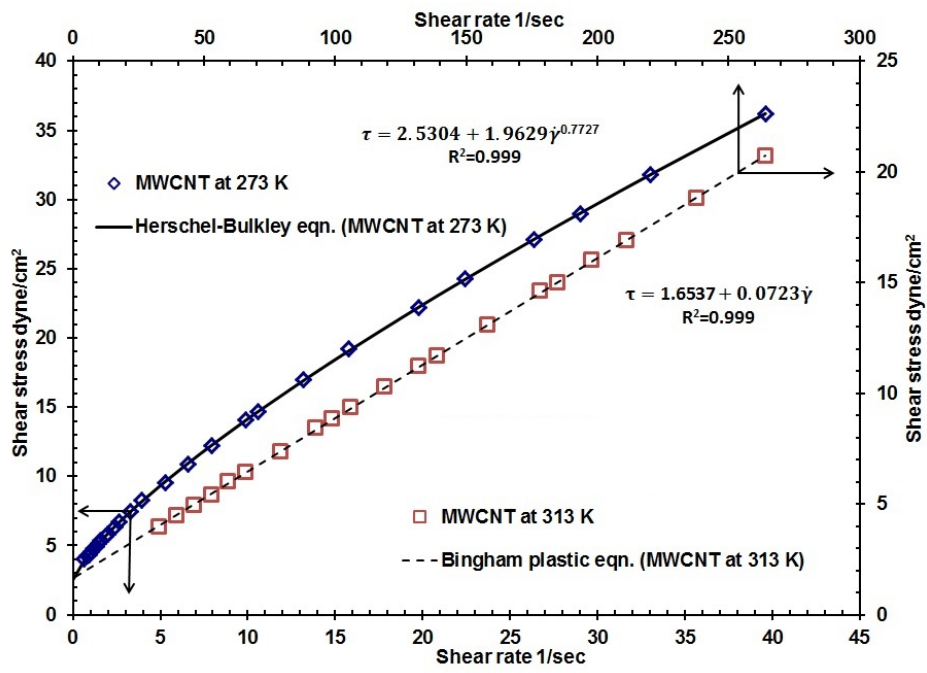


(a)



(b)

Figure 4.18. Shear stress versus shear strain rate at 273 K and 313 K for a 0.229% particle volume concentration of (a) SWCNT, (b) BWCNT and (c) MWCNT after 90 minutes of ultrasonication.



(c)

Figure 4.18 continued...

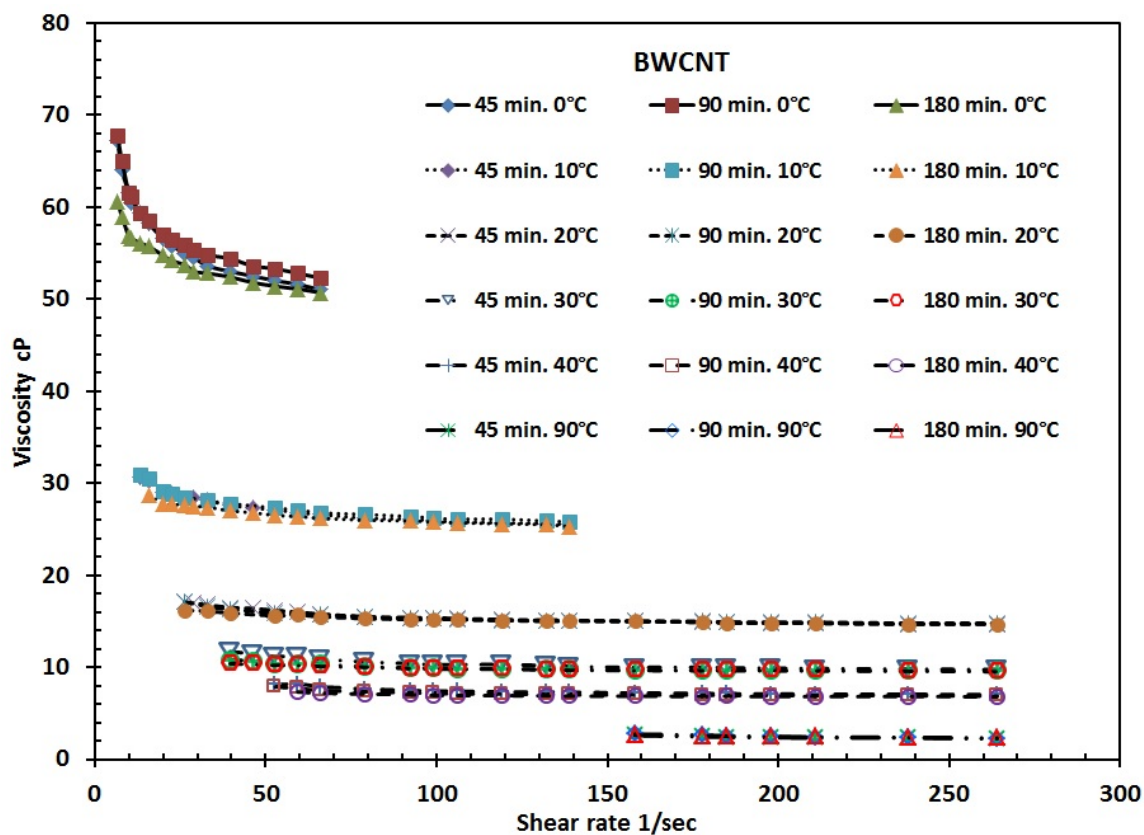


Figure 4.19. Effect of ultrasonication time on the viscosity of BWCNT.

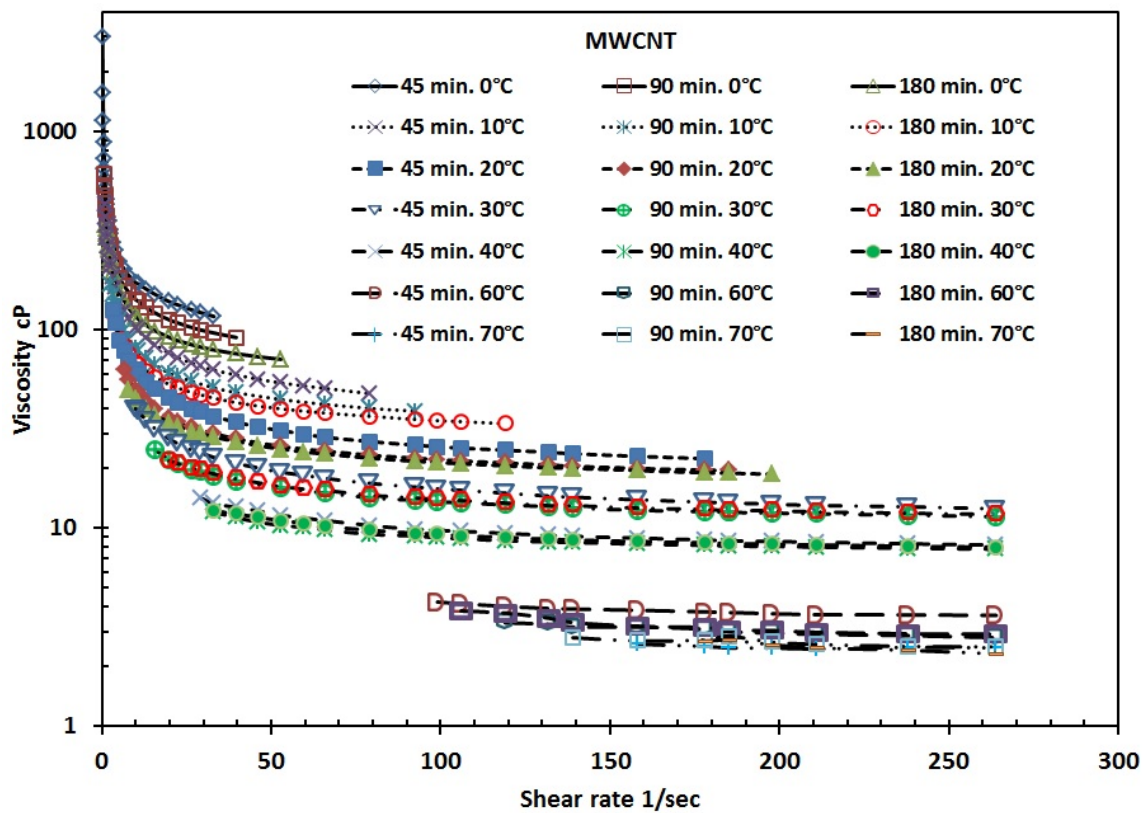


Figure 4.20. Effect of ultrasonication time on the viscosity of MWCNT.

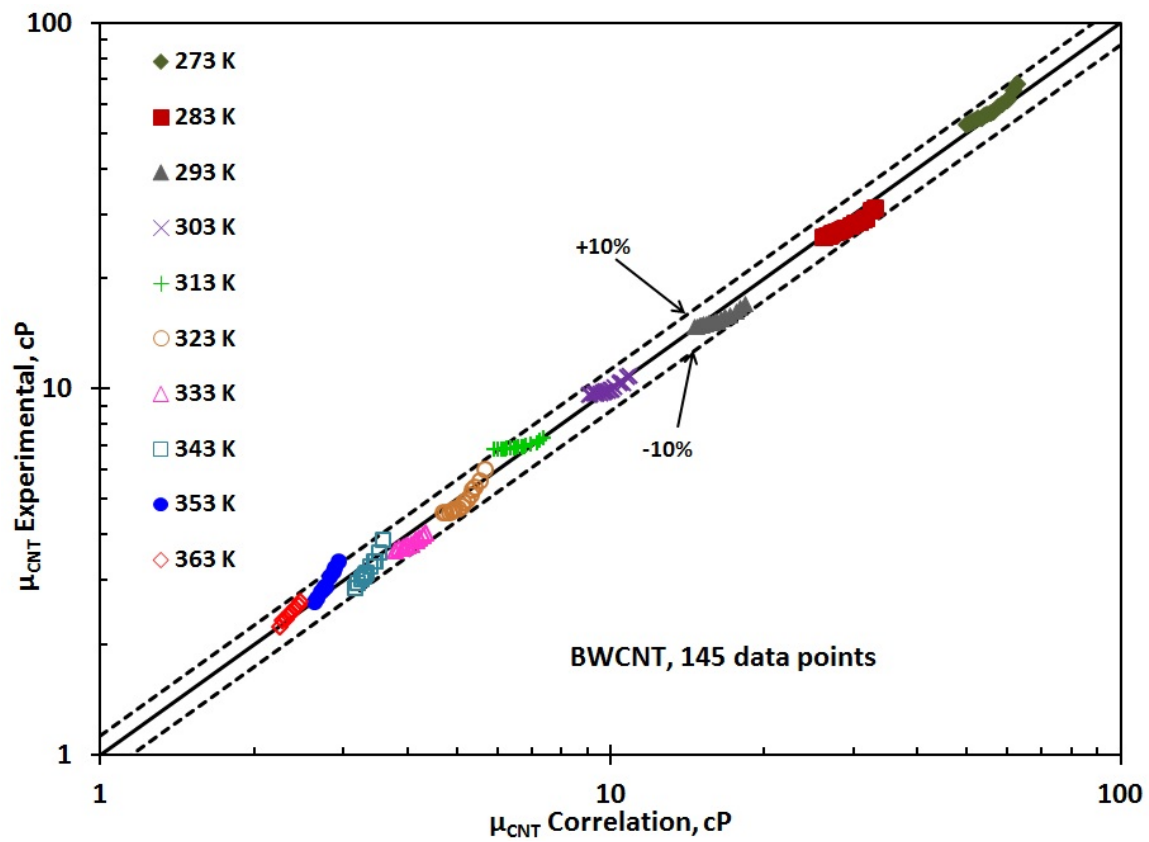


Figure 4.21. Comparison of the viscosity values calculated from the present correlation, Eq. (4.7) with the values obtained from the experiments for the BWCNT at different shear rates.

Chapter 5. Development of New Correlations for the Nusselt Number and the Friction Factor under Turbulent Flow of Nanofluids in Flat Tubes^{*}

5.1 Abstract

A three-dimensional turbulent flow and heat transfer of two different nanofluids, containing aluminum oxide (Al_2O_3) and copper oxide (CuO) nanoparticles, dispersed in ethylene glycol and water mixture (EG/W) in the flat tubes of an automotive radiator have been numerically studied to evaluate their performance. Computations have been carried out for nanoparticles volumetric concentrations up to 6% and over a Reynolds number range typically encountered in automobile radiators. Appropriate correlations for density, viscosity, specific heat and thermal conductivity of nanofluids as a function of particle volume concentration and temperature, developed from experiments have been used in this study. Numerical results have been first validated for the flow of single phase liquids, such as water and EG/W by comparing the computed values of Nusselt number and friction factor with those given by accurate correlations available in the literature. Inside the flat tube continuous reductions in the local heat transfer coefficient and wall shear stress are observed around the periphery of the flat tube, starting from the mid-point of the flat-wall and proceeding to the center of the curved wall. For the same Reynolds number, computations with nanofluids show an increase of friction factor and heat transfer coefficient with an increase in the particle volume concentration. The study reveals that under the basis of equal pumping power, Al_2O_3 and CuO nanofluids up to 3% and 2% particle volumetric concentrations respectively provide higher heat transfer coefficients than that of the base fluid. From the present study, several new correlations to determine the Nusselt number and friction factor for the nanofluids flowing in the flat tubes of a radiator have been proposed for the entrance as well as the fully developed regions.

^{*} Vajjha, R. S., Das, D. K., and Ray, D.R., 2015, "Development of New Correlations for the Nusselt Number and the Friction Factor under Turbulent Flow of Nanofluids in Flat Tubes," *International Journal of Heat and Mass Transfer*, 80, pp. 353-367.

5.2 Nomenclature

A	cross-sectional area, m^2
C_f	Fanning skin friction coefficient
C_p	specific heat, J/kg.K
d_p	nanoparticle diameter, m
D_h	hydraulic diameter of the tube, $D_h = 4A / P_m$, m
h	heat transfer coefficient, $h = q'' / (T_w - T_b)$, W/m ² K
k	thermal conductivity, W/m K
L	length of the tube, m
Nu	Nusselt number, $Nu = (hD_h/k)$
N_x, N_y, N_z	number of nodes in X, Y, Z directions
P	pressure, Pa
P_m	perimeter, m
Pr	Prandtl number, $Pr = (\mu C_p/k)$
q''	heat flux, W/m ²
Re	Reynolds number, $Re = (\rho VD_h/\mu)$
T	temperature, K
T_o	reference temperature, 273 K
\dot{W}	pumping power, W
V	velocity, m/sec
Z_H	hydrodynamic entry length, m
Z_T	thermal entry length, m
Z	axial distance from the inlet, m
Greek symbols	
ϕ	particle volumetric concentration, %
ρ	density, kg/m ³
μ	viscosity, mPa.s
κ	Boltzmann constant, 1.381×10^{-23} J/K
τ	shear stress, Pa

Subscripts

<i>avg</i>	peripheral average
<i>b</i>	bulk
<i>p</i>	nanoparticle
<i>nf</i>	nanofluid
<i>bf</i>	base fluid
<i>w</i>	wall
<i>Z</i>	local axial position
<i>ZA</i>	average on respective walls

Superscripts

—	average over the tube length
---	------------------------------

5.3 Introduction

The material need for automobiles can be diminished by reducing the size of radiators, which also present the added benefit of fuel efficiency due to the reduction in weight. Additionally, due to the steady rise in the cost of the fuel of automobiles, there is an increasing demand on improving their overall efficiency. To accomplish this, over the years, many new fin designs have evolved resulting in newer and compact designs to improve radiators. Kays and London [1] present a comprehensive collection of data on a variety of compact heat exchanger geometries. When it comes to the heat transfer fluid consideration, they have not been improved. Common coolants are: water, mixtures of ethylene glycol or propylene glycol mixed with water. The advent of nanofluids, which are stable suspensions of nanoscale particles (< 100 nm), promises to improve the performance of radiators by improving the coolant heat transfer capability.

A significant amount of literature is available on the performance of single phase fluids in radiators from the publications of the society of automotive engineers. However, literatures on nanofluids performance in radiators are quite limited. Therefore, the purpose of the present paper is to conduct a comprehensive analysis of nanofluids flow in the flat tube of an automotive radiator and compare their performance with single phase fluids.

Some literatures that compared the performance of commonly used single-phase heat transfer fluids in radiators are reviewed below. Gollin and Bjork [2] compared the heat transfer

and hydraulic performance of coolants, such as pure water, pure propylene glycol, 50/50 and 70/30 volume mixtures of both EG/W and propylene glycol/water (PG/W) for five automobile radiators through wind tunnel experiments. Based on their experiments, they concluded that in terms of heat transfer and lowest pressure drop, the most effective of coolants was pure water, followed by 50/50 EG/W, 50/50 PG/W, 70/30 EG/W, 70/30 PG/W and finally pure PG. JuGer and Crook [3] compared the heat transfer performance of 50/50 EG/W and 50/50 PG/W mixtures in two different geometries of truck radiator. They observed that heat transfer performance of 50/50 EG/W mixture is better than that of 50/50 PG/W mixture under the same operating conditions. This seems reasonable as EG/W has better thermophysical properties than PG/W. Cozzone [4] compared the heat transfer performance of EG/W with PG/W mixtures of various proportions ranging from 30% to 70 % in a 3.8 liter V6 gasoline engine. His study revealed that PG/W and EG/W mixtures showed almost equal heat transfer performance. He attributed this phenomenon to an improved heat transfer characteristics of the PG based coolants over the EG based coolants under nucleate boiling conditions, which may be occurring in the engine block.

The conventional approach of increasing the heat rejection rate of automobile radiators by the use of external fin geometries and various tube shapes have already been widely explored. Poor thermal properties of traditional heat transfer fluids have prompted the present day researchers to look for new technologies that will improve the fluid's heat transfer characteristics, thereby improving the cooling efficiency of automobile radiators. As explained earlier, one such technology that shows the potential to improve the traditional heat transfer fluids is the concept of nanofluids. Nanofluids are the stable dispersions of nanometer-sized particles in conventional base fluids [5, 6]. With the suspension of high thermal conductivity metals or metallic oxide nanoparticles in these traditional coolants, the thermal conductivity of the resulting mixture is increased [7-9]. Up until now two most widely studied nanoparticles are the Al_2O_3 and CuO. Minkowycz et al. [10] summarize the latest developments in nanofluids research upto 2013 in a treatise addressing different aspects through a systematic exposition in ten chapters.

Only a limited number of publications have appeared thus far on the application of nanofluids in automotive radiators. Vasu et al. [11] theoretically analyzed using the effectiveness-number of transfer unit (ϵ -NTU) method for the application of the Al_2O_3 nanoparticles dispersed in water as a coolant in flat tube plain fin compact heat exchanger. Their

analysis showed a substantial increase in the cooling capacity of the Al_2O_3 nanofluid compared to the base fluid. They also observed an increase in the pressure drop of nanofluid over the base fluid. Leong et al. [12] performed similar analysis using copper nanoparticles of up to 2% particle volumetric concentration suspended in ethylene glycol base fluid. They observed a heat transfer enhancement of 3.8% over the base fluid at the Reynolds number of 6000 and 5000 for air and coolant respectively, for a 2% particle volumetric concentration of nanofluid. Vajjha et al. [13] numerically studied a three-dimensional laminar flow and heat transfer performance of Al_2O_3 and CuO nanoparticles dispersed in ethylene glycol/water mixture circulating through the flat tubes of a Chrysler minivan radiator. For a 10% Al_2O_3 and a 6% CuO nanofluids, their analysis showed an increase in the average heat transfer coefficient of about 94% and 89% respectively over the base fluid, at a Reynolds number of 2000. They also observed that for the same amount of heat transfer, the Al_2O_3 nanofluid of 10% concentration and the CuO nanofluid of 6% concentration showed a reduction in pumping power of about 82% and 77% respectively when compared to the base fluid. Peyghambarzadeh et al. [14] experimentally investigated the heat transfer performance of the Al_2O_3 nanoparticles dispersed in different base fluids including pure water, pure EG and mixtures of EG and water (5, 10, 20 vol.% EG) as coolants in an automobile radiator. Their experiments showed that the heat transfer characteristics of the nanofluids were strong functions of particle volume concentration and the flow conditions. At optimal conditions, they obtained heat transfer enhancement of 40% when compared to the base fluids. Chavan and Pise [15] conducted an experimental study on the Al_2O_3 nanoparticles suspended in pure water in an automobile radiator. With the addition of 1% volume concentration of nanoparticles to the base fluid water, they presented a heat transfer enhancement of 40-45% over the base fluid. Hussein et al. [16] studied numerically the friction factor and heat transfer enhancement of a TiO_2 nanofluid flow in turbulent regime through circular, elliptical and flat shaped tubes. They observed that with the addition of the titanium oxide nanoparticles in water, the friction factor and the heat transfer coefficient increased. On the other hand, they reported that with an increase in the Reynolds number, the friction factor decreased and the heat transfer coefficient increased. They concluded that the flat tube gave the lowest friction factor and a higher heat transfer coefficient when compared to the elliptical and circular tubes. Ray and Das [17] compared the performance of three different nanofluids containing Al_2O_3 , CuO and SiO_2 nanoparticles dispersed in a base fluid of 60:40 EG/W using the effectiveness-number of

transfer unit method. They determined that a dilute 1% volume concentration of nanoparticles performed better than higher concentrations under the equal pumping power basis. Their results showed that under the same heat transfer basis, the Al_2O_3 , CuO and the SiO_2 nanofluids showed a reduction in pumping power of 35.3%, 33.1% and 26.2% respectively.

The present paper explores an important application of nanofluids in the automotive cooling system. The heat transfer and pumping power characteristics of EG/W based nanofluids were studied under the turbulent flow condition in the flat tubes of a radiator. The flat tube geometry and the fin geometries used in the present study correspond to radiators used in Chrysler minivan. This paper proves an increase in heat transfer coefficient resulting in the reduction in radiator size and the pumping power with nanofluid as coolants using the computational fluid dynamics (CFD) method, which would improve the fuel efficiency of automobiles. The two nanofluids used in this study were the Al_2O_3 and the CuO nanoparticles of up to 6% particle volumetric concentrations dispersed in a base fluid of 60% ethylene glycol and 40% water by mass (60:40 EG/W). A mixture of 60:40 EG/W by mass was selected in the present analysis as it is most commonly used heat transfer fluid in the cold regions of the world due to its low freezing temperature of $-48.3\text{ }^\circ\text{C}$ [18]. Recently developed correlations for the thermophysical properties of the 60:40 EG/W based nanofluids have been incorporated in to the numerical code to ascertain that accurate values of the heat transfer and frictional loss data are obtained.

5.4 Mathematical modeling

5.4.1 Problem geometry

Figure 5.1A presents the typical geometric configuration of a corrugated louver fin radiator commonly used in automobiles now-a-days [19] and Fig. 5.1B presents the geometry and dimensions of flat tube adopted in the present numerical study. The advantages of using a flattened tube over a circular tube are its increased heat transfer area and relatively smaller pressure drop on the air side explained by Fraas [20]. The cross-sectional dimensions of the flattened tube for the computational modeling in the present study are taken from Fraas. The length of the radiator tube was taken from the paper of Gollin and Bjork [2], who analyzed the radiator of a Chrysler minivan.

5.4.2 Governing equations

A three dimensional steady state, forced turbulent flow and conjugate heat transfer in the flat tube of the radiator with nanofluid flow inside is considered here. The flow and thermal fields are symmetric with respect to the X-axis and Y-axis as shown in Fig. 5.1B. Therefore, only one quarter of the flat tube cross section is considered. A uniform axial velocity and temperature were assumed for the fluid at the inlet section of the tube. The dispersion of low volume concentration of nanoparticles in the base fluids can be treated as a single phase fluids [22-24]. The base fluid as well as the nanofluid is incompressible and for the fluid flow inside radiators, the compression work and the viscous dissipation are usually considered negligible. Under these conditions, the governing equations for turbulent mean continuity, momentum, and thermal energy are presented below as Eqs. (5.1)–(5.3) [25]. The energy equation of heat conduction through the solid wall of the flat tube is given by Eq. (5.4).

Continuity:

$$(\nabla \cdot \bar{V}) = 0 \quad (5.1)$$

Momentum:

$$\rho(\nabla \cdot \bar{V})\bar{V} = -\nabla\bar{P} + \mu(\nabla^2\bar{V}) - \rho(\nabla \cdot \overline{V'V'}) \quad (5.2)$$

Energy equation for fluid:

$$\rho C_p(\bar{V} \cdot \nabla)\bar{T} = k(\nabla^2\bar{T}) - \rho C_p(\nabla \cdot \overline{V'T'}) \quad (5.3)$$

Energy equation for solid:

$$\nabla^2 T = 0 \quad (5.4)$$

where \bar{V} , \bar{P} , \bar{T} represent the time averaged mean values and V' and T' are turbulent fluctuations. The terms $\rho\overline{V'V'}$ and $\rho C_p\overline{V'T'}$ represent the turbulent momentum transport and turbulent

transport of temperature respectively. These additional time-averaged terms which appear in turbulence modeling can be solved if the Reynolds stresses and extra temperature transport terms can be related to the mean flow velocity and heat quantities.

In order to predict the Reynolds stresses and the scalar transport terms and close the system of governing equations, several turbulence models have been developed. White [26] describes 6 turbulence models, which are: one, two and four-equation models, such as turbulent kinetic energy, $(\kappa - \varepsilon)$, $(\kappa - \omega)$, $(\kappa - L)$, $(\kappa - \omega^2)$ and $(\kappa - \varepsilon - v^2 - f)$ model. Of the above turbulence models, the most widely used and validated is the $(\kappa - \varepsilon)$ model. Therefore, in the present computational analysis, the $(\kappa - \varepsilon)$ model has been adopted. This model uses the following additional transport equations for the turbulent kinetic energy κ and the rate of dissipation of turbulent energy ε .

$$\frac{\partial}{\partial x_i} (\rho \kappa \bar{u}_i) = \frac{\partial}{\partial x_j} \left[\left(\mu + \frac{\mu_t}{\sigma_\kappa} \right) \frac{\partial \kappa}{\partial x_j} \right] + \mu_t \frac{\partial \bar{u}_i}{\partial x_j} \left(\frac{\partial \bar{u}_i}{\partial x_j} + \frac{\partial \bar{u}_j}{\partial x_i} \right) - \rho \varepsilon \quad (5.5)$$

$$\frac{\partial}{\partial x_i} (\rho \varepsilon \bar{u}_i) = \frac{\partial}{\partial x_j} \left[\left(\mu + \frac{\mu_t}{\sigma_\varepsilon} \right) \frac{\partial \varepsilon}{\partial x_j} \right] + C_{1\varepsilon} \mu_t \frac{\varepsilon}{\kappa} \frac{\partial \bar{u}_i}{\partial x_j} \left(\frac{\partial \bar{u}_i}{\partial x_j} + \frac{\partial \bar{u}_j}{\partial x_i} \right) - C_{2\varepsilon} \rho \frac{\varepsilon^2}{\kappa} \quad (5.6)$$

where σ_κ and σ_ε are the effective Prandtl numbers that relate turbulent kinetic energy κ and rate of dissipation of turbulent energy ε respectively to the momentum eddy viscosity μ_t . The eddy viscosity is given as:

$$\mu_t = \frac{C_\mu \rho \kappa^2}{\varepsilon} \quad (5.7)$$

The above equations, Eqs. (5.5)–(5.7), contain five adjustable constants: $\sigma_\kappa=1.00$, $\sigma_\varepsilon=1.30$, $C_{1\varepsilon}=1.44$, $C_{2\varepsilon}=1.92$ and $C_\mu=0.09$. As explained by Launder and Spalding [27], the values for these constants have been arrived at by comprehensive data fitting for a wide range of turbulent flows. Equations (5.1) to (5.4) combined with Eqs. (5.5) to (5.7) are solved by the control volume approach using computational fluid dynamics software Ansys Fluent [28]. The governing equations are discretized using a second-order upwind scheme. A staggered grid was

used where scalar variables (pressure, temperature and other turbulent quantities) are stored in the cell centers of the control volumes, whereas the velocity or momentum variables are evaluated at the cell faces. The well-known SIMPLE (semi-implicit method for pressure-linked equations) [29] scheme was adopted in order to link the pressure with the velocity for an incompressible flow. Ansys Fluent solves a system of linear or non-linear algebraic equations resulting from the discretization methods for the partial differential equations using a point-by-point Gauss-Siedel method. During the numerical computations, the residuals were carefully monitored and the solution were considered to be converged when all the residuals for all governing equations (5.1)–(5.6) were lower than 10^{-6} . From the post-processing of these data, we compute the bulk fluid temperature, the wall shear stress, the skin friction coefficient, heat flux and the convective heat transfer coefficient around the periphery at various axial locations along the tube.

5.4.3 Boundary conditions

In solving the numerical model, uniform axial velocity, temperature, turbulent intensity and hydraulic diameter are prescribed at the inlet of the flat tube. From the inlet velocity of the tube, Reynolds number was determined and the inlet temperature of 90 °C (363 K) was adopted, which is typical for automotive radiators. An outflow boundary condition was applied at the outlet of the tube geometry since the flow and temperature fields are fully developed at the outlet section. This boundary condition assumes a zero normal gradient for all flow variables except pressure. The solver extrapolates the required information from the interior. All along the tube wall, a no-slip boundary condition is imposed for velocity. For an automobile radiator, a realistic thermal boundary condition on the outside of the wall is a prescribed convective heat transfer coefficient h_o on the air-side and a fixed free stream temperature. In our simulations, the air side effective convective heat transfer coefficient, which considers the fin geometry was $h_o=206$ W/m² K. An ambient air temperature of 30°C (303 K) was selected. This h_o value corresponds to an automobile operating under the city driving conditions [17].

5.5 Thermophysical properties

5.5.1 Conventional coolant (60:40 EG/W)

The thermophysical properties of the base fluid 60:40 EG/W used widely in cold regions were obtained from the ASHRAE Handbook [18] and curve-fitted as functions of temperature. The validity of these correlations are over a temperature range of $238 \text{ K} (-35 \text{ }^\circ\text{C}) \leq T \leq 398 \text{ K} (125 \text{ }^\circ\text{C})$. Table 5.1 presents the thermophysical property correlations of 60:40 EG/W and the maximum deviations observed between the curve-fit data and the ASHRAE data. The reference temperature T_0 was taken to be 273 K. The viscosity correlation follows the log-quadratic equation recommended by White [26] for the viscosity of liquids. Since viscosity is a strong function of temperature, the temperature range was split into two segments in order to maintain the maximum deviation to less than 1% between the data from ASHRAE and the correlation.

5.5.2 Nanofluids

5.5.2.1 Viscosity

Namburu et al. [30, 31] conducted measurements of viscosity of Al_2O_3 and CuO nanoparticles dispersed in a base fluid of 60:40 EG/W. The experiments were performed between a temperature range of $238 \text{ K} (-35 \text{ }^\circ\text{C}) \leq T \leq 323 \text{ K} (50 \text{ }^\circ\text{C})$, which is well suited to the cold regions applications. From their experimental data, they presented an empirical correlation for both the Al_2O_3 and CuO nanofluids as function of temperature T and particle volumetric concentration ϕ .

$$\log\mu_{nf} = Ae^{-BT} \quad (5.8)$$

where A and B were cubic polynomials derived as a function of the particle volumetric concentration. The curve-fit constants of these cubic polynomial functions were different for the Al_2O_3 and CuO nanofluids. Sahoo et al. [32] extended the work of Namburu's with additional measurements for the Al_2O_3 nanofluid up to a temperature of $90 \text{ }^\circ\text{C}$ and proposed two new correlations for the viscosity; one in lower temperature regime ($-35 \text{ }^\circ\text{C}$ to $0 \text{ }^\circ\text{C}$) and the other in the upper temperature regime ($0 \text{ }^\circ\text{C}$ to $90 \text{ }^\circ\text{C}$).

$$\mu_{nf} = C e^{\left(\frac{D}{T} + E\phi\right)} \quad (5.9)$$

where C , D and E are pure constants and are different for each temperature regime. Following up on the studies of Namburu et al. and Sahoo et al., Vajjha and Das [33] proposed a new correlation by expressing the viscosity in a non-dimensional form given by Eq. (5.10). This equation follows the early research of Einstein [34] and Batchelor [35], where the temperature dependence is accounted by including the viscosity of the base fluid. Therefore, the correlation is simply a function of particle volumetric concentration ϕ . This equation was used in calculating the viscosity of nanofluids in the present numerical study.

$$\frac{\mu_{nf}}{\mu_{bf}} = A_1 e^{(A_2\phi)} \quad (5.10)$$

In the above equation, A_1 and A_2 are constants and are given in Table 5.2. The above correlation has a maximum deviation of $\pm 8\%$ between the experimental data and curve-fit values.

5.5.2.2 Thermal conductivity

Vajjha and Das [9] measured thermal conductivities of the Al_2O_3 and CuO nanoparticles dispersed in a base fluid of 60:40 EG/W. From their experimental data, they proposed a correlation which was a combination of the static part proposed long ago by Maxwell and a dynamic part due to the Brownian motion of nanoparticles.

$$k_{nf} = \frac{k_p + 2k_{bf} - 2(k_{bf} - k_p)\phi}{k_p + 2k_{bf} + (k_{bf} - k_p)\phi} k_{bf} + 5 \times 10^4 \beta \phi \rho_{bf} C_{pbf} \sqrt{\frac{\kappa T}{\rho_p d_p}} f(T, \phi) \quad (5.11a)$$

$$f(T, \phi) = (2.8217 \times 10^{-2} \phi + 3.917 \times 10^{-3}) \left(\frac{T}{T_0}\right) + (-3.0669 \times 10^{-2} \phi - 3.91123 \times 10^{-3}) \quad (5.11b)$$

where $f(T, \phi)$ is given by Eq. (5.11b) and the expressions of β for Al_2O_3 and CuO nanofluids are presented in Table 5.3. This equation has maximum deviations of $\pm 2.8\%$ for the Al_2O_3 nanofluid and $\pm 7\%$ for the CuO nanofluid when compared with the experimental data.

5.5.2.3 Specific heat

An early equation for the specific heat of nanofluids was presented by Pak and Cho [24], taking the idea from the liquid-particle mixture theory. Subsequently, Xuan and Roetzel [23] presented an improved correlation by assuming thermal equilibrium between the nanoscale solid particles and the liquid phase.

$$C_{p,nf} = \frac{\phi \rho_p C_{pp} + (1 - \phi) \rho_{bf} C_{p,bf}}{\rho_{nf}} \quad (5.12)$$

However, the equations proposed by Pak and Cho and Xuan and Roetzel were all theoretical correlations. Vajjha and Das [36] conducted the specific heat measurements on three nanofluids containing Al_2O_3 , ZnO and SiO_2 nanoparticles. From their experiments, they observed that the solid phase particles and the base fluid are not in thermal equilibrium. This is because, the nanoparticles whose thermal diffusivities are higher than the base fluid, absorb more heat faster than the base fluid and attain a higher temperature. Therefore, they proposed a new correlation from their experimental data given by Eq. (5.13). The curve-fit coefficients A , B and C for the Al_2O_3 nanofluid are listed in Table 5.4.

$$\frac{C_{p,nf}}{C_{p,bf}} = \frac{(A(T/T_0) + B(C_{p,p}/C_{p,bf}))}{(C + \phi)} \quad (5.13)$$

Since no experimental data was available, the specific heat of the CuO nanofluid was calculated from Xuan and Roetzel relation.

5.5.2.4 Density

The equation for the density of micrometer size solid particles suspended in liquid-phase fluids is available in the literature on slurry flows [37], which is presented as Eq. (5.14). The

same equation was adopted by Pak and Cho [24] for nanometer size particles, by conducting the experiment at room temperature for the γ -Al₂O₃ and TiO₂ nanofluids of up to 4.5% particle volumetric concentrations. Later, Vajjha et al. [38] measured the density of Al₂O₃, ZnO and antimony-tin oxide (Sb₂O₅:SnO₂) nanoparticles suspended in 60:40 EG/W using the Anton-Paar digital densitometer. Their experimental data showed a good agreement with the theoretical equation. Therefore, Eq. (5.14) was adopted for computing the density of nanofluids in the present numerical study.

$$\rho_{nf} = \phi\rho_p + (1 - \phi)\rho_{bf} \quad (5.14)$$

5.6 Numerical computation

Numerical simulations were performed for the Al₂O₃ and CuO nanofluids in the turbulent regime with the Reynolds numbers varying from 3000 to 8000 in equal increments of 500. This low turbulent Reynolds number range covers the automotive radiator operating in idle, city and highway conditions from the compilation of operational data by Ray and Das [17]. Furthermore, simulations were carried out for the particle volumetric concentrations of 0 to 6%. The hydraulic diameter of the flat tube under consideration is 4.577×10^{-3} m. Therefore, the hydrodynamic and thermal entry length is calculated to be $Z_H = Z_T = 10D_h = 0.04577$ m [39]. So, the flow is fully developed hydrodynamically and thermally at the outlet section.

5.6.1 Mesh independence study

Figure 5.2 shows a three-dimensional mesh, generated using Ansys ICEM CFD [40]. The generated mesh was then exported to Ansys Fluent [28] to solve for the governing equations of mass, momentum and energy conservation. The mesh independence study was performed to ensure that all the flow details are captured, employing the least number of elements that can yield accurate computational results. The four mesh sizes used in verifying the mesh independence are summarized in Table 5.5. For each mesh size, velocity and temperature were obtained by solving the governing equations and the results were plotted for comparison. Figure 5.3 illustrates the mesh independence test conducted using the axial velocity and temperature distributions in the Y-direction at the outlet of the duct. It is clear that the results of meshes III

and IV overlap on one another verifying that the mesh independence was achieved from mesh III and further refinement is not necessary. Additionally, since the flow inside the channel is turbulent in nature, it is highly desirable that the mesh density near the channel walls should be sufficiently high to accurately capture the flow physics in the viscous sub-layer region. In order to resolve this, we have adopted the enhanced wall treatment function which is one of the near-wall treatment functions available in the Ansys Fluent software. When using this function, Ansys Fluent recommends that the dimensionless distance normal to the wall, y^+ , should be on the order of 1 and also at least 10 cells should be used within the viscosity-affected near-wall region to be able to resolve the mean velocity and turbulent quantities in that region. Similarly, at the entrance region of the channel where the flow is not fully developed, the rapidly diminishing friction and heat transfer variables must be captured with a finer mesh. Accordingly, to minimize errors and to optimize the CPU resources, all computations were run with the mesh III (95 x 35 x 200).

5.6.2 Validation of the computational procedure

The computational model was validated by comparing the numerical results with the theoretical data available for the convective fluids. Figures 5.4 and 5.5 show the comparison of the Nusselt number and friction factor in the fully developed turbulent flow of pure water and 60:40 EG/W with the correlations reported by various researchers. Table 5.6 presents the Nusselt number correlations given by Gnielinski [41] and Dittus and Boelter [42] with the maximum and average deviations between the present computational results and the correlations. A good agreement was observed between the numerical results and the theoretical correlations validating the present computational model. Table 5.7 presents the theoretical correlations used to compare the friction factor values obtained from the present numerical study. The table also presents the average and maximum deviations observed between the present computational results and the correlations for the two conventional fluids. The computational skin friction results agreed within 12% of all correlations presented in Table 5.7 and plotted in Fig. 5.5. The best agreement is with the Colebrook [43] correlation.

5.7 Results and discussion

5.7.1 Peripheral variation

The variations of the local heat transfer coefficient and the local shear stress along the inner peripheral surface of the flat tube are shown in Fig. 5.6. The horizontal axis of the figure presents the node numbers of the meshed geometry in the X-Y plane, taken in a clockwise direction starting from the midpoint of the upper wall. The left and right vertical axes represent the local heat transfer coefficient and shear stress obtained at the corresponding node numbers respectively. The results shown in the figure were obtained at a particular axial location of $Z=0.42\text{m}$ and from the simulation at a Reynolds number of 5000 with 60:40 EG/W base fluid. From the figure, we observe that in the rectangular region of the cross-section, the magnitudes of local shear stress and local heat transfer coefficient values are significantly higher compared to those in the semicircular region of the tube. As an example, the local shear stress and heat transfer coefficient at the center of the semicircular wall is 34.9% and 25.5% lower than that at the center of the upper and lower wall of the flat section respectively. This is due to the redistribution of momentum across the semicircular region assisted turbulent secondary flows (Fig. 5.7a). There are mean velocities u (in X-direction) and v (in Y-direction) of small magnitudes in the plane of the cross section. Figure 5.7a shows Y-velocity contours. It is observed that magnitudes of secondary flow velocity are generally higher in the curved region than those in the flat region, thus promoting secondary flows. The secondary flow reduces the mean axial velocity in the curved region causing a continuous reduction in the wall shear stress from the center of the flat wall to the curved wall. White [44] explains the same phenomenon for noncircular cross sections. The reduction in the axial velocity and the effect of secondary flow in the curved region also reduces the turbulent kinetic energy as observed in Fig. 5.7b. The turbulent kinetic energy decreases steadily from the center toward the curved wall. This results in poor promotion of mixing to convect the heat, ensuing a gradual decrease in the convective heat transfer coefficient along the wall, reaching the lowest value at the midpoint of the curved wall (node number 95) [39]. Similar observations of reductions in h_z and τ_z along the periphery of the tube were made by Vajjha et al. [13] while analyzing the flow under laminar condition in the flat tube of a radiator.

The variation of average convective heat transfer coefficient and shear stress on the upper and semicircular wall with axial distance is shown in Fig. 5.8. At a given Z -location, h_{ZA} and τ_{ZA} are average values along the upper, lower and curved walls. The values computed for lower wall are found to be same as those on the upper wall. The computed results shown are for the 60:40 EG/W base fluid flowing at a Reynolds number of 6000. Figure 5.8 shows that at the entrance to the tube, where the thermal and hydraulic boundary layers are minutely thin, the locally averaged heat transfer coefficient (h_{ZA}) and the locally averaged shear stress (τ_{ZA}) asymptotically approach extremely high values. With the development of both velocity and thermal boundary layers, the h_{ZA} and τ_{ZA} decay rapidly until the constant values associated with the fully developed conditions are reached [45]. In the present study, the velocity and thermal entrance lengths are found to be $Z_H = Z_T = 0.04577$ m beyond which it is fully developed flow. Therefore, in the Fig. 5.8 we can observe that after $Z/L = 0.09154$, the velocity and temperature are fully developed and h_{ZA} and τ_{ZA} become constant thereafter. From the figure we also observe that the average heat transfer coefficient and average shear stress on the semicircular wall are 11.7% and 26.19% lower respectively than that of the upper wall.

5.7.2 Effect of nanoparticle concentration on local skin friction coefficient

Figure 5.9 displays the peripheral average local Fanning skin friction coefficient $C_{f\ avg}$ computed along the length of the flat tube for various particle volumetric concentrations of 0% to 6% of the CuO nanofluid. The computations were performed for a constant uniform velocity of 1.8 m/s which corresponds to Reynolds numbers of 9643 for the 60:40 EG/W base fluid and 3488 for a 6% concentration of the CuO nanofluid as shown in the figure. The Reynolds number for a 6% CuO nanofluid, due to its high viscosity value, is lower on the basis of equal velocity. It is observed that as the nanoparticle volume concentration increased the local skin friction coefficient also increased resulting in a higher pressure drop and higher pumping power across the flat tube. In the fully developed region of the flat tube ($Z/L=0.09154$), the $C_{f\ avg}$ for a 6% particle volume concentration of the CuO nanofluid is 1.47 times that of the base fluid, 60:40 EG/W. The Al_2O_3 nanofluid exhibits similar distribution.

5.7.3 Effect of nanoparticle concentration on local heat transfer coefficient

Figure 5.10 presents the effect of increasing particle volumetric concentration of a CuO nanofluid on the peripheral average local heat transfer coefficient h_{avg} , along the tube length for a

uniform inlet velocity of 1.8 m/s. It is observed from the figure that the 1% CuO nanofluid provide highest h_{avg} when compared to the base fluid. But as we increase the nanoparticle volume concentration, the magnitude of h_{avg} gradually decreases and above a particle concentration of 3%, the CuO nanofluid's h_{avg} is lower than that of the base fluid. As an example, in the fully developed region the h_{avg} of 1% and 3% CuO nanofluid increases by 14.5% and 1.6% respectively over the base fluid while the h_{avg} of a 4% CuO nanofluid decreases by 4.5% compared to that of a base fluid. This is because, for the same inlet velocity, with the increase in particle volume concentration the nanofluid viscosity increases rapidly causing the Reynolds number to drop down diminishing the Nusselt number. Although, the thermal conductivity of nanofluid increases with an increase in the nanoparticle volume concentration, the increase in viscosity is proportionately much higher. This increase brings down the performance of nanofluids. This phenomenon is also temperature related as both k and μ are functions of temperature. For example, at a temperature of 363K, by adding the CuO nanoparticles of a 1% volume concentration, the thermal conductivity and viscosity increases by 35% and 15% respectively over the base fluid. While, at the same temperature, with the addition of 6% CuO nanoparticles, the thermal conductivity and viscosity increases by 51.7% and 129% respectively over the base fluid. This makes the decrease in the Reynolds number become more dominant. There is also a smaller impact on the Prandtl number. The net effect is that a high concentration diminishes the advantage of nanofluids over the base fluid. Therefore, a low nanoparticle volume concentration is preferable which maintains a higher Reynolds number while giving thermal conductivity enhancement, thereby achieving a higher heat transfer coefficient. The Al_2O_3 nanofluid also follows a similar trend.

Figure 5.11 shows the comparison of the average heat transfer coefficient for the base fluid 60:40 EG/W, Al_2O_3 and CuO nanofluids, as the velocity was varied from 0.8 – 1.8 m/s. The computations predict higher average heat transfer coefficient with the Al_2O_3 and CuO nanofluids than those with the base fluid at any given velocity over the full range. It was observed that on an equal velocity, the 1% volume concentration of the Al_2O_3 and CuO nanofluids showed the highest percentage increase in the average heat transfer coefficient over the base fluid. Thereafter, with the increase in the particle volume concentration, the percentage increase over the base fluid diminished. For example, at a liquid velocity of 1.2 m/s, the average heat transfer coefficient of a 1% Al_2O_3 and CuO nanofluids increases by 14% and 16%

respectively over the 60:40 EG/W base fluid. Under the same conditions, the average heat transfer coefficient of a 2% Al₂O₃ and CuO nanofluids increases by 10.5% and 10% respectively over the base fluid. This reduction is due to the higher values of viscosity of the Al₂O₃ and CuO nanofluids when compared with the base fluid. As concentration increases, the increasing viscosity reduces the Reynolds number thereby decreasing the heat transfer coefficient.

Figure 5.12 predicts what concentrations of Al₂O₃ and CuO nanofluids can yield better performance than the base fluid. This determination could be made following the work of Kays and London [1], who presented a performance comparison relation given by Eq. (5.15). A plot of average heat transfer coefficient versus friction power expended per unit of surface area given by Eq. (5.15) has been shown in Fig. 5.12. The average heat transfer coefficient plotted on the Y-axis and the average skin friction coefficient values used in Eq. (5.15) were obtained from the present numerical computations at various Reynolds numbers. From Fig. 5.12, we observe that the Al₂O₃ nanofluid of particle volume concentrations 1-3% and the CuO nanofluid of 1% and 2% volume concentrations provide higher heat transfer coefficients than the base fluid (60:40 EG/W) for a given friction power value (E). As the nanoparticles volume concentration increases the heat transfer coefficient diminishes, falling below that of the base fluid. Therefore, a 1% concentration of Al₂O₃ or CuO nanofluids appears to be the best choice, similar to the observation made in Fig. 5.11.

$$E = \frac{\bar{C}_f}{2\rho^2} \left(\frac{\mu Re_{D_h}}{D_h} \right)^3 \quad (5.15)$$

5.7.4 Effect of Reynolds number on average heat transfer coefficient

Figure 5.13 displays the variation of the average heat transfer coefficient, defined as $(\bar{h} = \frac{1}{L} \int_0^L h_{avg} dZ)$, with the Reynolds number over the entire tube length of 0.5 m for particle volumetric concentrations varying from 0 to 6% of the Al₂O₃ nanofluid. It is observed from the figure that the average heat transfer coefficient increases with an increase in the Reynolds number. For example, as the Reynolds number increases from 3000 to 8000, the average heat transfer coefficient \bar{h} increases by about 2.17 times for the base fluid 60:40 EG/W as well as for

all the particle volume concentrations of the Al_2O_3 nanofluid. This is because, at constant particle volume concentration, the average heat transfer coefficient is solely dependent upon the Reynolds number. At a fixed Reynolds number, the \bar{h} increases with an increase in particle volumetric concentration. For example, at a Reynolds number of 5500, the 6% concentration Al_2O_3 nanofluid produces \bar{h} which is 61% higher than that of the base fluid.

Figure 5.14 shows the variation of the average heat transfer coefficient \bar{h} with the Reynolds number over the entire tube length of 0.5 m for particle volume concentrations from 0 to 6% of the CuO nanofluid. As observed earlier, the average heat transfer coefficient increases with an increase in the Reynolds number as well as particle volumetric concentration. As an example, between the Reynolds numbers of 3000 to 8000, the average heat transfer coefficient \bar{h} increases by about 2.17 times for all the particle volume concentrations of the CuO nanofluid. Similarly, at a fixed Reynolds number of 5500, the average heat transfer coefficient \bar{h} of the 6% CuO nanofluid is 92.5% higher than that of the base fluid. This higher increase in the average heat transfer coefficient \bar{h} is attributed to the higher thermal conductivity of the CuO nanoparticle.

5.7.5 New correlations of Nusselt Number in fully developed and entrance regions of the flat tube

5.7.5.1 Fully developed region

The computational Nusselt number results of nanofluids were found to be quite different from the empirical predictions given by Gnielinski [41] and Dittus and Boelter [42] correlations for single phase liquid. This clearly indicated that the existing single phase correlations are not suitable for nanofluids. This is observed from the fact that the Nusselt number, Reynolds number and Prandtl number are functions of thermophysical properties (μ , k , C_p , ρ), which change significantly with ϕ , affecting h and C_f . Figures 5.9-5.14 showed for the nanofluids, both h and C_f vary with the particle volume concentration ϕ . Therefore, a new correlation for the Nusselt number must be a function of the particle volume concentration of the nanofluid. With this argument, a new correlation for the Nusselt number as a function of particle volume concentration, Reynolds number and Prandtl number was developed. Utilizing 132 data points from the numerical simulation obtained from the fully developed region, a new correlation, Eq.

(5.16) was developed using the statistical program Minitab [46]. This equation is patterned after the Dittus-Boelter correlation with an additional term containing particle volume concentration to account for the dependence of the Nusselt number on nanofluids. For the degenerate case, when $\phi = 0$, it matches with the single phase fluid correlation. This correlation has a maximum deviation of $\pm 2\%$ when compared with the numerical data as shown in Fig. 5.15.

$$\overline{Nu}_{nf} = 0.023 Re_{D_h}^{0.8} Pr^{0.3} (1 + 0.1771 \phi^{0.1465}) \quad (5.16)$$

$$1.988 \leq Pr \leq 13.44, 3000 \leq Re_{D_h} \leq 8000, 0 < \phi < 0.06.$$

Similarly, a correlation for the friction factor in the fully developed region was derived following the equation given by Colebrook [43] for the single-phase fluids. The variation of friction factor with concentration was considered by adding an additional ϕ term to the Colebrook equation. This correlation is presented as Eq. (5.17). The maximum deviation between numerical results and this correlation is $\pm 5\%$.

$$\overline{C}_{f_{nf}} = \left[\frac{1}{1.5635 \ln(Re_{D_h}/7)} \right]^2 (1 - 0.0640281 \phi^{0.103595}) \quad (5.17)$$

$$3000 \leq Re_{D_h} \leq 8000, 0 < \phi < 0.06.$$

5.7.5.2 Entrance region

In turbulent flow, the thermal and hydrodynamic entry lengths are much shorter than the corresponding lengths in laminar flow. As a result, it is often assumed that the average Nusselt number and the average friction factor calculated in the fully developed flow regions are assumed to be valid over the entire tube length including the hydrodynamic and thermal entrance regions. However, for short tubes, this assumption is not valid and in such cases the average Nusselt number can be calculated from an expression of the form given in Eq. (5.18) [45].

$$\frac{Nu_{avg,x}}{\overline{Nu}} = 1 + \frac{C}{(x/D_h)^m} \quad (5.18)$$

In the above equation, $Nu_{avg,x}$ is the circumferentially averaged but axially varying local Nusselt number, \overline{Nu} is the average Nusselt number for fully developed flow as defined earlier, C and m depend on the nature of the inlet, entry region, as well as on the Prandtl and Reynolds numbers [45]. Following this format, correlations for the Nusselt numbers in the entrance region of a smooth circular tube have been developed by various investigators. Reynolds et al. [43] studied analytically the low Reynolds number, turbulent flow of gases in circular tubes for the thermal entrance region and proposed a correlation of the form, Eq. (5.18), where C varies as a function of Reynolds number given by $C = 0.8(1 + 70000Re^{-3/2})$ and $m = 1$. Their correlation is valid for $3000 < Re < 50000$, $Pr = 0.71$ and $x/D_h \geq 2$. Al-Arabi [43] developed a similar correlation for the Nusselt number from his study on turbulent convection heat transfer in a tube for the thermally developing flow with the constant wall-temperature and constant heat flux boundary conditions. The constant C proposed by Al-Arabi is given in Eq. (5.19). This correlation is valid for $x/D_h \geq 3$, $500 < Re < 10^5$, and $0.7 < Pr < 75$.

$$C = \frac{(x/D_h)^{0.1}}{Pr^{1/6}} \left(0.68 + \frac{3000}{Re^{0.81}} \right) \quad (5.19)$$

Following the approaches of Reynolds and Al-Arabi, we developed correlations for the Nusselt number and the friction factor valid in the entrance region of the flat tubes. This new correlation presented in Eq. (5.20a & b) are similar to the correlation of Al-Arabi with an additional term for particle concentration to account for nanofluids. In order to limit the curve-fit errors to remain below $\pm 10\%$, the correlation have been split into two regions; one for smaller and the other for higher Z/D_h values.

$$\frac{Nu_{avg,z}}{\overline{Nu}} = \left[1 + \frac{1}{(Z/D_h)^{0.0714} Pr^{1/6}} \left(2.2642 + \frac{3000}{Re^{0.9742}} \right) \right] (1 + 2.07586\phi^{0.71209}) \quad (5.20a)$$

for $Z/D_h < 0.124$; $3000 < Re < 8000$; $1.98 < Pr < 13.4$

$$\frac{Nu_{avg,z}}{\overline{Nu}} = \left[1 + \frac{1}{(Z/D_h)^{0.5072} Pr^{1/6}} \left(0.77082 + \frac{3000}{Re^{1.0533}} \right) \right] (1 + 0.3437\phi^{0.5254}) \quad (5.20b)$$

for $0.124 < Z/D_h < 13.56$; $3000 < Re < 8000$; $1.98 < Pr < 13.4$

Figure 5.16 displays the comparison plot of the Nusselt number values obtained from the present numerical study and the values obtained from the correlation presented in Eq. (5.20 a & b). Nearly 92% of the 7652 local Nusselt number data points obtained from the present numerical computations, fall within $\pm 10\%$ of the values given by Eq. (5.20a & b).

A similar approach was followed to develop correlations for predicting the friction factor for the entrance region of the flat tube under turbulent flows of nanofluids. The correlations presented in Eq. (5.21a & b) have a maximum error of $\pm 10\%$ when compared with 7652 data points obtained from the numerical simulation.

$$\frac{C_{f,avg,z}}{\bar{C}_f} = \left[1 + \frac{1}{(Z/D_h)^{0.7062}} \left(0.5171 + \frac{3000}{Re^{1.176}} \right) \right] (1 + 0.08565\phi^{0.06248}) \quad (5.21a)$$

for $Z/D_h < 0.124$; $3000 < Re < 8000$

$$\frac{C_{f,avg,z}}{\bar{C}_f} = \left[1 + \frac{1}{(Z/D_h)^{0.7472}} \left(0.4994 + \frac{3000}{Re^{1.2051}} \right) \right] (1 + 0.0529\phi^{0.0941}) \quad (5.21b)$$

for $0.124 < Z/D_h < 13.56$; $3000 < Re < 8000$

5.7.6 Effect of nanoparticle concentrations on pumping power

Table 5.8 presents the performance of the Al_2O_3 nanofluid of particle volume concentration 0% to 6% under the condition of equal heat transfer coefficient. From figure 5.12, a constant average heat transfer coefficient of $6000 \text{ W/m}^2\cdot\text{K}$ was adopted which corresponds to a Reynolds number of 7894 for the 60:40 EG/W base fluid. From the same figure, for the same average heat transfer coefficient, the corresponding Reynolds number for different particle volume concentrations of Al_2O_3 nanofluid were found. Then, velocities were determined from the Reynolds number. The corresponding average skin friction coefficient ($\bar{C}_f = \frac{1}{L} \int_0^L C_{f,avg} dZ$) was obtained from the numerical computations. Then the corresponding pressure loss in the flat tube was calculated using Eq. (5.22).

$$\Delta P = \bar{C}_f \frac{4L}{D_h} \frac{1}{2} \rho V^2 \quad (5.22)$$

The pumping power required to circulate the fluid is

$$\dot{W} = AV(\Delta P) \quad (5.23)$$

The results are summarized in Table 5.8 for the Al_2O_3 . From this table, we notice that compared to the base fluid, the velocities of nanofluids were lower, up to particle volume concentration of $\phi = 5\%$. Above that they increased with an increase in particle volume concentration. The average skin friction coefficient increased with an increase in nanoparticle volume concentration. We also notice that the Al_2O_3 nanofluid require lower pumping power than the base fluid below a volume concentration of 3%. Figure 5.12 created from the correlation of Kays and London [1] agrees with this finding. The diminishing performance of nanofluids over the base fluid beyond 3% particle volumetric concentration is due to the higher percentage increase in viscosity. Similar analysis conducted for the CuO nanofluid showed that beyond 2% concentration, the pumping power exceeded that required by the base fluid.

5.8 Conclusions

Heat transfer computations for Al_2O_3 and CuO nanofluids with varying particle volumetric concentrations of 0 to 6% exhibit substantial increase in the average heat transfer coefficient with concentration. At a Reynolds number of 5500, the percentage increase in the average heat transfer coefficient over the base fluid for a 3% Al_2O_3 nanofluid is 36.6% and that for a 3% CuO nanofluid is 49.7%. For the particle volume concentrations of 1% and 3%, the h_{avg} in the fully developed region increases over the base fluid by 13.23% and 5.88% respectively for the Al_2O_3 nanofluid and by 14.5% and 1.6% respectively for the CuO nanofluid. Similarly, on the basis of equal inlet velocity, an increase in the nanoparticle volume concentration results in an increase in the peripheral averaged skin friction coefficient. At a constant inlet velocity of 1.8 m/s, the $C_{f\ avg}$ in the fully developed region of the flat tube for a 3% particle volume concentration of the Al_2O_3 and CuO nanofluids are 9.5% and 17.16% higher than that of the base fluid respectively. For the same amount of heat transfer, the Al_2O_3 nanofluid of a 1% concentration showed highest reduction in the pumping power over the base fluid and beyond 3% concentration, the pumping power increased for the Al_2O_3 nanofluid over that of the base fluid. New Nusselt number and skin friction coefficient correlations for turbulent flows of

nanofluids in the flat tubes of a radiator have been developed for the entrance as well as the fully developed regions.

5.9 Acknowledgement

Financial support from the Alaska NASA EPSCoR grant # AK- NNX11AM16A is gratefully acknowledged.

5.10 References

- [1] Kays, W. M., and London, A. L., 1984, Compact Heat Exchangers, Krieger Pub. Co.
- [2] Gollin, M., and Bjork, D., 1996, "Comparative Performance of Ethylene Glycol/Water and Propylene Glycol/Water Coolants in Automobile Radiators," International Congress and Exposition, SAE International (SAE Paper No. 960372), Detroit, Michigan, p. 9.
- [3] JuGer, J. J., and Crook, R. F., 1999, "Heat Trasfer Performance of Propylene Glycol Versus Ethyelene Glycol Coolant Solutions in Laboratory Testing," International Congress and Exposition, SAE International (SAE Paper No. 1999-01-0129), Detroit, Michigan, p. 11.
- [4] Cozzone, G. E., 1999, "Effect of Coolant Type on Engine Operating Temperatures," International Congress and Exposition, SAE International (SAE Paper No. 1999-01-0135), Detroit, Michigan, p. 6.
- [5] Choi, S. U. S., "Enhancing Thermal Conductivity of Fluids with Nanoparticles," Proc. Developments and Applications of Non-Newtonian Flows, D. A. Singer, and H. P. Wang, eds., ASME, pp. 99-105.
- [6] Choi, S. U. S., Yu, W., Hull, J. R., Zhang, Z. G., and Lockwood, F. E., 2001, "Nanofluids for Vehicle Thermal Management," Vehicle Thermal Management Systems Conference & Exhibition, SAE International (SAE Paper No. 2001-01-1706), Nashville, Tennessee, p. 6.
- [7] Eastman, J. A., Choi, S. U. S., Li, S., Yu, W., and Thompson, L. J., 2001, "Anomalously Increased Effective Thermal Conductivities of Ethylene Glycol-Based Nanofluids Containing Copper Nanoparticles," Applied Physics Letters, 78(6), pp. 718-720.
- [8] Das, S. K., Putra, N., Thiesen, P., and Roetzel, W., 2003, "Temperature Dependence of Thermal Conductivity Enhancement for Nanofluids," ASME Journal of Heat Transfer, 125(4), pp. 567-574.

- [9] Vajjha, R. S., and Das, D. K., 2009, "Experimental Determination of Thermal Conductivity of Three Nanofluids and Development of New Correlations," *International Journal of Heat and Mass Transfer*, 52(21-22), pp. 4675-4682.
- [10] Minkowycz, W. J., Sparrow, E. M., and Abraham, J. P., 2013, *Nanoparticle Heat Transfer and Fluid Flow*, CRC Press/Taylor & Francis Group, Boca Raton, FL.
- [11] Vasu, V., Rama Krishna, K., and Kumar, A. C. S., 2008, "Thermal Design Analysis of Compact Heat Exchanger Using Nanofluids," *International Journal of Nanomanufacturing*, 2(3), pp. 271-288.
- [12] Leong, K. Y., Saidur, R., Kazi, S. N., and Mamun, A. H., 2010, "Performance Investigation of an Automotive Car Radiator Operated With Nanofluid-Based Coolants (Nanofluid as a Coolant in a Radiator)," *Applied Thermal Engineering*, 30(17-18), pp. 2685-2692.
- [13] Vajjha, R. S., Das, D. K., and Namburu, P. K., 2010, "Numerical Study of Fluid Dynamic and Heat Transfer Performance of Al_2O_3 and CuO Nanofluids in the Flat Tubes of a Radiator," *International Journal of Heat and Fluid Flow*, 31(4), pp. 613-621.
- [14] Peyghambarzadeh, S. M., Hashemabadi, S. H., Hoseini, S. M., and Seifi Jamnani, M., 2011, "Experimental Study of Heat Transfer Enhancement Using Water/Ethylene Glycol Based Nanofluids as a New Coolant for Car Radiators," *International Communications in Heat and Mass Transfer*, 38(9), pp. 1283-1290.
- [15] Chavan, D., and Pise, A. T., 2013, "Performance Investigation of an Automotive Car Radiator Operated With Nanofluid as a Coolant," *Journal of Thermal Science and Engineering Applications*, 6(2), p. 5.
- [16] Hussein, A. M., Sharma, K. V., Bakar, R. A., and Kadirgama, K., 2013, "The Effect of Cross Sectional Area of Tube on Friction Factor and Heat Transfer Nanofluid Turbulent Flow," *International Communications in Heat and Mass Transfer*, 47, pp. 49-55.
- [17] Ray, D. R., and Das, D. K., 2014, "Superior Performance of Nanofluids in an Automotive Radiator," *Journal of Thermal Science and Engineering Applications*, 6(4), p. 16.
- [18] American Society of Heating, R., and Engineers, A.-C., 2009, *ASHRAE Handbook of Fundamentals*, ASHRAE, Atlanta, United States.
- [19] Webb, R. L., and Kim, N. H., 1994, *Principles of enhanced heat transfer*, Taylor & Francis, New York, NY.
- [20] Fraas, A. P., 1989, *Heat Exchanger Design*, John Wiley & Sons Inc., New York.

- [21] Jacobi, A. M., 2004, "Heat Transfer to Air-Cooled Heat Exchangers," Engineering Data Book III, J. R. Thome, ed., Wolverine Tube, Inc, Decatur, Alabama, p. 40.
- [22] Maïga, S. E. B., Palm, S. J., Nguyen, C. T., Roy, G., and Galanis, N., 2005, "Heat Transfer Enhancement by Using Nanofluids in Forced Convection Flows," *International Journal of Heat and Fluid Flow*, 26(4), pp. 530-546.
- [23] Xuan, Y., and Roetzel, W., 2000, "Conceptions for Heat Transfer Correlation of Nanofluids," *International Journal of Heat and Mass Transfer*, 43(19), pp. 3701-3707.
- [24] Pak, B. C., and Cho, Y. I., 1998, "Hydrodynamic and Heat Transfer Study of Dispersed Fluids With Submicron Metallic Oxide Particles," *Experimental Heat Transfer*, 11(2), pp. 151-170.
- [25] Tu, J., Yeoh, G. H., and Liu, C., 2007, *Computational Fluid Dynamics: A Practical Approach*, Elsevier.
- [26] White, F. M., 2005, *Viscous fluid flow*, McGraw-Hill New York, NY.
- [27] Launder, B. E., and Spalding, D. B., 1974, "The Numerical Computation of Turbulent Flows," *Computer Methods in Applied Mechanics and Engineering*, 3(2), pp. 269-289.
- [28] ANSYS FLUENT, 2012, "User's Guide," Release 14.5, Canonsburg, PA.
- [29] Patankar, S. V., 1980, *Numerical Heat Transfer and Fluid Flow*, Hemisphere, Washington, DC.
- [30] Namburu, P. K., Das, D. K., Tanguturi, K. A., and Vajjha, R. S., 2009, "Numerical Study of Turbulent Flow and Heat Transfer Characteristics of Nanofluids Considering Variable Properties," *International Journal of Thermal Sciences*, 48(2), pp. 290-302.
- [31] Namburu, P. K., Kulkarni, D. P., Misra, D., and Das, D. K., 2007, "Viscosity of Copper Oxide Nanoparticles Dispersed in Ethylene Glycol and Water Mixture," *Experimental Thermal and Fluid Science*, 32(2), pp. 397-402.
- [32] Sahoo, B. C., Vajjha, R. S., Ganguli, R., Chukwu, G. A., and Das, D. K., 2009, "Determination of Rheological Behavior of Aluminum Oxide Nanofluid and Development of New Viscosity Correlations," *Petroleum Science and Technology*, 27(15), pp. 1757-1770.
- [33] Vajjha, R. S., Das, D. K., and Kulkarni, D. P., 2010, "Development of New Correlations for Convective Heat Transfer and Friction Factor in Turbulent Regime for Nanofluids," *International Journal of Heat and Mass Transfer*, 53(21-22), pp. 4607-4618.

- [34] Einstein, A., 1906, "A new determination of the molecular dimensions," *Annalen der Physik*, 19(2), pp. 289-306.
- [35] Batchelor, G. K., 1977, "The effect of Brownian motion on the bulk stress in a suspension of spherical particles," *Journal of Fluid Mechanics*, 83, pp. 97-117.
- [36] Vajjha, R. S., and Das, D. K., 2009, "Specific Heat Measurement of Three Nanofluids and Development of New Correlations," *Journal of Heat Transfer*, 131(7), pp. 1-10.
- [37] Chermisinoff, N. P., 1988, *Encyclopedia of Fluid Mechanics: Rheology and non-Newtonian flows*, Gulf Publishing Company, Houston, United States.
- [38] Vajjha, R. S., Das, D. K., and Mahagaonkar, B. M., 2009, "Density Measurement of Different Nanofluids and Their Comparison With Theory," *Petroleum Science and Technology*, 27(6), pp. 612-624.
- [39] Bejan, A., 1993, *Heat Transfer*, John Wiley & Sons, Inc., New York, NY.
- [40] ANSYS ICEM CFD: Mesh Generation Software, 2012, Release 14.5, Canonsburg, PA.
- [41] Gnielinski, V., 1976, "New Equations for Heat and Mass Transfer in Turbulent Pipe and Channel Flow," *International Chemical Engineering*, 16, pp. 359-368.
- [42] Dittus, F. W., and Boelter, L. M. K., 1985, "Heat Transfer in Automobile Radiators of the Tubular Type," *International Communications in Heat and Mass Transfer*, 12(1), pp. 3-22.
- [43] Bhatti, M. S., and Shah, R. K., 1987, "Turbulent and Transition Flow Convective Heat Transfer in Ducts," In *Handbook of Single-Phase Convective Heat Transfer*, S. Kakaç, R. K. Shah, and W. Aung, eds., Wiley, New York.
- [44] White, F. M., 2011, *Fluid Mechanics*, McGraw-Hill, New York, NY.
- [45] Bergman, T. L., Lavine, A. S., Incropera, F. P., and DeWitt, D. P., 2011, *Introduction to Heat Transfer*, Wiley, New York.
- [46] "Minitab 16 Statistical Software (2013). [Computer software].", Minitab, Inc. (www.minitab.com), State College, PA.

Table 5.1. Thermophysical property correlations for 60:40 EG/W.

Property	Correlation	Max. deviation
Density (kg/m ³)	$\frac{\rho}{\rho_0} = -0.4642 \left(\frac{T_0}{T}\right)^2 + 1.0203 \left(\frac{T_0}{T}\right) + 0.4459$ 238 K ≤ T ≤ 398 K; ρ ₀ = 1091.657 kg/m ³ ; R ² =0.999	0.4%
Specific heat (J/kg. K)	$\frac{c_p}{c_{p_0}} = 0.3814 \left(\frac{T}{T_0}\right) + 0.6185$ 238 K ≤ T ≤ 398 K; c _{p0} = 3042.32 J/(kg. K) ; R ² =1	0.01%
Thermal conductivity (W/m. K)	$\frac{k}{k_0} = -0.6868 \left(\frac{T}{T_0}\right)^2 + 1.981 \left(\frac{T}{T_0}\right) - 0.2939$ 238 K ≤ T ≤ 398 K; k ₀ = 0.3422 W/(m. K) ; R ² =0.999	0.11%
Viscosity (kg/m. s)	$\ln\left(\frac{\mu}{\mu_0}\right) = 12.513 \left(\frac{T_0}{T}\right)^2 - 12.882 \left(\frac{T_0}{T}\right) + 0.3707$ 238 K ≤ T ≤ 273 K; μ ₀ = 0.011179 kg/(m. s) ; R ² = 1	-0.19%
	$\ln\left(\frac{\mu}{\mu_0}\right) = 6.9088 \left(\frac{T_0}{T}\right)^2 - 1.942 \left(\frac{T_0}{T}\right) - 4.976$ 273 K < T ≤ 398 K; μ ₀ = 0.011179 kg/(m. s) ; R ² = 1	-0.82%

Table 5.2. Constants of the viscosity correlation for the Al₂O₃ and CuO nanofluids.

Nanoparticles	A ₁	A ₂	APS (nm)	Concentration	Temperature (K)
Al ₂ O ₃	0.983	12.959	45	0 < φ < 0.1	273 K < T < 363
CuO	0.9197	22.8539	29	0 < φ < 0.06	273 < T < 363

Table 5.3. Curve-fit relations for β proposed from experiments of Vajjha and Das [9].

Type of particles	β	Concentration	Temperature (K)
Al ₂ O ₃	$8.4407(100\phi)^{-1.07304}$	$0.01 \leq \phi \leq 0.1$	$298 \leq T \leq 363$
CuO	$9.881(100\phi)^{-0.9446}$	$0.01 \leq \phi \leq 0.06$	$298 \leq T \leq 363$

Table 5.4. Curve-fit coefficients for the specific heat of Al₂O₃ nanofluids [36].

Nanofluid	A	B	C	Max. deviation %	Avg. absolute deviation %
Al ₂ O ₃	0.24327	0.5179	0.4250	5	2.28

Table 5.5. Mesh independence study.

Mesh (N _x x N _y x N _z)	Max. Velocity, m/sec	Max. Temperature, K
Mesh I 40 x 15 x 100	0.3429	359.53
Mesh II 65 x 25 x 150	0.37467	359.681
Mesh III 95 x 35 x 200	0.40611	359.774
Mesh IV 140 x 50 x 300	0.406436	359.776

Table 5.6. Fully developed turbulent flow Nusselt number correlations used for comparison in the present numerical study.

Researchers	Correlation	Fluid	Max. dev., Avg. dev. %
Gnielinski [41]	$Nu = 0.012(Re_{D_h}^{0.87} - 280)Pr^{0.4}$ $1.5 \leq Pr \leq 500, 3000 \leq Re_{D_h} \leq 10^6$	Water	-12.2 & 5.4
		60:40 EG/W	-13.6 & 6.2
Dittus and Boelter [42]	$Nu = 0.023Re_{D_h}^{0.8}Pr^{0.3}$ $0.7 \leq Pr \leq 120, 2500 \leq Re_{D_h} \leq 1.24 \times 10^5$	Water	3.2 & 0.8
		60:40 EG/W	-11.3 & 1.02

Table 5.7. Fully developed turbulent flow friction factor correlations used for comparison in the present study.

Researchers	Correlation	Fluid	Max. dev., & Avg. dev., %
Blasius [26]	$C_f = 0.0791Re_{D_h}^{-0.25}$	Water	-12.2 & 4.2
		60:40 EG/W	9.18 & 4.12
Churchill [18]	$C_f = 2 \left[\left(\frac{8}{Re_{D_h}} \right)^{12} + \frac{1}{(A+B)^{1.5}} \right]^{1/12}$ $A = \left[2.457 \ln \left(\frac{1}{(7/Re_{D_h})^{0.9} + (0.27\varepsilon/D_h)} \right) \right]^{16}$ $B = \left(\frac{37530}{Re_{D_h}} \right)^{16}$	Water	-11.1 & 3.41
		60:40 EG/W	9.34 & 3.35
Drew et al. [43]	$C_f = 0.0014 + 0.125Re_{D_h}^{-0.32}$	Water	-8.64 & 3.53
		60:40 EG/W	10.06 & 3.46
Bhatti and Shah [43]	$C_f = 0.00128 + 0.1143Re_{D_h}^{-0.311}$	Water	-11.54 & 3.74
		60:40 EG/W	8.1 & 3.67
Colebrook [43]	$\frac{1}{\sqrt{C_f}} = 1.5635 \ln \left(\frac{Re}{7} \right)$	Water	-7.73 & 2.73
		60:40 EG/W	7.94 & 2.7

Table 5.8. Comparison of various parameters for different concentrations of the Al₂O₃ nanofluid with the base fluid for a constant heat transfer.

Type of Nanofluid	Aluminum oxide (Al ₂ O ₃)						
Concentration (%)	0	1	2	3	4	5	6
Heat transfer coefficient h (W/m ² .K)	6000	6000	6000	6000	6000	6000	6000
Reynolds number, Re	7894	6150	5734	5363	5026	4673	4372
Density (kg/m ³)	1043.12	1064.89	1090.44	1116.09	1141.60	1167.25	1192.90
Viscosity (kg/m.s)	0.000891	0.000992	0.001132	0.001287	0.001470	0.001679	0.001909
Velocity (m/s)	1.4735	1.2521	1.3011	1.3515	1.4139	1.4684	1.5284
Average skin friction coefficient C_f	0.008803	0.009625	0.009876	0.010137	0.010398	0.010699	0.011000
Pressure loss (Pa)	4356.02	3511.08	3983.23	4515.29	5184.87	5882.82	6697.36
Power (W)	0.29632	0.20295	0.23925	0.28172	0.33843	0.39877	0.47255
% Power reduction		31.51	19.26	4.93	-14.21	-34.58	-59.48

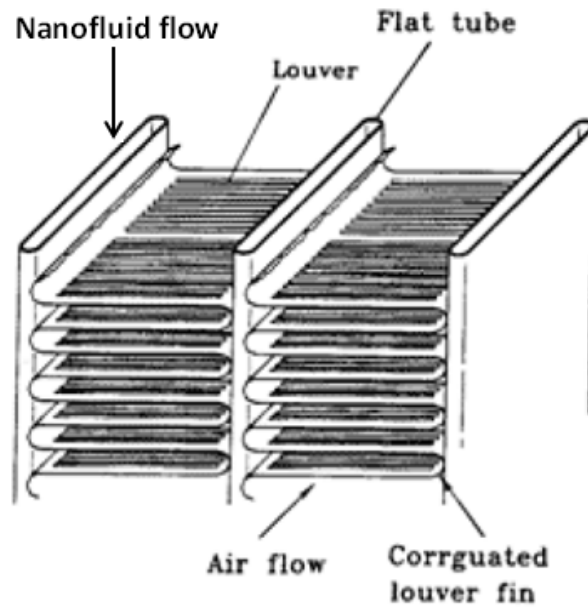


Figure 5.1A. Typical configuration of an automobile radiator adopted from [21].

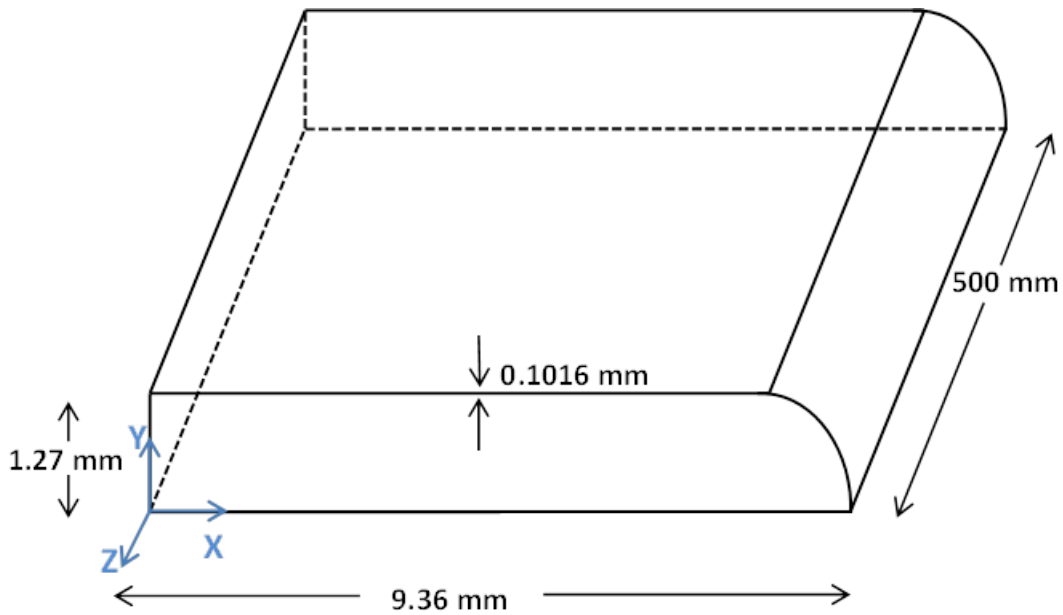


Figure 5.1B. Dimensions and coordinate system of one quarter of a flat tube used in the present numerical study.

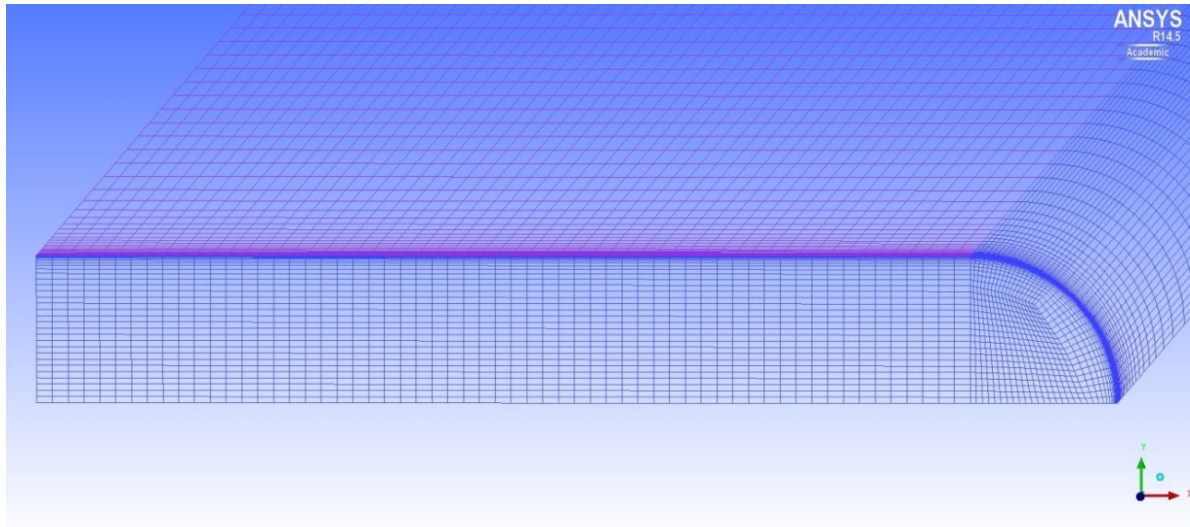


Figure 5.2. Mesh layout used in the present analysis.

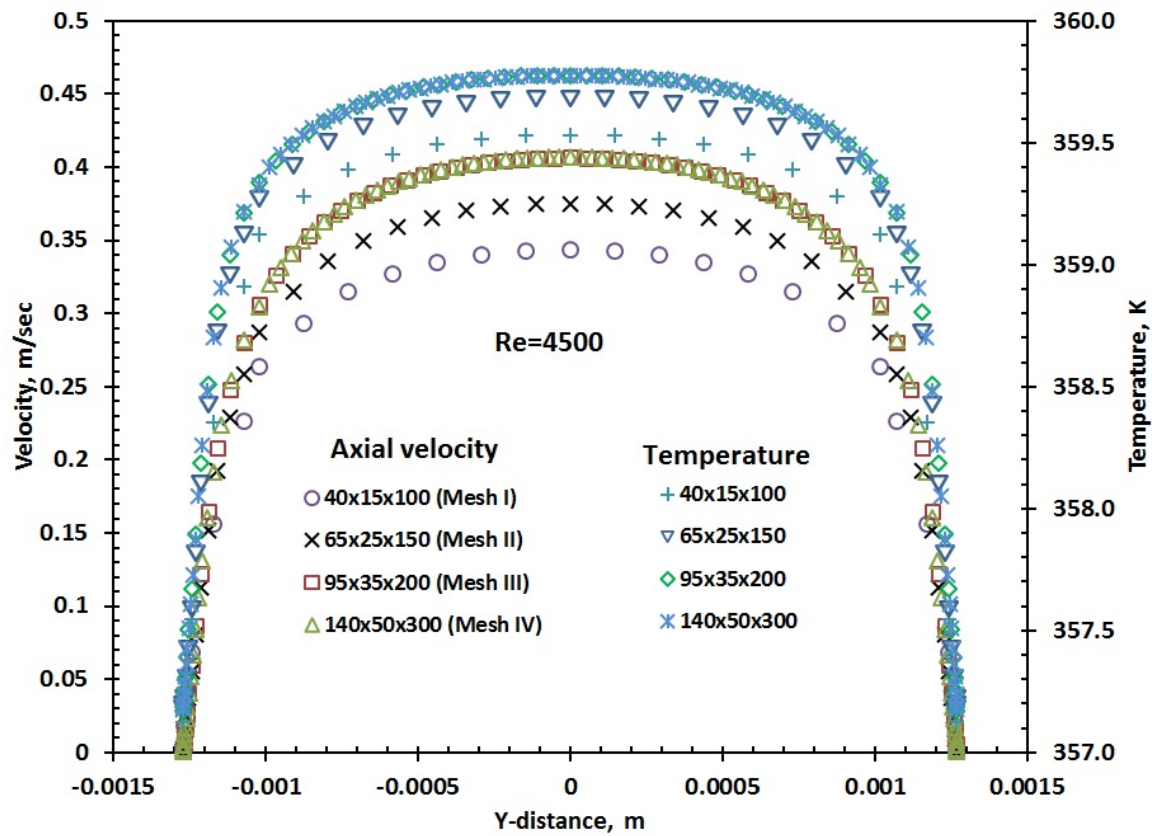


Figure 5.3. Axial velocity and temperature profiles in the Y-Z plane at the outlet of the duct ($Z=0.5\text{m}$) and at the center ($X=0$) for four different mesh sizes.

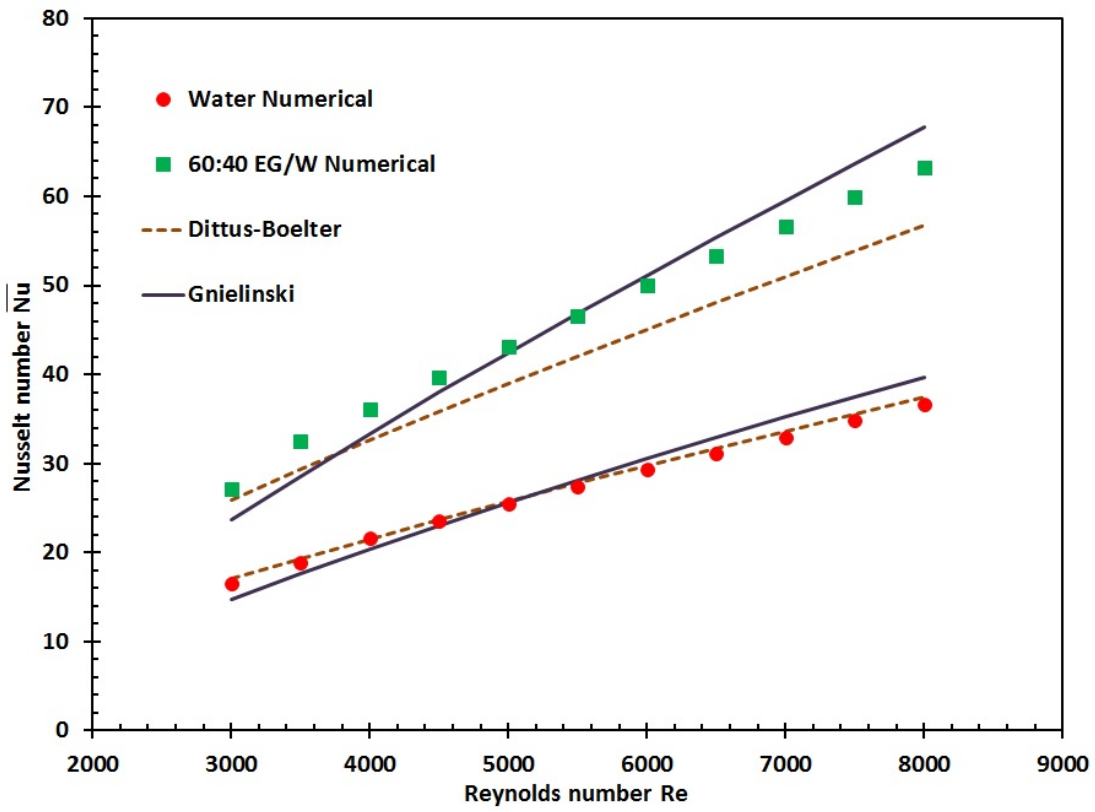


Figure 5.4. Comparison of \overline{Nu} of the present numerical computations with the theoretical results for various Reynolds numbers in a flat tube.

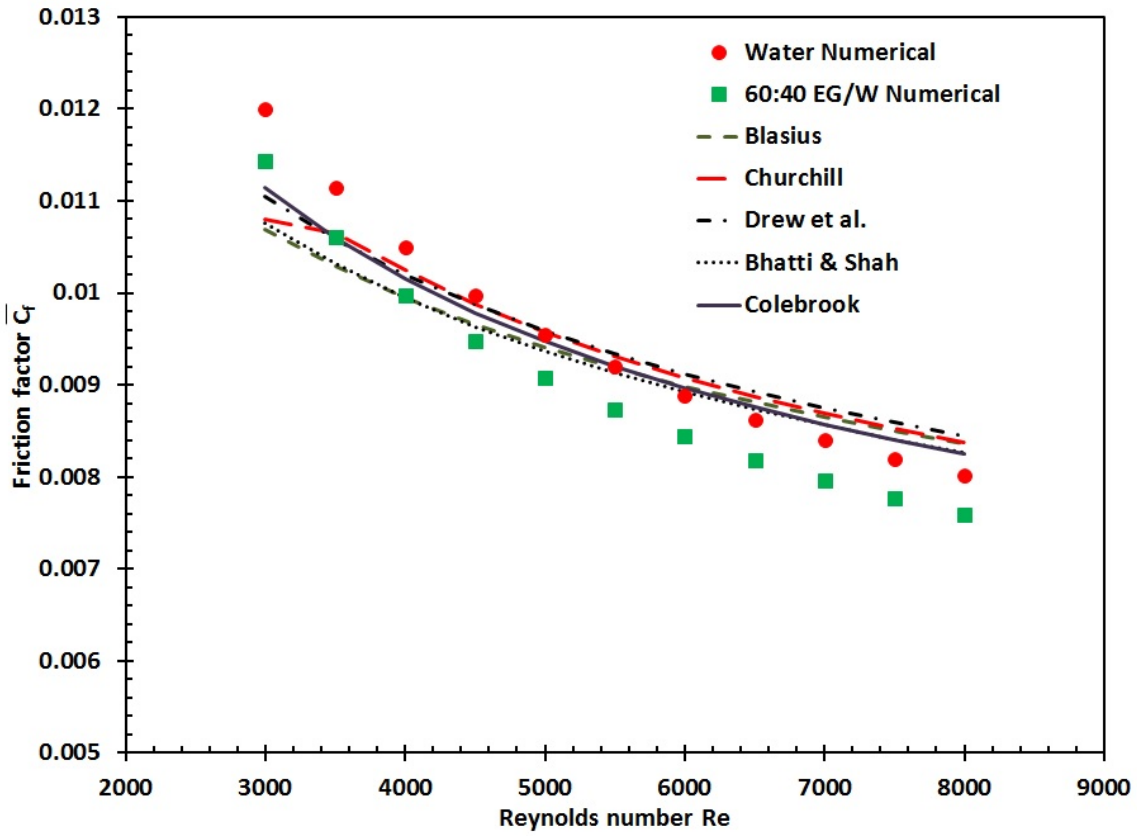


Figure 5.5. Comparison of \bar{C}_f of the present numerical computations with the correlations of other researchers for various Reynolds numbers.

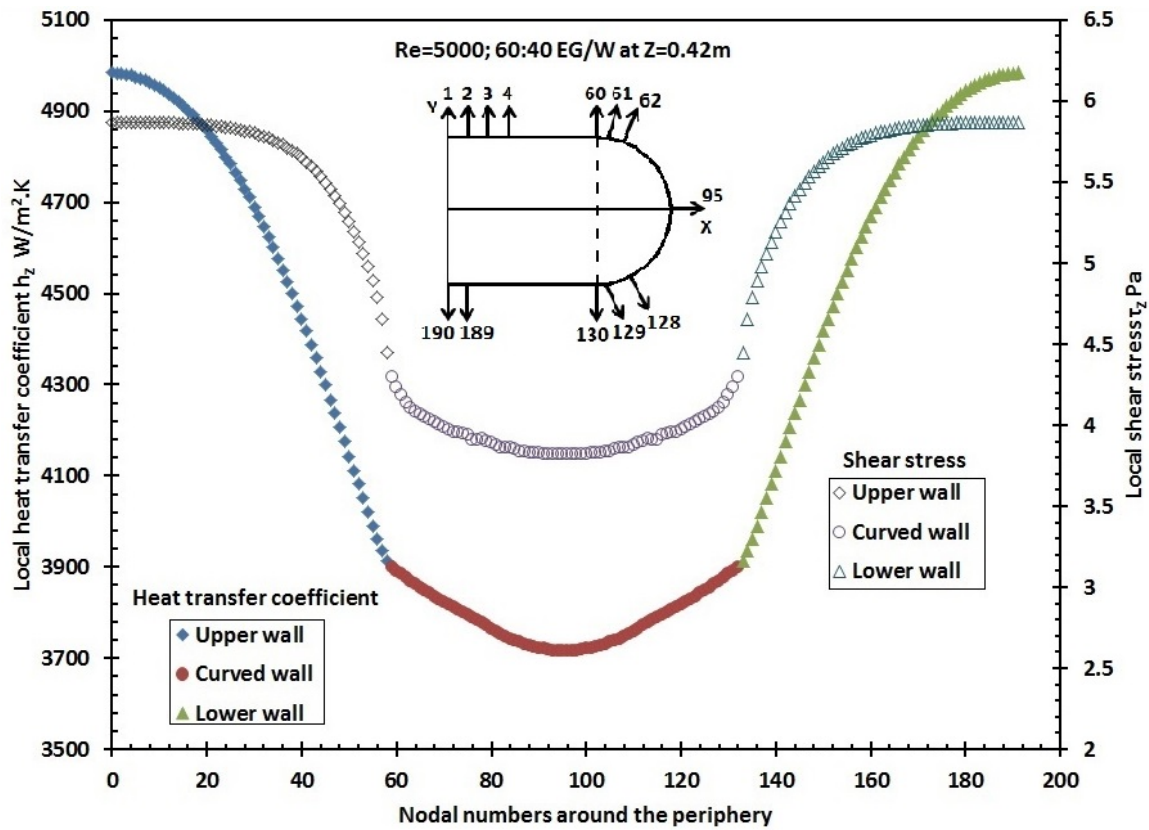
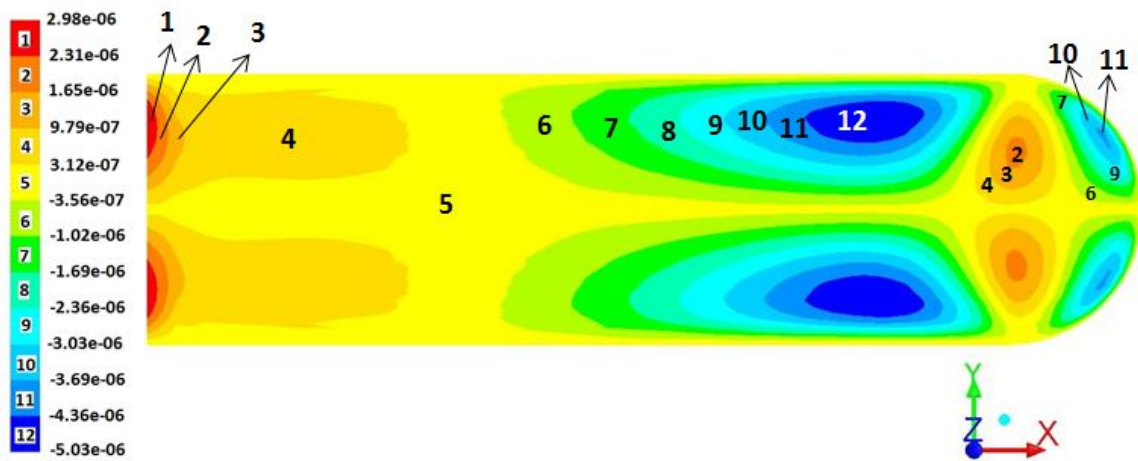
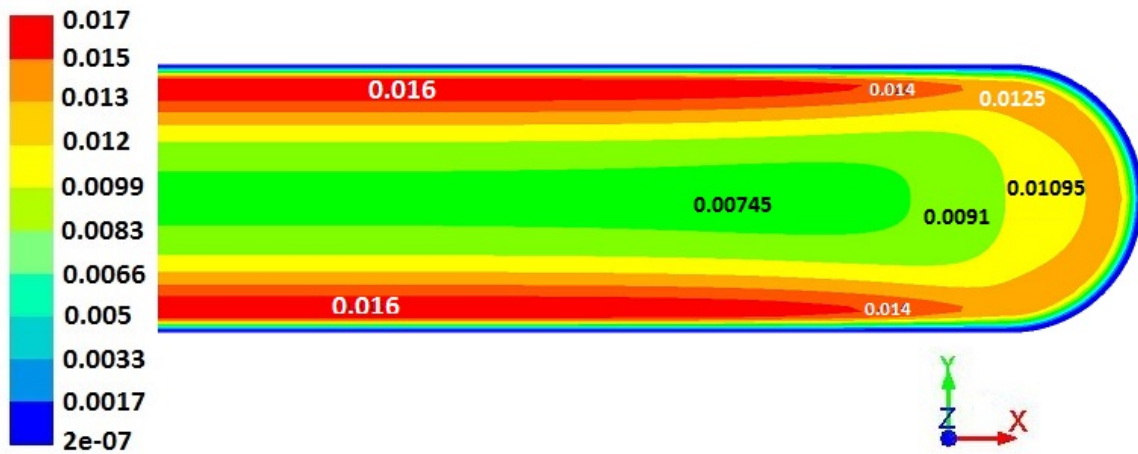


Figure 5.6. Local heat transfer coefficient and local shear stress variation along the circumference (1-60 upper wall, 61-130 curved wall and 131-190 lower wall) of the tube at Z=0.42 m for the base fluid.



(a) Y-velocity (m/s)



(b) Turbulent Kinetic Energy (m^2/s^2)

Figure 5.7. Contour plots of (a) Y velocity (m/s) and (b) Turbulent Kinetic Energy (m^2/s^2) at $Z = 0.25$ m and $Re = 5000$.

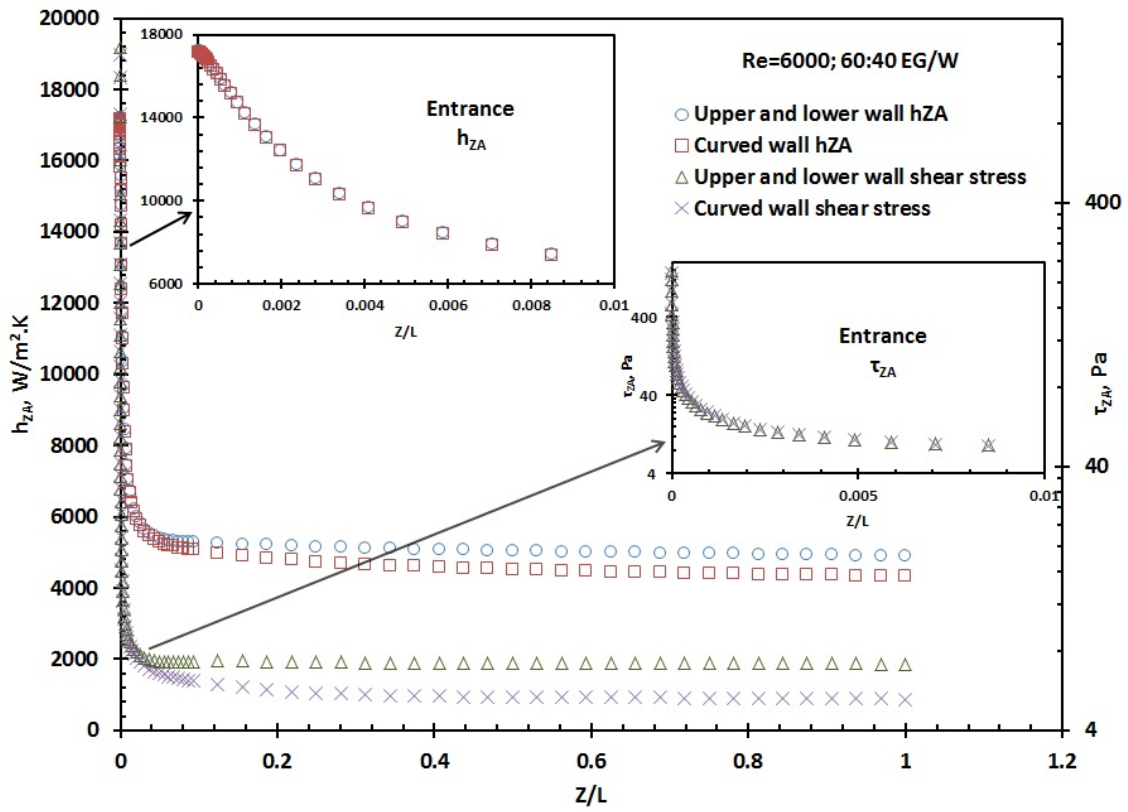


Figure 5.8. Variation of h_{ZA} and τ_{ZA} on the upper, lower and semicircular walls along the length of the tube for the base fluid.

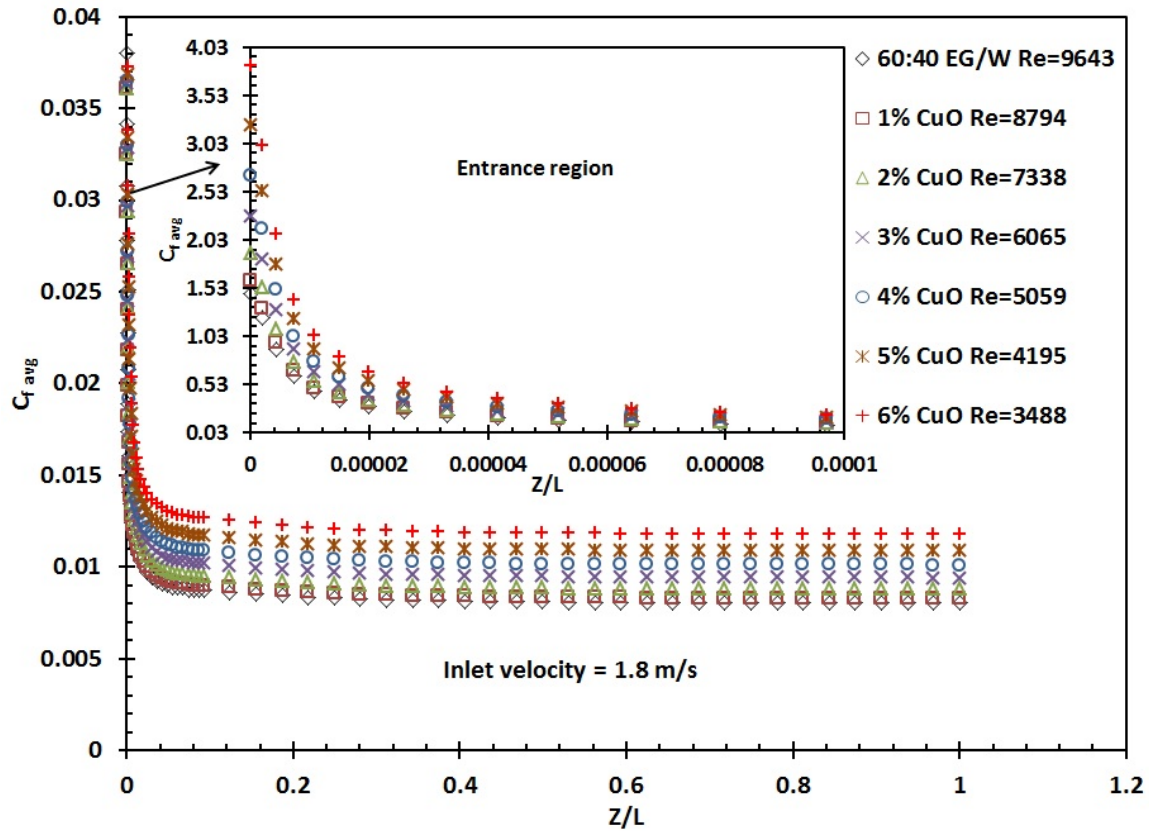


Figure 5.9. Variation of $C_{f, avg}$ along the tube length for different particle volumetric concentrations of the CuO nanofluid.

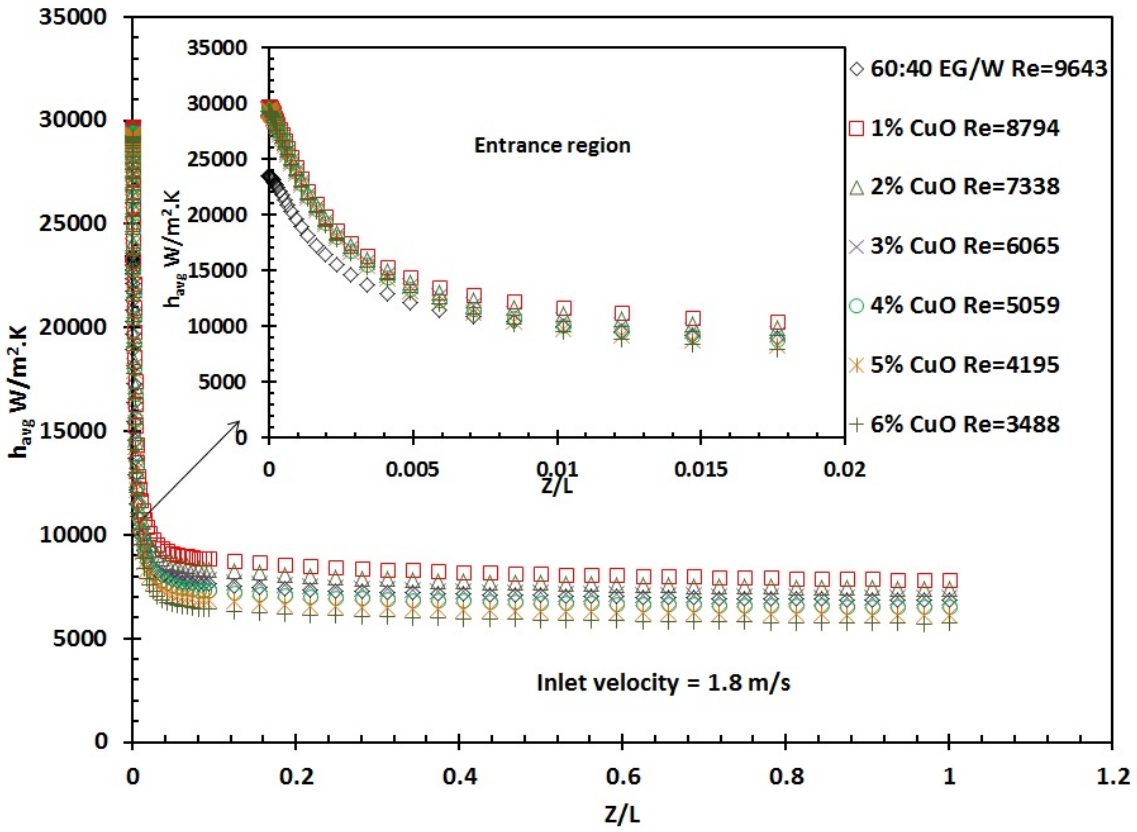


Figure 5.10. Variation of h_{avg} along the tube length for various concentrations of the CuO nanofluid.

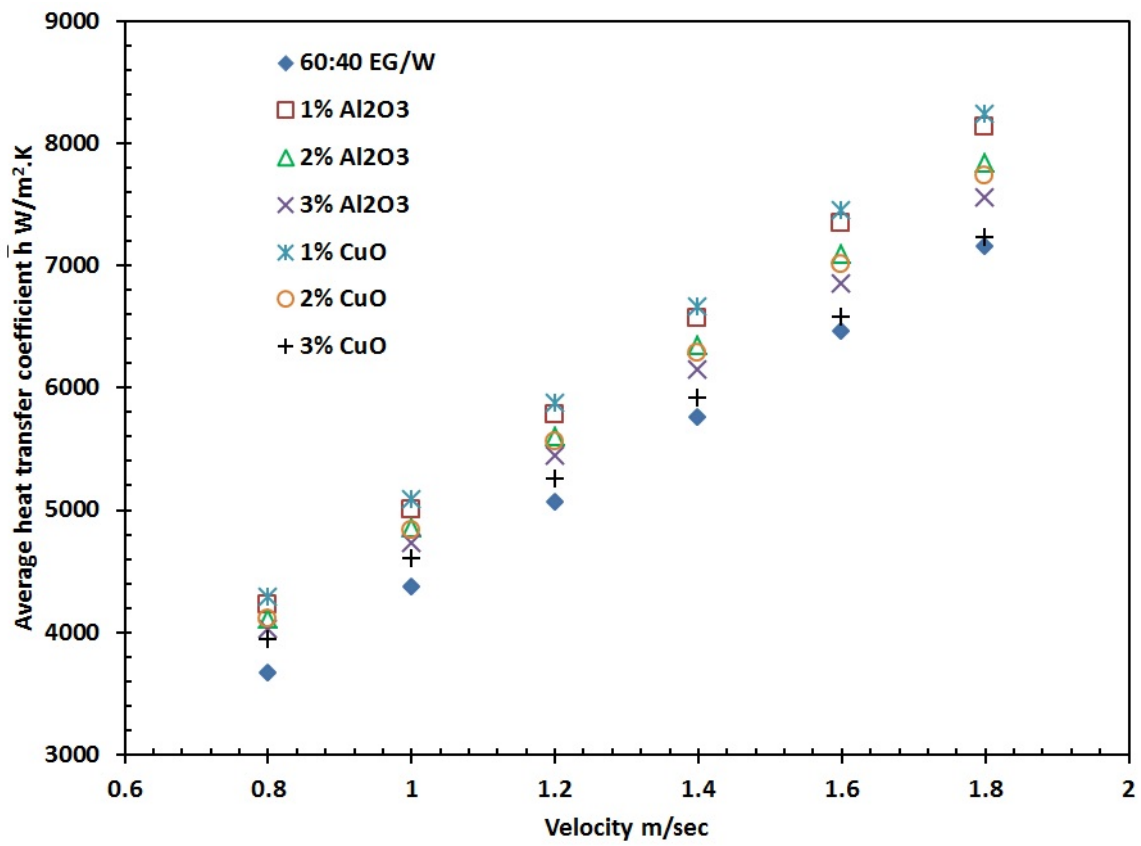


Figure 5.11. Variation of average heat transfer coefficient with velocity for base fluid and two nanofluids.

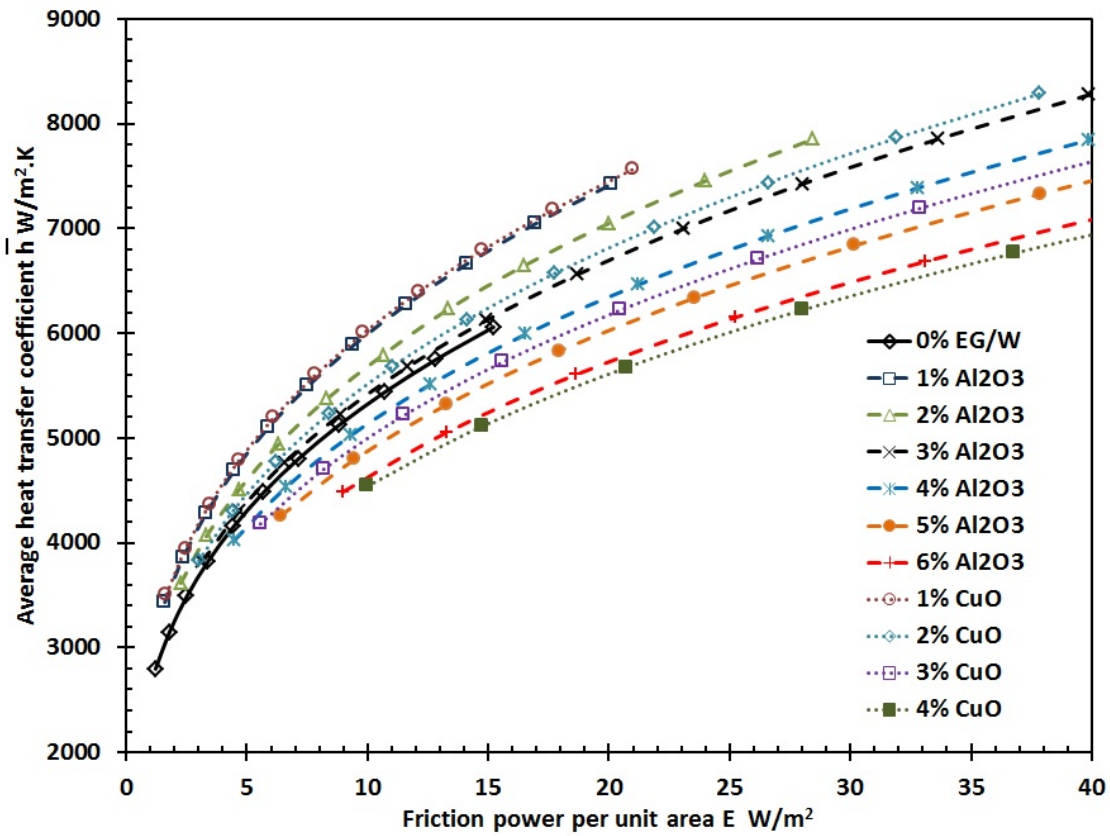


Figure 5.12. A comparison of the heat transfer coefficient at different friction powers per unit area for Al₂O₃, CuO nanofluids of different concentrations and the base fluid.

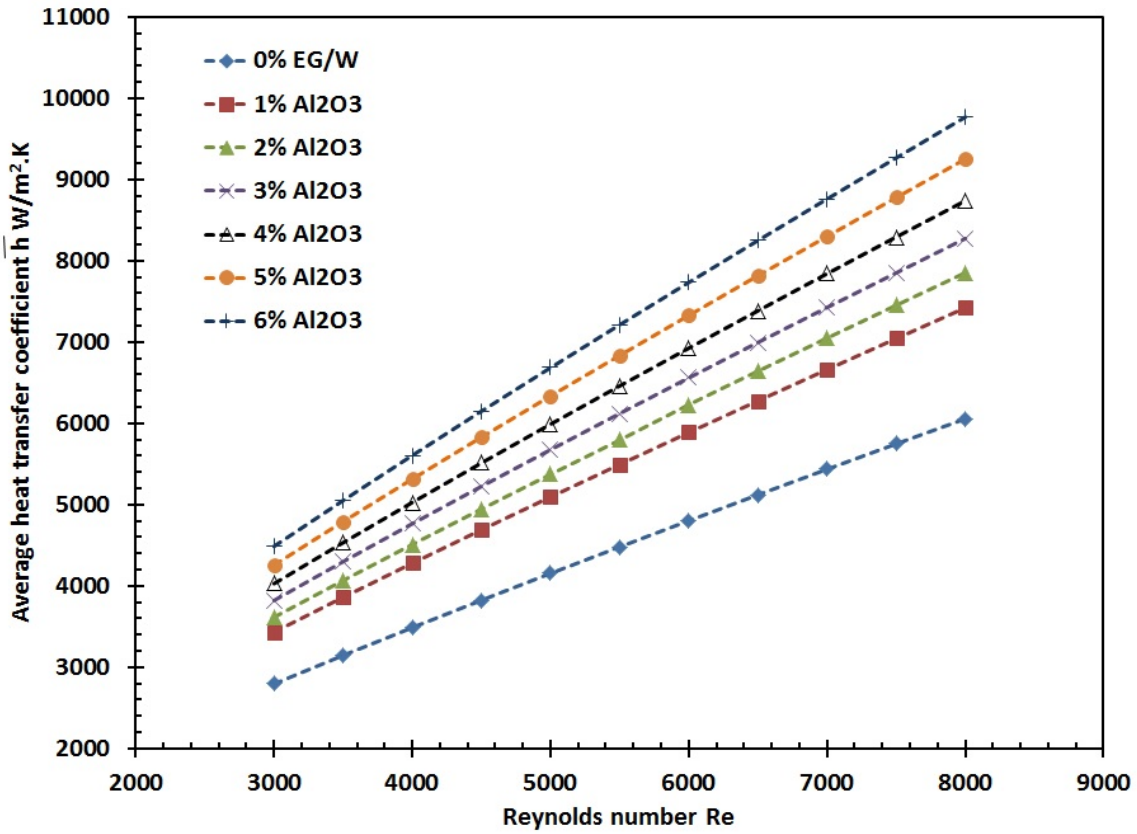


Figure 5.13. Variation of the \bar{h} with Reynolds number for different particle volumetric concentrations of the Al₂O₃ nanofluid.

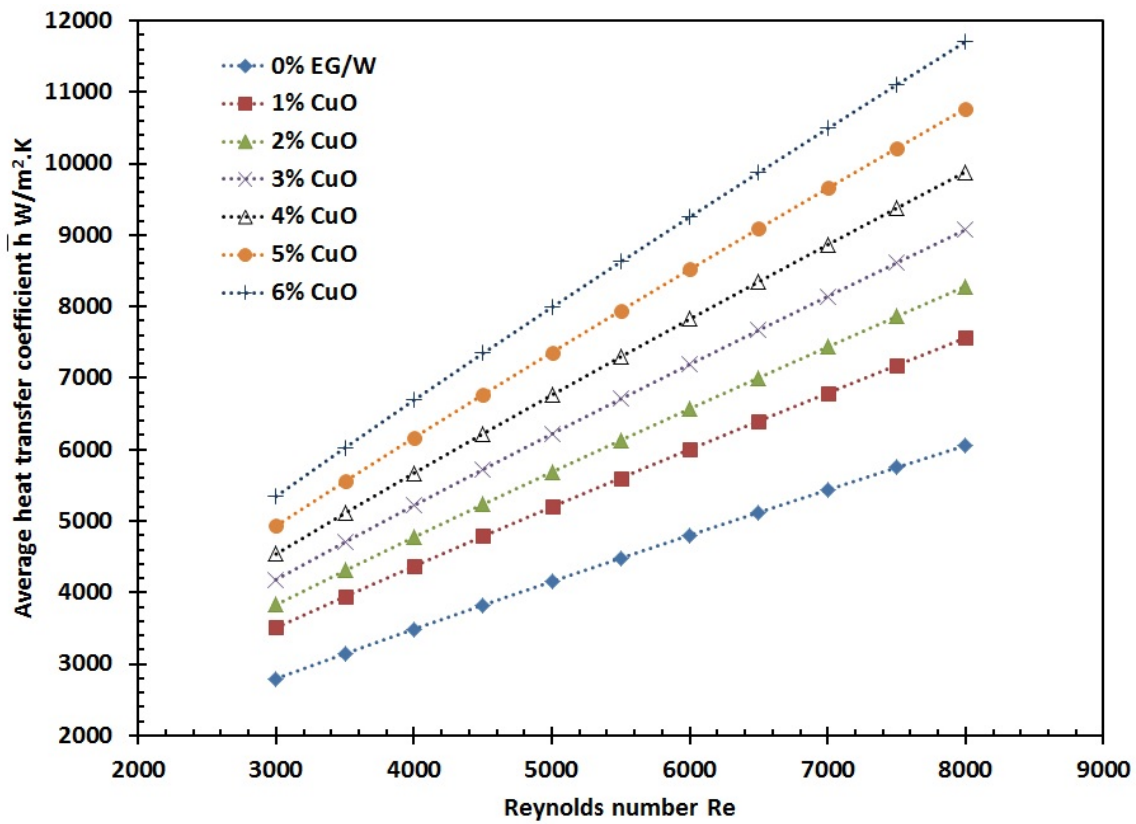


Figure 5.14. Variation of the \bar{h} with Reynolds number for different particle volumetric concentrations of the CuO nanofluid.

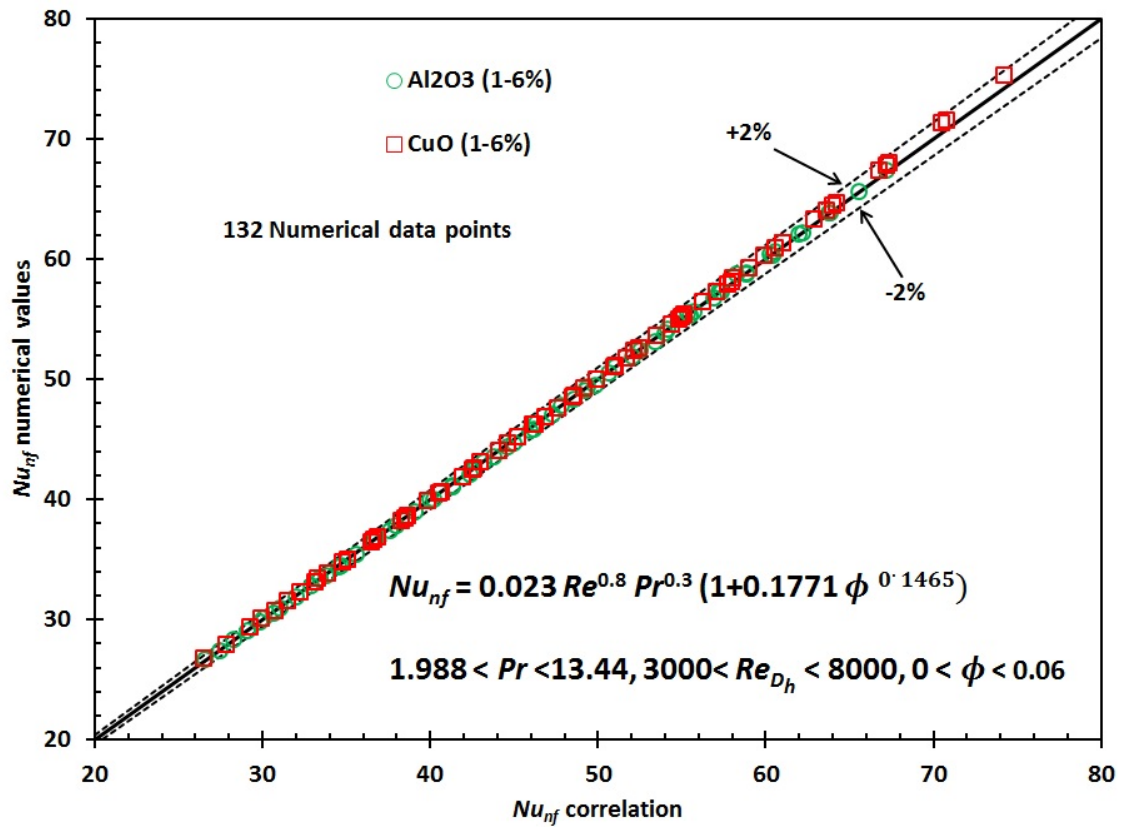


Figure 5.15. Comparison of the Nusselt number values calculated from the present correlation, Eq. (5.16) with the values obtained from the present numerical study in the fully developed region.

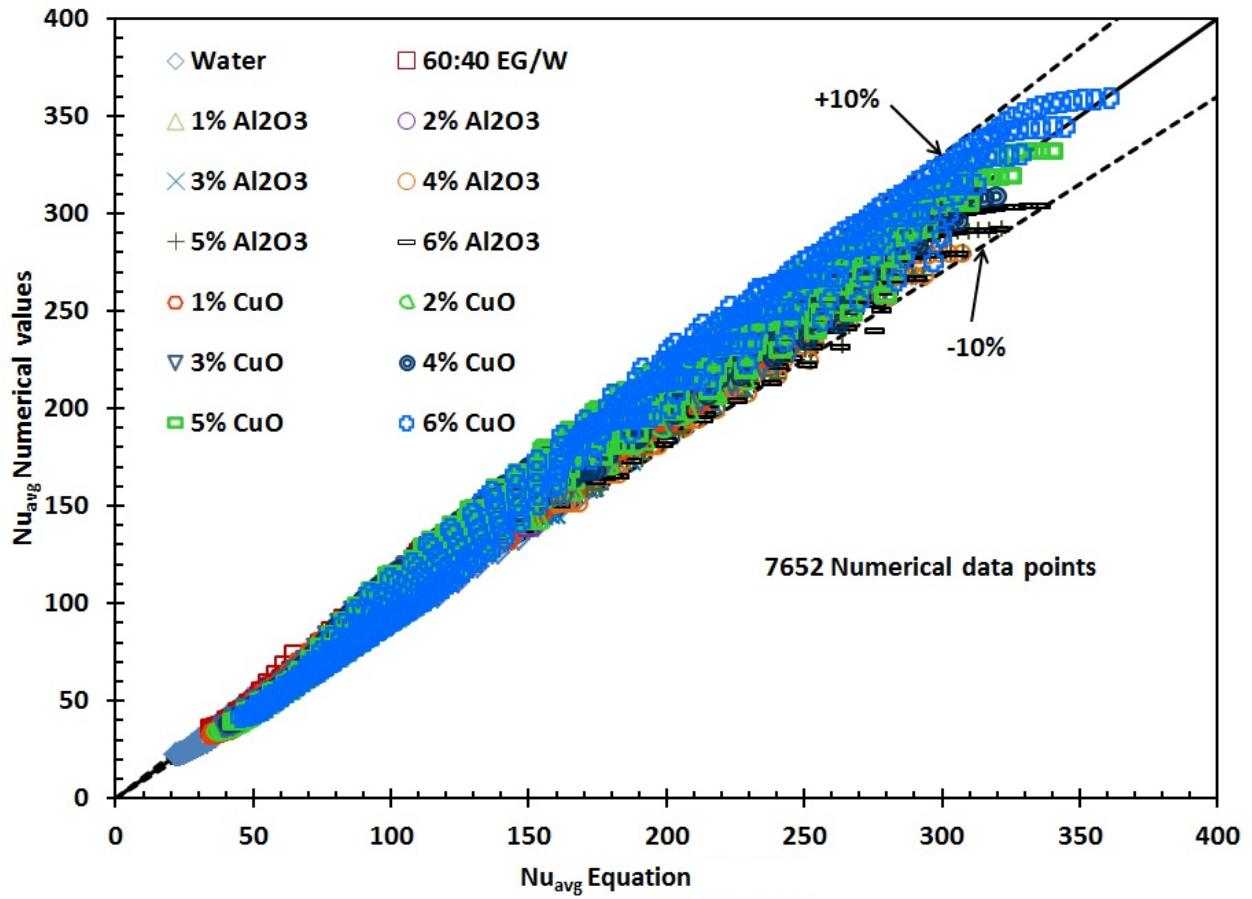


Figure 5.16. Comparison of the local Nusselt number values calculated from the correlation, Eq. (5.20a & b) with the values obtained from the present numerical study.

Chapter 6. Overall Conclusions

The following conclusions are drawn from the preceding chapters:

6.1 Conclusions for Development of New Correlations for Convective Heat Transfer and Friction Factor in Turbulent Regime for Nanofluids

- Experimental results showed that for all the three nanofluids, with an increase in the particle volumetric concentration the heat transfer coefficient increases. For example, at a Reynolds number of 7240, the percentage increase in the heat transfer coefficient over the base fluid for a 10% Al_2O_3 nanofluid is 81.74%.
- The pressure loss of nanofluids also increases with an increase in particle volume concentration. The increase of pressure loss for a 10% Al_2O_3 nanofluid at a Reynolds number of 6700 is about 4.7 times than that of the base fluid. This is due to the increase in the viscosity of the nanofluid with concentration.
- A new Nusselt number correlation similar to the Gnielinski equation for single phase liquid has been developed. This new equation is a function of the nanoparticle volume concentration in addition to the Reynolds number and the Prandtl number.
- Furthermore, a new correlation for the friction factor has been developed following the Blasius friction factor equation including in consideration density and viscosity of nanofluids.

6.2 Conclusions for a Review and Analysis on Influence of Temperature and Concentration of Nanofluids on Thermophysical Properties, Heat Transfer and Pumping Power

- Addition of nanoparticles to a liquid increases the viscosity significantly and the thermal conductivity moderately; however, the specific heat and density change modestly. For example, the viscosity of the Al_2O_3 nanofluid of 6% volumetric concentration increases by 91% in comparison to the base fluid of 60:40 EG/W at the room temperature of 293 K. Under the same conditions the thermal conductivity of the same nanofluid increases by 22.4%, the density by 13.9% and the specific heat decreases by 13.2%.

- The Prandtl number of nanofluids increases with an increase in particle volumetric concentration (e.g. for the CuO nanofluid of 6% concentration the increase is 124%), and decreases with an increase in the temperature.
- For a specified geometry and velocity, the Reynolds number of nanofluid increases with temperature and decreases with an increase in particle volumetric concentration. As an example, for the SiO₂ nanofluid of 4% concentration, the Reynolds number increases from 3900 at 293 K to 11395 at 333 K, an increase of 192%, predominantly due to the decrease in viscosity.
- The convective heat transfer coefficient of nanofluids increases with an increase in temperature and concentration and is significantly higher than that of the base fluid. As an example, for a 1% Al₂O₃ nanofluid the convective heat transfer coefficient can increase by 31.9% compared to the base fluid at room temperature.
- There exists an optimal range of temperature and concentration at the dilute level, where the benefits of nanofluids can be maximized.
- With an increase in particle volumetric concentration and temperature, the thermal diffusivity of nanofluid increases which is primarily due to the increase in thermal conductivity while the product of (ρC_p) remains nearly constant. For example, the increase in thermal diffusivity for a 2% CuO nanofluid at 333 K is 28%.
- For a constant rate of heat transfer, the pumping power for the nanofluid can be lower than that of the base fluid. For example, the 60:40 EG/W base fluid would require 83.3% higher pumping power in comparison to a 2% Al₂O₃ nanofluid at the room temperature of 293 K for the same amount of heat transfer.
- The figure of merit (FOM) of heat transfer rates for various nanofluids was compared based on the Mouromtseff number. Results showed that the Mouromtseff numbers of nanofluids are higher than that of the base fluid proving that nanofluids can be more efficient than the conventional fluids under both laminar and turbulent flow conditions.
- The energy ratio (ER) for the nanofluid is higher than that of the base fluid at an equal Reynolds number.
- From the pumping power requirement study, we observe that a dilute concentration of the Al₂O₃ nanofluid has the best combination of properties over the CuO and SiO₂ nanofluids to

yield a superior level of heat transfer at lower pumping power and may become an effective new generation heat transfer fluid.

6.3 Conclusions for an Experimental Determination of the Viscosity of Propylene Glycol/Water based Nanofluids and Development of New Correlations

- The viscosities of nanofluids with five nanoparticles (Al_2O_3 , CuO, SiO_2 , TiO_2 and ZnO) dispersed in a base fluid of 60:40 PG/W exhibit a non-Newtonian behavior within a lower temperature range of 243 K to 273 K and a Newtonian behavior within the higher temperature range of 273 K to 363 K.
- The non-Newtonian behavior followed a Bingham plastic viscosity model with small yield stress values.
- The viscosity of nanofluids increases with an increase in particle volumetric concentration and decreases with an increase in temperature.
- The viscosity was found to be exponential function of temperature for all the particle volumetric concentrations of nanofluids.
- For a given nanoparticle concentration, as the diameter of nanoparticles decreased, the viscosity of the nanofluid increased.
- Existing correlations in the literature do not predict the viscosity of nanofluids accurately.
- Therefore, a new model was developed from 458 experimental data points of five nanofluids.
- The present study also covers the experiments on rheological properties (Shear stress, shear strain) of three different types of carbon nanotubes; single walled carbon nanotubes (SWCNT), bamboo-like structured multi walled carbon nanotubes (BWCNT) and multi walled carbon nanotubes (MWCNT) dispersed in a base fluid of 20:80 PG/W with a particle volumetric concentration of 0.229% (weight concentration of 0.3%).
- The measurements revealed that the SWCNT and MWCNT suspensions behaved like a pseudoplastic fluid up to a temperature of 313 K (30°C) and thereafter they behaved as Bingham plastic fluid. On the other hand, the BWCNT behaved like a Bingham plastic fluid with over the entire temperature range of 273 K to 363 K.
- For a fixed volume concentration and temperature of the fluid, it was observed that at same shear rate, the viscosity of MWCNT > BWCNT > SWCNT.

- At a given concentration, the viscosity of the MWCNT is higher compared to that of the BWCNT and the SWCNT at the same temperature and shear rate.
- The SWCNT and BWCNT showed that the viscosity practically did not change after an ultrasonication time of 45 minutes under a prescribed power and sample volume.
- A correlation for the viscosity of CNT nanofluids as a function of temperature and shear rate, involving the Péclet number has been proposed from the measured values for SWCNT and BWCNT at a fixed volumetric concentration.

6.4 Conclusions for Development of New Correlations for the Nusselt Number and the Friction Factor under Turbulent Flow of Nanofluids in Flat Tubes

- Numerical simulation for the Al_2O_3 and CuO nanofluids with varying particle volumetric concentrations of 0 to 6% exhibit substantial increase in the average heat transfer coefficient with an increase in concentration.
- At a Reynolds number of 5500, the enhancement in the average heat transfer coefficient (h_{avg}) over the base fluid for a 3% Al_2O_3 nanofluid is 36.6% and that for a 3% CuO nanofluid is 49.7%.
- For the particle volume concentrations of 1% and 3%, the h_{avg} in the fully developed region increases over the base fluid by 13.23% and 5.88% respectively for the Al_2O_3 nanofluid and by 14.5% and 1.6% respectively for the CuO nanofluid.
- On the basis of equal inlet velocity, the peripheral averaged skin friction coefficient ($C_{f,avg}$) increases with an increase in the nanoparticle volumetric concentration. For example, at a constant inlet velocity of 1.8 m/s, the $C_{f,avg}$ in the fully developed region of the flat tube for a 3% particle volumetric concentration of the Al_2O_3 and CuO nanofluids are 9.5% and 17.16% higher than that of the base fluid respectively.
- For the same amount of heat transfer, the Al_2O_3 nanofluid of a 1% concentration showed highest reduction in the pumping power over the base fluid and beyond 3% concentration, the pumping power increased for the Al_2O_3 nanofluid over that of the base fluid.
- Similar analysis conducted for the CuO nanofluid showed that beyond a 2% particle concentration, the pumping power exceeded that required by the base fluid.

- New Nusselt number and skin friction coefficient correlations for turbulent flows of nanofluids in the flat tube of a radiator have been developed for the entrance as well as the fully developed regions.

6.5 Suggestions for Future Research

The present research has demonstrated that nanoparticles can be used to enhance the thermal performance of conventional heat transfer fluids used currently. However, additional research should be done in the following areas for better understanding of nanofluids and to improve the efficiency of nanofluids.

- The long term suspension stability of the nanofluids should be studied to prevent agglomeration, if nanofluids are to be successful in practical heat exchanger systems.
- Entropy generation analysis due to fluid friction and heat transfer in nanofluids should be investigated and compared with that of the base fluid.
- Enhancing the thermal emissivity of nanofluids with highly emissive nanoparticles is another important area to explore. This would extend the application of nanofluids to radiative cooling of space crafts in the outer space.
- Our experimental viscosity data of several ethylene glycol based nanofluids are limited up to a temperature of 50°C. With some additional experimental work, this data can be extended up to 90°C. Finally, the viscosity data of propylene glycol based nanofluids from the present research and the viscosity data of ethylene glycol based nanofluids from the past research can be combined to develop a new unified correlation for the viscosity of glycol based nanofluids, valid for both EG and PG.
- Nanofluid performance can be improved by exploring new nanoparticles such as aluminum nitride and boron nitride. These particles have much higher thermal conductivity than the Al_2O_3 and CuO . Therefore, they are promising candidates in enhancing the thermal conductivity of these nitride particles based nanofluids.
- The work on carbon nanotubes should be extended to fully understand the effect of particle volume concentration on the viscosity of different types of carbon nanotubes. Excessive sonication results in the breakage of CNT and lower than optimum sonication time cannot separate the agglomerated bunch. Therefore, further studies are recommended to establish an appropriate period of ultrasonication for the multi-

walled carbon nanotubes to reach an equilibrium state, beyond which the rheological properties do not change appreciably.

Appendices

During my Ph.D. research in the past five years, in addition to the four chapters presented in the main body of the dissertation, I worked on several research projects with the fellow graduate students of the Nanofluids group.

Several journal publications were produced from those studies in which I participated and did a portion of research. The abstracts of those papers are presented in this Appendix.

Appendix 1. Experimental and Numerical Investigations of Nanofluids Performance in a Compact Minichannel Plate Heat Exchanger*

ABSTRACT

Three nanofluids comprising of aluminum oxide, copper oxide and silicon dioxide nanoparticles in ethylene glycol and water mixture have been studied theoretically to compare their performance in a compact minichannel plate heat exchanger (PHE). The study shows that for a dilute particle volumetric concentration of 1%, all the nanofluids show improvements in their performance over the base fluid. Comparisons have been made on the basis of three important parameters; equal mass flow rate, equal heat transfer rate and equal pumping power in the PHE. For each of these cases, all three nanofluids exhibit increase in convective heat transfer coefficient, reduction in the volumetric flow rate and reduction in the pumping power requirement for the same amount of heat transfer in the PHE. On the cold fluid side of the heat exchanger, a coolant, HFE-7000, has been studied, which has the potential for application in extremely low temperatures, but has not been investigated widely in the literature. Experimental data measured from a minichannel PHE in a test loop using water as the base fluid have validated the test apparatus with excellent agreement of predicted heat transfer rate and the overall heat transfer coefficient with the experimental values. From experiments on a 0.5% aluminum oxide nanofluid, preliminary correlations for the Nusselt number and the friction factor for nanofluid flow in a PHE has been derived. This apparatus will be useful to test different kinds of nanofluids to ultimately determine the effects of parameters such as: volumetric concentration, particle size and base fluid properties on thermal and fluid dynamic performance of nanofluids in compact heat exchangers.

* Ray, D. R., Das, D. K., and Vajjha, R. S., 2014, "Experimental and numerical investigations of nanofluids performance in a compact minichannel plate heat exchanger," *International Journal of Heat and Mass Transfer*, 71, pp. 732-746.

Appendix 2. Measurements of the pH of Three Nanofluids and Development of New Correlations *

ABSTRACT

In this study the pH of aluminum oxide (Al_2O_3), silicon dioxide (SiO_2) and zinc oxide (ZnO) nanoparticles dispersed in propylene glycol and water mixture were measured in the temperature range of 0 °C to 90 °C. The volumetric concentration of nanoparticles in these fluids ranged from 0 to 10% for different nanofluids. The average particle sizes (APS) considered were from 10 nm to 70 nm. The pH measuring apparatus and the measurement procedure were validated by measuring the pH of a calibration fluid, whose properties are known accurately. The measured pH values agreed within less than $\pm 0.5\%$ with the published data reported by the manufacturer. Following the validation, the pH values of different nanofluids were measured. The measurements showed that pH of nanofluids decreased with an increase in temperature and increased with an increase in particle volumetric concentration. For the same nanofluid at a fixed volumetric concentration, the pH was found to be higher for larger particle sizes. From the experimental data, empirical models were developed for three nanofluids to express the pH as functions of temperature, volumetric concentration and the size of the nanoparticles.

* Konakanchi, H., Vajjha, R. S., Chukwu, G., and Das, D. K., 2014, "Measurements of pH of Three Nanofluids and Development of New Correlations," In Press: Heat Transfer Engineering.

Appendix 3. Measurement of the Thermal Conductivity of Silicon Dioxide Nanofluid and Development of Correlations *

ABSTRACT

Experimental investigations were carried out for the determination of thermal conductivity of silicon dioxide (SiO₂) nanoparticles dispersed in 60% ethylene glycol and 40% water by mass. Experiments conducted in a temperature range of 20 °C to 90 °C and for several particle volumetric concentrations up to 10% showed that the ratio of thermal conductivity of nanofluid to that of the base fluid increased with an increase in temperature and volumetric concentration. As an example, as much as a 20% enhancement in thermal conductivity was evidenced for a particle volumetric concentration of 10 % at 87 °C. Comparison of experimental results of this non-metallic nanoparticles suspension with the well-known model developed by Hamilton and Crosser for microparticles suspensions, exhibits that this model underpredicts the thermal conductivity of nanofluids. Therefore, a new correlation has been derived following recent models developed for metallic nanoparticles suspensions, which is a combination of the Hamilton-Crosser model plus a term due to the Brownian motion. This new correlation expresses the thermal conductivity of silicon dioxide nanofluid as a function of temperature, volumetric concentration and the properties of the base fluid and the nanoparticles.

* Sahoo, B. C., Das, D. K., Vajjha, R. S., and Satti, J. R., 2013, "Measurement of the Thermal Conductivity of Silicon Dioxide Nanofluid and Development of Correlations," ASME Journal of Nanotechnology in Engineering and Medicine, 3(4), pp. 1-10.

Appendix 4. Electrical Conductivity Measurements of Nanofluids and Development of New Correlations *

ABSTRACT

In this study the electrical conductivity of aluminum oxide (Al_2O_3), silicon dioxide (SiO_2) and zinc oxide (ZnO) nanoparticles dispersed in propylene glycol and water mixture were measured in the temperature range of 0 °C to 90 °C. The volumetric concentration of nanoparticles in these fluids ranged from 0 to 10% for different nanofluids. The particle sizes considered were from 20 nm to 70 nm. The electrical conductivity measuring apparatus and the measurement procedure were validated by measuring the electrical conductivity of a calibration fluid, whose properties are known accurately. The measured electrical conductivity values agreed within $\pm 1\%$ with the published data reported by the manufacturer. Following the validation, the electrical conductivities of different nanofluids were measured. The measurements showed that electrical conductivity of nanofluids increased with an increase in temperature and also with an increase in particle volumetric concentration. For the same nanofluid at a fixed volumetric concentration, the electrical conductivity was found to be higher for smaller particle sizes. From the experimental data, empirical models were developed for three nanofluids to express the electrical conductivity as functions of temperature, volumetric concentration and the size of the nanoparticles.

* Konakanchi, H., Vajjha, R., Misra, D., and Das, D., 2011, "Electrical Conductivity Measurements of Nanofluids and Development of New Correlations," *Journal of Nanoscience and Nanotechnology*, 11(8), pp. 6788-6795.

Appendix 5. Comparison of the Performance of Copper Oxide Nanofluid with Water in Electronic Cooling*

ABSTRACT

A numerical study to compare the performance of water and copper oxide (CuO) nanofluid flowing under laminar regime in a parallel-plate channel, serving as a heat sink in an electronic device, has been presented. The geometry considered here is commonly used in the design of heat sinks suitable for cooling an array of microprocessor chips for which air cooling is insufficient. The influence of nanofluids concentration on local and average skin friction coefficients, Nusselt numbers and convective heat transfer coefficients in the channel have been analyzed in detail. The increases in the skin friction and heat transfer with volumetric concentration of nanoparticles have been evaluated from numerical simulations in the Reynolds number range of 100 to 2000. The analysis shows that the flow in this heat sink is hydrodynamically and thermally developing, for which the axial variations of local skin friction and local Nusselt number are presented. As an example, computational results for a 8% volumetric concentration of CuO nanofluid shows that at a Reynolds number of 2000, the average heat transfer coefficient increases nearly by a factor of 2 in comparison with pure water. From a detailed analysis summarized in a table, it is observed that there is an increase in the pressure loss as the particle concentration increases. For the CuO nanofluid of dilute concentration of 2%, a slightly higher pumping power of about 10% compared to water is predicted. This may be tolerable for the thermal protection of expensive electronic chips, in applications where the chip cost is the dominant factor.

* Namburu, P. K., Das, D. K., and Vajjha, R. S., 2012, "Comparison of Performance of Copper Oxide Nanofluid with Water in Electronic Cooling," *Journal of ASTM International* 9(5), pp. 1-15.

Appendix 6. Application of Nanofluids in Heating Buildings and Reducing Pollution *

ABSTRACT

This paper presents nanofluid convective heat transfer and viscosity measurements, and evaluates how they perform heating buildings in cold regions. Nanofluids contain suspended metallic nanoparticles, which increases the thermal conductivity of the base fluid by a substantial amount. The heat transfer coefficient of nanofluids increases with volume concentration. To determine how nanofluid heat transfer characteristics enhance as volume concentration is increased; experiments were performed on copper oxide, aluminum oxide and silicon dioxide nanofluids, each in an ethylene glycol and water mixture. Calculations were performed for conventional finned-tube heat exchangers used in buildings in cold regions. The analysis shows that using nanofluids in heat exchangers could reduce volumetric and mass flow rates, and result in an overall pumping power savings. Nanofluids necessitate smaller heating systems, which are capable of delivering the same amount of thermal energy as larger heating systems using base fluids, but are less expensive; this lowers the initial equipment cost excluding nanofluid cost. This will also reduce environmental pollutants because smaller heating units use less power, and the heat transfer unit has less liquid and material waste to discard at the end of its life cycle.

* Kulkarni, D. P., Das, D. K., and Vajjha, R. S., 2009, "Application of Nanofluids in Heating Buildings and Reducing Pollution," *Applied Energy*, 86(12), pp. 2566-2573.